Assessing the Emerging Environmental Concerns from Bio-originated Organic Pollutants in Cropping Systems

Mengfan Cai

A Thesis

In the Department

of

Building, Civil and Environmental Engineering

Presented in Partial Fulfillment of the Requirements

For the Degree of

Doctor of Philosophy (Civil Engineering) at

Concordia University

Montreal, Quebec, Canada

July 2023

CONCORDIA UNIVERSITY

SCHOOL OF GRADUATE STUDIES

This is to certify that the thesis prepared

By: *Mengfan Cai*

Entitled: *Assessing the Emerging Environmental Concerns from Bio-originated Organic Pollutants in Cropping Systems*

and submitted in partial fulfillment of the requirements for the degree of

DOCTOR OF PHILOSOPHY **(***Civil Engineering***)**

complies with the regulations of the University and meets the accepted standards with respect to originality and quality.

Signed by the final examining committee:

_____Chair
Dr. Rabin Raut

_____External Examiner
Dr. Lei Liu

_____Examiner
Dr. Fariborz Haghighat

_____Examiner
Dr. Wen-Fang Xie

_____Examiner
Dr. Sang Hyeok Han

_____Thesis Supervisor
Dr. Chunjiang An

Approved by _____
Dr. Samuel Li, Chair, Department of Building,
Civil and Environmental Engineering

July 2023 _____
Dr. Mourad Debbabi, Dean,
Gina Cody School of Engineering and Computer Science

ABSTRACT

Assessing the Emerging Environmental Concerns from Bio-originated Organic Pollutants in Cropping Systems

Mengfan Cai, Ph.D.

Concordia University, 2023

Agriculture plays a significant role in achieving the goal of carbon neutrality and emission reduction through practices such as crop residue management. Crop residues can be utilized to produce biodegradable mulches (BMs), which can increase crop production and carbon sequestration potential. However, agricultural health and safety are facing new challenges, particularly concerning bio-originated organic pollutants in cropping systems, including biogenic volatile organic compounds (BVOCs) and biodegradable microplastics (BMPs). The main purpose of the research presented in this dissertation is to assess these emerging environmental concerns, including the appropriate assessment of BVOC emissions and the degradation and fragmentation of BMs.

BVOC emissions were generally influenced by various factors, including temperature, drought, solar radiation, humidity, nutrient availability, carbon dioxide (CO_2), ozone (O_3), etc. Among these factors, growth length, air temperature, solar radiation, and leafage were found to be the most important variables affecting the spatial-temporal variations of methanol (MeOH) emissions from spring wheat during the growing period in a Canadian province. The seasonality of MeOH emissions was positively correlated with concentrations of carbon monoxide (CO), filterable

particulate matter (FPM), and coarse particulate matter (PM_{10}), but negatively related to nitrogen dioxide (NO_2) and O_3. Compared with paper mulch, bioplastic mulch contributed a higher amount of aromatic structure-containing chemicals and carboxylic acids, to the water environment, but released fewer and smaller plastic particles. After entering the soil-water environment, the rough microstructure and oxygenated functional groups on BMP surfaces played a crucial role in the adsorption of aromatic compounds and heavy metals from soils.

Scientometric analysis can provide researchers with an in-depth understanding of BVOC emission mechanisms, while also offering decision-makers insights into emission mitigation and environmental management. The newly developed BVOC assessment approach, designed to evaluate the biogenic MeOH emitted from crops during growing seasons, can help uncover the relationships between BVOC emissions and key influencing factors. The characterization and quantification of BMPs in cropping systems focused on examining the fragmentation and degradation of BMPs under UV irradiation using visual inspection and quantitative analysis. This dissertation offers scientific support for researching and further developing the impact of BVOC emissions and BMP generation on environmental management.

ACKNOWLEDGEMENTS

During the most creative and passionate five years, I am deeply grateful to all the individuals and institutions who have contributed to the completion of this Ph.D. thesis.

First and foremost, I would like to express my profound gratitude to my supervisor, Dr. Chunjiang An, for his scholarly insights, unwavering support, and immense patience throughout this research. Dr. An is a dedicated professor and a highly respected scholar. I consider myself incredibly fortunate to have had the privilege of being mentored by him throughout my entire doctoral journey.

I wish to express my sincere appreciation for the funding, scholarships, or grants that have financially supported my research endeavors.

I sincerely thank the members of my dissertation committee, namely Dr. Lei Liu, Dr. Sang Hyeok Han, Dr. Fariborz Haghighat, Dr. Wenfang Xie, and Dr. Chunjiang An, for their rigorous examination and invaluable suggestions, which have significantly enriched the depth and breadth of my research.

I would also like to acknowledge the indispensable assistance provided by Dr. Christophe Guy from University of Technology of Compiègne, Dr. Xiujuan Chen from the Department of Civil Engineering at the University of Texas at Arlington, Dr. Zhiming Qi from the Department of Bioresource Engineering at McGill University, Ms. Hong Guan from the Department of Building, Civil & Environmental Engineering, and Dr. Dmytro Kevorkov from the Department of Chemical

and Materials Engineering at Concordia University. Their support in training and conducting measurements for my research has been instrumental.

Additionally, I am deeply grateful to my colleagues in Dr. An's Lab, who have not only provided valuable insights but have also become cherished friends, greatly enriching my Ph.D. experience.

Last but certainly not least, my heartfelt gratitude goes to my family and friends, whose understanding and inspiration have been invaluable in helping me overcome moments of doubt and difficulty.

TABLE OF CONTENTS

LIST OF FIGURES

LIST OF TABLES

LIST OF ACRONYMS

ABA	Abscisic Acid
ACS	Agricultural Carbon Sequestration
AMPs	MPs from Artificial Weathering Processes
ARGs	Antibiotic Resistance Genes
As	Arsenic
ASOA	Anthropogenic SOA
ATR−FTIR	Attenuated Total Reflection−Fourier Transform Infrared Spectroscopy
AVOC	Anthropogenic VOC
BECCS	Bioenergy with Carbon Capture and Storage
BMaPs	Biodegradable Macroplastics
BMs	Biodegradable Mulches
BMPs	Biodegradable Microplastics
BNPs	Biodegradable Nanoplastics
BTEX	Benzene, Toluene, Ethylbenzene and Xylenes
BOVOCs	Biogenic Oxygenated VOCs
BPA	Bisphenol A
BSOA	Biogenic SOA
BTEX	Benzene, Toluene, Ethylbenzene and Xylenes
BVOCs	Biogenic Volatile Organic Compounds
Ca	Calcium

CA_w	Water Contact Angle
CCN	Cloud Condensation Nuclei
CCS	Carbon Capture and Storage
Cd	Cadmium
CDF	Cumulative Distribution Function
Cfb	Temperate Oceanic Climate
CI	Carbonyl Index
CK	Cytokinin
CLS	Canadian Light Source
CMEM	Crop Methanol Emission Model
CMIP6	Coupled Model Intercomparison Project Phase 6
CO	Carbon Monoxide
CO_2	Carbon Dioxide
CTM	Chemistry and Transport Model
Cu	Copper
CW	Cell Wall
DBP	Dibutyl Phthalate
DE	Author Keywords
DEC-MS	Disjunct Eddy Covariance by Mass Scanning Technique
DEHP	Di-(2-Ethylhexyl) Phthalate
Dfb	Warm-Summer Humid Continental Climate
DLS	Dynamic Light Scattering

DOE	Design of Experiments
DOM	Dissolved Organic Matter
DOM_{BMP}	BMP-Derived DOM
D_p	Aerodynamic Diameter
ES	Enclosure System
ET	Electron Transfer
FAO	Food and Agriculture Organization
FPM	Filterable Particulate Matter
GC	Gas Chromatography
GC-FID	Gas Chromatograph in Conjunction with Flame Ionization Detectors
GHGs	Greenhouse Gases
GIS	Geospatial Information Systems
G_L	Latex Glove
GL	Growth Length
Glove_S	Glove After Wave and Sand Friction
GLVs	Green Leaf Volatiles
G_N	Nitrile Glove
GPP	Gross Primary Production
G_V	Vinyl Glove
HBCDDs	Hexabromocyclododecanes
HCHO	Formaldehyde
HDPE	High-Density Polyethylene

HG	Homogalacturonan
HI	Harvest Index
HMPs	High-Intensity Weathered MPs
HNPs	High-Intensity Weathered NPs
$IF_{p<0.05}$	Significant Interactive Factors
IR	Infrared Detector
LAI	Leaf Area Index
LDF	Light-Dependent Fraction
LDPE	Low-Density Polyethylene
LISST	Laser In-Situ Scattering and Transmissometer
LLR	Log-Likelihood Ratio
LN	Liquid Nitrogen
LPJ-GUESS	Lund-Potsdam-Jena General Ecosystem Simulator
LUE_{max}	Maximum Light Use Efficiency
MACR	Methacrolein
MaPs	Macroplastics
Mask_S	Mask After Wave and Sand Friction
MCT	Mercury Cadmium Telluride
Me	Methyl group
MEGAN	Model of Emissions of Gases and Aerosols from Nature
MeOH	Methanol
MEP	Methylerythritol 4-Phosphate

MERRA	Modern-Era Retrospective Analysis for Research and Applications
MGL	Maximum Growing Length
MGO	Methylglyoxal
M_I	Inner Layer of the Mask
MI	Mutual Information
MID-IR	Mid Infrared Spectromicroscopy
MLG	Mixed Layer Gradient
M_M	Middle Layer of the Mask
M_O	Outer Layer of the Mask
MOHYCAN	Model of Hydrocarbon Emissions by the Canopy
MPs	Microplastics
MTs	Monoterpenes
MTS	Material Test System
MVK	Methyl Vinyl Ketone
MVOCs	Microbial VOCs
MW	Molecular Weight
Ni	Nickel
NMPs	MPs from Natural Sources
NMVOC	Non-Methane VOC
NO	Nitrogen Monoxide
NO_2	Nitrogen Dioxide
NO_x	Nitrogen Oxides

NPP	Net Primary Production
NPs	Nanoplastics
O_3	Ozone
•OH	Hydroxyl Radical
-OH	Hydroxyl Groups
OM	Organic Matter
OMI	Ozone Monitoring Instrument
OVOC	Oxygenated VOCs
PA	Polyamide
PAHs	Polycyclic Aromatic Hydrocarbons
PAR	Photosynthetically Active Radiation
PBAT	Polybutylene Adipate Terephthalate
PBVOCs	Plant BVOCs
PCA	Principal Component Analysis
PCBs	Polychlorinated Biphenyls
PE	Polyethylene
PES	Polyethersulfone
PET	Polyester
PHAs	Polyhydroxyalkanoate
Phe	Phenanthrene
PLA	Polylactide
PM	Particulate Matter

PM_{10}	Coarse Particulate Matter
$PM_{2.5}$	Fine Particulate Matter
PME	Pectin Methylesterase
PMMA	Polymethylmethacrylate
POMBMP	Bmp-Derived Particulate Organic Matter
PP	Polypropylene
PPFD	Photosynthetic Photon Flux Density
PSU	Polysulfone
PTFE	Polytetrafluoroethylene
PTR-MS	Proton-Transfer-Reaction Mass Spectrometry
PTR-TOF	Proton Transfer Reaction Time-Of-Flight
PTR-TOF-MS	Proton Transfer Reaction - “Time-Of-Flight” - Mass Spectrometer
QA/QC	Quality Assurance/Quality Control
RCMs	Regional Climate Models
RCPs	Representative Concentration Pathways
REA	Relaxed Eddy Accumulation
REA-EC	Relaxed Eddy Accumulation - Eddy Covariance
RH	Relative Humidity
ROS	Reactive Oxygen Species
RS	Remote Sensing
SBVOCs	Soil BVOCs
SD	Standard Deviation

SDGs	Sustainable Development Goals
SEM	Scanning Electron Microscope
SESI-MS	Secondary Electrospray Ionization Mass Spectrometry
$SF_{p<0.05}$	Significant-Single-Factors
$SF_{p>0.05}$	Insignificant-Single-Factors
SIA	Secondary Inorganic Aerosol
SLG	Surface Layer Gradient
SO_2	Sulfur Dioxide
SCS	Soil Carbon Sequestration
SOA	Secondary Organic Aerosol
SOM	Soil Organic Matter
SPME	Solid Phase Microextraction
SQTs	Sesquiterpenes
SR-XRF	Synchrotron X-Ray Fluorescence
SSP2-4.5	A Medium Development (SSP2) Achieving Forcing Levels of 4.5 $W \cdot M^{-2}$
SSP5-8.5	A High Economic Growth (SSP5) Achieving Forcing Levels of 8.5 $W \cdot M^{-2}$
SSPs	Shared Socioeconomic Pathways
TBBPA	Tetrabromobisphenol A
TCD	Thermal Conductivity Detector
TF*IDF	Term Frequency and Inversed Document Frequency
THF	Tetrahydrofolate
UN	United Nations

UV	Ultraviolet
VE	Vacuum Extraction
VESPERS	Very Sensitive Elemental and Structural Probe Employing Radiation from A Synchrotron
VOCs	Volatile Organic Compounds
VPD	Vapor Pressure Deficit
VPM	Vegetation Photosynthesis Model
WRF-CHEM	Weather Research and Forecasting (WRF) model coupled with Chemistry
WGP	Weedguardplus
WoS	Web of Science
WoSCC	Web of Science Core Collection
ZP	Zeta Potential
Zn	Zinc

CHAPTER 1. INTRODUCTION

1.1. Problem statement

As per the Food and Agriculture Organization (FAO) of the United Nations (UN), the global agricultural land area is estimated to be around five billion hectares, constituting approximately 38 percent of the Earth's total land surface (FAOSTAT, 2020). Roughly one-third of this land is designated for cropland, while the remaining two-thirds serve as meadows and pastures for grazing livestock. The world's burgeoning population has more than doubled between 1961 and 2016, resulting in an increased demand for food resources (FAOSTAT, 2020). Thus, the pressure on land resources has similarly intensified, necessitating the augmentation of crop production with finite resources.

The Paris Agreement and UN Sustainable Development Goals (SDGs) are urging us to shift from fossil fuels to sustainable and renewable energy resources for the goal of carbon neutrality and emission reduction. Agriculture plays a significant role in achieving this goal and it can sequester carbon through practices such as soil carbon sequestration (SCS), crop residue management, and renewable energy generation. Agricultural carbon sequestration (ACS) refers to the process of capturing and storing carbon dioxide (CO_2) from the atmosphere through the above agricultural practices. Bioenergy with carbon capture and storage (BECCS) related to agriculture combines carbon capture and storage (CCS) technologies with the use of biomass such as crops, agricultural residues, and bioenergy crops for energy production. It has the potential to achieve significant CO_2 removals from the atmosphere and results in negative net emissions through the natural photosynthesis process of the biomass used for energy production (Gaurav et al., 2017). Generally, bioenergy production primarily depends on CO_2 capture and solar energy storage in energy crops,

followed by carbon storage in litterfalls, residues, and soils (Monforti et al., 2015). Agricultural practices, such as crop residue management, enhance crop production and SCS. For example, retaining crop residues (e.g., stalks, stubble) on the soil surface instead of burning or removing them allows for the slow release of carbon back into the soil. Crop residues, such as straw, hay, or corn stalks, can be utilized to produce biodegradable mulches (BMs) which are used to improve soil structure and increase carbon sequestration potential. By increasing carbon storage in soils, vegetation, and agricultural biomass, agriculture can help mitigate climate warming and contribute to carbon neutrality by offsetting the emissions of greenhouse gases (GHGs) from other sectors. However, agricultural health and safety are facing some new challenges, especially bio-originated organic pollutants in cropping systems, including biogenic volatile organic compounds (BVOCs) and biodegradable microplastics (BMPs).

BVOCs, as a proportion of carbon loss that is released back to the atmosphere during processes such as photosynthesis, respiration, and biomass burning, have caused controversy over the role of bioenergy in climate warming mitigation (Favero et al., 2020). Besides GHGs, these volatiles should be considered in climate research due to their high reactivity and large bio-sources (Covey et al., 2021). Methanol (MeOH, CH_3OH) is typically the second-most plentiful volatile organic compound (VOC), after methane (CH_4), in the remote troposphere. Due to its plenitude and long lifetime compared to other VOCs, MeOH has an important impact on air quality, human health, and climate change (Caravan et al., 2018; Mozaffar, 2017). Biogenic MeOH emission from plants is a primary source of ambient MeOH (accounting for 80%–89%) and it generally exceeds emissions of all other VOCs except terpenoids measured above a variety of different ecosystems (Harley et al., 2007; Heikes et al., 2002). However, most previous studies have not distinguished

the individual contribution of plants or soil microbes to the BVOC emissions of an ecosystem. The effects of anthropogenic activities and soil processes have barely been quantified when modeling ecosystem-BVOC emissions. Furthermore, previous estimates have focused primarily on MeOH emissions from forests and grasses. Croplands cover a significant proportion of the Earth's surface and, although they are negligible isoprene emitters, they may be a significant source of MeOH (Custer and Schade, 2007). To date, though, no specific emission model for crop MeOH spanning the different developmental stages has been proposed, which will promote the assessment of MeOH emission to encompass this scope (Bachy et al., 2016; Guenther et al., 2012; Stavrakou et al., 2011). Understanding their emissions could help better achieve SDG13 which is to "take urgent action to combat climate change and its impact".

BMPs, as one of the bio-originated organic pollutants, have potential environmental concerns in ACS and BECCS systems. The application of BMs in cropping systems can increase crop production and carbon sequestration potential. After exposure to the soil, the fragmentation of BMs caused by abiotic and biotic processes will elevate the mobility of BMPs in the soil, aquatic environment, and atmosphere (Cai et al., 2017; 2019b; Wang et al., 2021c). BMPs can be the carbon addition to agricultural soils, which will change the composition of soil-dissolved organic matter (DOM), such as aromatic functional groups (Feng et al., 2020). BMPs have a stronger affinity to soil pollutants, such as organic pollutants and heavy metals; thus, BMPs may have a greater negative impact than non-BMPs in certain conditions (Qin et al., 2021). Although there are scarce studies on the ecotoxicity of BMPs on terrestrial organisms, we can speculate their hazards to crops, animals, and humans considering the transfer of BMPs via the terrestrial food web in the agroecosystem. Notably, the effects of BMPs on soil microbiological and physicochemical

properties are controlled by polymer type, size, dose, and shape (Wang et al., 2022a). Therefore, it is necessary to explore the degradation and fragmentation of BMs after the use of mulching in future studies.

1.2. Research objectives

Bio-originated organic pollutants, such as BVOCs and BMPs, pose potential environmental concerns in cropping systems. Conducting an appropriate assessment of BVOC emissions and exploring the degradation and fragmentation of BMs are prerequisites for investigating the impact of BVOC emissions and BMP generation on environmental management. Three objectives are expected to be addressed:

- Scientometric analysis of BVOCs emitted from terrestrial systems – This study analyzed the overall structure and characterizations of the intellectual landscape in the research field of BVOC emissions using scientometric analysis tools. It aims to grasp the features and emerging trends in existing research, identify consensus on salient topics and anticipate future research directions. The insights gained from these findings can provide a systematic and comprehensive review of the emissions and drivers of BVOCs and their contributions to air pollutants and GHGs, aiding in the achievement of sustainable environmental management for human-dominated terrestrial ecosystems.
- Assessment of biogenic MeOH emitted from crops – This study seeks to fill these gaps by modeling, for the first time, MeOH emissions from spring wheat in its various developmental stages. Moreover, it seeks to provide an updated method for assessing MeOH emissions from spring wheat or other crops using limited weather data. The study seeks to uncover the

relationships between MeOH emissions and major influencing factors. The results obtained can be utilized to enhance the adaptation and mitigation strategies for agricultural systems.

- Characterization and quantification of the BMPs in cropping systems – This study aims to examine the effects of weathering on BMs under abiotic conditions, particularly UV irradiation. It seeks to investigate the physicochemical changes of weathered BMPs, the particle distributions of micro- and nano-plastics, and the chemical characteristics of BMP leachate released into the soil-water environment. The findings can contribute to the management of environmental risks and aid in determining appropriate disposal strategies following the use of mulching in cropping systems.

1.3. Thesis outline

This dissertation contains six chapters:

- Chapter 1 is a general introduction providing the background information relevant to this dissertation.
- Chapter 2 is a comprehensive literature review, providing a comprehensive understanding and the latest developments of BVOCs and BMPs, as well as the current research limitations. It includes emission sources of BVOCs, estimation methods of BVOC emissions, uncertainties in the response of BVOC emissions to influencing factors, and emerging microplastic (MP) and nanoplastic (NP) pollution from mulching films applied in cropping systems.
- Chapter 3 conducts a scientometric analysis of 2,762 journal papers related to BVOC emissions from the Web of Science Core Collection (WoSCC) between 1991 and 2020 using CiteSpace and Carrot^2. It highlights three main knowledge domains in the field of BVOC emissions, namely BVOC emissions and drivers, BVOCs and their oxidation products in

biosphere-atmosphere exchange, and soil BVOCs in plant-microbe interactions. Additionally, it suggests that incorporating BVOC emissions and their relationships with pollutants, biomass, and energy into environmental management and decision-making shows promise as a future direction.

- Chapter 4 proposes an emission model to assess the temporal and spatial variations of MeOH emissions of spring wheat during the growing period in a Canadian province. It highlights that growth length, air temperature, solar radiation, and leaf age are the most important factors influencing MeOH emissions. Additionally, it mentions that the seasonality of MeOH emissions is positively correlated with concentrations of carbon monoxide (CO), filterable particulate matter (FPM), and coarse particulate matter (PM_{10}), but negatively related to nitrogen dioxide (NO_2) and ozone (O_3).
- Chapter 5 demonstrates the physicochemical characteristics of weathered BMPs and their derived leachate through particle size analysis and spectral analysis. It compares the differences between paper mulch and bioplastic mulch in terms of the chemicals released into the water environment and the size of plastic particles. The spectral mapping results reveal the spatial distributions of metal elements and functional groups on the surface of BMPs, indicating that ultraviolet (UV) radiation promotes the adsorption of aromatic compounds and heavy metals from soils onto BMPs.
- Chapter 6 summarizes the overall conclusions and major findings of the dissertation. It highlights the main contributions and significance of the research and provides recommendations for future research directions.

CHAPTER 2. LITERATURE REVIEW

2.1. Emission sources of BVOCs

2.1.1. Extension of the definition of BVOCs

BVOCs can be classified into plant BVOCs (PBVOCs) and soil BVOCs (SBVOCs) according to their producers, i.e., living organisms in terrestrial ecosystems (particularly vegetation and soil microbes). PBVOCs, predominantly isoprene (C_5H_8), monoterpenes (MTs, $C_{10}H_{16}$), and sesquiterpenes (SQTs, $C_{15}H_{24}$), are generally produced as a defence mechanism against oxidative and thermal stresses or as a communication mechanism for above-ground plants or below-ground microbial organisms (Loreto and Schnitzler, 2010; Maki et al., 2019). SBVOCs, meanwhile, primarily consisting of MTs and biogenic oxygenated VOCs (BOVOCs). Soils could produce and emit BVOCs through various soil processes, e.g., microbial decomposition of litter and soil organic matter (SOM), stored-BVOCs evaporation from litterfall and soil, living root emission, as well as other physicochemical processes, and they could also work as a sink of BVOCs through dry and wet deposition or biotic and abiotic uptake (Maki et al., 2019; Penuelas et al., 2014). Notably, soils are the principal habitat of the soil microbes (i.e., bacteria, actinomycetes, fungi, protozoa, and nematodes) that emit microbial VOCs (MVOCs), and they also contain large amounts of shedding vegetation and living roots that emit PBVOCs (Tang et al., 2019a). As such, SBVOCs are a non-negligible source of BVOC emissions from terrestrial ecosystems.

The schematic diagram of the interactions of BVOCs with subsequent derivatives in terrestrial ecosystems is shown in Figure 2.1. These BVOCs participate in many atmospheric reactions as the precursors to CO_2, O_3, secondary organic aerosol (SOA), and particulate matter (PM) because of their high reactivity and emissions (Fares et al., 2012). SOA, it should be noted, accounts for a

large proportion of fine particulate matter ($PM_{2.5}$) and has significant effects on human health and climate change (Rohr, 2013). Aerosol particles, as an important component of the GHGs, not only have a direct effect on global warming but also cause changes in cloud properties that will have a long-term impact on the global climate and environmental chemistry (Cai et al., 2019b; Way et al., 2013). Therefore, in recent decades, many efforts have been made to estimate BVOC emissions and their contributions to these oxidation products (Calfapietra et al., 2013; Prendez et al., 2013).

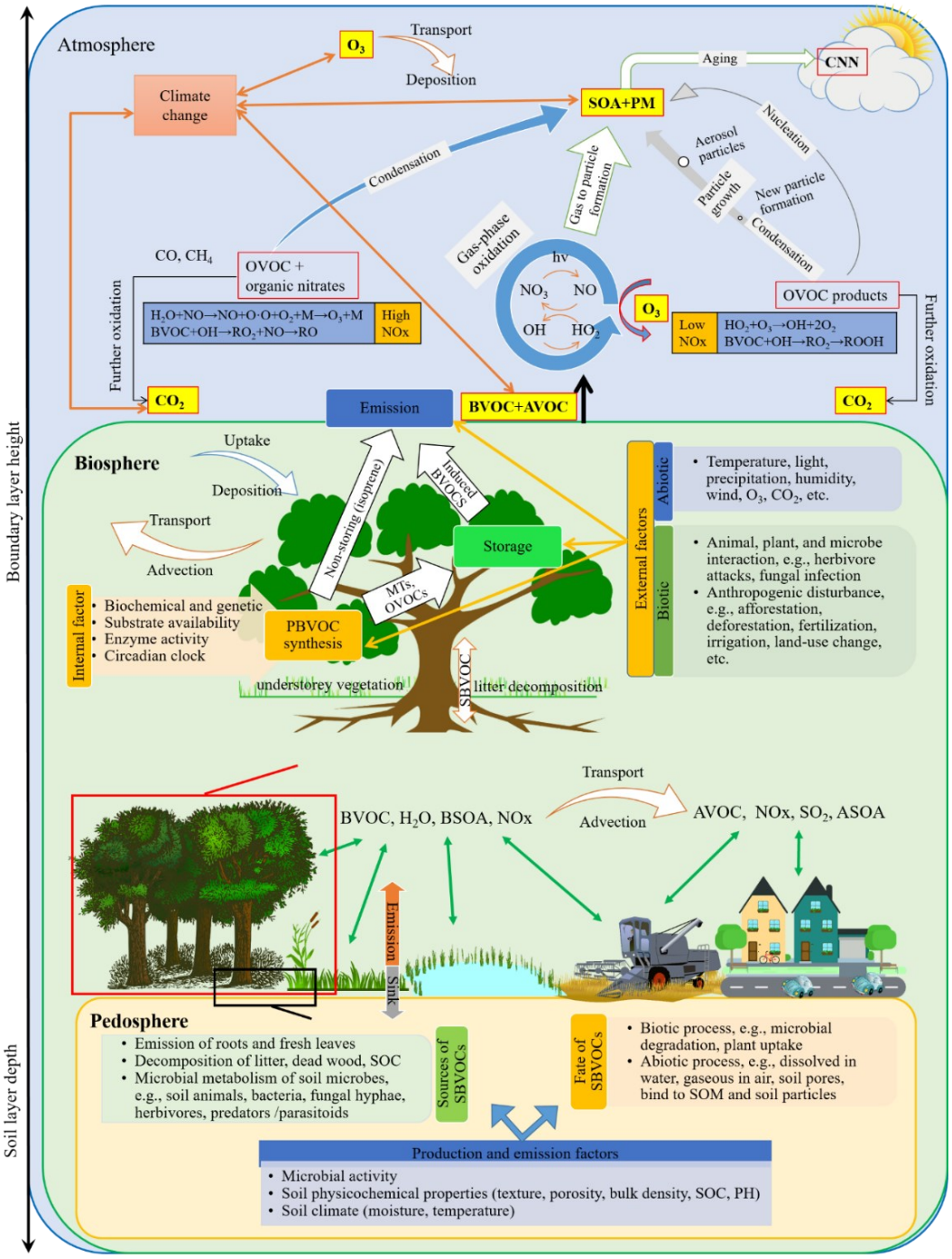

Figure 2.1. Schematic diagram of the interactions of BVOCs with subsequent derivatives in terrestrial ecosystems. AVOC: anthropogenic VOC; BSOA: biogenic SOA; ASOA: anthropogenic SOA.

2.1.2. Biogenic MeOH emission from plants

Biogenic MeOH is generally produced in plant cells through biochemical processes such as cell-wall loosening during cell expansion, tetrahydrofolate pathways, protein repair, and pectin methylesterase (PME) (Figure 2.2). The MeOH produced in plant cells can be stored in water and tissue and can be utilized in plant cells through many metabolic pathways. It evaporates to the atmosphere through stomata or is oxidized by hydroxyl radical (•OH) to form formaldehyde (HCHO) and, ultimately, CO_2. MeOH emission may be affected by environmental factors (e.g., light intensity and air temperature) and vegetation factors (e.g., stomatal conductance, leaf development, MeOH pool size, and methylotrophs). Stresses such as hypoxia, high ozone concentration, frost, injury (e.g., cutting, insect or animal attacks), senescence, dehydration of plant leaves, and biomass burning can also cause MeOH emissions (Brunner et al., 2007; Galbally and Kirstine, 2002). It has been reported that young leaves are higher emitters compared to mature leaves, and, similarly, that herbivore-attacked leaves are higher emitters than unattacked leaves (Fall and Benson, 1996; Penuelas et al., 2005). Understanding biogenic MeOH emission could help better achieve the UN SDG 13 which is to "take urgent action to combat climate change and its impact".

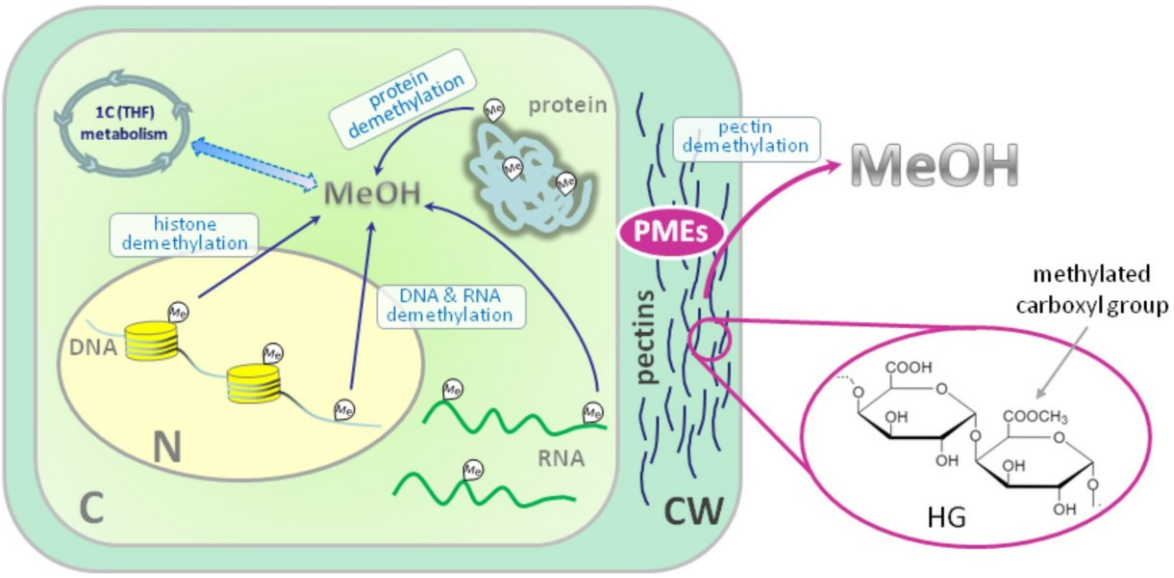

Figure 2.2. Sources of endogenous MeOH in plant cells (Dorokhov et al., 2018). 1C: one-carbon; C: cytoplasm; N: nucleus; CW: cell wall; HG: homogalacturonan; Me: methyl group; PMEs: pectin methylesterases; THF: tetrahydrofolate.

2.1.3. MVOCs in plant-microbe communications

Several reviews have introduced information about the chemical species, structures, biosynthetic pathways, and biological functions of MVOCs, such as SQTs and microbial terpenes emitted from fungal species (Kramer and Abraham, 2012). According to the database of VOCs emitted by microorganisms as described by Effmert et al. (2012), 300 rhizosphere and soil microbes could produce approximately 800 MVOCs with distinct action potentials, which can play a dominant role in microbe-microbe and microbe-plant interactions below ground. MVOCs could alter the physiology, growth, and defence mechanisms of plants across complex processes concerning abscisic acid (ABA) and cytokinin (CK), but most bioactive MVOCs could hardly experience specific VOC-mediated interactions (Ameztoy et al., 2019). These microbe-to-plant signal

compounds can promote biomass production, sustainable energy supply, and climate change mitigation (Antar et al., 2021; Singh et al., 2021).

2.2. Estimation methods of BVOC emissions

2.2.1. Measurements of BVOC emissions

Spatial-temporal trends of emissions and their drivers vary depending on the scale (Cai et al., 2017). BVOC emission trends have been described in different studies in terms of time scale (ranging from diurnal to phenological, seasonal, and annual) and spatial scale (ranging from leaf to individual, regional, national, and global). The emission trends at large scales (e.g., seasonal and annual time scales, or regional, national, and global spatial scales) tended to be expressed in the form of simulation results; observation results were a better choice for small scales (e.g., diurnal and phenological time scales or leaf and individual spatial scales) due to the large uncertainty associated with modeling at these scales. When there were fewer simulation data such as in the cases of BOVOCs and SQTs, large-scale emission trends were typically supplemented by measurements.

Since the 1990s, observations and simulations of BVOC emissions have gradually been attracting increasing attention. In terms of BVOC sampling and composition identification, measurement techniques mainly included enclosure system (ES), proton-transfer-reaction mass spectrometry (PTR-MS), relaxed eddy accumulation (REA), mixed layer gradient (MLG), and surface layer gradient (SLG), ranging in spatial scale from leaves (10 cm^2) to landscapes (100 km^2) with a time resolution of several seconds (de Gouw and Warneke, 2007; Guenther et al., 1996). Among these, a chamber controlling light and leaf temperature was a commonly used ES. It can be used to

measure BVOC emissions of individual leaves and entire branches as well as their short-term environmental controllers, such as light, temperature, and mechanical wounding (Staudt and Bertin, 1998). REA was a universal approach in micrometeorological flux measurement that was commonly used to observe local BVOC fluxes from vegetation canopies, varying from tall forests (e.g., *Norway spruce*, orange orchard, beech) to short crops (e.g., wheat and barley), as well as to measure their response to regional meteorological changes (Arnts et al., 2013; Valentini et al., 1997). PTR-MS was one of the useful techniques for identifying and measuring both field and laboratory BVOC emissions with high sensitivity and rapid response time. The operation theory, operating conditions, and improvement work of PTR-MS have been described in several reviews (de Gouw and Warneke, 2007). The complementary use of proton transfer reaction time-of-flight (PTR-TOF) and gas chromatograph in conjunction with flame ionization detectors (GC-FID), as another measurement method, can improve the accuracy of chemical identification and source apportionment as well as the time resolution of flux quantification (Ouyang et al., 2016; Pallozzi et al., 2016). There were natural and rich stable carbon isotope ratios in BVOCs, which might offer a useful method to evaluate diverse metabolic pathways under field conditions (Haberstroh et al., 2019).

2.2.2. Simulations of BVOC emissions

Apart from revealing BVOC emission trends, observations can also be applied to verify and improve models. Model of Emissions of Gases and Aerosols from Nature (MEGAN) was a widely known bottom-up model to estimate BVOC emissions from terrestrial ecosystems at both the global and regional scales. This model was based on early MT and isoprene models and suggested parameters (Guenther et al., 2006). It was a phenomenological model encompassing standard

emission factors for any species (ε), environmental correction factors (γ), and input data (Figure 2.3). Most studies on model improvement have focused on γ algorithms and input data at both time scales and spatial scales (Grote et al., 2013). Besides key factors affecting BVOC emissions, such as temperature and light, additional driving factors like leafage, soil moisture, and CO_2 (Guenther et al., 1999; 2006), were subsequently considered in the models, e.g., MEGAN 2.1 (Guenther et al., 2012), an update of previous versions such as MEGAN 2.0 for isoprene emissions (Guenther et al., 2006) and MEGAN 2.02 for MT and SQT emissions (Sakulyanontvittaya et al., 2008). MEGAN estimated the global BVOC flux to be 1,150 Tg C yr^{-1}, composed of isoprene (49%), t-β-ocimene, β-pinene, α-pinene, ethene, propene, limonene, acetone, ethanol, acetaldehyde, and MeOH (30% combined), MTs (15%), SQTs (3%), and more than 100 additional compounds rounding out the remaining 3%. It was found that tropical forestlands (like rainforests, savanna, and drought-deciduous forests) covered about 18% of the global land areas and contributed nearly half of global BVOC emissions; shrubs, crops, and other forests were found to cover about the same area as tropical forestlands but contributed only 10% to 20% apiece. However, soil moisture stress was found to decrease global emissions by 20% to 50% (Müller et al., 2007; Sindelarova et al., 2014). For example, Sindelarova et al. (2014) deployed MEGAN coupled with Modern-Era Retrospective Analysis for Research and Applications (MERRA) and estimated global BVOC emissions to be 760 Tg C yr^{-1}, including isoprene (70%), MTs (11%), SQTs (2.5%), MeOH (6%), acetone (3%), and other VOCs (7.5%). Leaf traits, such as thickness, area, and pigments, vary significantly with canopy height, so the physiological status of leaves should be considered in efforts to improve emission algorithms (Simpraga et al., 2013). In this context, MEGAN 3 features a modified canopy environmental model, stress response, controlling processes, over 40,000 plant types, and more than 200 BVOC compounds (Jiang et al., 2018).

From 1991–2020, the emission models have developed from an isoprene emission model of individual leaves to a global BVOC emission model which can simulate past and future BVOC emissions by coupling climate models, e.g., regional climate models (RCMs), and canopy models, e.g., Model of HYdrocarbon emissions by the CANopy (MOHYCAN) (Bauwens et al., 2018). Apart from field measurements, Remote Sensing (RS) and Geospatial Information Systems (GIS) can provide land use, forest area, leaf area index (LAI), foliar densities, etc. These interpretative data of RS images have been applied to estimate a finer spatial-temporal resolution of BVOC emissions, including source distributions and emission profiles of different chemical species. Simulations of BVOC emissions can also be conducted using top-down models, i.e., inversion studies based on HCHO columns observed from space using an ozone monitoring instrument (OMI) (Bauwens et al., 2018). HCHO observations offered useful insights on reactive hydrocarbon emissions when a chemistry and transport model (CTM) was applied to evaluate the time-dependent HCHO yield from BVOCs such as isoprene, 2-methyl-1-butanol, and α- and β-pinenes (Choi et al., 2019; Palmer et al., 2007).

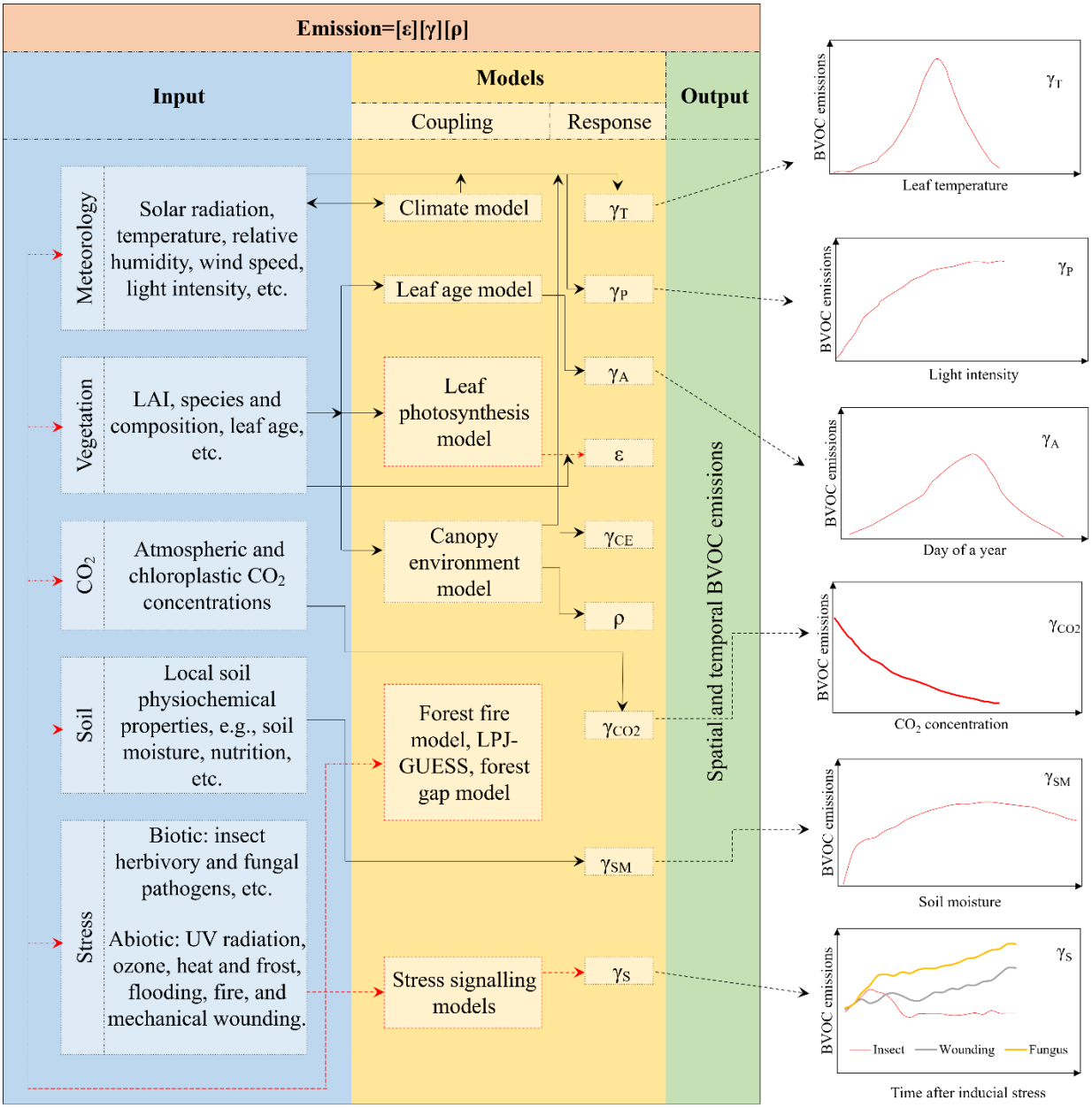

Figure 2.3. A schematic of the main structure and components of the BVOC emission model. LPJ-GUESS: Lund-Potsdam-Jena General Ecosystem Simulator. ε is the standard BVOC emission. ρ is a factor explaining the production and loss of BVOC within plant canopies. γ is a non-dimensional emission activity factor accounting for emission changes considering the light

(γ_P), temperature (γ_T), soil moisture (γ_{SM}), canopy environment (γ_{CE}), leaf age (γ_A), CO_2 inhibition and fertilization (γ_{CO2}), and induced stresses such as insects, fungus, and wounding (γ_{stress}).

The surface soil is also a significant contributor to stand-scale BVOC emissions due to the synthesis and release of BVOCs from shedding vegetation and living roots as well as the microbial decomposition of litter and SOM (Cai et al., 2020). Decaying and dried vegetation is an important source of C_1−C_3 BOVOCs. Thus, litter BVOC emissions are dependent on the major influences of temperature, moisture content, and labile carbon content of the litter, consistent with the format of the MEGAN landscape emission model (Guenther et al., 2006). This simple model is described by the expression:

$$E = \varepsilon \cdot \gamma_{SM} \cdot \gamma_T \cdot \gamma_C \tag{2.1}$$

$$\gamma_{SM} = exp\,(a \cdot (\%m - \%m_0)) \tag{2.2}$$

$$\gamma_T = exp\,(b \cdot (T - T_0)) \tag{2.3}$$

$$\gamma_C = exp\,(-c \cdot (T - T_0)) \tag{2.4}$$

where ε is the emission capacity of BVOC at standard surface soil temperature (T_0 = 30) and soil moisture ($\%m_0$ = 6%), which are determined empirically to match gradient flux observations; γ_C is the emission activity factor of available soil carbon; $\%m$ is the moisture content in percent; and T is the soil surface temperature. Available carbon decreases with time, and the initial carbon input could be also estimated with crop yield. Constants *a, b* and *c* have been determined experimentally for each BVOC in the gradient experiments (Greenberg et al., 2012).

2.2.3. Emission drivers and model development

Empirical algorithms in phenomenological models have been widely adopted to explore relationships between environmental variables and BVOC emissions (Arneth et al., 2011). Generally, BVOC emissions were affected by temperature, drought, solar radiation, humidity, availability of nutrients, CO_2, O_3, etc. The magnitude of stress-induced emissions was dominated by stress tolerance, timing, duration, and strength. The combined effects of two or more stresses, moreover, were sometimes additive or had priority in one stress (Holopainen and Gershenzon, 2010; Niinemets, 2010). A recent meta-analysis quantifying the effect of medium-term (nearly 7 days) climate change on leaf-scale BVOC emissions found isoprene emissions to be inhibited by drought (−15%), elevated CO_2 (−23%), and O_3 (−8%) but stimulated by warming (+53%). However, these climate drivers were found to have little effect on MT emissions, except for elevated O_3 (limited to evergreens with storage organs and plants that are not sensitive to O_3) and warming (+39%) (Feng et al., 2019). Squire et al. (2014) projected a future scenario (for the year 2095) in a simulation study with a 55% reduction in isoprene emissions in contrast with the year 2000 with individual contributions from climate change (+30%), land-use change (−73%, mainly cropland expansion) and CO_2 inhibition (−57%).

There were significant uncertainties in predicting changes in a dynamic global environment, especially when using multipliers based on single-factor relationships derived from short-term experiments to illustrate the synergistic effects of several environmental variables (Pacifico et al., 2009). It is not necessarily reliable to use empirical algorithms for long-term predictions, and the key to establishing realistic and reliable models is to quantify the stress effects of induced and constitutive BVOC emissions. Several reviews summarized key advances in BVOC models,

stressing the importance of incorporating process understanding of leaf BVOC production into BVOC emission modeling (Arneth et al., 2011; Harrison et al., 2013a). Process-based models had the potential to capture the influence of environmental variables. Some models based on cell structure and metabolic processes, such as pectin demethylation in cell walls or metabolism processes in the chloroplast, were proposed to describe the production and emission of BOVOCs (e.g., acetone, acetaldehyde, C_3/C_4 carbonyls, MeOH, and acetic acid) and volatile isoprenoid (e.g., isoprene) (Harrison et al., 2013a). Combining leaf models with whole-plant models physiologically would be an encouraging direction. For example, the mechanistic treatment of photosynthesis, including photosynthetic electron transport and calculation of intermediate compounds, can be introduced into vegetation emission models (Arneth et al., 2007; Grote, 2007). It was promising to consider the possible feedback of BVOC emissions on the physiological conditions of plants, e.g., the mitigation of thermal and oxidative stresses resulting from plant isoprenoids (Grote and Niinemets, 2008). However, these mechanism-based models had the limitation of lacking validation data. It is important to standardize experiments and algorithms and critically examine past studies for developing accurate databases of emission factors for specific plant species and chemical species.

2.2.4. Gaps in empirical models and future directions

Overall, empirical models (e.g., MEGAN) have been widely used in modeling BVOC emissions, particularly volatile isoprenoids. Successive modifications, including incorporating more valuable parameters and coupling process-based models, have been applied to BVOC emission models to minimize uncertainties. However, plants and soils not only emit MTs and isoprene, but also emit BOVOCs, mainly including alcohols, aldehydes, ketones, etc., and their synthesis pathways are

different. There have been many studies on monoterpene and isoprene, but few on the formation and emission mechanism of OVOCs. SBVOC fluxes have not been considered when modeling global BVOC emissions from terrestrial ecosystems. The source and quality of basic parameters (including the vegetation cover type, LAI, and ε of an underlying surface) are critical in governing the accuracy and rationality of spatial emissions. Data calibration using ground measurements and RS images for BVOC emission modeling could largely reduce the uncertainties in BVOC emissions caused by land cover data. Furthermore, models derived from MEGAN, although robust in their consideration of natural factors, rarely include the effects of human activities on metabolic processes in ecosystems, e.g., landscape planning, technical policy, and growing population. Interestingly, forest wildfires may significantly alter emission factors and BVOC emissions from plants and soils, thereby influencing the ambient concentration of SOA and O_3, as well as the composition and evolution of vegetation and soil microbes within the ecosystem (Ciccioli et al., 2014). Biological stress and mechanical damage can cause some green leaf volatiles (GLVs) to emit almost immediately (Ameye et al., 2018). However, wildfire-driven fluxes and instantaneous emissions have not been considered in the modeling of global BVOC estimates from the terrestrial biosphere, shown in red dotted boxes in Figure 2.3. Additionally, there are large uncertainties in long-term emission modeling due to a lack of long-term BVOC measurements and the chronic response to environmental changes. Future observations from laboratory control experiments and long-term fields might contribute to revealing the interactive and comprehensive impacts of multiple drivers and bridge gaps in the modeling of BVOC emissions, especially for BOVOCs and high-latitude plants. Future attention should be given to manipulated or long-term measurements of SBVOC emissions, including root and litter emissions and microbial decomposition responding to diverse environmental factors in primary soil types at stand scales. Moreover, it is difficult to

determine how one or multiple environmental drivers may influence the emission of different chemical species of BVOCs from various biological species in terms of plant physiology and soil biology. Therefore, the improvement of a conceptual and estimation model based on MEGAN regarding the above problems could be a promising direction for future research. A meta-analysis, multi-factor regression, or scenario analysis based on all studies mentioned could be carried out to offer a better understanding of these relationships and anticipate trends in future studies. Moreover, more observation of the production and emission of BVOC, especially BOVOCs, from the perspective of plant physiology at the cell level is required for verification and validation of these emission models.

2.3. Uncertainties in the response of PBVOC emissions to influencing factors

2.3.1. Biological drivers of PBVOC emissions

The production and emission of PBVOCs can be understood as a response to the negative consequences of stresses in terms of stress gradient and response time (Figure 2.4). Several reviews in this area have noted that the emission rates and components of BVOC are affected by biotic stresses (e.g., ecological succession, tree age, leaf age, photosynthetic rate, transpiration rate, stomatal conductance, intercellular CO_2 concentration, etc.), environmental stresses (light, temperature, relative humidity, soil nutrition, salt stress, drought stress, elevated CO_2 and O_3, etc.), and disturbances related to animal activity or anthropogenic activities (e.g., afforestation, deforestation, herbivore attacks, fertilization, irrigation, land-use change, etc.) (Monson et al., 1994; Niinemets, 2010; Peñuelas and Staudt, 2010).

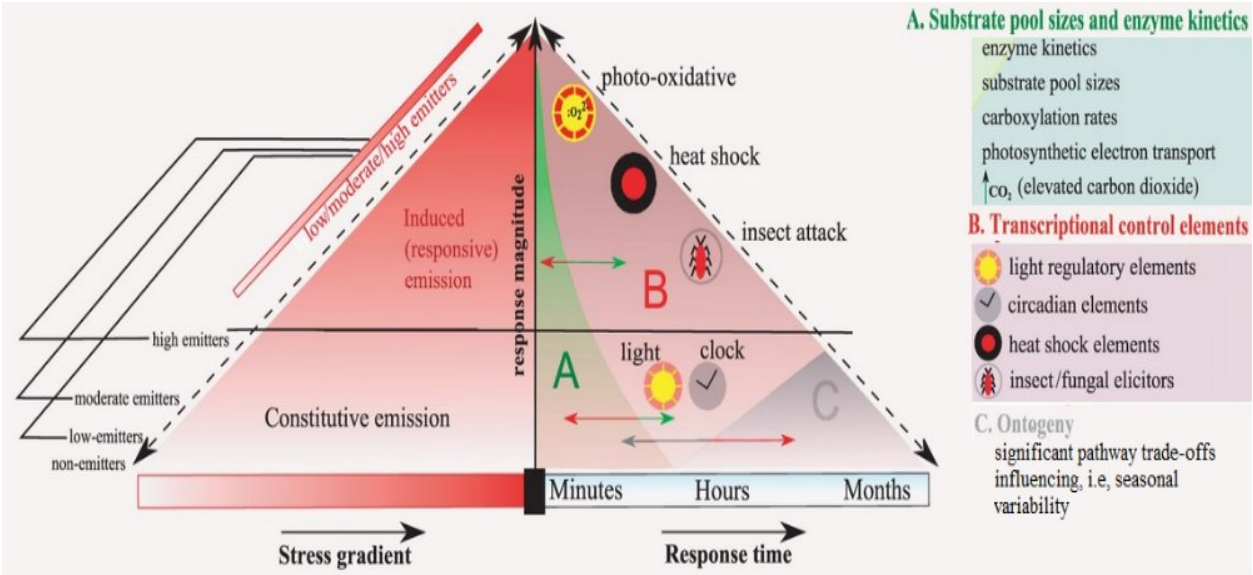

Figure 2.4. Conceptual diagram of constitutive and inducible BVOC emissions in terms of plant species and biochemical factors at multi-response timescales (Harrison et al., 2013a).

There is a fundamental difference between the short-term biological and environmental drivers (e.g., herbivore attacks, mechanical damage, light, temperature, CO_2 concentration, humidity, and extreme weather events) of instantaneous PBVOC emission rates and the long-term biological drivers (e.g., species composition, soil fertility, and foliar biomass) (Niinemets et al., 2010). On short-term scales, herbivore attacks and mechanical damage are the main biological drivers. Generally, ecosystem BVOC emissions will periodically increase because of insect outbreaks associated with climate change (Rinnan et al., 2013). Infested trees emit new VOCs, but the composition and quantities are related to the plant species. For example, a study by Staudt and Lhoutellier (2007) found that infested *Quercus ilex L.* released new PBVOCs (primarily SQTs, a homoterpene and an MT alcohol), accounting for 16% of the total. However, Amin et al. (2013) found that infested spruce trees induced a nine-fold increase in the total PBVOC emissions, with

these emissions dominated by 3-carene, β-pinene, and α-pinene. Similarly, other studies have noted that mechanical damage, such as cutting of vegetation, will increase instantaneous BVOC emissions (mainly C_8 compounds and SQTs) up to 20-fold, with these emissions dominated by plant oil emissions (in the case of plants with stored oils) and leaf wound defence emissions (in the case of other plants) (Kim et al., 2011; Rinnan et al., 2013).

At long-term scales, soil fertility, such as nitrogen and phosphorus fertilization, is an important factor affecting PBVOC emissions due to the changes in leaf photosynthetic capacity and foliar biomass. In general, higher isoprene and isoprenoid emissions are stimulated by higher nitrogen concentrations and lower phosphorus concentrations in the soil (Blanch et al., 2007; Ormeno et al., 2009). However, MT and monoterpenoid emissions are inhibited by nitrogen fertilization, because the rising nitrogen fertilizer causes an increase in photosynthetic products for plant growth and a decrease in non-structural carbohydrates for MT synthesis (Bryant et al., 1983; Muzika et al., 1989). Additionally, long-term PBVOC emissions are affected by anthropogenic land-use changes (i.e., tropical deforestation, European afforestation, and plant selection) and natural vegetation alteration (i.e., forest wildfires). Tropical deforestation has been shown to significantly decrease isoprene emission by 29% and increase MeOH emission by 22% at global scales. European afforestation, meanwhile, has been found to have increased PBVOC emissions by 54% in Europe but to have had little effect on global PBVOC emissions (Lathiere et al., 2006; Rosenkranz et al., 2015). Guo et al. (2013) showed that PBVOC emissions in low-latitude subtropical Ningbo, China, could be reduced by planting low-emitting trees in urban areas and converting bamboo forests to broad-leaved forests in rural areas. Conversion of slow-growing evergreens (e.g., *E. hermaphroditum*) to deciduous shrubs (e.g., *Betula and Salix*), meanwhile, may increase emissions

of PBVOCs such as isoprene, MTs, and non-isoprenoids in the Arctic (Vedel-Petersen et al., 2015). Zhang-Turpeinen et al. (2020a) have noted that PBVOC emissions will also strongly decrease due to forest wildfires in boreal areas resulting from climate warming, though they may be expected to recover from the forest floor within about 20 years after a wildfire. In general, global decreasing isoprene emission largely results from anthropogenic land-use changes, such as the conversion of forests in rural areas to croplands, pastures and urban areas, while global MT emissions primarily decrease due to changes in natural vegetation composition (Hantson et al., 2017; Tai et al., 2013; Wiedinmyer et al., 2006).

2.3.2. Temperature-driven PBVOC emissions under extreme conditions

From the environmental perspective, climate and global changes, including warming, drought, elevated CO_2, O_3, and UV irradiation, will alter PBVOC emissions depending on the doses and timing of environmental factors, as well as the affected PBVOC compositions (Penuelas and Staudt, 2010). Stored volatiles (MTs, acetaldehyde, green leaf volatiles, MeOH, and ethanol) are emitted when cellular membranes or cell walls of the storage pools become seriously damaged at temperatures >45 °C (Guidolotti et al., 2019). Similarly, plants such as *Thymus vulgaris*, *Lavandula stoechas*, and *Cistus albidus* have been found to emit large amounts of terpenoids, e.g., thymol, l-fenchone, and 3-hexen-1-ol at elevated temperatures in the range of 70 ℃ to 180 ℃ (Courty et al., 2014). This may be attributable to the competition among compounds with a similar function for substrates and enzymes, such as a trade-off between isoprene and stored volatiles of the Methylerythritol 4-phosphate (MEP) pathway at very high temperatures (>45 °C) (Guidolotti et al., 2019). Interestingly, the emissions of volatile isoprenoids and MTs in the sun leaves may also decrease with the synthesis of more photo-protective carotenoids because of competition

among the same biochemical precursors (Simpraga et al., 2013). Thus, it requires identifying the response of PBVOC emissions to high temperatures.

In the long term, temperature, resulting in changes in vegetation coverage and species composition, is also the primary driver of seasonal and inter-annual changes in PBVOC emissions. This is especially true of subarctic and Arctic areas, which are seeing an increase in air temperatures at twice the global mean rate and a corresponding increase in plant biomass and change in vegetation composition (Huang et al., 2015b). For example, an air temperature increase of 1.9–2.5°C will result in a doubling of emissions of MTs and SQTs from a wet subarctic tundra heath (Faubert et al., 2010). In this regard, a study by Kellomaki et al. (2001) projected that the emissions of MTs and isoprene over the whole of Finland will increase by 17% and 60%, respectively, due to the increase of forest resources with elevated temperature (+4 °C) and precipitation (+10%) by the year 2100. However, the emissions from *Empetrum hermaphroditum*, *Cassiope tetragona*, *Betula nana*, and *Salix arctica* in the subarctic and high Arctic are only slightly affected by elevated temperature in long-term field experiments because the significant changes in leaf anatomy of these species in response to the elevated temperature appear to differ from those of low-latitude species (Schollert et al., 2015). Given this, more observations of high-latitude species should be conducted to improve the modeling in terms of evaluating the temperature and light-dependency of PBVOC emissions.

2.3.3. Drought-driven PBVOC emissions at different temporal scales

Drought, generally represented by low precipitation and soil moisture is a major environmental factor constraining the performance and survival of plants and the production and emission of

PBVOCs. The drought effects on PBVOC emissions, effects that are closely related to plant photosynthesis, are controversial, with some researchers concluding that drought causes a decrease in PBVOC emissions, while others suggest that PBVOC emissions are unaffected or even increased by drought. Niinemets (2010) has asserted that, in general, the short-term mild drought stress will cause a significant increase in isoprenoid emissions but a slightly negative effect on terpenoid emissions. Acute drought stress, though, may cause a sudden burst in non-MT emission because of certain stress-related green leaf volatiles (GLVs) (Simpraga et al., 2011). Others have noted that a severe drought or prolonged moderate drought will result in significant reductions in isoprene and MT emissions (Grote et al., 2014; Jiang et al., 2018). For example, in a study by Ormeno et al. (2007), *Rosmarinus officinalis* showed nearly equal MT emissions with or without water stress, while a decrease in MT emissions from *Pinus halepensis* occurred when the severe drought stress inhibited primary metabolism because isoprenoid formation depended on metabolites primarily formed by photosynthesis. Another study observed that the summer drought stress in a holm oak forest caused a strong and repeated inhibition of PBVOC emissions, with a negative effect on isoprene emission (−23%) but a slight positive effect on MT emissions. This is presumably because of stomatal closure and internal CO_2 reduction resulting in decreased leaf carbon availability and photosynthetic rate (Feng et al., 2019; Lavoir et al., 2009). Furthermore, the response and adaptability of terpenoid emissions to drought stress have been found to vary among terpenoid species, showing inhibited MT emission but unaffected or enhanced emissions of α-pinene, camphene, and manoyl oxide (Haberstroh et al., 2018). Under moderate and severe stress conditions, the emissions of phenols, flavonoids, and oxygenated MTs (e.g., Camphor) have been shown to increase while SQTs (e.g., Germacrene D) decrease (Caser et al., 2018). Although the effects of soil moisture or drought stress on isoprene emission have been considered in

modeling, the response and adaptability of different plant species and PBVOC species to various drought stress scenarios should be considered in further laboratory and field experiments.

2.4. Emerging Microplastic Pollution from Mulching Films Applied in Cropping Systems

2.4.1. Application of biodegradable mulching films in cropping systems

Plastic film mulching is an effective agronomical practice to enhance crop production because it can conserve soil and water, regulate soil temperature, and prevent weeds (Cai et al., 2020; Kader et al., 2017; Wang et al., 2022a). Non-biodegradable mulches, such as polyethylene (PE), are usually required to be removed after use. Over the past decades, biodegradable mulches (BMs) have been regarded as an alternative mulch material to replace traditional non-degradable mulching to mitigate the environmental and disposal problems caused by plastic residues (Miles et al., 2017). BMs are generally composed of polysaccharides such as starch, cellulose, chitosan, chitin, and polyesters (e.g., polybutylene adipate terephthalate (PBAT), polyhydroxyalkanoate (PHAs), and polylactide (PLA)). Different countries have various regulations regarding the use of BMs in organic agriculture. According to the European Standard EN-17033, issued by the European Committee for Standardization in 2018, BMs are allowed in certified organic agriculture without a biobased requirement across the European Union (EN-17033, 2018). In the United States and Canada, BMs for organic food are required to be 100% derived from bio-based sources rather than fossil resources or genetically engineered sources (CAN/CGSB-32.311, 2020; OMRI, 2015). Most commercially available BMs contain certain fossil fuel-based ingredients or additives, which limits their use in organic agriculture. For example, BioAgri is one of the BMs that has been widely used worldwide for many years. Its main composition is PBAT, which is a biobased polymer derived from petroleum sources. Since 2015, BioAgri has no longer been regarded as an allowable

input to certified organic farming in Canada (CAN/CGSB-32.311, 2015). Notably, organic farmers are hoping that organic certification bodies strike a balance between idealistic organic movements and realistic market standards in organic agriculture (Bandopadhyay et al., 2018). The main concerns include whether the biodegradation capacity of BMs will be affected by the ingredients derived from fossil sources and whether fossil fuel-based BMs have negative environmental impacts.

2.4.2. Fragmentation of different plastic materials under different weathering processes

After exposure to the soil, the further fragmentation from mulches to macroplastics (MaPs) and then MPs elevates the mobility of MPs in the soil, aquatic environment, and atmosphere (Cai et al., 2017; 2019b; Wang et al., 2021c). The size distribution of MPs in different environments can be described by a conditional fragmentation model (Wang et al., 2021c):

$$F(x) = \left(1 - e^{-\lambda x^{\alpha}}\right)(0 \leq x \leq 5) \tag{2.5}$$

where x is MP size (mm); $F(x)$ is the simulated cumulative distribution function (CDF) of microparticles (or nanoparticles); λ is the range parameter ($mm^{-\alpha}$) that depicts the relative location of $F(x)$, decided by the size range of MPs; and α is the fragmentation parameter (dimensionless) that describes the shape of $F(x)$, representing the fragmentation process with a focus on debris stability. Notably, a higher value of α (>1) means that larger debris has a higher probability of weathering and downsizing than smaller ones. A lower value of α (<1) indicates that smaller debris has a higher probability of downsizing than larger ones. If $\alpha = 1$, MP size has no significant effect on the subsequent fragmentation process.

The modeling parameters (α and λ) for MPs separated from different natural sources were summarized in previous studies (Wang et al., 2021c). Some results with previous findings from artificial weathering processes (Cai et al., 2023; Wang et al., 2021d; Wang et al., 2022c) were calculated and shown in Figure 2.5 and Table 2.1. In Figure 2.5 (a), a higher α indicated stable MPs which meant these MPs had a stable size distribution pattern, whereas a higher λ suggested smaller-size MPs. Larger particles are generally susceptible to fragmentation at the low level of α and λ. With the increase of λ and α, the large particles experienced fragmentation and downsizing, shifting to smaller but stable ones. A proportion of MPs from natural sources (NMPs) and artificial weathering processes (AMPs) were distributed in the range of λ [1, 10] and α [0.5, 1], which suggested that the downsizing of larger MPs would be suppressed compared with smaller ones. Therefore, the small MPs and NPs migrated more easily than the large ones. For NMPs with a certain value of $\alpha > 1$, larger α indicated that the mobility of larger NMPs tended to inhibit in natural environments. For AMPs with a certain value of $\alpha > 1$, larger λ suggested that the sizes of AMPs shifted to smaller ones. Moreover, the size distribution of AMPs was affected by plastic materials and weathering processes. Regarding different materials (Figure 2.5 (c-d)), the MP median size followed the order: Mask > BioAgri > WGP > Glove, whereas the NP median size followed the order: PBAT > LDPE > WGP ≈ BioAgri. During the formation of MPs and NPs in ultrapure water after UV irradiation, the high-intensity weathered MPs (HMPs) had relatively higher values of α (>1), whereas the high-intensity weathered NPs (HNPs) had relatively lower values of α (<1), compared with the low-intensity weathered ones. This suggested that HMPs were more stable with downsizing accelerated by UV irradiation, whereas HNPs were still affected by sequent downsizing caused by the decrease in pH (Pace et al., 2012). Overall, artificial processes,

such as grinding, oxidation, UV irradiation, as well as wave and sand friction, can accelerate the fragmentation of MPs.

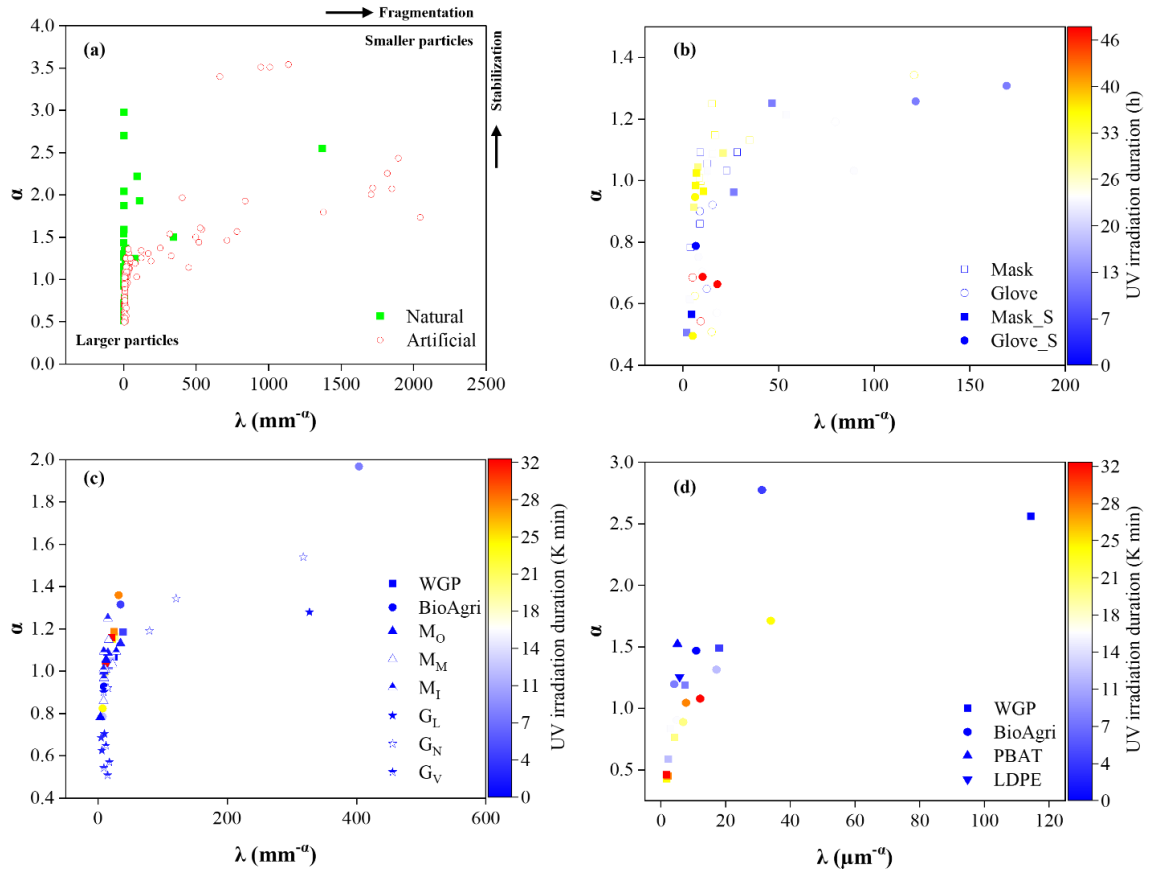

Figure 2.5. The fragmentation of different plastic materials under different weathering processes. MP formation in (a) natural and artificial weathering processes; (b) UV irradiation as well as wave and sand friction; (c) ultrapure water after UV irradiation. NP formation in (d) ultrapure water after UV irradiation. LDPE: low-density polyethylene; WGP: Weedguardplus; Mask_S: mask after wave and sand friction; Glove_S: glove after wave and sand friction; M_O: outer layer of the mask; M_M: middle layer of the mask; M_I: inner layer of the mask; G_L: latex glove; G_N: nitrile glove; G_V: vinyl glove.

Table 2.1. Particle size parameters of the conditional fragmentation model describing the MP and NP formation after various artificial weathering processes.

Weathering processes	**Materials**	**D50 (µm)**	**D90 (µm)**	**Range parameter λ ($mm^{-\alpha}$) ***	**Fragmentation parameter α**	**Adjusted R^2**	***p***	**Reference**
MP formation after mechanical milling through nominal sieve fraction	PBAT	45.8–522.0	48.2–587.9	>370.0	7.60–13.73	0.777–0.999	<0.001	(Astner et al., 2019)
	LDPE	43.9–586.2	46.1–661.2	>155.2	7.27–15.02	0.750–0.999	<0.001	(Astner et al., 2019)
MP formation at different discharge plasma treatment times at different oxidizing intensities	PVC	139.9–145.7	196.3–201.3	945.7–1135.9	3.51–3.54	>0.99	<0.001	(Zhou et al., 2020)
MP formation in different solutions after different sunlight irradiation durations	PS	50.4–83.0	83.1–102.6	>181435.9	4.00–4.89	>0.98	<0.001	(Zhu et al., 2020b)
MP formation after different heat-activated $K_2S_2O_8$ treatment times	PS	9.5–28.9	22.8–47.5	519.1–7782.5	1.44–2.64	>0.99	<0.001	(Liu et al., 2019)
	PE	10.5–33.3	12.7–59.0	251.2–3296.1	1.14–2.53	>0.99	<0.001	(Liu et al., 2019)
MP formation after different Fenton treatment times	PS	14.1–42.4	31.4–62.5	527.6–33094.3	1.61–3.41	>0.99	<0.001	(Liu et al., 2019)
	PE	11.0–39.3	25.1–60.6	188.3–6686.7	1.22–2.64	>0.99	<0.001	(Liu et al., 2019)
MP formation in ultrapure water after	Mask	20.9–115.8	62.6–439.5	3.9–159.7	0.78–1.43	0.898–0.998	<0.001	(Wang et al., 2021d)

different UV irradiation durations	Glove	1.9–72.5	10.5–285.3	5.0–327.2	0.5–3.0	0.972–0.997	<0.001	(Wang et al., 2022c)
MP formation in ultrapure water and sand after different	Mask	16.6–206.3	63.3–458.4	2.0–983.2	0.51–2.03	0.817–0.994	<0.001	(Wang et al., 2021d)
UV irradiation durations	Glove	5.8–105.3	11.4–375.7	5.1–994.3	0.5–2.9	0.872–0.999	<0.001	(Wang et al., 2022c)
MP formation in ultrapure water after	WGP	28.9–46.5	121.1–199.5	17.6–25.7	1.02–1.19	>0.99	<0.001	(Cai et al., 2023)
different UV irradiation durations	BioAgri	36.4–60.0	152.2–284.2	7.3–403.8	0.79–1.97	>0.99	<0.001	(Cai et al., 2023)
NP formation through high-performance wet	PBAT	0.288	0.569	5.10	1.52	>0.99	<0.001	(Astner et al., 2019)
grinding using 106 μm MP	LDPE	0.196	0.470	5.74	1.26	>0.99	<0.001	(Astner et al., 2019)
NP formation in ultrapure water after	WGP	0.108–0.182	0.275–0.661	1.8–18.1	0.43–1.49	>0.96	<0.001	(Cai et al., 2023)
different UV irradiation durations	BioAgri	0.089–0.242	0.170–0.559	4.1–34.0	0.89–2.78	>0.99	<0.001	(Cai et al., 2023)

PVC: polyvinylchloride; PS: polystyrene. D50 (d50) and D90 (d90) mean that 50% and 90% of the total particles were smaller than the corresponding size in the CDF of MPs (NPs), respectively. * For NP, the unit of range parameter (λ) is $\mu m^{-\alpha}$.

2.4.3. Environmental risks of microplastic pollution in agroecosystems

Agricultural health and safety are facing some new challenges (Eryiğit and Engel, 2022; Yang et al., 2022a). Generally, soil contains various metal elements, such as Cu, Pb, Cr, Cd, Co, Zn, and Ni. It was found that the adsorption of metals (e.g., Cu, Pb, and Cd) by MPs was primarily driven through physical sorption and electrostatic interaction (Zou et al., 2020). In addition, the binding between heavy metals and the surface ligands of MP was related to the amount of oxygenated functional groups, which was probably affected by the MP-induced pH changes (Uchimiya et al., 2011). For example, carboxyl groups had a strong coordination affinity with metal ions such as Fe, Pb, and Cu (Uchimiya et al., 2011; Yue et al., 2022).

As shown in Figure 2.6, MP-derived DOM had lower mean values of $SUVA_{254}$ and $S_{275–295}$ compared with biomass-pyrogenic smoke, natural water, soil, and biochar, which meant that the MP-derived DOM had a larger molecular size and higher aromaticity than other media. Thus, MPs can be the carbon addition into the agricultural soils, which will change DOM composition, such as aromatic functional groups. This may result in excessive carbon input into the soil and carbon emission into the air (Cai et al., 2021a; Cai et al., 2021b; Liu et al., 2022a).

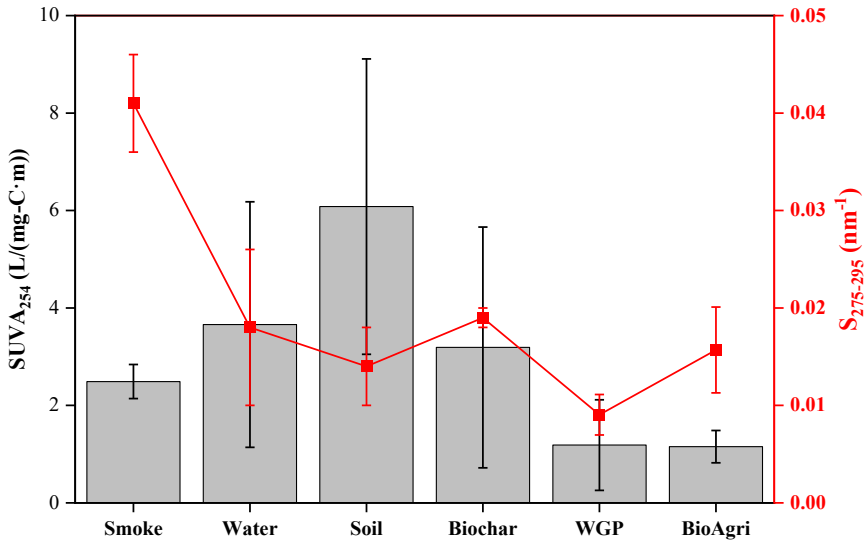

Figure 2.6. UV-vis indexes of DOM of biomass-pyrogenic smoke, natural water, soil, biochar, and BMPs. $S_{275–295}$ (nm^{-1}) is the slope of linear regression on the log-transformed spectra in the range of 275-295 nm; $SUVA_{254}$ [L/ (mg-C · m)] is the absorption coefficient at 254 nm divided by DOC concentration.

Figure 2.7 and Table 2.2 describe the transfer of MPs via the terrestrial food web in the agroecosystem. The fragmented MPs from natural environments have a larger range (range: 24.1–2930.0, median: 716.0, mean: 944.2) in particle size (D90 of each case, μm) than those from artificial processes (range: 10.5–458.4, median: 140.3, mean: 159.8), such as grinding, oxidation, and UV irradiation. The particle size (maximum size of each case, μm) of ingested MPs follows the order: humans (range: 0.05–5000, median: 90, mean: 1805) > animals (range: 0.04–3000, median: 150, mean: 929) > crops (range: 0.02–250, median: 3, mean: 3967). Notably, there is scarce direct evidence of MP ingestion by humans, so the findings of human feces and food sources are summarized. The biological effects of MPs on human health are investigated using in vitro studies on human-derived cell lines because in vivo studies of humans are scarce. Therefore,

human-ingested MPs showed a bimodal distribution in the range of 0.05–40 and 140–5000 μm. The size range of the fragmented MPs from natural and artificial processes has a large overlap with the ingested MPs by terrestrial organisms, indicating that a wide range of terrestrial organisms is exposed to the risk of fragmented MPs due to the high availability of ingestion via the terrestrial food web.

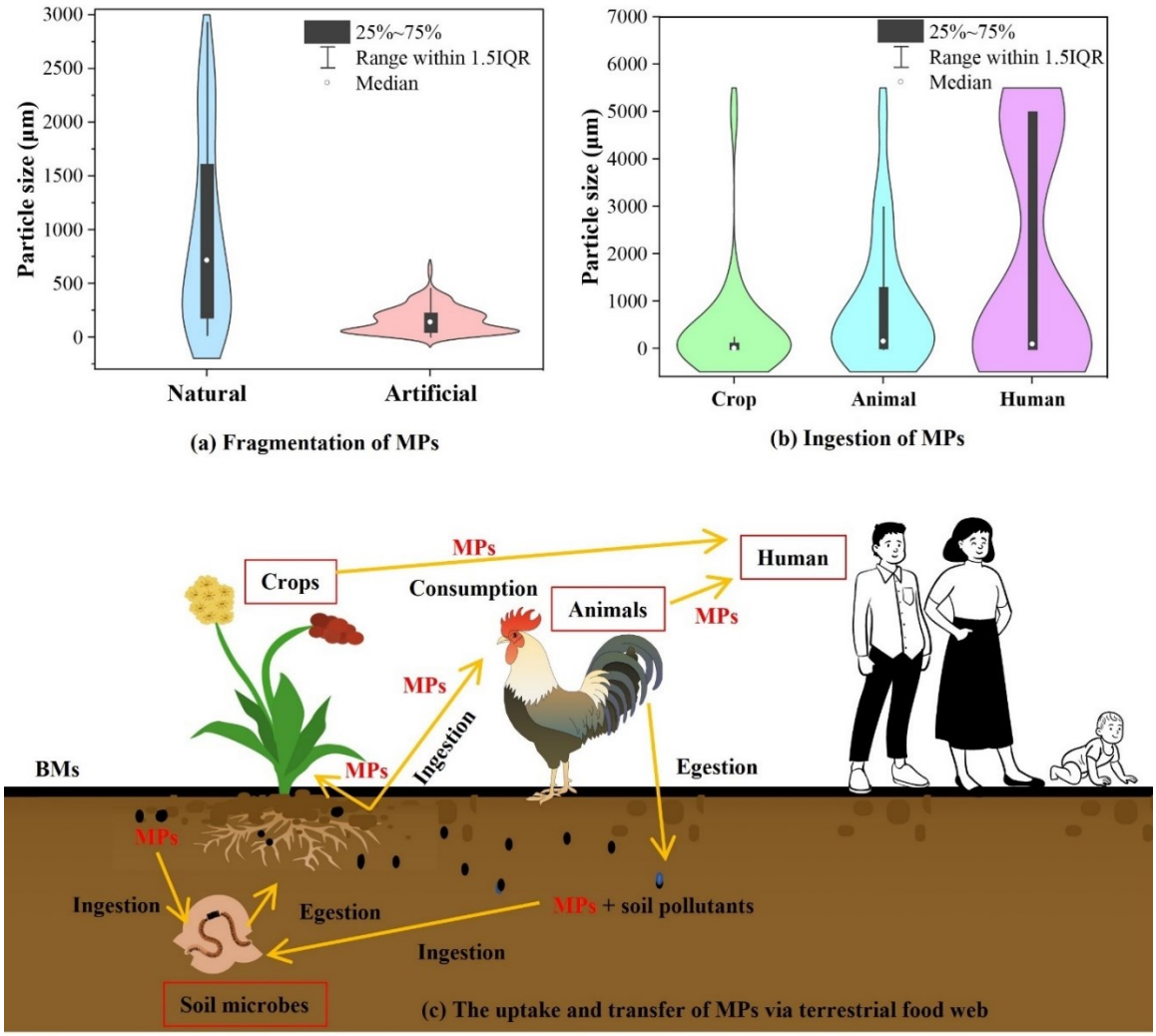

Figure 2.7. The transfer of MPs via terrestrial food web in the agroecosystem.

Table 2.2. The uptake and biological impacts of MPs and NPs in terrestrial biota at different trophic levels (Wang et al., 2022b).

Species	Plastics	Size (μm)	Concentration	Co-present contaminants	Biologic effects	Reference
Plant						
Rice (*Oryza sativa* L.)	PS	≤1	40 mg/L			(Liu et al., 2022b)
Rice (*Oryza sativa* L.)	PS	0.02	10–100 mg/L	/	Oxidative stress; Decrease in root length; alternations in root metabolism processes.	(Zhou et al., 2021)
Rice (*O. sativa* L.)	PS & PTFE	10	0.04–0.2 g/L	As (1.6–4 mg/L)	Decrease in plant biomass and photosynthesis; Reduced uptake of As; Oxidative stress.	(Dong et al., 2020b)
Maize (*Zea mays* L.)	PS-NH_2 & PS-COOH	0.02	2 μL of 1 mg/L PS solution per 0.3 cm^2 leaf surface			(Sun et al., 2021)
Maize (*Zea mays* L.)	PE	3	0.0125–100 mg/L	/	Decrease in biomass and transpiration.	(Urbina et al., 2020)
Mung bean (*Vigna radiata*)	PS	0.03	10–100 mg/kg			(Chae and An, 2020)
Broad bean (*Vicia faba*)	PS	0.1–5	10–100 mg/L	/	Decrease in root length, plant biomass, and cell proliferation; Oxidative stress; Genotoxicity.	(Jiang et al., 2019b)
Soybean (*Glycine* max L. *Merrill*)	PS	0.1–100	10 mg/kg	Phe (1 mg/kg)	Oxidative damage; Decrease in root activity; Genotoxicity; Reduced uptake of Phe.	(Xu et al., 2021)
Wheat (*Triticum aestivum* L.)	LDPE	<1000	1% (w/w in soil)	/	Decrease in plant growth and biomass.	(Qi et al., 2018)
Wheat (*Triticum aestivum* L.)	PE	200–250	0.5–8% (w/w in soil)	Phe (100 mg/kg)	Decrease in shoot height; Reduced uptake of Phe.	(Liu et al., 2021)

Wheat (*Triticum aestivum* L.) & lettuce (Lactuca sativa L.)	PS & PMMA	≤2	0.5–50 mg/L or 150–500 mg/kg			(Li et al., 2020a)
Lettuce (*Lactuca sativa* L.)	PS	0.1	0.1–1 mg/L			(Lian et al., 2021)
Lettuce (*Lactuca sativa* L.)	PE	10–500	0.1–10% (w/w in soil)	Cd (0.5–4.4 mg/kg)	Decrease in plant biomass; Increase in plant uptake of Cd	(Wang et al., 2021a)
Lettuce (*L. sativa* L.)	PE	–23	0.25–1 g/L	DBP (5 mg/L)	Decrease in root growth and activity; Damage in cell structure; Oxidative stress; Reduced uptake of DBP.	(Gao et al., 2021)
Carrot (*Daucus carota* L.)	PS	≤1	10–20 mg/L			(Dong et al., 2021)
Cucumber (*Cucumis sativus* L.)	PS	0.1–0.7	50 mg/L			(Li et al., 2020a)
Spring onion (*Allium fistulosum*)	PA, PS, HDPE, PP, & PET	<5000	0.2–2.0% (w/w in soil)	/	Polymer-dependent changes in plant total biomass, root traits, and leaf elemental composition.	(de Souza Machado et al., 2019)
Onion (*Allium cepa* L.)	PS	0.02–0.19	0.01–1.0 g/L	/	Oxidative stress; Cytological abnormalities; Genotoxicity.	(Giorgetti et al., 2020)
Thale cress (*Arabidopsis thaliana*)	PS-NH2 & PS-COOH	0.2	10–100 mg/L			(Sun et al., 2020)
Garden cress (*Lepidium sativum* L.)	PE, PP, & PVC	≤130	0.02% (w/w in soil)	/	Decrease in seed germination and plant biomass; Oxidative stress.	(Pignattelli et al., 2020)

Festuca brevipila, *Holcus lanatus*, *Calamagrostis epigejos*, *Achillea millefolium*, *Hieracium pilosella*, *Plantago lanceolata*, & *Potentilla argentea*	PET	1300	4 g/kg	/	Alterations in plant community structure; Decrease in community shoot-to-root ratio.	(Lozano and Rillig, 2020)
Animal						
Earthworm (*Lumbricus terrestris*)	PE	<150	7–60% (w/w in litter)	/	Ingestion and egestion of PE; Increase in mortality; Reduced growth rate.	(Huerta Lwanga et al., 2016)
Earthworm (*Metaphire californica*)	PVC	/	2 g/kg	As (40 mg/kg)	Decrease in bioaccumulation of total As; Alleviation of As toxicity to the gut microbiome.	(Wang et al., 2019a)
Earthworm (*Eisenia fetida* & *Metaphire guillelmi*)	PS	<2000	0.25% (w/w in soil)	HBCDDs (–40 μg/kg)	Ingestion of PS; Increased bioaccumulation of HBCDDs;	(Li et al., 2019)
Earthworm (*E. fetida*)	PE	30–100	0.1–10% (*w*/w in soil)	Ni2+ (40 mg/kg) & Cu2+ (100 mg/kg)	Increased bioaccumulation of metals; Oxidative stress; Alterations in gene expression.	(Li et al., 2021)
Earthworm (*E. fetida*)	LDPE & PS	<300	0.1–10% (w/w in soil)	PAHs (510–740 μg/kg) & PCBs (180–220 μg/kg)	Ingestion of LDPE and PS; Oxidative stress; Decreased bioaccumulation of PAHs and PCBs	(Wang et al., 2019b)
Worm (*E. crypticus*)	PS	0.05–0.1	1 g/kg in oats	Tetracycline (10 mg/kg)	Ingestion of PS; Increased bioaccumulation of tetracycline; Increase in the diversity and abundance of ARGs in gut	(Ma et al., 2020)

					microbiome; Gut microbiome dysbiosis.	
Worm (*Enchytraeus crypticus*)	PA	13–150	2–12% (w/w in soil)	/	Ingestion of PA; Reduced reproduction.	(Lahive et al., 2019)
Woodlice (*P. scaber*)	PET	10–3000	0.5% (w/w in soil)	Chlorpyrifos (0.2–2 mg/kg)	Decreased bioaccumulation of chlorpyrifos; Increase in total hemocyte count; Slight alterations in immune processes.	(Dolar et al., 2021)
Woodlice (*Porcellio scaber*)	PET	10–3000	0.02–1.5% (w/w in soil)	/	Ingestion of PET; Reductions in energy reserve and feeding activity.	(Selonen et al., 2020)
Collembolan (*Crypto pygus antarcticus*)	PS	0.1–100	/	/	Ingestion of PS.	(Bergami et al., 2020)
Nematode (Caenorhabditis elegans)	PS	1	1–100 μg/L	/	Ingestion of PS; Increase in ROS production; Intestinal damage.	(Yu et al., 2020)
Springtail (*Folsomia candida*)	PE	<500	0.1–1% (w/w in dry soil)	/	Avoidance behavior; Decrease in reproduction; Changes in the gut microbial community; Mortality.	(Ju et al., 2019)
Snail (*Achatina fulica*)	PET	1300	0.01–0.71 g/kg soil	/	Ingestion and egestion of PET; Reduced food intake and excretion; Decrease in total antioxidant capacity in the liver; Intestinal villi damage.	(Song et al., 2019c)
Silkworm (*Bombyx mori*)	PS	0.05–6	10 μg/L PS solution sprayed on mulberry leaves.	/	Accumulation of PS in gut tissue and lumen; Alterations in gene expression; Oxidative stress; Reduced immunity to pathogens.	(Muhammad et al., 2021)
Mosquito (*Culex pipiens*)	PS	2–15	50–200 particles/mL	/	Ingestion of PS; Ontogenic transference of PS; No impact on the growth or mortality.	(Al-Jaibachi et al., 2019)

Honey bees (*Apis mellifera L.*)	PS	25	0.5–10 mg/L	/	Ingestion of PS; Alterations in gene expression; Changes in the gut microbiome.	(Wang et al., 2021b)
Rat	PS	0.04	1–10 mg/kg body weight day	/	Uptake of PS; High accumulation of PS in the testis; Endocrine disruption; Tissue and cell impairment; Reproductive toxicity; Alterations in gene expression.	(Amereh et al., 2020)
Terrestrial birds	Man-made plastic	500–5000	10.6 ± 6.4 items/individual	/	Ingestion of man-made plastic.	(Zhao et al., 2016)
Chicken feces	LDPE	100–1000	129.8 ± 82.3 particles/g	/	Ingestion of LDPE; Reduced food consumption and the volume of the gizzards.	(Huerta Lwanga et al., 2017)
Human *						
Commercial bivalves	PE, PET, & PA	5–5000	2.1–10.5 items/g			(Li et al., 2015a)
Canned sardines & sprats	PP, PET, PE, & PVC	200–3800	A total of 6 items in 4 out of 16 brands.			(Karami et al., 2018)
Chicken gizzard	/	100–5000	10.2 ± 13.8 items/individual			(Huerta Lwanga et al., 2017)
Animal medicinal materials	PET, rayon, PE, nylon, PP, PVC	10–5000	1.80–7.80 items/individual or 1.59–43.56 items/g (dry weight)	/	/	(Lu et al., 2020)

Carrot, lettuce, broccoli, potato, apple, & pear	/	1.5–2.5	26,000–310,000 items/g			(Conti et al., 2020)
Take-out food	Mainly, PS, PE, PET, & PP	40–5000	3–29 items/container			(Du et al., 2020)
Edible salts	Mainly, PE, PP, & PET	100–5000	Sea salt: 0–13,629 items/kg; Rock salt: 0–148 items/kg; Lake salt: 28–462 items/kg			(Kim et al., 2018)
Honey	/	>40	Fiber: 10–336 items/kg; Fragment: 2–82 items/kg			(Liebezeit and Liebezeit, 2015)
Beer and tap water	/	100–5000	0–14.3 items/L & 0–61 items/L			(Kosuth et al., 2018)
Milk	PES & PSU	100–5000	3–11 items/L			(Kutralam-Muniasamy et al., 2020)
Human feces	/	50–500	2 items/g	/	/	(Schwabl et al., 2019)
Intestinal epithelial cells (Caco-2)	PS	0.05–0.1	25–200 μg/mL	/	Cellular internalization of PS; Slight cytotoxic/genotoxic effects.	(Cortés et al., 2020)
Intestinal epithelial cells (Caco-2)	PE	30–140	100–1000 μg/mL	TBBPA (10–50 mg/L)	Decrease in cell viability; Increased ROS generation; Reduction in mitochondrial membrane potential; Increased release of lactate dehydrogenase;	(Huang et al., 2021)

					Joint toxicity of PE with TBBPA to a certain degree.	
Intestinal epithelial cells (Caco-2)	PS	0.3–6	20–120 μg/mL	BPA (20–120 ng/mg)	Cellular internalization of PS; Reduced cell viability; Increase in intracellular ROS production; Mitochondrial depolarization; Synergistic toxicity of PS with BPA.	(Wang et al., 2020b)
Colorectal cells (Caco-2 & HT-29-MTX) & lymphoblast cells (Raji-B)	PS	0.05–0.1	1–200 μg/mL	/	Cellular internalization of PS; No significant effects on cell viability, membrane integrity, ROS production, DNA, and gene expression.	(Domenech et al., 2020)
Lung epithelial cells (BEAS-2B)	PS	1.7–2.2	1–1000 μg/cm^2	/	Reduction in cell viability; Alterations in cell morphology; Increased ROS production; Cellular inflammatory response.	(Dong et al., 2020a)
Alveolar epithelial cells (A549)	PS	0.025–0.07	1.1–25 μg/mL	/	Cellular internalization of PS; Decrease in cell viability under high exposure concentrations; Cellular inflammatory response; Disturbance in cell cycle and apoptosis; Alterations in gene and protein expressions.	(Xu et al., 2019)
Alveolar epithelial cells (A549)	PS	0.1	10–1000 μg/mL	DBP & DEHP (5 μg/mL)	Cellular internalization of PS; Increase in cytotoxicity of DBP and DEHP under higher concentrations of PS; Decreased bioavailability of DBP and DEHP.	(Shi et al., 2021a)

Hepatic cells (HepG2)	PS, PS-COOH, & PS-NH2	0.05	10–100 µg/mL	/	Cellular internalization of NPs; Decrease in cell viability; Cellular oxidative stress.	(He et al., 2020)
Cerebral cells (T98G) & cervical epithelial cells (HeLa)	PE & PS	PE: 0.1–16; PS: 0.04–10	0.01–10 µg/mL	/	No significant effects on cell viability; Cellular generation of ROS in PE-treated T98G cells and PS treatments.	(Schirinzi et al., 2017)
Peripheral blood mononuclear cells (PBMCs), mast cells (HMC-1), & dermal fibroblasts (HDFs)	PP	20–200	10–1000 µg/mL	/	No cytotoxicity for PP of >25 µm; Decreased cell viability and increased ROS production under exposure to 1000 µg/mL of –20 µm PP.	(Hwang et al., 2019)

Plastics: HDPE: high-density polyethylene; PA: polyamide; PAHs: polycyclic aromatic hydrocarbons; PES: polyethersulfone; PET: polyester; PMMA: polymethylmethacrylate; PP: polypropylene; PSU: polysulfone; PTFE: polytetrafluoroethylene.

Contaminants: As: arsenic; Cd: cadmium; DBP: dibutyl phthalate; Phe: phenanthrene; HBCDDs: hexabromocyclododecanes; Ni: nickel; Cu: copper; PCBs: polychlorinated biphenyls; TBBPA: tetrabromobisphenol A; BPA: bisphenol A; DBP: dibutyl phthalate; DEHP: di-(2-ethylhexyl) phthalate.

Indicators: ARGs: antibiotic resistance genes; ROS: reactive oxygen species.

* There is scarce direct evidence of MP ingestion by humans, so the findings of human feces and food sources are summarized. The biological effects of MPs on human health are investigated using in vitro studies on human-derived cell lines because in vivo studies of humans are scarce.

CHAPTER 3. SCIENTOMETRIC ANALYSIS OF BVOCS EMITTED FROM TERRESTRIAL SYSTEMS

3.1. Background

The Paris Agreement and SDGs are urging us to shift from fossil fuels to sustainable and renewable energy resources for the goal of carbon neutrality and emission reduction. Bioenergy is considered one of the promising alternatives because carbon sequestration and energy storage can be achieved through biological carbon capture and storage in biomass during solar-driven photosynthesis (Gaurav et al., 2017). Biofuel production primarily depends on CO_2 capture and solar energy storage in terrestrial plants such as forests and energy crops, followed by carbon storage in litterfalls, residuals, and soils (Monforti et al., 2015). There is also a proportion of carbon loss that is released back to the atmosphere in the form of CO_2 and VOCs during processes such as photosynthesis, respiration, and biomass burning, causing a controversy over the role of bioenergy in climate change mitigation (Favero et al., 2020). Besides GHGs, these volatiles should be considered in climate research due to their high reactivity and large bio-sources (Covey et al., 2021). As the precursors to CO_2, O_3, PM, and SOA in many atmospheric reactions, VOCs are closely related to atmospheric chemistry and climate effects (Fares et al., 2012; Tani and Mochizuk, 2021). Understanding their emissions could help better achieve SDG13 which is to "take urgent action to combat climate change and its impact".

BVOCs account for nearly 90% of total VOC emissions (Guenther et al., 2006). Studies related to BVOC emissions have ranged in terms of both spatial scale (e.g., leaf, individual, canopy, regional, national, global) and temporal scale (e.g., diurnal, phenological, seasonal, and annual). Based on measurements and simulations of BVOC emission rates and fluxes performed worldwide,

researchers have addressed diverse topics in the area of BVOC emissions, focusing particularly on isoprene and MTs, including biosynthesis mechanism, ecophysiological functions, emission inventories, and responses of BVOC emission to plant or microbe physiology and environmental factors (e.g., temperature, light, drought, etc.) (Li et al., 2017; Tang et al., 2019b). Although there have been efforts focusing on the assessment of BVOC emissions of forests at different scales, studies on the emissions from crops, including biofuel crops, are limited. Most previous studies also have not distinguished the individual contribution of plants or soil microbes to BVOC emissions from an ecosystem. Consequently, BVOC emissions have been regarded in most of these studies as emissions of PBVOCs, especially from vegetation such as trees, mosses, and ferns. SBVOCs, consisting of PBVOCs released from shedding vegetative parts (e.g., leaves, branches, bark, and stems) and living roots, and MVOCs, produced in the microbial decomposition of litter and SOM, have rarely been included in the emission estimates of ecosystem-BVOCs.

Some efforts have been made to profile the literature on BVOC emissions in critical reviews. For example, Harrison et al. (2013a) reviewed volatile isoprenoid emissions from cell physiology to atmospheric remote sensing; Holopainen and Gershenzon (2010) outlined the main factors stressing PBVOC emissions; Calfapietra et al. (2013) summarized BVOC emissions from urban trees and their interactions with ozone concentration; Lun et al. (2020) provided a comprehensive review about BVOC emissions in Asia and their impacts on air quality and human health. SBVOC emissions and drivers for its sink and emission processes have been compiled in recent works (Peñuelas et al., 2014; Tang et al., 2019b). However, many previous reviews have been qualitative and subjective, largely based on personal knowledge and understanding, leading to a lack of overall structure in their characterizations of the intellectual landscape in this field. Although some

literature reviews on PBVOCs characterized the global scientific production and distribution through bibliometric analysis (Cheng et al., 2019; Li et al., 2017), few studies have analyzed in depth the body of research on BVOC emissions from plants and soils using advanced scientific tools such as burst detection. Consequently, it is difficult to grasp the features and emerging trends in existing research, identify consensus on salient topics, or anticipate future research directions.

To bridge the above research gaps, there is an urgent need to conduct an in-depth scientometric study on BVOC emissions, encompassing SBVOCs, to provide a systematic and comprehensive review of the emissions and drivers of BVOCs and their contributions to air pollutants and GHGs. In the present study, scientometric characteristics and relationships among journal papers about BVOC emissions from the WoSCC spanning the period between 1991 and 2020 were analyzed and visualized using CiteSpace and Carrot^2 (Chen, 2006). A network of keywords was created through co-word analysis to identify research hotspots during different time intervals and to visualize links between each selected keyword in CiteSpace. Besides, the evolution of popular research hotspots over time across fields was visualized through keyword clustering to clarify knowledge domains and emerging trends in CiteSpace and Carrot^2. New research trends, mutations over time, and promising avenues of future research in this field were identified based on the burst detection of keywords or references in CiteSpace. This study expanded the definition of BVOCs, including PBVOCs and SBVOCs according to their producers, and analyzed the research evolution of BVOC emissions using scientometric analysis tools. Insights gained from these findings can be used to mitigate the negative impact of BVOC emissions and achieve sustainable environmental management for human-dominated terrestrial ecosystems.

3.2. Methodology

3.2.1. Data collection and processing

The framework of scientometric analysis is shown in Figure 3.1.

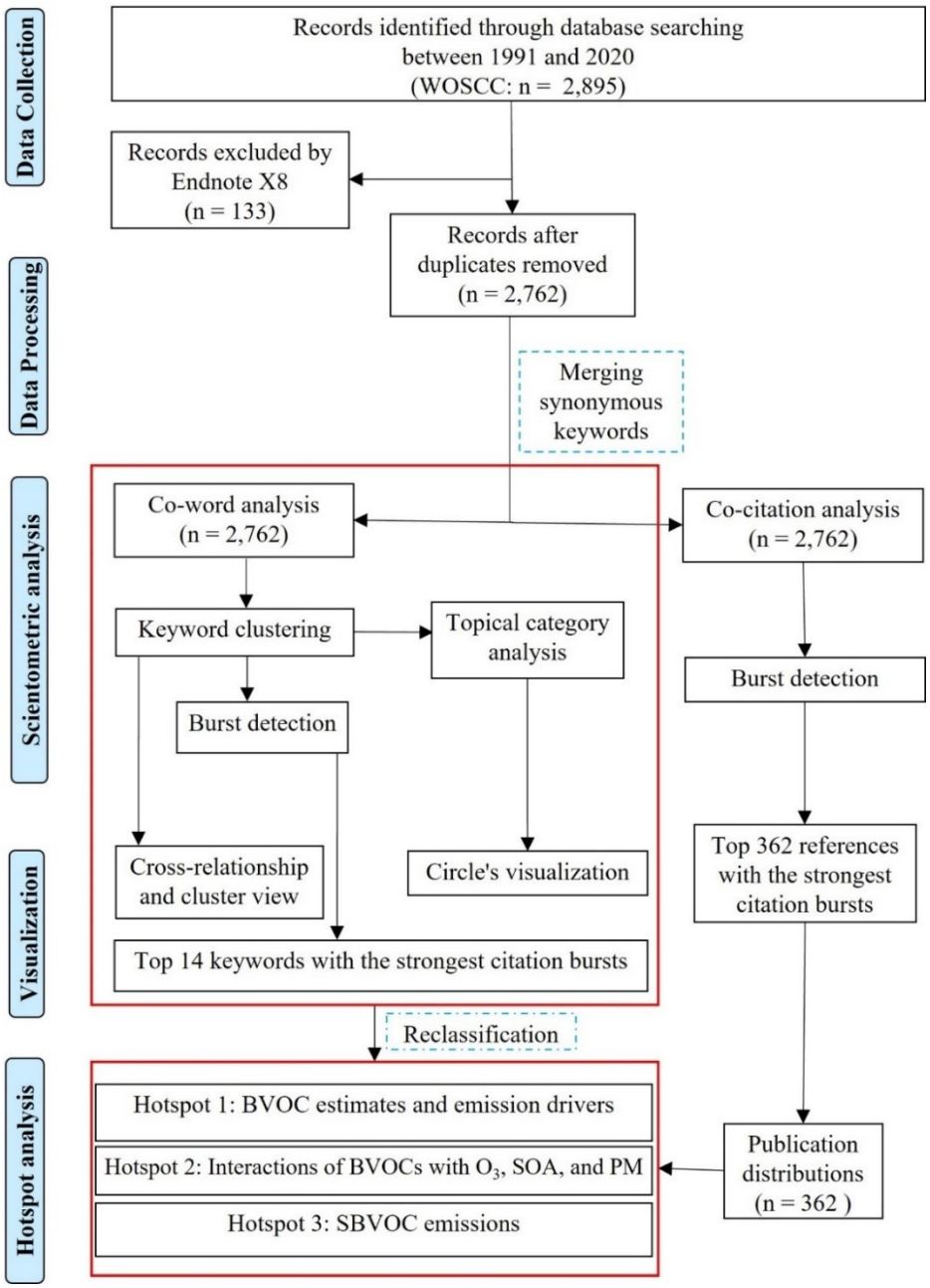

Figure 3.1. The framework of scientometric analysis.

Various databases might yield different results, but the Web of Science (WoS) database is regarded as one of the most common and reliable databases in most fields (Ouyang et al., 2018). Notably, abstracts were not included in documents before 1991, so only those published between 1991 and 2020 were systematically reviewed and discussed based on the frequency of literature keywords over the past three decades (Li et al., 2017). Thus, studies were identified through a comprehensive search on WoSCC (Thomson Reuters, NY, USA) spanning the period from January 1991 to March 2020. The search string was TS (Topic Search) = (T1) AND (T2) = (K_{B1} OR K_{B2} OR …) AND (K_{E1} OR K_{E2} OR …). Topic 1 (T1) represented BVOC-related keywords (K_{Bi}), including "biogenic volatile*", “BVOC*”, "biogenic VOC*", "microbial VOC*", "microbial volatile*", "biogenic emission*", "biogenic isopren*", "biogenic *terpen*", “MVOC*”, "biogenic NMVOC*", “BOVOC*”, "biogenic oxygenated volatile organic compound*", "non-methane volatile organic compound*". Topic 2 (T2) represented emission-related keywords (K_{Ei}), including “release*”, “emit*”, “emission*”, “flux*”, “exchange*”, “flow*”, “discharge*”, “uptake*”, “suspen*”, “deposit*”, “estimat*”, “model*”, “simulat*”, “measure*”, “observ*”. “AND” was used to link keywords between two topics, while “OR” was used to link keywords of T1 and T2, respectively. This search yielded 2,895 articles and reviews published in 72 countries or regions between 1991 and 2020, with “Full Record and Cite References” in “Plain text” format for further scientometric analysis. The "Full Record" means the detailed bibliographic information of a particular research paper, mainly including author names, article titles, publication years, keywords, etc. The "Cite References" means the list of references cited within that paper. Duplicate papers were removed using Endnote X8, resulting in a revised total of 2,762 papers. KeyWords Plus terms must appear more than once in the bibliography and are ordered from multi-word phrases to single terms, while author keywords are included in records of articles from 1991 forward. Thus, KeyWords Plus terms

were deleted and only author keywords were included in this study. Synonymous keywords were merged, and synonyms used for this task were listed in Table 3.1.

Table 3.1. Synonyms list

Label	Replaced term
VOC	Volatile organic compounds, volatile organic compound
BVOC	Biogenic volatile organic compounds, biogenic volatile organic compound, biogenic voc, Biogenic vocs, biogenic volatile organic compounds(bvocs), biogenic volatile organic compounds (bvocs), biogenic volatile organic compound (bvoc), biogenic volatile organic compound(bvoc)
MVOCS	Microbial volatile organic compounds, microbial volatile organic compound, microbial vocs, microbial volatile organic compounds (mvocs), microbial volatile organic compounds(mvocs)
Sesquiterpene	Sesquiterpenes
SOA	Secondary organic aerosol, secondary organic aerosols
Aerosol	Aerosols
CO_2	Carbon dioxide
O_3	Ozone
$PM_{2.5}$	Fine particles
GC	Gas chromatography
SPME	Solid phase microextraction (spme), solid- phase microextraction (spme)
MEGAN	Model of emissions of gases and aerosols from nature (megan), model of emissions of gases and aerosols from nature
PTR-TOF-MS	Proton-transfer reaction time-of-flight mass spectrometer (ptr-tof-ms), proton-transfer reaction time-of-flight mass spectrometer
PTR-MS	Proton transfer reaction mass spectrometry (ptr-ms), proton-transfer-reaction mass spectrometry
PCA	Principal component analysis (pca), principal component analysis
SESI-MS	Secondary electrospray ionization mass spectrometry (sesi-ms), secondary electrospray ionization mass spectrometry

3.2.2. Scientometric analysis

In the present study, CiteSpace 5.6.R3 and Carrot[2] were used to analyze and visualize research trends of BVOC emissions. CiteSpace 5.6.R3 is a free scientometric tool for the visualization of co-citation and co-word networks. Co-word analysis burst detection of keywords or references and

keyword clustering was conducted to identify hot research topics and frontiers and to detect sudden changes and emerging trends over time. Given that keywords signify the core content of a paper, based on the occurrence frequency and publication year of keywords, the co-word analysis conducted by CiteSpace reflected emerging trends, tracked changes in research topics over time, and uncovered useful information for projecting future research directions (Fang et al., 2017). The frequency of and cross-relationships between hot keywords were identified in this study. Any sharp increases in interest in a given research field were detected according to burst terms extracted from the title, author keywords, and abstract of each paper through a burst detection algorithm (Xiao et al., 2017). The citation bursts of keywords or references were detected, respectively. The cluster analysis of keywords divided the author keywords extracted from the 2,762 papers into multiple clusters, with a high similarity among keywords in each cluster and a high dissimilarity between various clusters (Su et al., 2019). Diverse research subtopics in all selected papers were identified. "Circles visualization", created by Carrot[2], was used to extract keywords of significance for the topical category analysis of each cluster (Fang et al., 2020).

Notably, the parameter settings shown in Table 3.2 were set before conducting the above analysis. According to the CiteSpace manual (Chen, 2014), links and nodes are the cornerstones of visualization maps. A color spectrum shows the chronological occurrence of links and items, and a node indicates one keyword or reference. The node's size reflects the frequency of keyword occurrence or reference citation. In a node, concentric circles with various colors indicate articles in different time series, where orange and blue respectively denote the newest and oldest occurrence, and an outer purple ring indicates good centrality. Links between nodes describe their relationships of co-occurrence or co-citation, where its color denotes the first year to establish

relationships and the thickness shows the connection strength between two nodes (de Castilhos Ghisi et al., 2020; Fang et al., 2017). Additionally, the modularity and homogeneity of a network are represented by the module value and overall mean silhouette, respectively. In our study, the clusters were numbered in descending order of cluster size, i.e., ID #0 represented the largest cluster, and so on. Cluster labels were summarized from literature keywords with mutual information (MI). However, labels varied due to different clustering methods, including the term frequency and inversed document frequency (TF*IDF, also namely LSI), log-likelihood ratio (LLR), and MI, so the top three terms of different methods were identified to improve context interpretation.

Table 3.2. Parameter settings.

Settings	Value	Description
Publication Years	1991-2020	Divide the time zone into 1 year
Threshold	Top50	Selected the top 50 high-frequency nodes in each time zone
Pruning	No pruning	N. A
Type of keywords	Author keywords	Author keywords (DE)
Types of nodes	Keywords	N. A

3.3. Results and discussion

3.3.1. Overview of keywords for BVOC studies

Among the 2,762 documents from the period under study (1991–2020), 311 keywords on BVOC emissions with a total occurrence of 2,738 were found. Among them, 194 (62.4%) appeared twice each, 42 (13.5%) appeared over ten times each, while the large number of keywords used only once was not detected with this method. Previous scientometric studies conducted in this area

found that 62.4% to 81.0% appeared only once (Hu et al., 2010; Xie et al., 2008) and 10.0% to 12.8% appeared twice (Hu et al., 2010; Li et al., 2017). This prevalence of keywords appearing only once in the literature likely suggested a lack of research continuity and emphasis discrepancy among studies in this field (Chuang et al., 2007); as such, we focused on high-frequency keywords and the relationships between them. Table 3.3 lists the top 30 keywords with the highest frequency in 1991–2020. This period was divided into three 10-year intervals (1991–2000, 2001–2010, and 2011–2020) to ensure reasonable time spans for temporal analysis. Overall, the keyword frequency was found to increase over time, indicating that increasing attention has been paid to BVOC emissions. A network graph was created using CiteSpace based on keyword occurrences to reveal the relationships between these keywords. Figure 3.2 exhibits the cross-relationship between keywords.

Table 3.3. Top 30 keywords with the highest frequency in 1991–2020.

1991–2020		1991–2000		2001–2010		2011–2020	
K[a]	F[b]	K[a]	F[b]	K[a]	F[b]	K[a]	F[b]
BVOC	270	Biogenic emission	47	Isoprene	93	BVOC	184
Isoprene	222	Isoprene	41	Biogenic emission	81	VOC	109
Biogenic emission	194	Monoterpene	31	BVOC	77	Isoprene	88
VOC	205	VOC	24	Monoterpene	75	O_3	85
Monoterpene	182	O_3	13	VOC	72	Monoterpene	76
O_3	140	BVOC	9	O_3	42	Biogenic emission	66
SOA	62	Terpene	9	Sesquiterpene	22	SOA	50
Air quality	52	Emission	6	MVOC	14	Air quality	42
Climate change	48	Tropospheric ozone	6	Climate change	14	PM	40
Sesquiterpene	45	Biogenic hydrocarbon	5	Modeling	12	Source apportionment	35

Source apportionment	45	Hydrocarbon	4	SOA	12	Climate change	34
PM	43	NOx	4	Air quality	10	Air pollution	27
Emission	39	Nitric oxide	4	Emission	10	Emission	23
Air pollution	37	Temperature	4	Source apportionment	10	MVOC	21
MVOC	37	Seasonal variation	4	Terpene	10	Sesquiterpene	21
Emission inventory	31	Pinus pinea	3	Air pollution	8	Emission inventory	21
Terpene	26	Biomass burning	3	Emission inventory	8	Aerosol	19
Temperature	21	Quercus ilex	3	Seasonal variation	7	Temperature	15
Tropospheric ozone	21	Vegetation	3	Emission factor	6	Biomass burning	14
Aerosol	19	Relaxed Eddy Accumulation	3	Formaldehyde	6	Drought	13
Biomass burning	19	Mediterranean vegetation	3	Nitric oxide	6	PTR-MS	12
PTR-MS	17	Sesquiterpene	2	Forest	6	Tropospheric ozone	12
CO_2	17	Branch enclosure	2	Emission rate	5	BVOC emission	11
Atmospheric chemistry	15	Light	2	Monoterpene emission	5	CO_2	11
Drought	13	MVOC	2	PTR-MS	5	Photosynthesis	10
Seasonal variation	13	Micrometeorology	2	Dry deposition	4	Fungi	10
Fungi	13	Boreal forest	2	Alpha-pinene	4	MEGAN	10
Photosynthesis	12	Leaf temperature	2	Model	4	WRF-CHEM	9
Anthropogenic emission	12	Air pollution	2	Spatial distribution	4	Nitrogen oxide	9
Modeling	11	Plant physiology	2	PM	4	Anthropogenic emission	9
Total	1862		247		636		1077

Note: [a] Keywords; [b] Frequency. WRF-CHEM: Weather Research and Forecasting (WRF) model coupled with Chemistry.

Results showed “BVOC”, “biogenic emission”, “VOC”, “isoprene”, and “monoterpene” were the top five keywords, much higher than other keywords analyzed in 1991–2020 (Table 3.3 and Figure 3.2). The advancement of “isoprene” and “monoterpene” suggested that compound-based research has been an area of special focus during the period investigated. Isoprene and MTs are the top abundant VOCs with high reactivity produced by deciduous and coniferous plants, respectively (Feng et al., 2019). The frequency was found to be over 45 for several keywords, including “O_3”, “SOA”, “air quality”, and “climate change”, which are all closely related to atmospheric chemistry and climate effects. BVOCs may participate in many atmospheric processes as precursors to CO_2, O_3, SOA, and PM. SOA accounts for a large proportion of $PM_{2.5}$ and has significant effects on human health and climate change (Rohr, 2013). Aerosol particles, as an important component of the GHGs, not only have a direct effect on global warming but also cause changes in cloud properties that will have a long-term impact on the global climate and environmental chemistry (Cai et al., 2019a; Cai et al., 2019b). Increased SOA might increase aerosol scattering and further diffuse radiation, making clouds more reflective and providing cooling effects (Sporre et al., 2019).

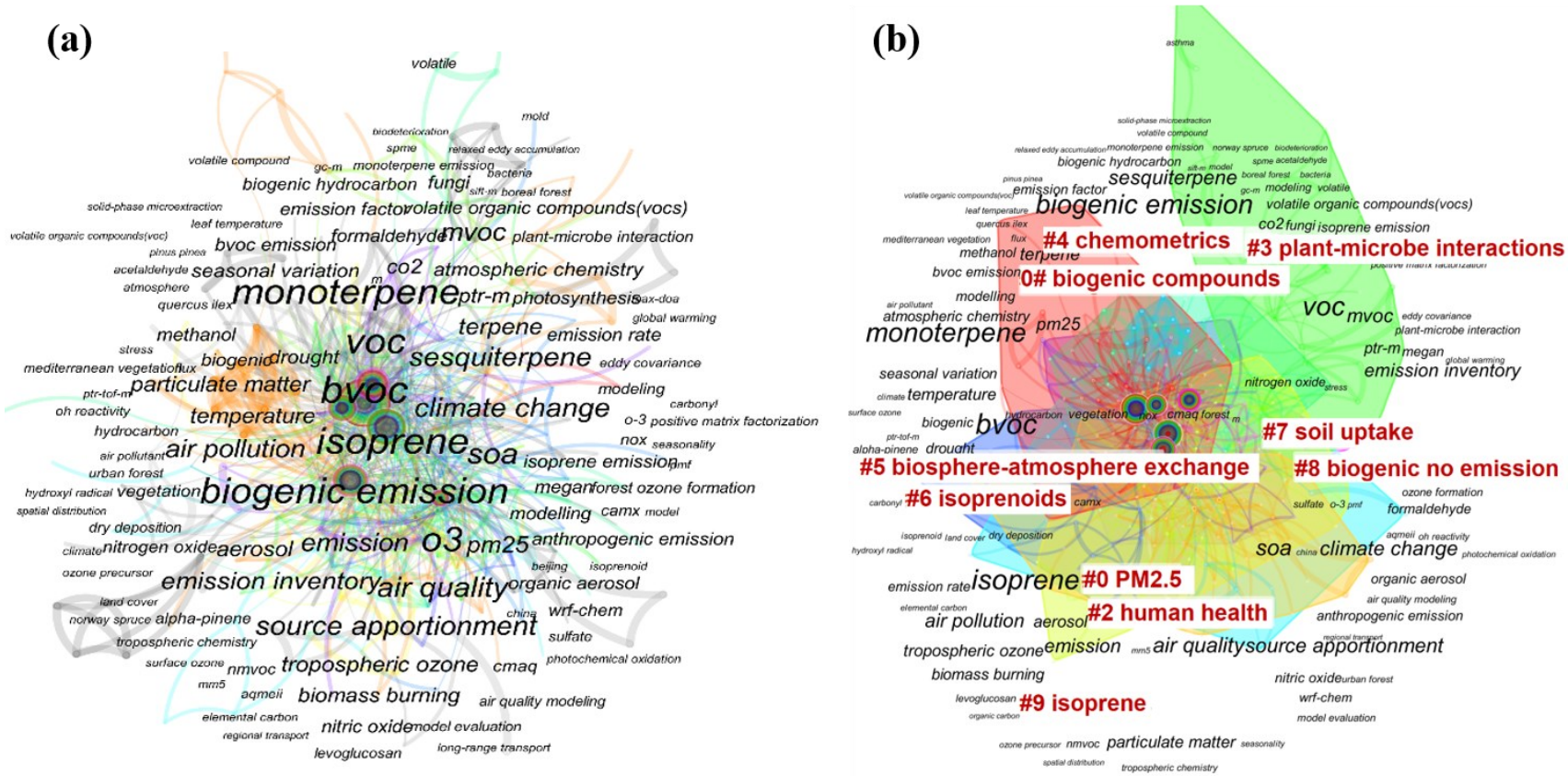

Figure 3.2. Co-keyword analysis of research related to BVOC emissions during 1991-2020 from the view of (a) cross-relationship and (b) cluster network (produced by CiteSpace).

3.3.2. Research hotspots based on cluster analysis

Cluster analysis reveals a clear structure of underlying subtopics. Figure 3.2 (b) illustrates ten clusters in BVOC emission research, with the largest and smallest size respectively being #0 and #9, labelled with keywords using the MI algorithm. The modularity Q of 0.4442 was not very high. This indicated that the research network was reasonably categorized into coupling clusters, but these clusters had small overlapping parts. The overall average silhouette score was 0.3523 (Table 3.4). This meant that the average homogeneity of ten clusters was not quite high, possibly because of the effect of overlapping parts. The silhouette of each cluster exceeded 0.5 and over half of the clusters had a value greater than 0.8. This indicates that keywords matched well to their clusters but poorly to adjacent clusters; therefore, it can be concluded that the cluster results of this research were typical, valid, and reliable.

Table 3.4. Parameter description.

Parameters	**Description**
Version	V. 5.6.R4 (64-bit)
Network N=311, E=1055 (density=0.0219)	Number of network nodes: 311, number of connections: 1055, network density: 0.0219
Modularity Q=0.4442	The network module value is generally in the [0,1) interval. If Q>0.3, it means that the separated community structure is significant.
Overall Mean Silhouette S=0.3523	When S>0.7, the clustering is significant. If S>0.5, the clustering is reasonable.

The top three terms of the three clustering methods were summarized to improve context interpretation, as presented in Table 3.5, while only labels generated by the MI method were shown in Figure 3.2 (b) and Figure 3.3 to avoid meaningless and repetitive information. Figure 3.3 summarizes ten clusters of BVOC emission studies with changes over time using CiteSpace.

Further analysis on the topical category of each cluster was conducted using Carrot[2], shown in Figure 3.4-3.6. Overall, research in BVOC emission mainly included: (a) BVOCs: composition, emission, and drivers (Cluster #0, #4, #6); (b) biosphere-atmosphere exchange: source and fate, oxidation products (Cluster #1, #2, #5, #9); and (c) plant-microbe interactions: microbial and soil BVOCs (Cluster #3, #7, #8).

Table 3.5. Summary of 10 clusters for the research hotspots during 1991-2020.

Hotspot ID	Cluster ID	Size	Silhouette	Mean (year)	Label (LSI)	Label (LLR)	Label (MI)
(a)	0	53	0.535	2008	monoterpenes; seasonal variation; bvoc composition	isoprene; monoterpenes; bvoc	biogenic compounds; benzenoids; plant wounding
	4	25	0.874	2005	erica arborea; myrtus communis; quercus cerri	pinus pinea; sift-ms; ptr-ms	chemometrics; acetaldehyde; nonan-2-one
	6	23	0.775	2008	forest fires; biomass burning; isoprenoids	forest fires; air chemistry; flash pyrolysis	isoprenoids; ec-tracer; uncertainty analysis
(b)	1	43	0.729	2011	source apportionment; methyl vinyl ketone; methacrolein	source apportionment; cmaq; land use	pm2.5; leaf temperature; pearl river delta
	2	41	0.68	2009	particulate matter; model evaluation; central-eastern Europe	model evaluation; regional transport; nitrogen oxides	human health; pm2.5 speciation; photochemical reactivity
	5	25	0.868	2009	biogenic emissions; solid-phase microextraction; nondestructive analysis	vacuum-assisted extraction; grape skin; solid-phase microextraction	biosphere-atmosphere exchange; atmosphere-biosphere trace gas exchanges; Amazonia
	9	6	0.937	2008	speciated voc oxidation; tropospheric chemistry; degradation mechanisms	mechanism reduction; degradation mechanisms; speciated voc oxidation	isoprene; bvoc; mechanism reduction

(c)	3	36	0.879	2012	photosynthesis; radial stem growth; European beech	bacteria; fungi; rhizobacteria	plant-microbe interactions; conservation biology; hormone signalling
	7	16	0.851	2009	temperature; seasonality; decomposition	decomposition; temperature; climate change	soil uptake; chemistry; Mediterranean woody species
	8	11	0.851	2011	sensible heat; boundary layer; vertical profiles	omi; ch4; ndvi	biogenic no emission; boreal pine forest; meteorological effects

Size is the number of references that a cluster contains. Clusters are referred to in terms of the labels selected by the LLR, TF*IDF, and MI tests.

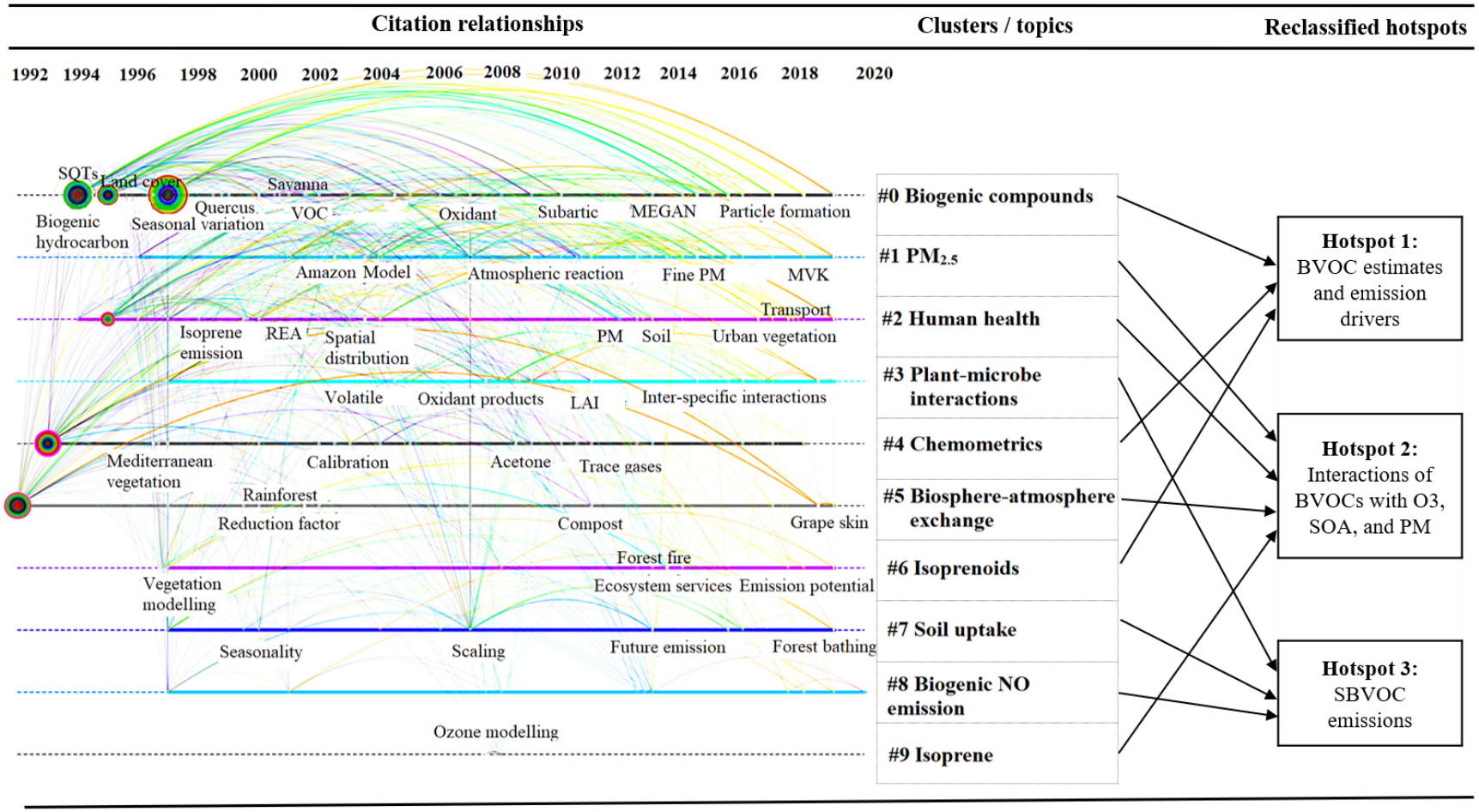

Figure 3.3. Citation relationship and logical grouping of relevant topics about BVOC emissions during 1991-2020 (produced by CiteSpace).

The first significant hotspot was focused on BVOCs and consisted of three subclusters, as per Table 3.5 and Figure 3.3-3.4. Studies in this hotspot have been related to (1) estimation methods (e.g., chemometrics, symptoms, uncertainty analysis, gas chromatography, model); (2) BVOC compounds and emission trends (e.g., isoprene, MTs, isoprenoids, benzenoids, acetaldehyde, nonan-2-one, seasonal and regional variation, plant species); and (3) emission drivers (e.g., mechanical wounding, climate warming, elevated CO_2, forest fires). Three articles in this area with the strongest bursts were all related to a BVOC emission model, namely MEGAN, with the strengths of 66.8, 90.9, and 107.5, as well as citations of 140, 266, and 310, during the periods, 1996–2003, 2007–2014, and 2014–2020, respectively. This indicates that MEGAN was a widely known bottom-up model to estimate BVOC emissions from terrestrial ecosystems at both the global and regional scales throughout the study period.

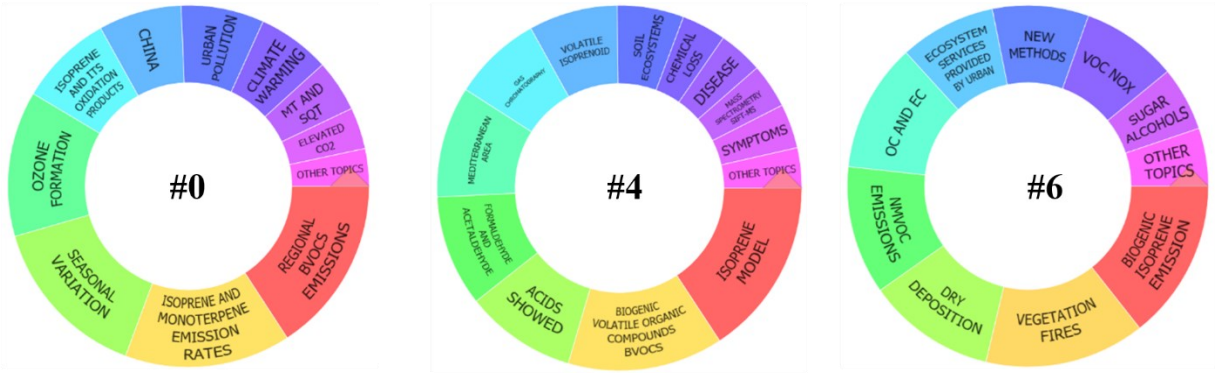

Figure 3.4. Subclusters of BVOCs: composition, emission, and drivers (Cluster #0, #4, #6) (produced by Carrot[2]).

The second significant hotspot was the biosphere-atmosphere exchange, consisting of four subclusters as per Table 3.5, Figure 3.3, and Figure 3.5. Studies in this hotspot were related to the

fate of BVOCs in biosphere-atmosphere exchange, including (1) source apportionment (model evaluation, photochemical reactivity, human health, climate change); and (2) degradation mechanisms and oxidation products (O_3, SOA, PM, nondestructive analysis, vacuum extraction (VE), solid-phase microextraction (SPME)).

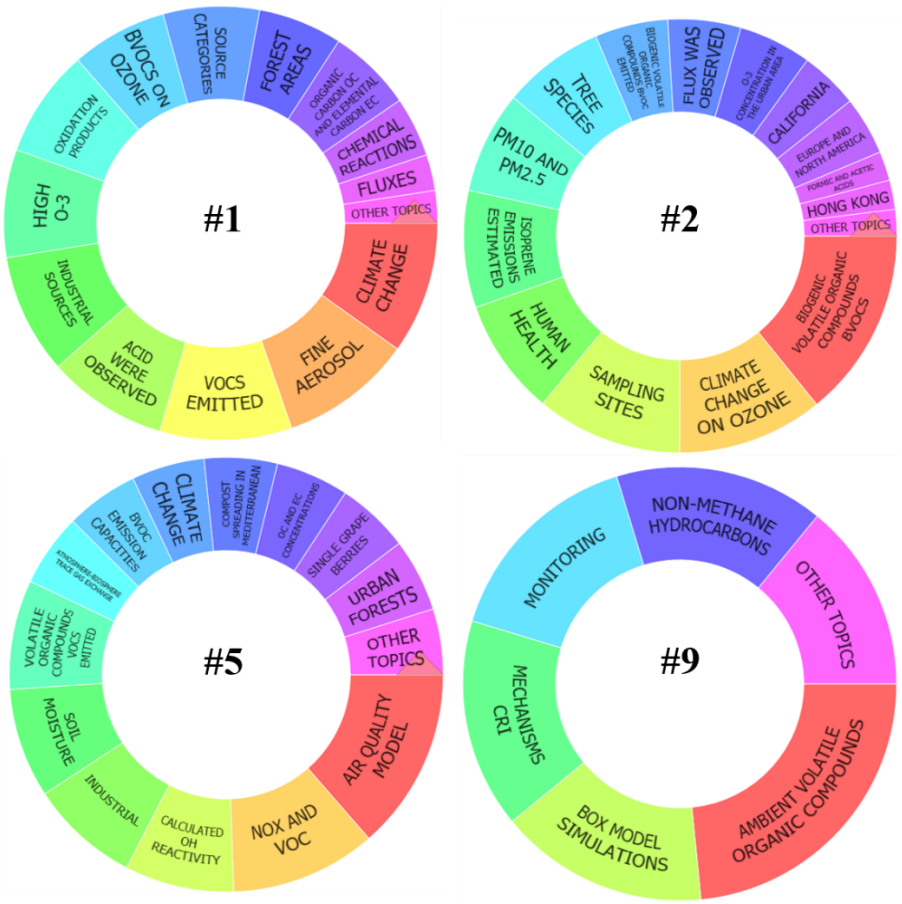

Figure 3.5. Subclusters of biosphere-atmosphere exchange: source and fate, oxidation products (Cluster #1, #2, #5, #9) (produced by Carrot[2]).

"O_3" has consistently drawn attention in atmospheric chemistry research since 1991, while some new research areas have also emerged in this field, such as "SOA" during 2001–2010 and "PM"

during 2010–2020 (Table 3.3). The top ten articles with the strongest bursts, published during 2005–2015 and frequently cited during 2006–2020, were primarily related to isoprene degradation and SOA formation, with strengths between 23.5 and 51.7 and citations between 94 and 193 (Table 3.6). This indicates that SOA has drawn widespread public attention due to its adverse effects on air quality and human health. Researchers worldwide have studied the mechanism of SOA formation with different BVOCs (e.g., isoprene, MTs, SQTs, and other reactive chemicals). The diversity of SOA formation pathways (e.g., gas-phase reactions, aqueous-phase oxidation, heterogeneous acid-catalyzed reactions, and oligomerization reactions) has caused large discrepancies and uncertainties in findings (Amin et al., 2013; Hansel et al., 2015). Moreover, studies on PM, including the contribution of BVOCs to PM concentrations, the mechanism of new particle formation, as well as BVOC and PM fluxes over forests, have become increasingly popular research topics during 2010–2020. Combining high BVOC emissions with active photochemical reactions enhanced various gas- and particle-phase SOA and likely promoted the synchronous formation and growth of $PM_{2.5}$ and O_3 at regional scales (Wang et al., 2016a). For example, BVOC-derived SOA has been found to account for 9–29% of total $PM_{2.5}$ in urban districts in Birmingham, UK (Heal et al., 2011).

Table 3.6. Top 362 references with the strongest citation bursts (produced by CiteSpace).

References	Year	Strength	Begin	End	1991 - 2020
TRAINER M, 1987, J GEOPHYS RES-ATMOS, V92, P11879, DOI	1987	3.8932	1991	1995	
JUUTI S, 1990, J GEOPHYS RES-ATMOS, V95, P7515, DOI	1990	3.9379	1991	1998	
JACOB DJ, 1988, J GEOPHYS RES-ATMOS, V93, P1477, DOI	1988	8.1922	1991	1996	
TRAINER M, 1987, NATURE, V329, P705, DOI	1987	5.8421	1991	1995	
LAMB B, 1987, ATMOS ENVIRON, V21, P1695, DOI	1987	14.9572	1991	1995	
CHAMEIDES WL, 1988, SCIENCE, V241, P1473, DOI	1988	16.4122	1991	1996	
ZIMMERMAN PR, 1988, J GEOPHYS RES-ATMOS, V93, P1407, DOI	1988	5.038	1991	1996	
Davidson E A, 1991, MICROBIAL PRODUCTION AND CONSUMPTION OF GREENHOUSE GASES: METHANE, V0, P0	1991	3.6122	1992	1997	
ANDERSON IC, 1987, J GEOPHYS RES-ATMOS, V92, P965, DOI	1987	4.7597	1992	1993	
SLEMR F, 1991, J GEOPHYS RES-ATMOS, V96, P13017, DOI	1991	3.6122	1992	1997	
DAVIDSON EA, 1991, J GEOPHYS RES-ATMOS, V96, P15439, DOI	1991	7.8337	1992	1997	
ANDERSON IC, 1988, J GEOPHYS RES-ATMOS, V93, P3893, DOI	1988	5.7095	1992	1996	
WILLIAMS EJ, 1991, J GEOPHYS RES-ATMOS, V96, P1033, DOI	1991	3.6122	1992	1997	

SHEPHERD MF, 1991, ATMOS ENVIRON A-GEN, V25, P1961, DOI	1991	4.8176	1992	1997
JOHANSSON C, 1988, J GEOPHYS RES-ATMOS, V93, P7180, DOI	1988	7.6156	1992	1996
SANHUEZA E, 1990, J GEOPHYS RES-ATMOS, V95, P22481, DOI	1990	7.3781	1992	1998
Levine JS, 1988, GLOBAL BIOGEOCHEM CY, V2, P445, DOI	1988	3.8048	1992	1996
WINER AM, 1992, ATMOS ENVIRON A-GEN, V26, P2647, DOI	1992	9.4586	1993	2000
ATKINSON R, 1990, ATMOS ENVIRON A-GEN, V24, P1, DOI	1990	5.8116	1994	1998
KUZMA J, 1993, PLANT PHYSIOL, V101, P435, DOI	1993	5.8116	1994	1998
MACDONALD RC, 1993, ATMOS ENVIRON A-GEN, V27, P1709, DOI	1993	4.991	1994	2001
JANSON RW, 1993, J GEOPHYS RES-ATMOS, V98, P2839, DOI	1993	14.5094	1994	2001
LAMB B, 1993, ATMOS ENVIRON A-GEN, V27, P1673, DOI	1993	21.5531	1994	2001
AREY J, 1991, ATMOS ENVIRON A-GEN, V25, P1063, DOI	1991	7.558	1994	1998
AREY J, 1991, J GEOPHYS RES-ATMOS, V96, P9329, DOI	1991	4.4276	1994	1999
MONSON RK, 1989, PLANT PHYSIOL, V90, P267, DOI	1989	4.5363	1994	1996
MCKEEN SA, 1991, J GEOPHYS RES-ATMOS, V96, P15377, DOI	1991	4.648	1994	1998
GUENTHER AB, 1993, J GEOPHYS RES-ATMOS, V98, P12609, DOI	1993	46.9194	1994	2001
FUJITA EM, 1992, J AIR WASTE MANAGE, V42, P264, DOI	1992	4.6712	1994	1995

GERY MW, 1989, J GEOPHYS RES-ATMOS, V94, P12925, DOI	1989	6.1618	1994	1997
Fehsenfeld F, 1992, GLOBAL BIOGEOCHEM CY, V6, P389, DOI	1992	31.8719	1994	2000
GUENTHER AB, 1991, J GEOPHYS RES-ATMOS, V96, P10799, DOI	1991	23.9069	1994	1999
[Anonymous], 1991, RETHINKING OZONE PRO, V0, P0	1991	7.3444	1994	1995
SILLMAN S, 1990, J GEOPHYS RES-ATMOS, V95, P1837, DOI	1990	5.2297	1994	1998
PIERCE TE, 1991, J AIR WASTE MANAGE, V41, P937, DOI	1991	5.2788	1995	1998
CRUTZEN PJ, 1990, SCIENCE, V250, P1669, DOI	1990	5.2788	1995	1998
MARTIN RS, 1991, J ATMOS CHEM, V13, P1, DOI	1991	5.0308	1995	1999
GERON CD, 1994, J GEOPHYS RES-ATMOS, V99, P12773, DOI	1994	22.8985	1995	2002
CORCHNOY SB, 1992, ATMOS ENVIRON B-URB, V26, P339, DOI	1992	5.3321	1995	2000
SHARKEY TD, 1991, PLANT CELL ENVIRON, V14, P333, DOI	1991	5.0308	1995	1999
SHARKEY TD, 1991, [No title captured], V0, P153	1991	8.2169	1995	1998
ROSELLE SJ, 1991, J GEOPHYS RES-ATMOS, V96, P7371, DOI	1991	5.2788	1995	1998
CHAMEIDES WL, 1992, J GEOPHYS RES-ATMOS, V97, P6037, DOI	1992	17.6487	1995	2000
GRINSPOON J, 1991, PLANT PHYSIOL, V97, P170, DOI	1991	4.1047	1995	1998
GUENTHER A, 1994, ATMOS ENVIRON, V28, P1197, DOI	1994	19.5414	1995	2002

GROSJEAN D, 1993, ENVIRON SCI TECHNOL, V27, P830, DOI	1993	5.2788	1995	1998	
MONTZKA SA, 1993, J GEOPHYS RES-ATMOS, V98, P1101, DOI	1993	3.6439	1996	1998	
MONSON RK, 1992, PLANT PHYSIOL, V98, P1175, DOI	1992	8.5113	1996	1998	
MONSON RK, 1994, OECOLOGIA, V99, P260, DOI	1994	10.923	1996	2002	
Harley P, 1996, TREE PHYSIOL, V16, P25	1996	5.2199	1996	1999	
SILVER GM, 1991, PLANT PHYSIOL, V97, P1588, DOI	1991	4.2517	1996	1998	
GERON CD, 1995, ATMOS ENVIRON, V29, P1569, DOI	1995	5.1595	1996	2003	
GUENTHER A, 1995, J GEOPHYS RES-ATMOS, V100, P8873, DOI	1995	66.7762	1996	2003	
SHARKEY TD, 1995, NATURE, V374, P769, DOI	1995	7.5438	1996	1999	
Tingey D T, 1991, TRACE GAS EMISSIONS, V0, P93	1991	8.1251	1996	1999	
MONSON RK, 1995, ATMOS ENVIRON, V29, P2989, DOI	1995	8.0334	1997	2000	
WILLIAMS EJ, 1992, J GEOPHYS RES-ATMOS, V97, P7511, DOI	1992	3.5942	1997	1999	
YIENGER JJ, 1995, J GEOPHYS RES-ATMOS, V100, P11447, DOI	1995	7.214	1997	2002	
Loreto F, 1996, PLANT PHYSIOL, V110, P267, DOI	1996	7.214	1997	2002	
Staudt M, 1995, FRESEN ENVIRON BULL, V4, P743	1995	5.9935	1997	1999	
ATKINSON R, 1995, INT J CHEM KINET, V27, P941, DOI	1995	3.8125	1997	2001	

STAUDT M, 1995, NATURWISSENSCHAFTEN, V82, P89, DOI	1995	9.2799	1997	2002	
CICCIOLI P, 1993, ATMOS ENVIRON A-GEN, V27, P1891, DOI	1993	3.5942	1997	1999	
Kesselmeier J, 1996, ATMOS ENVIRON, V30, P1841, DOI	1996	20.0716	1997	2004	
Sharkey TD, 1996, TREE PHYSIOL, V16, P649	1996	5.1502	1997	2002	
SHARKEY TD, 1993, OECOLOGIA, V95, P328, DOI	1993	5.7351	1997	2000	
KONIG G, 1995, ATMOS ENVIRON, V29, P861, DOI	1995	12.7213	1997	2003	
SIMPSON D, 1995, J GEOPHYS RES-ATMOS, V100, P22875, DOI	1995	17.1448	1997	2003	
Guenther A, 1996, TREE PHYSIOL, V16, P17	1996	7.1941	1997	1999	
CARDENAS L, 1993, J GEOPHYS RES-ATMOS, V98, P14783, DOI	1993	4.1938	1997	1999	
Benjamin MT, 1996, ATMOS ENVIRON, V30, P1437, DOI	1996	11.4482	1998	2004	
Goldan PD, 1995, J GEOPHYS RES-ATMOS, V100, P25945, DOI	1995	8.7609	1998	2002	
Guenther A, 1996, J GEOPHYS RES-ATMOS, V101, P25859, DOI	1996	6.7676	1998	2003	
AREY J, 1995, ATMOS ENVIRON, V29, P2977, DOI	1995	3.46	1998	2001	
SIMPSON D, 1995, J GEOPHYS RES-ATMOS, V100, P22891, DOI	1995	7.2892	1998	2003	
Biesenthal TA, 1997, ATMOS ENVIRON, V31, P2049, DOI	1997	4.6829	1998	2003	
Harley P, 1997, TREE PHYSIOL, V17, P705	1997	5.4713	1998	2002	

Geron CD, 1997, J GEOPHYS RES-ATMOS, V102, P18889, DOI	1997	4.3759	1998	2002	
Guenther A, 1996, J GEOPHYS RES-ATMOS, V101, P18555, DOI	1996	10.9753	1998	2001	
Hoffmann T, 1997, J ATMOS CHEM, V26, P189, DOI	1997	9.6885	1998	2005	
Andreae MO, 1997, SCIENCE, V276, P1052, DOI	1997	10.45	1998	2004	
Street RA, 1996, J GEOPHYS RES-ATMOS, V101, P22799, DOI	1996	4.9235	1998	2002	
MONTZKA SA, 1995, J GEOPHYS RES-ATMOS, V100, P11393, DOI	1995	4.162	1998	2003	
Kesselmeier J, 1997, ATMOS ENVIRON, V31, P119, DOI	1997	8.7635	1998	2005	
Guenther A, 1996, J GEOPHYS RES-ATMOS, V101, P1345, DOI	1996	9.9511	1998	2004	
Odum JR, 1996, ENVIRON SCI TECHNOL, V30, P2580, DOI	1996	3.7221	1999	2004	
Steinbrecher R, 1997, ATMOS ENVIRON, V31, P79, DOI	1997	7.9378	1999	2005	
SINGH HB, 1995, NATURE, V378, P50, DOI	1995	7.571	1999	2002	
Seufert G, 1997, ATMOS ENVIRON, V31, P5, DOI	1997	6.6667	1999	2003	
Kinnee E, 1997, ECOL APPL, V7, P46, DOI	1997	6.447	1999	2005	
Staudt M, 1997, ATMOS ENVIRON, V31, P145, DOI	1997	13.4123	1999	2002	
Valentini R, 1997, ATMOS ENVIRON, V31, P229, DOI	1997	3.8419	1999	2000	
Bertin N, 1997, ATMOS ENVIRON, V31, P135, DOI	1997	12.2381	1999	2003	

Makela JM, 1997, GEOPHYS RES LETT, V24, P1219, DOI	1997	4.7868	1999	2004	
Guenther A, 1997, ECOL APPL, V7, P34, DOI	1997	14.9104	1999	2005	
Lerdau M, 1997, PLANT CELL ENVIRON, V20, P569, DOI	1997	4.0735	1999	2002	
Larsen B, 1997, ATMOS ENVIRON, V31, P35, DOI	1997	3.6617	2000	2005	
Benjamin MT, 1997, ATMOS ENVIRON, V31, P3087, DOI	1997	6.9975	2000	2003	
Owen S, 1997, ATMOS ENVIRON, V31, P101, DOI	1997	11.1913	2000	2005	
Kesselmeier J, 1999, J ATMOS CHEM, V33, P23, DOI	1999	36.8306	2000	2007	
Schuh G, 1997, J ATMOS CHEM, V27, P291, DOI	1997	7.8545	2000	2005	
Simpson D, 1999, J GEOPHYS RES-ATMOS, V104, P8113, DOI	1999	27.4351	2000	2007	
Griffin RJ, 1999, J GEOPHYS RES-ATMOS, V104, P3555, DOI	1999	8.7895	2000	2007	
Hakola H, 1998, ATMOS ENVIRON, V32, P1825, DOI	1998	6.3956	2000	2001	
Street RA, 1997, ATMOS ENVIRON, V31, P89, DOI	1997	10.4795	2000	2005	
Calogirou A, 1999, ATMOS ENVIRON, V33, P1423, DOI	1999	5.0834	2000	2007	
Pierce T, 1998, J GEOPHYS RES-ATMOS, V103, P25611, DOI	1998	14.6865	2000	2005	
Ciccioli P, 1997, J GEOPHYS RES-ATMOS, V102, P23319, DOI	1997	4.2664	2000	2002	
Atkinson R, 1997, J PHYS CHEM REF DATA, V26, P215, DOI	1997	11.7664	2000	2004	

Street RA, 1997, J GEOPHYS RES-ATMOS, V102, P15875, DOI	1997	5.7553	2000	2001	
Helmig D, 1999, CHEMOSPHERE, V38, P2163, DOI	1999	9.375	2001	2006	
Fall R, 1999, J GEOPHYS RES-ATMOS, V104, P15963, DOI	1999	8.3019	2001	2007	
Kavouras IG, 1998, NATURE, V395, P683, DOI	1998	8.853	2001	2006	
Kirstine W, 1998, J GEOPHYS RES-ATMOS, V103, P10605, DOI	1998	10.4194	2001	2006	
Lindinger W, 1998, INT J MASS SPECTROM, V173, P191, DOI	1998	17.7452	2001	2006	
Guenther A, 2000, ATMOS ENVIRON, V34, P2205, DOI	2000	37.1775	2001	2008	
Benjamin MT, 1998, ATMOS ENVIRON, V32, P53, DOI	1998	4.4472	2001	2002	
de Gouw JA, 1999, GEOPHYS RES LETT, V26, P811, DOI	1999	6.3452	2001	2007	
Guenther AB, 1998, J GEOPHYS RES-ATMOS, V103, P13145, DOI	1998	5.0831	2001	2002	
Kavouras IG, 1999, GEOPHYS RES LETT, V26, P55, DOI	1999	5.2029	2001	2006	
Poisson N, 2000, J ATMOS CHEM, V36, P157, DOI	2000	4.3505	2002	2008	
Schade GW, 2001, J GEOPHYS RES-ATMOS, V106, P3111, DOI	2001	11.3821	2002	2007	
Guenther A, 1999, J GEOPHYS RES-ATMOS, V104, P30625, DOI	1999	17.6168	2002	2006	
FALL R, 1999, REACTIVE HYDROCARBON, V0, P41	1999	6.3565	2002	2005	
Staudt M, 1998, PLANT CELL ENVIRON, V21, P385, DOI	1998	5.1994	2002	2005	

Fuentes JD, 2000, B AM METEOROL SOC, V81, P1537, DOI	2000	22.3076	2002	2007	
Atkinson R, 2000, ATMOS ENVIRON, V34, P2063, DOI	2000	21.3655	2002	2008	
Shao M, 2001, J GEOPHYS RES-ATMOS, V106, P20483, DOI	2001	5.3186	2002	2008	
Helmig D, 1998, J GEOPHYS RES-ATMOS, V103, P25519, DOI	1998	3.6821	2002	2004	
Helmig D, 1998, J GEOPHYS RES-ATMOS, V103, P22397, DOI	1998	3.8228	2002	2003	
Heiden AC, 1999, ECOL APPL, V9, P1160, DOI	1999	3.4649	2002	2005	
Warneke C, 1999, GLOBAL BIOGEOCHEM CY, V13, P9, DOI	1999	4.4605	2002	2003	
Harley PC, 1999, OECOLOGIA, V118, P109, DOI	1999	6.5891	2002	2006	
Klinger LF, 1998, J GEOPHYS RES-ATMOS, V103, P1443, DOI	1998	4.043	2002	2005	
Staudt M, 2000, J ATMOS CHEM, V35, P77, DOI	2000	6.9473	2003	2006	
Griffin RJ, 1999, GEOPHYS RES LETT, V26, P2721, DOI	1999	4.5051	2003	2004	
Jenkin ME, 1997, ATMOS ENVIRON, V31, P81, DOI	1997	4.2517	2003	2005	
Schade GW, 1999, GEOPHYS RES LETT, V26, P2187, DOI	1999	4.05	2003	2006	
Thunis P, 2000, ATMOS ENVIRON, V34, P467, DOI	2000	4.8598	2003	2005	
Schmidt H, 2001, ATMOS ENVIRON, V35, P6277, DOI	2001	4.8598	2003	2005	
Stockwell WR, 1997, J GEOPHYS RES-ATMOS, V102, P25847, DOI	1997	9.1204	2003	2005	

Greenberg JP, 1999, ATMOS ENVIRON, V33, P855, DOI	1999	5.468	2003	2005	
Seinfeld J H, 1998, ATMOSPHERIC CHEM PHY, V0, P0	1998	13.9164	2003	2006	
Sillman S, 1999, ATMOS ENVIRON, V33, P1821, DOI	1999	6.9791	2004	2005	
de Gouw J, 2003, INT J MASS SPECTROM, V223, P365, DOI	2003	6.8017	2004	2010	
Karl TG, 2002, ATMOS CHEM PHYS, V2, P279, DOI	2002	7.2561	2004	2010	
Karl T, 2001, J GEOPHYS RES-ATMOS, V106, P24157, DOI	2001	4.4389	2004	2005	
Galbally IE, 2002, J ATMOS CHEM, V43, P195, DOI	2002	8.0283	2004	2007	
Wiedinmyer C, 2001, ATMOS ENVIRON, V35, P6465, DOI	2001	3.8043	2004	2005	
Warneke C, 2003, ENVIRON SCI TECHNOL, V37, P2494, DOI	2003	4.0779	2004	2010	
Wang KY, 2000, ATMOS ENVIRON, V34, P2909, DOI	2000	6.3055	2004	2007	
Rosenstiel TN, 2003, NATURE, V421, P256, DOI	2003	9.5297	2004	2010	
Kulmala M, 2001, TELLUS B, V53, P324, DOI	2001	3.8043	2004	2005	
De Gouw JA, 2000, ENVIRON SCI TECHNOL, V34, P2640, DOI	2000	3.8043	2004	2005	
Pare PW, 1999, PLANT PHYSIOL, V121, P325, DOI	1999	4.0105	2004	2007	
Andreae MO, 2001, GLOBAL BIOGEOCHEM CY, V15, P955, DOI	2001	5.1577	2004	2007	
Rinne HJI, 2002, ATMOS ENVIRON, V36, P2421, DOI	2002	4.584	2004	2007	

Ciccioli P, 1999, J GEOPHYS RES-ATMOS, V104, P8077, DOI	1999	7.2684	2004	2006	
Abbot DS, 2003, GEOPHYS RES LETT, V30, P0, DOI	2003	3.4809	2004	2009	
de Gouw JA, 2003, J GEOPHYS RES-ATMOS, V108, P0, DOI	2003	5.4393	2004	2010	
Klinger LF, 2002, J GEOPHYS RES-ATMOS, V107, P0, DOI	2002	3.812	2005	2010	
Owen SM, 2002, ATMOS ENVIRON, V36, P3147, DOI	2002	3.6451	2005	2009	
Horowitz LW, 2003, J GEOPHYS RES-ATMOS, V108, P0, DOI	2003	10.9552	2005	2009	
Owen SM, 2001, ATMOS ENVIRON, V35, P5393, DOI	2001	8.3414	2005	2009	
Loreto F, 2001, PLANT PHYSIOL, V127, P1781, DOI	2001	4.1664	2005	2009	
Fiedler K, 2001, INT J HYG ENVIR HEAL, V204, P111, DOI	2001	3.6451	2005	2009	
Penuelas J, 2003, TRENDS PLANT SCI, V8, P105, DOI	2003	3.8053	2005	2011	
Loreto F, 2004, TREE PHYSIOL, V24, P361, DOI	2004	3.6451	2005	2009	
Bey I, 2001, J GEOPHYS RES-ATMOS, V106, P23073, DOI	2001	8.4581	2005	2008	
Atkinson R, 2003, ATMOS ENV S2, V37, P197, DOI	2003	4.7717	2005	2007	
Heiden AC, 2003, J ATMOS CHEM, V45, P143, DOI	2003	4.1747	2005	2007	
Hakola H, 2003, ATMOS ENVIRON, V37, P1623, DOI	2003	11.8506	2005	2008	
Yu JZ, 1999, J ATMOS CHEM, V34, P207, DOI	1999	4.7717	2005	2007	

Lamanna MS, 1999, J GEOPHYS RES-ATMOS, V104, P21247, DOI	1999	5.0308	2005	2006
Sabillon D, 2001, ATMOS ENVIRON, V35, P4419, DOI	2001	4.7717	2005	2007
Palmer PI, 2003, J GEOPHYS RES-ATMOS, V108, P0, DOI	2003	10.9808	2005	2010
Kulmala M, 2004, ATMOS CHEM PHYS, V4, P557, DOI	2004	7.154	2005	2010
Komenda M, 2002, J GEOPHYS RES-ATMOS, V107, P0, DOI	2002	3.6451	2005	2009
Guenther A, 2002, CHEMOSPHERE, V49, P837, DOI	2002	5.9662	2005	2007
Spanke J, 2001, TELLUS B, V53, P406, DOI	2001	4.4013	2005	2006
Saunders SM, 2003, ATMOS CHEM PHYS, V3, P161, DOI	2003	7.2968	2005	2009
Janson R, 2001, ATMOS ENVIRON, V35, P4629, DOI	2001	4.4013	2005	2006
Claeys M, 2004, SCIENCE, V303, P1173, DOI	2004	29.0216	2006	2012
Sanderson MG, 2003, GEOPHYS RES LETT, V30, P0, DOI	2003	8.9212	2006	2009
Karl T, 2004, J GEOPHYS RES-ATMOS, V109, P0, DOI	2004	7.3078	2006	2012
Holzinger R, 2005, ATMOS CHEM PHYS, V5, P67, DOI	2005	13.4233	2006	2012
Kanakidou M, 2005, ATMOS CHEM PHYS, V5, P1053, DOI	2005	31.6311	2006	2013
Fall R, 2003, CHEM REV, V103, P4941, DOI	2003	8.2717	2006	2011
Kalberer M, 2004, SCIENCE, V303, P1659, DOI	2004	7.7994	2006	2008
Di Carlo P, 2004, SCIENCE, V304, P722, DOI	2004	17.1039	2006	2012

Claeys M, 2004, ATMOS ENVIRON, V38, P4093, DOI	2004	5.3967	2006	2008	
Kurpius MR, 2003, GEOPHYS RES LETT, V30, P0, DOI	2003	7.6975	2006	2010	
Jenkin ME, 2000, ATMOS ENVIRON, V34, P2499, DOI	2000	4.7965	2006	2008	
Atkinson R, 2003, CHEM REV, V103, P4605, DOI	2003	7.2456	2006	2009	
Streets DG, 2003, J GEOPHYS RES-ATMOS, V108, P0, DOI	2003	6.5977	2006	2008	
Lee A, 2005, ATMOS CHEM PHYS, V5, P505, DOI	2005	8.2117	2006	2010	
Singh HB, 2004, J GEOPHYS RES-ATMOS, V109, P0, DOI	2004	5.6947	2006	2007	
Goldstein AH, 2004, GEOPHYS RES LETT, V31, P0, DOI	2004	8.9363	2006	2012	
Spirig C, 2005, ATMOS CHEM PHYS, V5, P465, DOI	2005	10.5762	2006	2011	
Lathiere J, 2005, GEOPHYS RES LETT, V32, P0, DOI	2005	7.0336	2007	2009	
Jacob DJ, 2005, J GEOPHYS RES-ATMOS, V110, P0, DOI	2005	9.5718	2007	2012	
Bonn B, 2003, GEOPHYS RES LETT, V30, P0, DOI	2003	5.2731	2007	2009	
Hakola H, 2006, BIOGEOSCIENCES, V3, P93, DOI	2006	13.9405	2007	2012	
Niinemets U, 2004, TRENDS PLANT SCI, V9, P180, DOI	2004	12.7118	2007	2011	
de Gouw JA, 2005, J GEOPHYS RES-ATMOS, V110, P0, DOI	2005	14.6724	2007	2013	
Atkinson R, 2003, ATMOS ENVIRON, V37, P0, DOI	2003	21.0697	2007	2011	

Lee A, 2006, J GEOPHYS RES-ATMOS, V111, P0, DOI	2006	11.2407	2007	2011	
Tie X, 2003, GEOPHYS RES LETT, V30, P0, DOI	2003	4.8791	2007	2011	
Loreto F, 2006, PLANT CELL ENVIRON, V29, P1820, DOI	2006	5.2731	2007	2009	
Guenther A, 2006, ATMOS CHEM PHYS, V6, P3181, DOI	2006	90.8911	2007	2014	
Tarvainen V, 2005, ATMOS CHEM PHYS, V5, P989, DOI	2005	10.4447	2007	2012	
von Kuhlmann R, 2004, ATMOS CHEM PHYS, V4, P1, DOI	2004	5.8598	2007	2009	
Karl T, 2005, ATMOS CHEM PHYS, V5, P3015, DOI	2005	5.3677	2007	2011	
Shim C, 2005, J GEOPHYS RES-ATMOS, V110, P0, DOI	2005	4.2007	2008	2012	
Henze DK, 2006, GEOPHYS RES LETT, V33, P0, DOI	2006	11.6513	2008	2014	
Helmig D, 2007, ENVIRON SCI TECHNOL, V41, P1545, DOI	2007	9.1921	2008	2010	
Hogrefe C, 2004, J GEOPHYS RES-ATMOS, V109, P0, DOI	2004	5.5646	2008	2009	
Millet DB, 2006, J GEOPHYS RES-ATMOS, V111, P0, DOI	2006	4.5913	2008	2010	
Fu TM, 2007, J GEOPHYS RES-ATMOS, V112, P0, DOI	2007	8.4111	2008	2012	
Lathiere J, 2006, ATMOS CHEM PHYS, V6, P2129, DOI	2006	16.0449	2008	2014	
Sharkey TD, 2001, ANNU REV PLANT PHYS, V52, P407, DOI	2001	6.1837	2008	2009	
Volkamer R, 2006, GEOPHYS RES LETT, V33, P0, DOI	2006	13.8464	2008	2014	

Murazaki K, 2006, J GEOPHYS RES-ATMOS, V111, P0, DOI	2006	6.8029	2008	2009	
Arneth A, 2007, ATMOS CHEM PHYS, V7, P31, DOI	2007	7.0862	2008	2015	
Weber RJ, 2007, J GEOPHYS RES-ATMOS, V112, P0, DOI	2007	8.772	2008	2013	
Goldstein AH, 2007, ENVIRON SCI TECHNOL, V41, P1514, DOI	2007	28.9055	2008	2015	
Tunved P, 2006, SCIENCE, V312, P261, DOI	2006	15.0667	2008	2013	
Johnson D, 2006, ATMOS CHEM PHYS, V6, P403, DOI	2006	5.5646	2008	2009	
Tsigaridis K, 2003, ATMOS CHEM PHYS, V3, P1849, DOI	2003	6.1837	2008	2009	
Heald CL, 2005, GEOPHYS RES LETT, V32, P0, DOI	2005	8.8795	2008	2012	
Byun D, 2006, APPL MECH REV, V59, P51, DOI	2006	10.7544	2008	2012	
Kroll JH, 2005, GEOPHYS RES LETT, V32, P0, DOI	2005	7.4657	2008	2010	
Kuhn U, 2007, ATMOS CHEM PHYS, V7, P2855, DOI	2007	5.5646	2008	2009	
Edney EO, 2005, ATMOS ENVIRON, V39, P5281, DOI	2005	4.1713	2008	2013	
Arneth A, 2008, ATMOS CHEM PHYS, V8, P4605, DOI	2008	16.8037	2009	2013	
Ortega J, 2008, CHEMOSPHERE, V72, P343, DOI	2008	13.1131	2009	2014	
Lelieveld J, 2008, NATURE, V452, P737, DOI	2008	23.5151	2009	2016	
Wiedinmyer C, 2006, EARTH INTERACT, V10, P0, DOI	2006	4.8561	2009	2010	

Karl T, 2007, J GEOPHYS RES-ATMOS, V112, P0, DOI	2007	9.1278	2009	2014	
Palmer PI, 2006, J GEOPHYS RES-ATMOS, V111, P0, DOI	2006	8.0049	2009	2012	
Seco R, 2007, ATMOS ENVIRON, V41, P2477, DOI	2007	9.4165	2009	2011	
Rinne J, 2007, ATMOS CHEM PHYS, V7, P3361, DOI	2007	8.3065	2009	2011	
Steinbrecher R, 2009, ATMOS ENVIRON, V43, P1380, DOI	2009	9.8424	2009	2015	
Brilli F, 2007, NEW PHYTOL, V175, P244, DOI	2007	5.5341	2009	2011	
Folkers A, 2008, PLANT BIOLOGY, V10, P65, DOI	2008	7.1971	2009	2011	
de Gouw J, 2007, MASS SPECTROM REV, V26, P223, DOI	2007	22.9925	2009	2015	
Sharkey TD, 2008, ANN BOT-LONDON, V101, P5, DOI	2008	6.758	2009	2013	
Sakulyanontvittaya T, 2008, ENVIRON SCI TECHNOL, V42, P1623, DOI	2008	7.9626	2009	2012	
Kiendler-Scharr A, 2009, NATURE, V461, P381, DOI	2009	10.4862	2010	2016	
Ortega J, 2008, CHEMOSPHERE, V72, P365, DOI	2008	4.8818	2010	2012	
Donahue NM, 2006, ENVIRON SCI TECHNOL, V40, P2635, DOI	2006	5.7063	2010	2014	
Bouvier-Brown NC, 2009, ATMOS CHEM PHYS, V9, P5505, DOI	2009	9.2274	2010	2014	
Ortega J, 2007, ATMOS ENVIRON, V41, P5479, DOI	2007	4.8818	2010	2012	
Laothawornkitkul J, 2009, NEW PHYTOL, V183, P27, DOI	2009	20.5686	2010	2017	

Atkinson R, 2006, ATMOS CHEM PHYS, V6, P3625, DOI	2006	7.7508	2010	2011	
Hofzumahaus A, 2009, SCIENCE, V324, P1702, DOI	2009	15.8152	2010	2013	
DeCarlo PF, 2006, ANAL CHEM, V78, P8281, DOI	2006	7.466	2010	2014	
Helmig D, 2006, ATMOS ENVIRON, V40, P4150, DOI	2006	5.9599	2010	2011	
Duhl TR, 2008, BIOGEOSCIENCES, V5, P761, DOI	2008	13.2222	2010	2013	
Karl T, 2010, SCIENCE, V330, P816, DOI	2010	8.2194	2011	2012	
Loreto F, 2010, TRENDS PLANT SCI, V15, P154, DOI	2010	21.1869	2011	2018	
Canagaratna MR, 2007, MASS SPECTROM REV, V26, P185, DOI	2007	5.5608	2011	2015	
Penuelas J, 2010, TRENDS PLANT SCI, V15, P133, DOI	2010	28.7018	2011	2018	
Niinemets U, 2010, BIOGEOSCIENCES, V7, P1809, DOI	2010	7.8909	2011	2013	
Hallquist M, 2009, ATMOS CHEM PHYS, V9, P5155, DOI	2009	51.7047	2011	2017	
van der Werf GR, 2006, ATMOS CHEM PHYS, V6, P3423, DOI	2006	9.1893	2011	2014	
Niinemets U, 2010, BIOGEOSCIENCES, V7, P2203, DOI	2010	8.0621	2011	2013	
Peeters J, 2009, PHYS CHEM CHEM PHYS, V11, P5935, DOI	2009	14.5829	2011	2015	
Jimenez JL, 2009, SCIENCE, V326, P1525, DOI	2009	35.3983	2011	2017	
Karl M, 2009, BIOGEOSCIENCES, V6, P1059, DOI	2009	7.4313	2011	2016	

Zhang Q, 2007, GEOPHYS RES LETT, V34, P0, DOI	2007	17.4026	2011	2015
Forster P, 2007, CLIMATE CHANGE 2007: THE PHYSICAL SCIENCE BASIS, V0, P129	2007	12.9144	2011	2013
Aiken AC, 2008, ENVIRON SCI TECHNOL, V42, P4478, DOI	2008	11.1402	2011	2015
Pacifico F, 2009, ATMOS ENVIRON, V43, P6121, DOI	2009	8.1336	2011	2015
Robinson AL, 2007, SCIENCE, V315, P1259, DOI	2007	16.3069	2011	2015
Stavrakou T, 2010, ATMOS CHEM PHYS, V10, P9863, DOI	2010	7.0434	2011	2012
Paulot F, 2009, SCIENCE, V325, P730, DOI	2009	24.0116	2011	2017
Niinemets U, 2010, TRENDS PLANT SCI, V15, P145, DOI	2010	11.8662	2011	2018
Grell GA, 2005, ATMOS ENVIRON, V39, P6957, DOI	2005	9.4617	2012	2013
Arneth A, 2011, ATMOS CHEM PHYS, V11, P8037, DOI	2011	14.9179	2012	2016
Fowler D, 2009, ATMOS ENVIRON, V43, P5193, DOI	2009	7.0925	2012	2013
Seinfeld J H, 2006, ATMOSPHERIC CHEM PHY, V0, P0	2006	6.9818	2012	2014
Ervens B, 2011, ATMOS CHEM PHYS, V11, P11069, DOI	2011	6.9633	2012	2020
Curci G, 2009, ATMOS ENVIRON, V43, P1444, DOI	2009	9.2749	2012	2014
Heald CL, 2009, GLOBAL CHANGE BIOL, V15, P1127, DOI	2009	10.1971	2012	2014
Paulot F, 2009, ATMOS CHEM PHYS, V9, P1479, DOI	2009	11.4963	2012	2016

Jacob DJ, 2009, ATMOS ENVIRON, V43, P51, DOI	2009	14.9415	2012	2017	
Jordan A, 2009, INT J MASS SPECTROM, V286, P122, DOI	2009	7.6596	2013	2016	
Surratt JD, 2008, J PHYS CHEM A, V112, P8345, DOI	2008	8.1394	2013	2016	
Kleindienst TE, 2007, ATMOS ENVIRON, V41, P8288, DOI	2007	8.2691	2013	2014	
Heald CL, 2008, J GEOPHYS RES-ATMOS, V113, P0, DOI	2008	10.7957	2013	2016	
Carlton AG, 2009, ATMOS CHEM PHYS, V9, P4987, DOI	2009	18.8504	2013	2017	
Surratt JD, 2010, P NATL ACAD SCI USA, V107, P6640, DOI	2010	22.3307	2013	2018	
Zhang Q, 2009, ATMOS CHEM PHYS, V9, P5131, DOI	2009	18.4056	2013	2017	
Lamarque JF, 2010, ATMOS CHEM PHYS, V10, P7017, DOI	2010	16.3425	2013	2018	
Kroll JH, 2006, ENVIRON SCI TECHNOL, V40, P1869, DOI	2006	6.906	2013	2014	
Kim S, 2010, ATMOS CHEM PHYS, V10, P1759, DOI	2010	8.2691	2013	2014	
Spracklen DV, 2011, ATMOS CHEM PHYS, V11, P12109, DOI	2011	16.6	2013	2015	
Graus M, 2010, J AM SOC MASS SPECTR, V21, P1037, DOI	2010	8.1485	2013	2018	
Kerminen VM, 2012, ATMOS CHEM PHYS, V12, P12037, DOI	2012	7.6018	2014	2015	
Arneth A, 2010, NAT GEOSCI, V3, P525	2010	6.5297	2014	2017	
Mao J, 2012, ATMOS CHEM PHYS, V12, P8009, DOI	2012	8.1876	2014	2015	

Carlton AG, 2010, ENVIRON SCI TECHNOL, V44, P3376, DOI	2010	9.3353	2014	2017
Riipinen I, 2011, ATMOS CHEM PHYS, V11, P3865, DOI	2011	9.243	2014	2018
Kroll JH, 2008, ATMOS ENVIRON, V42, P3593, DOI	2008	18.6203	2014	2016
Guenther AB, 2012, GEOSCI MODEL DEV, V5, P1471, DOI	2012	107.4813	2014	2020
van der Werf GR, 2010, ATMOS CHEM PHYS, V10, P11707, DOI	2010	15.1521	2014	2018
Emmons LK, 2010, GEOSCI MODEL DEV, V3, P43, DOI	2010	18.1147	2014	2018
Carslaw KS, 2010, ATMOS CHEM PHYS, V10, P1701, DOI	2010	9.3597	2014	2015
Shilling JE, 2013, ATMOS CHEM PHYS, V13, P2091, DOI	2013	6.867	2014	2016
Crounse JD, 2011, PHYS CHEM CHEM PHYS, V13, P13607, DOI	2011	9.6644	2014	2018
Paasonen P, 2013, NAT GEOSCI, V6, P438	2013	18.9893	2014	2018
Kulmala M, 2013, SCIENCE, V339, P943, DOI	2013	14.7294	2014	2018
Ehn M, 2014, NATURE, V506, P476, DOI	2014	40.4109	2015	2020
Kurokawa J, 2013, ATMOS CHEM PHYS, V13, P11019, DOI	2013	7.2229	2015	2020
Scott CE, 2014, ATMOS CHEM PHYS, V14, P447, DOI	2014	6.1583	2015	2018
Carlton AG, 2011, ENVIRON SCI TECHNOL, V45, P4438, DOI	2011	6.2441	2015	2017
Riccobono F, 2014, SCIENCE, V344, P717, DOI	2014	10.4339	2015	2018
Mao JQ, 2013, J GEOPHYS RES-ATMOS, V118, P11256, DOI	2013	5.0953	2015	2020

Ulbrich IM, 2009, ATMOS CHEM PHYS, V9, P2891, DOI	2009	7.8134	2015	2017	
Goldstein AH, 2009, P NATL ACAD SCI USA, V106, P8835, DOI	2009	14.0765	2015	2017	
Niinemets U, 2011, BIOGEOSCIENCES, V8, P2209, DOI	2011	7.8081	2015	2017	
Makkonen R, 2012, ATMOS CHEM PHYS, V12, P10077, DOI	2012	3.7299	2015	2020	
Zhang X, 2014, P NATL ACAD SCI USA, V111, P5802, DOI	2014	7.2866	2015	2017	
Ng NL, 2010, ATMOS CHEM PHYS, V10, P4625, DOI	2010	6.7653	2015	2017	
Back J, 2012, BIOGEOSCIENCES, V9, P689, DOI	2012	11.4623	2015	2017	
Sindelarova K, 2014, ATMOS CHEM PHYS, V14, P9317, DOI	2014	26.926	2015	2020	
Muller JF, 2008, ATMOS CHEM PHYS, V8, P1329	2008	7.3476	2015	2016	
Jokinen T, 2015, P NATL ACAD SCI USA, V112, P7123, DOI	2015	26.5537	2016	2020	
Boyd CM, 2015, ATMOS CHEM PHYS, V15, P7497, DOI	2015	8.6411	2016	2017	
Holopainen JK, 2010, TRENDS PLANT SCI, V15, P176, DOI	2010	12.2688	2016	2018	
Xu L, 2015, P NATL ACAD SCI USA, V112, P37, DOI	2015	26.0675	2016	2020	
Darer AI, 2011, ENVIRON SCI TECHNOL, V45, P1895, DOI	2011	8.064	2016	2017	
Huang RJ, 2014, NATURE, V514, P218, DOI	2014	16.5026	2016	2020	
Hakola H, 2012, ATMOS CHEM PHYS, V12, P11665, DOI	2012	7.4102	2016	2018	

Noziere B, 2015, CHEM REV, V115, P3919, DOI	2015	9.7958	2016	2017	
Lee BH, 2014, ENVIRON SCI TECHNOL, V48, P6309, DOI	2014	6.7234	2016	2020	
Calfapietra C, 2013, ENVIRON POLLUT, V183, P71, DOI	2013	9.1286	2017	2020	
Canagaratna MR, 2015, ATMOS CHEM PHYS, V15, P253, DOI	2015	7.5147	2017	2020	
Stein AF, 2015, B AM METEOROL SOC, V96, P2059, DOI	2015	9.963	2017	2018	
Akagi SK, 2011, ATMOS CHEM PHYS, V11, P4039, DOI	2011	12.3601	2017	2020	
Crounse JD, 2013, J PHYS CHEM LETT, V4, P3513, DOI	2013	9.6668	2017	2020	
Kirkby J, 2016, NATURE, V533, P521, DOI	2016	11.7257	2017	2018	
Pye HOT, 2010, ATMOS CHEM PHYS, V10, P11261, DOI	2010	8.7886	2017	2018	
Hoyle CR, 2011, ATMOS CHEM PHYS, V11, P321, DOI	2011	4.0574	2017	2020	
Fry JL, 2014, ENVIRON SCI TECHNOL, V48, P11944, DOI	2014	12.3601	2017	2020	
Hu WW, 2015, ATMOS CHEM PHYS, V15, P11807, DOI	2015	8.7886	2017	2018	
Trostl J, 2016, NATURE, V533, P527, DOI	2016	12.3601	2017	2020	
Marais EA, 2016, ATMOS CHEM PHYS, V16, P1603, DOI	2016	7.5147	2017	2020	
Lelieveld J, 2015, NATURE, V525, P367, DOI	2015	8.2016	2017	2018	
Harrison SP, 2013, NEW PHYTOL, V197, P49, DOI	2013	6.8469	2017	2020	
Li M, 2014, ATMOS CHEM PHYS, V14, P5617, DOI	2014	4.2108	2017	2020	

Budisulistiorini SH, 2015, ATMOS CHEM PHYS, V15, P8871, DOI	2015	7.6148	2017	2018	
Lee BH, 2016, P NATL ACAD SCI USA, V113, P1516, DOI	2016	15.0568	2017	2020	
Ayres BR, 2015, ATMOS CHEM PHYS, V15, P13377, DOI	2015	8.3813	2018	2020	
Penuelas J, 2014, PLANT CELL ENVIRON, V37, P1866, DOI	2014	8.8309	2018	2020	
Jenkin ME, 2015, ATMOS CHEM PHYS, V15, P11433, DOI	2015	8.9811	2018	2020	
Lopez-Hilfiker FD, 2014, ATMOS MEAS TECH, V7, P983, DOI	2014	7.7816	2018	2020	
Zhang HF, 2018, P NATL ACAD SCI USA, V115, P2038, DOI	2018	8.3813	2018	2020	
Ng NL, 2017, ATMOS CHEM PHYS, V17, P2103, DOI	2017	11.9826	2018	2020	
Travis KR, 2016, ATMOS CHEM PHYS, V16, P13561, DOI	2016	7.1821	2018	2020	
Monks PS, 2015, ATMOS CHEM PHYS, V15, P8889, DOI	2015	8.3813	2018	2020	

The final significant hotspot identified in the literature was plant-microbe interactions, consisting of three subclusters as per Table 3.5, Figure 3.3, and Figure 3.6. Studies in this hotspot were related to topics including (1) plant-microbe communications (e.g., seasonality, microbe, soil, plant); and (2) SBVOCs emission (e.g., photosynthesis, decomposition, temperature, meteorological effects, climate change, vertical profiles). "MVOC" has drawn increasing public attention over time, with keyword frequencies ranging from 2 to 21 (Table 3.3). The top four articles with the strongest bursts, published during 1991–2014 and frequently cited during 1996–2020, were primarily related to the impact of airborne pollutants on plants through the uptake of soils and roots and the exchange of VOCs between soils and atmosphere, with the strengths of 8.1–8.9 (Table 3.6).

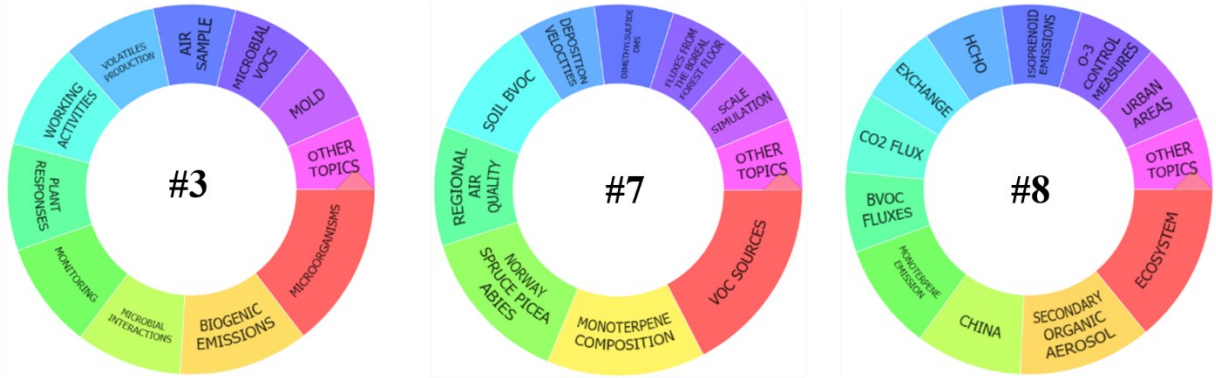

Figure 3.6. Subclusters of plant-microbe interactions: microbial and soil BVOCs (Cluster #3, #7, #8) (produced by Carrot[2]).

3.3.3. Preliminary evolution of the research hotspots

The evolution of research hotspots of BVOC emissions was ascertained preliminarily from keyword citation bursts, listed in Table 3.7, showing the top 362 references and 14 keywords with citation bursts, respectively. Biogenic hydrocarbon and isoprene emissions were identified as

research hotspots that have been trending since 1991, while MTs and SQTs were identified as topics that have been attracting researchers' attention since 2005. VOC emissions from rotted plant materials and soil microorganisms have also been an area of consideration in BVOC emission studies beginning in 2008. Notably, the formation of aerosols and PM through BVOC oxidation and the emission of BVOCs from ecosystems, including plants and soil microorganisms, were identified as topics that have garnered increasing attention since 2014, and which may continue to trend in this direction in future.

Table 3.7. Top 14 keywords with the strongest citation bursts (produced by CiteSpace).

Keywords	Year	Strength	Begin	End	1991 - 2020
Biogenic emission	1991	23.2934	1992	2003	
Isoprene	1991	11.9757	1994	2003	
Terpene	1991	3.6037	1994	2000	
Biogenic hydrocarbon	1991	4.3852	1995	2004	
Nitric oxide	1991	5.6375	1997	2002	
Seasonal variation	1991	4.1258	1997	2007	
Monoterpene	1991	4.7383	2005	2007	
Sesquiterpene	1991	8.1319	2006	2011	
MVOC	1991	3.6182	2008	2010	
PTR-MS	1991	3.8637	2011	2015	
Aerosol	1991	5.0014	2014	2020	
Drought	1991	4.1565	2015	2020	
PM	1991	3.4987	2016	2020	
Plant-microbe interaction	1991	3.5884	2017	2020	

Note: The small rectangles in the rightmost column denote the 30 years 1991–2020 and the red indicates that citations increase dramatically.

3.3.4. Publication distribution among reclassified hotspots

Of the 362 references with citation bursts, six lacked valid information, while 157, 142, and 19 publications were concentrated on hotspots (a), (b), and (c), respectively, as per Table 3.6 and Figure 3.7. Hotspots (a) and (b) were found to have been studied simultaneously in 38 publications since 1991, a finding which suggests that, within the field of atmospheric chemistry and climate change, BVOCs as precursors of aerosols and pollutants have drawn attention since the early stage of BVOC emission studies. Only three of 19 publications in the hotspot (c) were concentrated on SBVOC emissions, while others were related to soil fluxes of nitrogen oxides (NOx), which means that further work focused on SBVOC emissions is required. Among 362 references, nearly half of them were conducted with measurements while review papers had the highest average citation strengths compared to observations and simulations. This means that modeling BVOC emissions, especially from soils and their interactions with oxidation products is required in future.

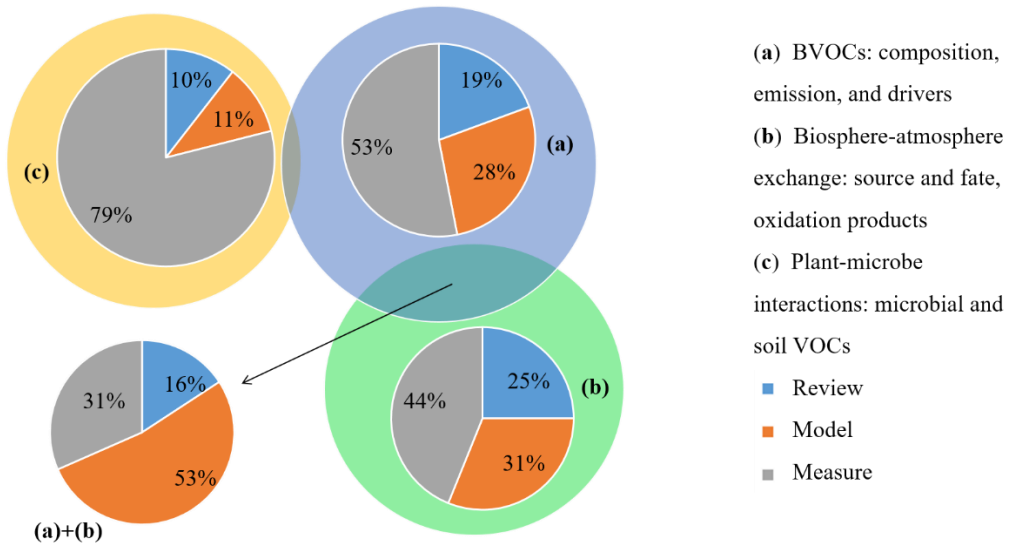

Figure 3.7. Publication distributions of the study methodology of different hotspots among 356 references with citation bursts.

After the search period, the pandemic began and caused a global lockdown, probably affecting anthropogenic activities and environmental impacts, so we further extended this search to May 2021. Recent studies found that emissions of AVOCs, e.g., benzene, toluene, ethylbenzene and xylenes (BTEX), were more affected by lockdown compared to BVOCs including HCHO and isoprene (Pakkattil et al., 2021; Sbai et al., 2021). This pandemic has caused the resurgence of studies on BVOCs and human health due to the healing effects of BVOCs, e.g., *α*-pinene, *d*-limonene, and 3-carene, on human physiological and mental health (Choi et al., 2021; Zabini et al., 2020). For example, Mediterranean plants reduced COVID-19 mortality in Italian forested areas due to some immuno-modulating PBVOCs (Roviello and Roviello, 2021; Sytar et al., 2021). This indicates that finding PBVOCs for the development of natural antivirals might be a future direction.

3.3.5. Sources and sinks of SBVOCs

Soil and litterfall released small amounts of ethanol but high amounts of terpenes (i.e., approximately 12% to 136% of canopy MT emissions) and BOVOCs (e.g., MeOH, acetaldehyde, and acetone) (Faiola et al., 2014; Schade et al., 2011). As an important source of C_1−C_3 BOVOCs, global decaying and dried vegetation emitted 6.8 to 15 Tg C yr^{-1} MeOH and 3.7 to 5 Tg C yr^{-1} acetone (Fall, 2003). Aldehydes (e.g., acrolein) were primarily produced by living and fresh leaves, and then subsequently volatilized more from green biomass than microbial degradation of decayed leaf litter (Figure 3.8). Notably, sustainable bioenergy resources, such as ethanol, CH_4, and hydrogen, could be produced from bioresources including agricultural and other biomass residues, i.e., corn stover, wheat straw and forest residues, through human-controlled microbial processes

(Gaurav et al., 2017). Although there were BVOC and GHG emissions from soils or residues, biomass stored in residues could significantly reduce GHG emissions from fossil energy burning and improve energy independence (Zheng and Qiu, 2020).

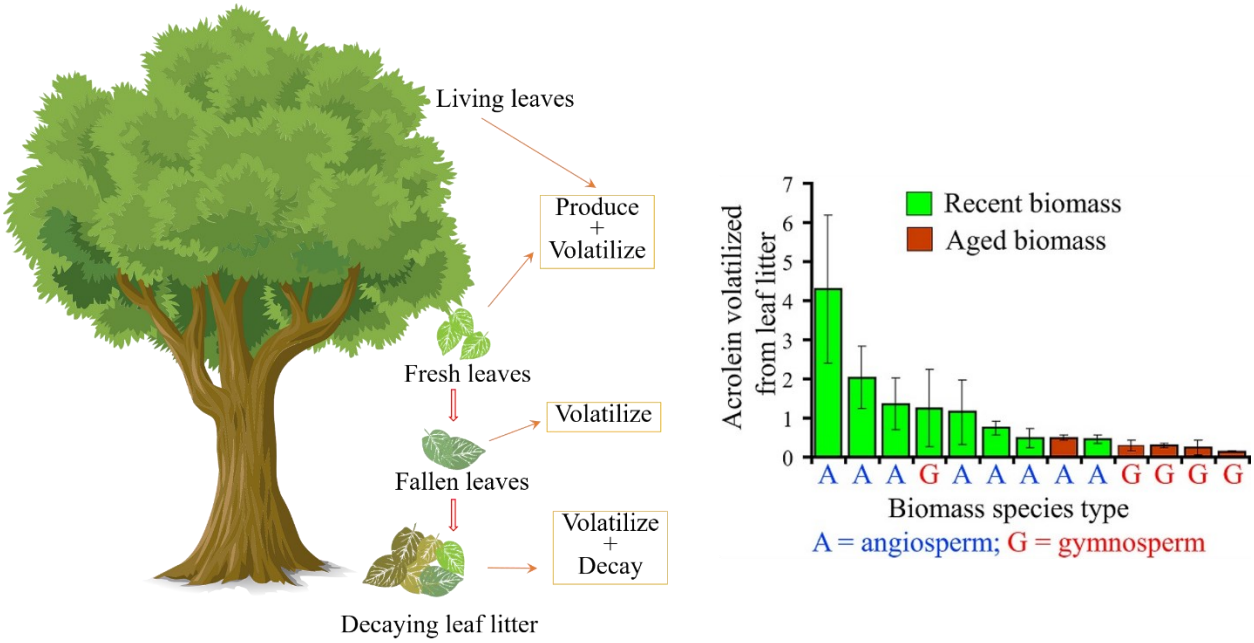

Figure 3.8. The presence of aldehydes (e.g., acrolein) in decaying leaf litter on the forest floor (Ehrlich and Cahill, 2018).

Previous studies found forest floor is an important contributor to forest-scale BVOC emissions due to the synthesis and emission of BVOCs from shedding vegetation and living roots as well as the microbial decomposition of litter and SOM (Cai et al., 2020; Feng et al., 2020). Its BVOC fluxes showed a seasonal trend with the greatest fluxes being in summer and spring, while its contributions of forest-stand fluxes varied between seasons with the smallest being in summertime (below 5% of forest-stand fluxes) and the greatest being in autumn. Compared to forest-scale

fluxes, SBVOC fluxes accounted for 1-72% of MeOH in spring and early summer and 2-93% of MT in spring and autumn in the northern hemisphere (Maki et al., 2019). BVOC emissions from soils were typically 1 to 2 orders of magnitude below those from above-ground plants (Penuelas et al., 2014). For example, net BVOC emissions from soil and roots contributed only negligibly to forest-scale emissions from well-drained heathlands beyond the growing period (Rinnan et al., 2013).

SBVOC emissions could reach the same magnitude as canopy emissions under the right combination of conditions, including temperatures, pH, SOM, and soil moisture, for specific ecosystems (Penuelas et al., 2014). For instance, frequent forest wildfires and permafrost thawing in boreal forests as a result of global warming will affect BVOC emissions, as these changes will increase microbial decomposition of SOM and alter the vegetation composition of the forest floor. MT emissions from high-temperature soils in summer, meanwhile, could increase with the increasing availability of nitrogen (Loreto and Sharkey, 1993). Forest wildfires will result in a decrease in vegetation coverage and SOM decomposition, and consequently lower BVOC emissions than before the wildfires (Zhang-Turpeinen et al., 2020a). SBVOC emissions tend to increase with the product of soil pH with SOM because pH can affect nutrient availability and microorganism physiology (Abis et al., 2018; Chen et al., 2020). Moreover, the increased soil moisture caused by SOM may promote the increased amount and diversity of BVOCs in anaerobic conditions—rather than CO_2 as the end product of microbial decomposition in aerobic conditions—emitted from soils in microsites (Seewald et al., 2010; Yao et al., 2020). Nonetheless, the increased soil moisture will cause a decrease in BVOC emissions from the hemi-boreal forest floor. This is due to decreases in gas diffusion in soil, together with increases in microbial VOC

uptake in soil, VOC dissolution into soil water, wet deposition of VOCs on the soil surface, and VOC leaching towards underlying soil layers and even the bedrock (Maki et al., 2019). In general, the net deposition of BVOCs is correlated inversely with ambient concentrations, and it will decrease due to the above-ground presence of non- or low-emitting plants (Spielmann et al., 2017). The sources and sinks of SBVOCs and the drivers for sink and emission processes, it should be noted, have been studied in recent work (Tang et al., 2019a). However, soil VOC fluxes have not been considered when modelling global BVOC emissions from terrestrial ecosystems. Future attention should be given to manipulated or long-term measurements of SBVOC emissions, including root and litter emissions and microbial decomposition responding to diverse environmental factors in primary soil types at stand scales.

3.3.6. Effects of anthropogenic activities on BVOC emissions

Studies related to the source apportionment and degradation mechanism of VOCs are essential for abatement measures of ground-level O_3, SOA, and PM. Compared to biogenic emissions, anthropogenic emissions from transportation and industrial sources played a key role in the production and emission of VOCs, O_3, SOA, and PM in urban areas (Figure 3.9 and Table 3.8). In most cases, the industry was the largest contributor to concentrations of VOCs, O_3, and SOA (7.5-66.1%, 11.5-65.0%, and 25.7-33.0%, respectively), followed by transportation emissions (15.0-64.3%, 12.5-39.0%, and 3.3-34.0%, respectively). Apart from traffic and industrial sources, SOAs and secondary inorganic aerosols (SIAs) were an important contributor to PM concentration (32.5±25.9%). Thus, the reduction of industrial solvents and daily automobiles using fossil energy sources may be beneficial to air quality in urban cities. However, concerning the VOC-derived pollutants, biogenic emissions were found to be a higher relative contributor compared to

automobile, residential, and industrial emissions during the summertime (Escudero et al., 2015). Isoprene emission was usually related to local emissions sources, while MTs trends were more likely associated with distant sources (Detournay et al., 2013). The contribution of biogenic sources to isoprene emission in rural areas was significantly higher than that in urban areas (over 90% for rural versus 30–40% for urban) (Kashyap et al., 2019).

Figure 3.9 (b-d) shows that the biogenic source was the largest contributor of O_3, SOA, and PM derived from precursor VOCs in most cases. Methylglyoxal (MGO) and HCHO were the major oxidation products of methyl vinyl ketone (MVK) and methacrolein (MACR), which were the main intermediate products of isoprene's photochemical oxidation (Ling et al., 2019). HCHO, mainly distributed in 0–100 m and derived from biogenic emissions (particularly oxidation of BVOCs with 37%) and biomass burning with energy transfers (Xing et al., 2020), was the top contributor to O_3 pollution in urban cities. As such, reducing VOC emissions of major chemical species was higher effective than controlling their total emissions for air pollution control (Kumar et al., 2019; Zhu et al., 2020a).

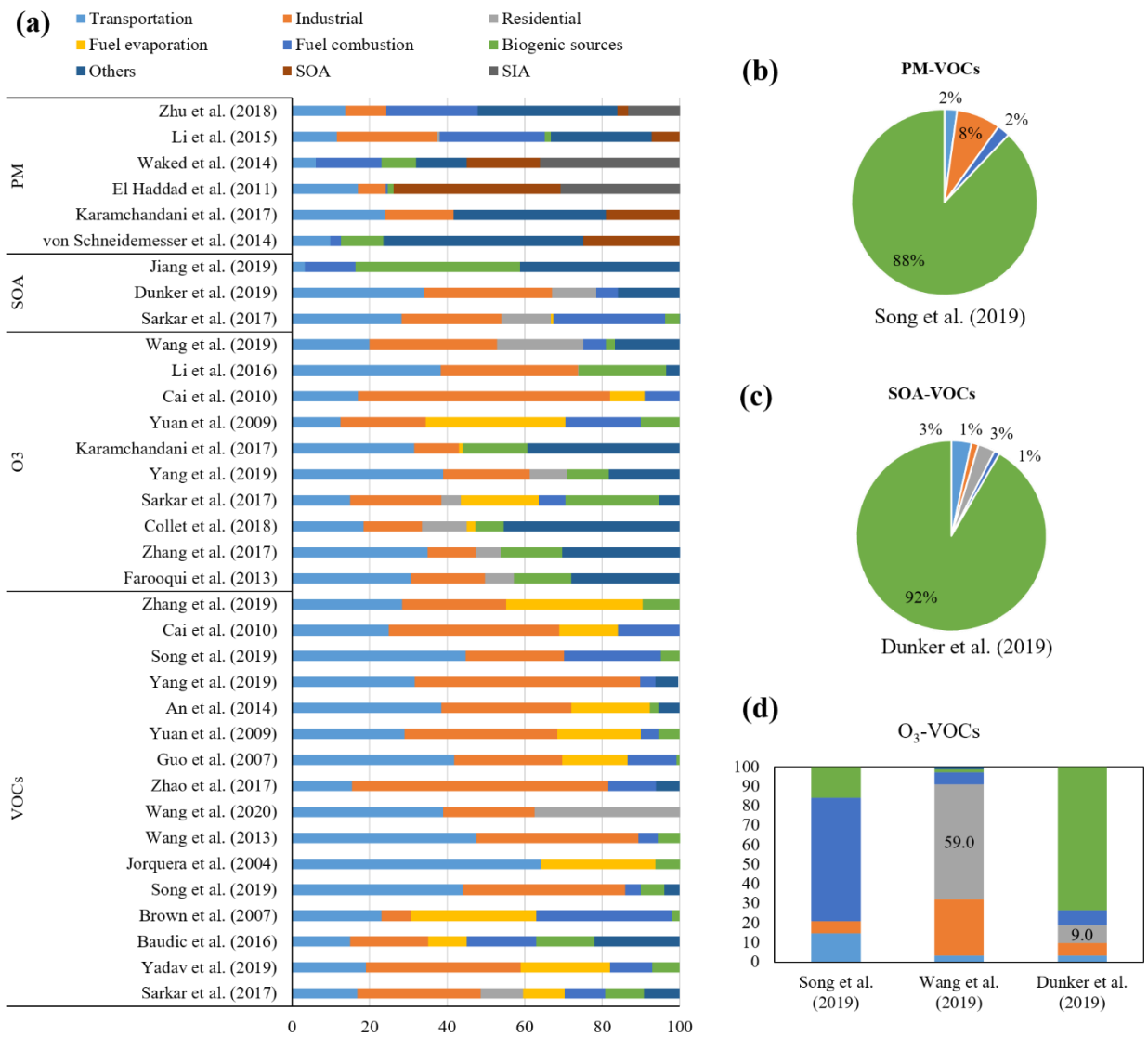

Figure 3.9. Source-sector contributions (%) to total VOCs, O_3, SOA, and PM (a) and to partial PM (b), SOA (c), and O_3 (d) derived from precursor VOCs. Detailed study information and references included in this figure are listed in Table 3.8.

Table 3.8. Previous studies about source appointment of VOCs, O_3, SOA, and PM.

Category	Study	Method	Region and time	T[a]	I[b]	R[c]	FE[d]	FC[e]	B[f]	Others	SOA	SIA
VOCs	Sarkar et al. (2017)	PMF[1]	Kathmandu Valley, Bagmati Pradesh, Nepal, 2012-2013	16.8	31.9	10.9	10.8	10.4	10.0	9.2		
	Yadav et al. (2019)	PMF	western India, 2015	19.0	40.0		23.0	11.0	7.0			
	Baudic et al. (2016)	PMF	Paris megacity, France, 2010	15.0	20.0		10.0	18.0	15.0	22.0		
	Brown et al. (2007)	PMF	Azusa and Hawthorne, USA, 2001	23.0	7.5		32.5	35.0	2.0			
	Song et al. (2019b)	CMB[2] / PMF / CTM[3]	Seoul, Korea, 2013-2015	44.0	42.0			4.0	6.0	4.0		
	Jorquera and Rappengluck (2004)	UNMIX[4] / PMF	Santiago, Chile, 1996 spring	64.3			29.5		6.3			
	Wang et al. (2013)	PMF	Shanghai, China, 2009-2010	47.6	41.7			5.0	5.8			
	Wang et al. (2020a)	PMF	Nanjing, China, 2016	38.9	23.6	37.6						
	Zhao et al. (2017)	PCA[5]/APCS[6]	Jiangsu, China, 2005-2014	15.4	66.1			12.4		6.0		
	Guo et al. (2007)	PCA/APCS	Hong Kong, China, 2002-2003	41.8	28.0		16.8	12.8	0.8			
	Yuan et al. (2009)	PMF	Beijing, China, 2006	29.0	39.5		21.5	4.5	5.5			

	An et al. (2014)	PCA/APCS	Nanjing, China, 2011-2012	38.5	33.5		20.3		2.3	5.5
	Yang et al. (2019)	NAQPMS[7]	PRD[15], China, 2016	31.7	58.2			3.8		6.0
	Song et al. (2019a)	PMF	Langfang, north China, 2016-2017	44.8	25.4			24.9	4.9	
	Cai et al. (2010)	PMF / MIR[8]	Shanghai, China, 2007-2010	25.0	44.0		15.0	16.0		
	Zhang et al. (2019)	PMF	Guilin, southwest China, 2018	28.3	26.9		35.3		9.5	
O_3	Farooqui et al. (2013)	CAMx[9] / OSAT[10]	Texas, USA, 2002 September	30.5	19.3	7.5			14.8	28.0
	Zhang et al. (2017)	CAMx / OSAT	USA, 2011 September	34.8	12.6	6.4			15.9	30.4
	Collet et al. (2018)	CMAQ[11] / ISAM[12]	USA, 2030 summer	18.3	15.2	11.6	2.2		7.4	45.4
	Sarkar et al. (2017)	PMF	Kathmandu Valley, Bagmati Pradesh, Nepal, 2012-2013	15.0	23.5	5.0	20.2	6.8	24.2	5.2
	Yang et al. (2019)	NAQPMS	PRD, China, 2016	39.0	22.3	9.8			10.8	18.3
	Karamchandani et al. (2017)	CAMx / OSAT / PSAT[13]	Europe, 2010	31.4	11.5		1.0		16.6	39.4
	Yuan et al. (2009)	PMF	Beijing, China, 2006	12.5	22.0		36.0	19.5	10.0	
	Cai et al. (2010)	PMF / MIR	Shanghai, China, 2007-2010	17.0	65.0		9.0	9.0		
	Li et al. (2016)	OSAT / CAMx	YRD[16], China, 2013 summer	38.3	35.5	0.2			22.5	3.5
	Wang et al. (2019c)	OSAT / CAMx	China, 2013 August	20.0	33.0	22.2		5.9	2.3	16.7

SOA	Sarkar et al. (2017)	PMF	Kathmandu Valley, Bagmati Pradesh, Nepal, 2012-2013	28.2	25.7	12.8	0.6	28.9	3.7	0.1		
	Dunker et al. (2019)	CMAQ / PIM	Houston, USA, 2013 September / 2028 summer	34.0	33.0	11.5		5.5		16.0		
	Jiang et al. (2019a)	CAMx / VBS[14]	Europe, 2011	3.3				13.0	42.5	41.2		
PM	von Schneidemesser et al. (2018)	CMB	Berlin, Germany, 2014 summer	9.8				2.7	11.1	51.5	24.9	
	Karamchandani et al. (2017)	CAMx / OSAT / PSAT	Europe, 2010	24.1	17.6					39.2	19.1	
	El Haddad et al. (2011)	CMB	Marseille, France), 2008 summer	17.0	7.1			0.5	1.6		43.0	31.0
	Waked et al. (2014)	PMF	Lens, France, 2012	6.0				17.0	9.0	13.0	19.0	36.0
	Li et al. (2015b)	PSAT / CAMx	YRD, China, 2013 January	11.6	25.9	0.6		27.1	1.5	26.1	7.2	
	Zhu et al. (2018)	CMB / PMF / PCA	China, 1987–2017	13.7	10.5			23.7		36.0	2.8	13.8
VOCs-O3	Song et al. (2019b)	CMB / PMF / CTM	Seoul, Korea, 2013-2015	14.7	6.3			63.2	15.8			
	Wang et al. (2019c)	OSAT / CMAQ	China, 2013 August	3.3	28.7	59.0		5.9	1.8	1.2		
	Dunker et al. (2019)	CMAQ / PIM	Houston, USA, 2013 September / 2028 summer	3.4	6.4	9.0		7.8	73.5			

VOCs-SOA	Dunker et al. (2019)	CMAQ / PIM	Houston, USA, 2013 September / 2028 summer	3.4	1.2	2.9	0.9	91.6
VOCs-PM	Song et al. (2019b)	CMB / PMF / CTM	Seoul, Korea, 2013-2015	2.2	7.7		2.2	87.9

Note: [a] Transportation; [b] Industrial; [c] Residential; [d] Fuel evaporation; [e] Fuel combustion; [f] Biogenic sources. [1] Positive Matrix Factorization; [2] Chemical Mass Balance; [3] Chemical Transport Model; [4] EPA's Unmix Model; [5] Principal Component Analysis; [6] Absolute Principal Component Scores; [7] Nested Air Quality Prediction Modeling System; [8] Maximum Incremental Reactivity; [9] Comprehensive Air Quality Model with Extensions; [10] Ozone Source Apportionment Technology; [11] Community Multiscale Air Quality Modeling System; [12] Integrated Source Apportionment Method; [13] Particulate Matter Source Apportionment Technology; [14] Volatility Basis Set; [15] Pearl River Delta; [16] Yangtze River Delta.

Anthropogenic activities such as crop cultivation and urban greening may affect the emission of BVOCs and the formation of some BVOC-derived pollutants (e.g., O_3, SOA, and PM). As shown in Figure 3.10, BVOC-derived SOAs were possibly accelerated by anthropogenic precursors/aerosols. Biofuel plantations close to polluted areas could affect the living environment of surrounding people (Karlsson et al., 2020). There was a concern about ground-level O_3 related to biogenic and anthropogenic VOC emissions in large forested and agricultural areas at local scales (Gao et al., 2020). Urban trees, as a natural strategy for local climate regulation and air purification, emitted BVOCs which can significantly increase surface O_3 and SOA concentrations in urban areas (Margarita et al., 2013). Generally, BVOC photochemistry significantly contributed to local O_3 formation, showing a positive correlation between isoprene concentration and O_3 levels, especially in the NO-saturated atmosphere (Kim et al., 2013; Simon et al., 2019). Transported NOx and anthropogenic VOCs interacted with local BVOCs and then promoted chemical O_3 production and biogenic SOA formation (Wu et al., 2020). The concentration of isoprene-derived SOAs significantly decreased with reductions in SO_2 and NOx emissions because they were directly affected by sulfate abundance rather than particle acidity and/or moisture (Xu et al., 2015a). Interestingly, isoprenoids (particularly MTs and SQTs) could help to reduce O_3 concentrations in the canopy and sub-canopy because of their high atmospheric reactivity (Fares et al., 2012; Pallozzi et al., 2016). Thus, it is a challenge for plant selection considering the effect of BVOC emissions on O_3 uptake and formation (Calfapietra et al., 2013). For example, Eller et al. (Eller et al., 2011) proposed that BVOC emissions should be an important factor when selecting bioenergy crops. This is because most bioenergy crops were strong BVOC emitters, releasing several grams of BVOC per liter of fuel produced (Graus et al., 2013; Rosenkranz et al., 2015). BECCS and efficient agroforestry management might lead to net carbon benefits by storing carbon in

ecosystems and by producing renewable material and energy products (Favero et al., 2020; Gustavsson et al., 2021). Taking Qingdao City in China as an example, although BVOC emissions from green areas have been predicted to more than triple by 2050, the planting of low-emitting vegetation might mitigate BVOCs by up to 34% (Ren et al., 2017). Another study demonstrated that exotic plant species could emit 28-fold terpenes compared to natives in the same family (Prendez et al., 2013). Thus, native species and lower-emitting species with no or small reactive BVOC emissions would be selected to mitigate carbon emission and energy loss as well as to reduce the biogenic sources of O_3, SOA, and $PM_{2.5}$ from crop cultivation and urban greening (Tiwary and Kumar, 2014).

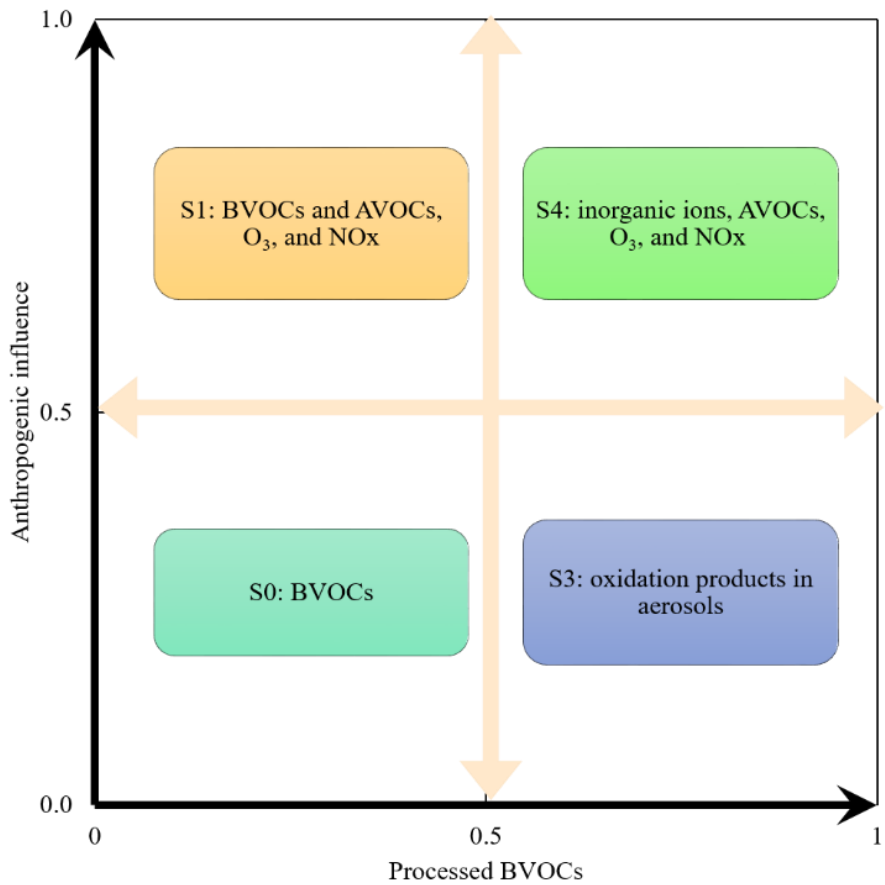

Figure 3.10. Controlling factors of BSOA formation concerning the extent of anthropogenic influence and BVOC processing under four scenarios with different dominated compositions (Mochizuki et al., 2015).

Those involved in decision-making in this area may consider trade-offs between the costs and benefits of ecosystem services. For example, the ratio of BVOC emissions to biomass production or energy transformation would be an effective tool for designers and decision-makers to incorporate BVOC emissions into urban landscaping (Giuntoli et al., 2020; Ren et al., 2017). The implementation of different management strategies will affect BVOC emissions and interacting atmospheric processes, which can jointly influence the concentration of major BVOCs and their oxidation products. Climate models and atmospheric chemical models can be coupled to evaluate these interactive processes. However, these models have not implemented bidirectional coupling with emission models. A coupling system for observing BVOC measurements and modeling atmospheric chemical processes is a promising direction for future work. Such a system, incorporating current climate models, would refine the description of aerosol conversion, together with its direct and indirect impacts. As such, it would assist in forming an earth system model that can express real-time online feedback on atmosphere vegetation. Based on the results of climate models and BVOC emission models, an index system that integrates key ecosystem service values and negative impacts could be established to support decision-making in plant selection and environmental management.

3.4. Summary

This study applied CiteSpace and Carrot^2 to analyze and visualize the BVOC emission-related studies published in journals between 1991 and 2020. BVOC emissions are closely related to atmospheric chemistry and climate effects. The main hotspots included BVOC emissions and drivers, BVOCs and their oxidation products in biosphere-atmosphere exchange and SBVOCs in plant-microbe interactions. Generally, BVOC emissions were affected by temperature, drought, solar radiation, humidity, availability of nutrients, CO_2, O_3, etc. Soils can act as both the sink and source of BVOCs through various soil processes that are affected by soil temperature, pH, SOM, and soil moisture. Anthropogenic activities might affect BVOC emissions and promote the formation of BVOC-derived pollutants (e.g., O_3, SOA, and PM). With the in-depth study of BVOC emissions, research hotspots and research frontier hotspots were found to vary at different stages. From the detected results of citation bursts, biogenic hydrocarbon and isoprene emissions have been the most significant research hotspots overall since 1991, while MTs and SQTs have attracted increasing attention from researchers since 2005. Beginning in 2008, research topics such as "MVOC" have emerged. There are some new directions in BVOC emission research, such as BVOC emissions from plant-soil ecosystems, BVOC-derived pollutants, and natural antivirals originating from PBVOCs. Incorporating BVOC emissions and their relationships with pollutants, biomass, and energy into environmental management and decision-making is a promising direction. The findings of this study can provide researchers with an in-depth understanding of BVOC emission mechanisms, and decision-makers with insights on emission mitigation and environmental management. The scientometric analysis conducted in this study can help minimize the subjectivity and bias compared to critical reviews, offer a holistic and quantitative analysis of previous BVOC studies, and identify the research gap and future directions in this area.

CHAPTER 4. ASSESSMENT OF BIOGENIC MEOH EMITTED FROM CROPS DURING GROWING SEASONS

4.1. Background

MeOH is typically the second-most plentiful VOC, after CH_4, in the remote troposphere. As the precursor of CO, HCHO, and O_3, it can be related to harmful oxidant concentration and air quality deterioration in urban regions (Bachy et al., 2018; Wells et al., 2014). In less polluted rural areas, MeOH can react with •OH, reduce atmospheric oxidation capacity, and increase CH_4 lifetime (Caravan et al., 2018). It can also act as a precursor for SOAs and PM that scatter solar radiation and increase cloudiness as cloud condensation nuclei (CCN) (Cai et al., 2017; 2019b; Shrivastava et al., 2017). Due to its plenitude and long lifetime compared to other VOCs, MeOH has an important impact on air quality, human health, and climate change (Caravan et al., 2018; Mozaffar, 2017). Biogenic MeOH emission from plants is a primary source of ambient MeOH (accounting for 80%–89%) and it generally exceeds emissions of all other VOCs except terpenoids measured above a variety of different ecosystems (Harley et al., 2007; Heikes et al., 2002).

Previous estimates have focused primarily on MeOH emissions from forests and grasses. For example, several studies have estimated the global biogenic MeOH emission based on the empirical algorithms proposed by Guenther et al. (1995) and Galbally and Kirstine (2002). These estimates have varied considerably—from 70 to 350 $Tg \cdot yr^{-1}$—with a mean of approximately 100 $Tg \cdot yr^{-1}$ (Harley et al., 2007; Stavrakou et al., 2011; Tie et al., 2003). Huve et al. (2007) proposed that cell wall expansion and stomatal conductance govern the dynamics of MeOH emission from plants during the growing stage. Brunner et al. (2007), meanwhile, simulated the temporal MeOH emissions from grasslands according to a simple parameterization of the LAI and water vapor flux.

However, croplands cover a significant proportion of the Earth's surface and, although they are negligible isoprene emitters, they may be a significant source of MeOH (Custer and Schade, 2007). Wheat was selected for this study due to its large farming in the world —accounting for 15.1% of the global cultivated area (FAO, 2018)—and because it is one of the fast-growing crops and large MeOH emitters (Mozaffar, 2017). Although crops such as wheat are regarded as a significant source of MeOH, there is scarce information regarding its emission inventories and controlling mechanisms from a crop ecosystem in the diverse development phases (Mozaffar, 2017). A few studies have measured MeOH emissions from wheat in chamber experiments or field observations. For example, Gomez et al. (2019) measured BVOC (including MeOH) emissions from wheat at the plant level using dynamic automated chambers only under controlled weather conditions during a 7-d ripening period. Bachy et al. (2020) observed ecosystem-scale BVOC (including MeOH) fluxes over a winter wheat field throughout the plant development period using an eddy covariance method without distinguishing plant and soil sources.

To date, though, no specific emission model for wheat MeOH spanning the different developmental stages has been proposed. The emission model proposed in the present study, then, extends these previous empirical models for BVOC emissions to encompass this scope (Bachy et al., 2016; Guenther et al., 2012; Stavrakou et al., 2011). Some meteorological parameters, such as ambient temperature, precipitation, solar radiation, etc., are collected and used to investigate the crop biomass and emission activity factor. The purpose of the present research is to (1) develop an emission model to simulate temporal differences and spatial distribution of MeOH emissions of spring wheat in different stages during the growing period; (2) evaluate the uncertainty and sensitivity in emission estimates; (3) quantify the effect of climate change on wheat MeOH

emissions; and (4) explore the relationships between biogenic MeOH and air pollutants. This study seeks to fill these gaps by modeling, for the first time, MeOH emissions from spring wheat in its various developmental stages. Moreover, it seeks to provide an updated method for the assessment of MeOH emission from spring wheat or other crops using limited weather data. The results can be used to develop appropriate strategies for regional emission management.

4.2. Methodology

4.2.1. The general process of biogenic MeOH emission from spring wheat during the growing period in Saskatchewan

The Canadian prairie province of Saskatchewan has a continental climate, with temperatures and precipitation varying greatly between seasons, and has over 40% of Canada's farmland (more than 60 million acres). This province is the largest contributor (approximately 30%) to Canada's crop production, including spring wheat, which is the principal crop in Canada, accounting for around 20% of crop production. In 2018, the total spring wheat production from Saskatchewan was approximately 8.7 million tonnes, accounting for 18% of Saskatchewan's total crop production and ranked as the third contributor except for all wheat and canola (Government of Canada, 2018). The cropping area in Saskatchewan is mainly in the southern and central regions of the province. From the southeast to the northwest, the crop area is divided into 17 crop districts in our study. The seeding of spring wheat in 2018 was collected (Government of Saskatchewan, 2018). It is assumed to be evenly distributed among the crop districts, as shown in Figure 4.1 (a). The northern crop districts have a comparatively higher seeding area, with the largest value seen in crop district 13 (D13), while no seedings are seen in D4 and D15. The historical weather data and solar resource data are collected (Government of Canada, 2016; 2018). Among the 17 crop districts, the mean

(T_{mean}, °C), minimum (T_{min}, °C), and maximum (T_{max}, °C) daily air temperatures, global solar radiation (R_s, Wh·m^{-2}), and mean daily wind speed at a height of 2 m (v, m·s^{-1}) are generally found to increase when moving from the northwest to the southeast, although this trend does not hold for the mean daily precipitation (P, mm), relative humidity (RH, %), and dewpoint temperature (T_d, °C), as shown in Figure 4.1 (b-i).

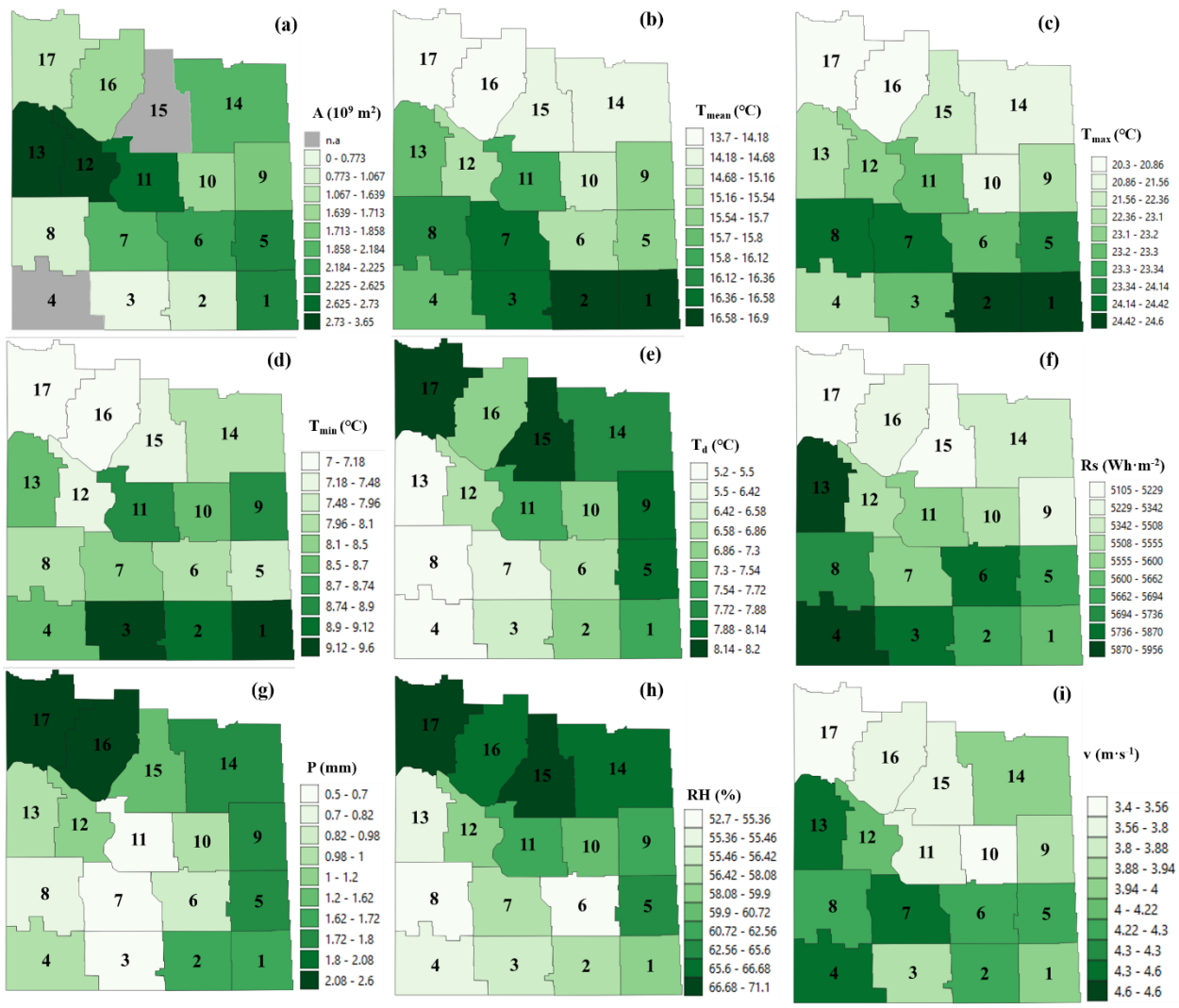

Figure 4.1. Seeding area of spring wheat and meteorological variables of different crop districts in Saskatchewan during growing stages in 2018. (a) Seeding area (A, 10^9 m^2); (b) Mean daily air temperature (T_{mean}, °C); (c) Maximum daily air temperature (T_{max}, °C); (d) Minimum daily air

temperature (T_{min}, °C); (e) Mean daily dewpoint temperature (T_d, °C); (f) Global solar radiation (Rs, Wh·m^{-2}); (g) Mean daily precipitation (P, mm); (h) Mean daily relative humidity (RH, %); (i) Mean daily wind speed at 2-m height (v, m·s^{-1}).

Although crop residue decomposition and soil-related emission phenomena continue throughout the spring, summer, and autumn until the soil becomes frozen in winter (Shi et al., 2021b), emissions from the leaves during the growing period are considered the principal source of MeOH emission by spring wheat. The growing season is assumed to span the period from May 1, 2018, to September 17, 2018, for the present study. According to Saskatchewan Crop Reports (Government of Saskatchewan, 2018), although the seeding and harvesting periods vary slightly among the different crop districts, the growing period of spring wheat generally can be divided into seven stages: germination (*G*: Day 1-7), emergence (*E*: Day 8-21), tillering (*T*: Day 22-42), heading (*H*: Day 43-70), flowering (*F*: Day 71-91), yield formation (*YF*: Day 92-126) and ripening (*R*: Day 127-140) (Figure 4.2). During the growing period, solar radiation and air temperature are generally higher in the T, H, F and YF stages than in the other stages (*S*, *E*, and *R*), while all meteorological variables are at a high level in the *T* stage.

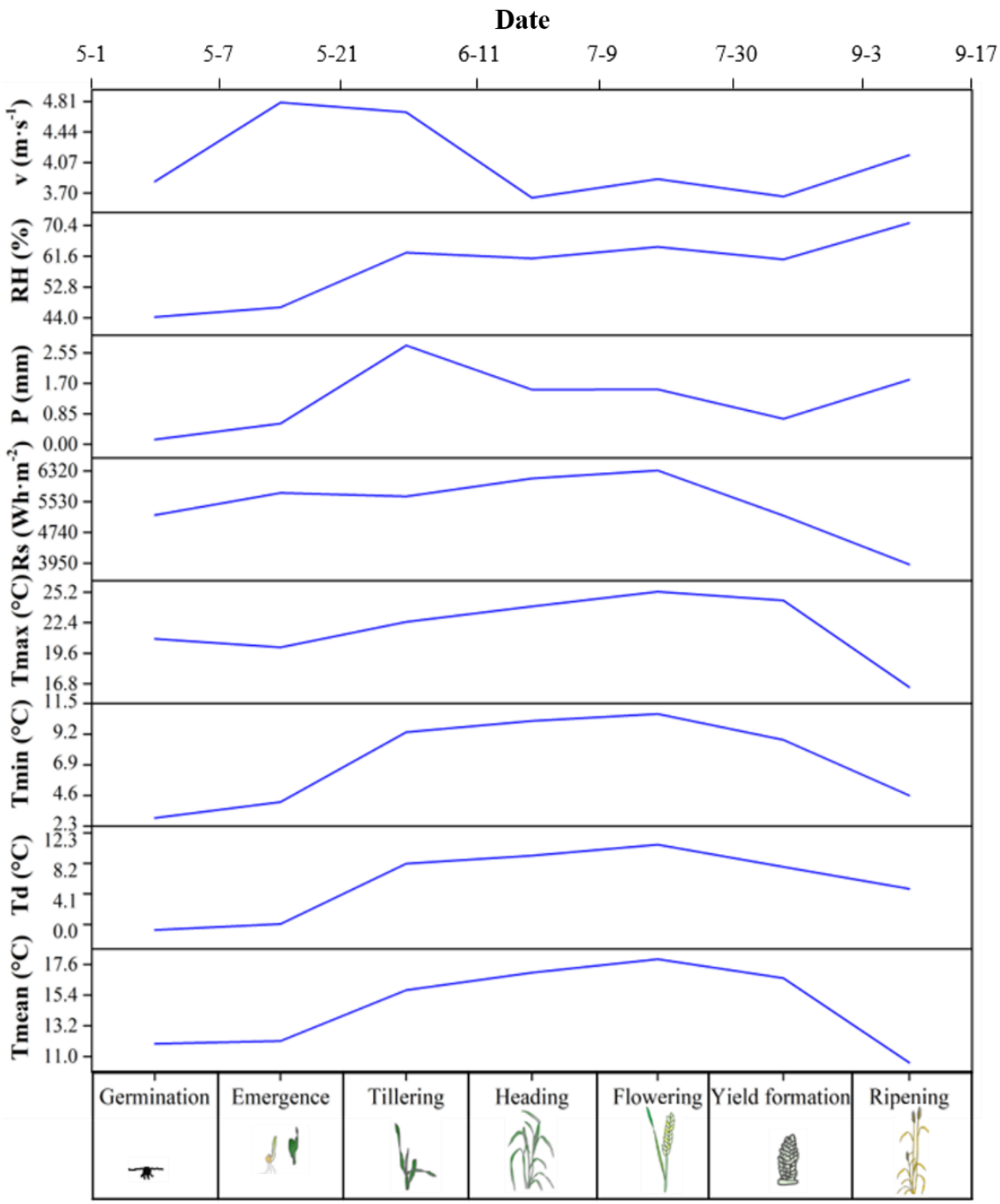

Figure 4.2. Changes in meteorological variables with the spring wheat phenology.

4.2.2. Biogenic MeOH emissions from crops during growing seasons

BVOCs are closely related to the amount of carbon accumulating in the growing period which depends on the balance (net primary production, *NPP*) of photosynthesis (gross primary production, *GPP*) and respiration (Collalti et al., 2020). Empirical models have been widely adopted to estimate BVOC emissions based on vegetation factors, emission factors, and environmental factors (Bachy et al., 2016; Guenther et al., 1995; 2006; 2012; Pierce and Waldruff, 1991; Stavrakou et al., 2011). The present study builds upon and extends these models to develop a Crop MeOH Emission Model (CMEM) to estimate the net MeOH emissions from spring wheat during growth (E, μg compound·m^{-2} earth surface·h^{-1}) into the atmosphere above the canopy at a specific time and location:

$$E_i = D_r \cdot \sum NPP_i \cdot \varepsilon \cdot \gamma \cdot \rho \tag{4.1}$$

$$NPP_i = 0.77 \times GPP = 0.77 \times PAR_i \cdot f_{PAR} \cdot LUE_{max} \cdot f_T \cdot f_W \cdot f_P \cdot f_{CO_2} \approx \frac{Yield}{HI} \tag{4.2}$$

$$\gamma = \gamma_{CE} \cdot \gamma_{PT} \cdot \gamma_{Age} \cdot \gamma_{SM} \cdot \gamma_{CO_2} \cdot \gamma_{Stress} \tag{4.3}$$

In the above equations, i represents the different growing stages of spring wheat. D_r is an ecosystem-dependent empirical coefficient and a constant value of 0.75 is selected for spring wheat that retains its foliage for less than one year (Guenther et al., 1995). ε is the standard MeOH emission (μg·g^{-1}·h^{-1}) into the canopy at standard conditions at a photosynthetically active radiation (PAR) flux of 1,000 μmol photons·m^{-2}·s^{-1} and a leaf temperature of 303 K. Due to the lack of experimental data for standard MeOH emission of spring wheat, a constant value of 1.0 μg·g^{-1}·h^{-1} is used in this model based on the dynamic MeOH emissions from common wheat (*Triticum aestivum*) at the ripening stage (Gomez et al., 2019). ρ is a factor explaining the production and loss of MeOH within plant canopies. It is assumed to be a constant value of 0.96 (Guenther et al., 2006).

NPP_i is the net primary production of wheat biomass in the growing period, i, in g dry matter·m^{-2}, which is estimated by the vegetation photosynthesis model (VPM). This model has been widely applied to estimate the *GPP* and *NPP* of crops including wheat (Patel et al., 2010; Sánchez et al., 2015). Wheat has been found to have a constant NPP/GPP ratio over the growing period with a value of 0.77 (Albrizio and Steduto, 2003). Harvest index (*HI*), meanwhile, can be used to obtain a rough estimate of biomass using the measured grain yield of spring wheat (*Yield*, g·m^{-2}) (Bolinder et al., 2007a; Dai et al., 2016a), as follows:

$$PAR_i = 0.0036R_s \times \eta_r \tag{4.4}$$

$$f_{PAR} = 0.9 \times (1 - exp\,(-K \times LAI) \tag{4.5}$$

$$LAI = \begin{cases} O & 0.0084 \times GL - 0.1024 < 0 \\ 0.0084 \times GL - 0.1024 & 0 < GL < 60 \\ -0.0021 \times GL^2 + 0.5014 \times GL - 21.828 & 60 \le GL \le 140 \end{cases} \tag{4.6}$$

$$f_T = \begin{cases} \dfrac{(T_{mean} - T_1)\ (T - T_2)}{(T_{mean} - T_1)(T_{mean} - T_2) - (T_{mean} - T_0)^2}, & T_1 < T_{mean} < T_2 \\ 0, & T_{mean} < T_1 \ or\ T_{mean} > T_2 \end{cases} \tag{4.7}$$

$$f_w = \begin{cases} 1 - K_y(1 - \dfrac{P}{ET_m}), & P \le ET_m \\ 1, & P > ET_m \end{cases} \tag{4.8}$$

$$ET_m = K_w \times ET_0 \tag{4.9}$$

$$ET_0 = 0.077 \times (T_{max} - T_{min}) + 0.114 \times T_{mean} + 0.832 \times \frac{2503 \exp\left(\frac{17.27 \times T_{mean}}{T_{mean} + 237.3}\right)}{(T_{mean} + 237.3)^2} \times R_s - 2.77 \times e + 0.269 \times v + 0.053 \tag{4.10}$$

$$e_a = e^o(T_d) = 0.6108 \times \exp\left(\frac{17.27T_d}{237.3 + T_d}\right) \tag{4.11}$$

In these equations, PAR (MJ·m^{-2}) is the proportion of shortwave radiation utilized by plants for photosynthesis. f_{PAR} means a fractional interception for PAR. R_s is the global solar radiation (Wh·m^{-2}), and η_r is the photosynthetic effective coefficient, ranging from 0.47 to 0.53 and usually being a constant value of 0.5 (Monteith, 1977). LUE_{max} is the maximum light use efficiency of wheat, ranging from 1.92 to 3.42 gC·MJ^{-1} (Gower et al., 1999; Sánchez et al., 2015). For the present study, this is assumed to be a constant value of 2.55 gC·MJ^{-1}, following similar studies in North America (He et al., 2018). f_T, f_W, f_P, and f_{CO2}, meanwhile, are the LUE response to temperature, soil moisture, phenology and CO_2, respectively. The values of f_P and f_{CO2} for spring wheat during growth are assumed to be 1.

The relationship between LAI and a fractional interception for PAR (f_{PAR}), meanwhile, can be calculated using Equation (4.5) (Acevedo et al., 2006). Here, K is the canopy extinction coefficient, ranging from 0.3 to 0.7 for wheat crops. LAI, meanwhile, is closely correlated to leaf development, i.e., growth length (GL, d), and it can be estimated using a fitted LAI-GL curve based on the findings of Martre and Dambreville (2018), shown in Equation (4.6).

f_T is estimated using the method developed by Patel et al. (2010), expressed as Equation (4.7) above, T (°C) is the mean daily air temperature as recorded at local weather stations, and T_0, T_1, and T_2, are the optimal, minimum, and maximum air temperatures, respectively, for photosynthetic activities, these being 22.0 °C, 5.0 °C, and 35.0 °C, respectively, for wheat.

The effect of water stress on photosynthesis (f_W) is calculated using a series of empirical calculations (Hassanzadeh et al., 2014; Maulé et al., 2006; Xu et al., 2015b), expressed as

Equations (4.8-(4.11) above. Here, P, ET_m, and ET_0 are the cumulative precipitation (mm), water requirement (mm), and reference evapotranspiration (mm), respectively, during different crop growth stages. K_y and K_w are the sensitivity to water scarcity and water demand coefficient, respectively, which are shown in Table 4.1. e_a refers to the actual vapor pressure (KPa); v is the daily wind speed ($m \cdot s^{-1}$); T_{mean}, T_{min}, T_{max}, and T_d are the mean, minimum, maximum, and dewpoint daily temperature, respectively, in °C.

γ is a non-dimensional emission activity factor accounting for emission changes considering the light and temperature (γ_{PT}), soil moisture (γ_{SM}), canopy environment (γ_{CE}), leaf age (γ_A), CO_2 inhibition and fertilization (γ_{CO2}), and induced stresses such as insects, fungus, and wounding (γ_{stress}). γ_{CE} and γ_A, it should be noted, vary among different growing stages (Bachy et al., 2020), as shown in Table 4.1. γ_{CO2} and γ_{stress} are both assumed to be 1 in this study.

Table 4.1. Model input parameters varying growing stages.

Stages / Parameters	Germination (G)	Emergence (E)	Tillering (T)	Heading (H)	Flowering (F)	Yield formation (Y)	Ripening (R)	References
Water demand coefficient (K_w)	0.3-0.4	0.7-0.8	0.7-0.8	1.05-1.2	1.05-1.2	0.65-0.75	0.2-0.25	(Xu et al., 2015b)
Sensitivity to water scarcity (K_y)	0.2	0.6	0.6	0.6	0.6	0.5	0	(Xu et al., 2015b)
Optimal photosynthetic temperature (T_0, °C)	18	18	24	27	27	25	18	(Xu et al., 2015b)
Minimum photosynthetic temperature (T_1, °C)	5	5	7	14	14	14	10	(Xu et al., 2015b)
Maximum photosynthetic temperature (T_2, °C)	27	27	30	33	33	33	30	(Xu et al., 2015b)
Canopy environment factor (γ_{CE})	0.42	0.42	0.42	0.42	0.42	0.31	0.31	(Bachy et al., 2020)
Leaf age factor (γ_A)	1.02	1.02	1.02	1.02	1.02	2.74	2.74	(Bachy et al., 2020)
Light-dependent fraction of the emissions (LDF)	0.93	0.93	0.93	0.93	0.93	0.8	0.8	(Bachy et al., 2020)

MeOH emissions increase exponentially with the rising light intensity and air temperature (Stavrakou et al., 2011). In our study, the response factor to temperature and light (γ_{PT}) is calculated using empirical algorithms from Stavrakou et al. (2011), expressed as Equations (4.12)-(4.18). The temperature difference between leaf and air, it should be noted, has a strong quadratic relationship with mean daily vapor pressure deficit (*VPD*, kPa), so leaf temperature (T_{leaf},°C) can be simulated based on air temperature (*T*, °C), relative humidity (*RH*, %) and *VPD* using Equation (4.16)(4.17) (Chen et al., 2011). Meanwhile, water stress may cause stomatal closure and photosynthesis reduction, and change vegetation composition, further affecting MeOH emissions (Svendsen et al., 2016). Moreover, soil moisture is closely related to air humidity, so a fitted γ_{SM} -RH curve based on experimental data from dynamic chambers (Gomez et al., 2019), is applied to calculate γ_{SM} using Equation (4.18).

$$\gamma_{\mathrm{PT}} = [(1 - LDF) \cdot \gamma_{T-li} + LDF \cdot \gamma_P \cdot \gamma_{T-ld}] \tag{4.12}$$

$$\gamma_{T-ld} = E_{opt} \cdot \left[\frac{C_{T2} \cdot \exp\left(C_{T1} \cdot \frac{\left(\frac{1}{T_{opt}} - \frac{1}{T_{leaf}}\right)}{0.00831} \right)}{C_{T2} - C_{T1} \cdot \left(1 - \exp\left(C_{T2} \cdot \frac{\left(\frac{1}{T_{opt}} - \frac{1}{T_{leaf}}\right)}{0.00831} \right) \right)} \right] \tag{4.13}$$

$$\gamma_{T-li} = \exp\left(\beta\left(T_{leaf} - 303\right)\right) \tag{4.14}$$

$$\gamma_P = \frac{\alpha \cdot PPFD \cdot C_P}{(1 + \alpha^2 \cdot PPFD^2)^{0.5}}, PPFD = uPAR \tag{4.15}$$

$$T_{leaf} = 0.56VPD^2 - 3.596VPD + 2.7248 + T_{mean} \tag{4.16}$$

$$VPD = e_s - e_a = \frac{e^o(T_{max}) + e^o(T_{min})}{2} - e^o(T_d) \tag{4.17}$$

$$\gamma_{SM} = \frac{1.388}{1 + \frac{1.388 \times 0.763 \times RH}{100}} \tag{4.18}$$

where *LDF* is the light-dependent fraction of the MeOH emissions (Bachy et al., 2020; Stavrakou et al., 2011), shown in Table 4.1; γ_P is the light-dependent response factor; $\gamma_{T\text{-}ld}$ and $\gamma_{T\text{-}li}$ are the temperature response factors of light-dependent and light-independent MeOH emissions, respectively; and T_{leaf} is the leaf temperature (K). Here, E_{opt}, T_{opt}, C_{T1}, and C_{T2} are set to 1.61, 313 K, 60 kJ·mol^{-1}, and 230 kJ·mol^{-1}, respectively. Meanwhile, the β-factor is set to 0.08 K^{-1}, and C_P and α are set to 1.066 and 0.0027, respectively. Finally, the photosynthetic photon flux density (*PPFD*, expressed in μmol·m^{-2}·s^{-1}) is defined as the photon flux density of *PAR* (W·m^{-2}); and *u* is the *PPFD*/*PAR* conversion coefficient (μmol·J^{-1}), ranging from 4.40 μmol·J^{-1} to 4.80 μmol·J^{-1}, and usually assumed as a constant value of 4.61 μmol·J^{-1} (Carruthers et al., 2001).

4.2.3. Uncertainty and sensitivity analysis

The uncertainty analysis can help obtain a better understanding of the environmental processes. There is uncertainty in the estimation of both biomass and emissions. To determine the significant factors affecting MeOH emission from spring wheat, the Monte Carlo simulations are used to assess the sensitivities and uncertainties in the emission estimate considering 14 variables and 17 parameters using the Crystal Ball software (v11.1.2.4) in this study. 10,000 trials are performed when each parameter is sampled independently with its respective applicable distribution. Normal, lognormal, and uniform distributions are employed based on publicly available data and data from peer-reviewed literature (Table 4.2). A ±10% change is assumed when only the mean value of a

variable is available. A sensitivity analysis is conducted to determine the correlation and contribution of each input variable to the MeOH emissions.

However, the sensitivity analysis using the Crystal Ball software can only reveal the single effect rather than the joint effects of multiple factors. In contrast, factorial analysis has been widely applied to study the main and interaction effects of several factors on a response. In the present study, the Minitab software (v15) is adopted to conduct the design of experiments (DOE). When experimenting, two 2-level fractional factorial designs with 15 factors (128 runs) considering two situations — (1) input data and model parameters and (2) only model parameters—are conducted with DOE capabilities, respectively. The range for those factors for which data is available is set according to the literature, while a ±10% variation range is considered for those factors for which data ranges are not available (Table 4.2).

Table 4.2. Probabilistic distributions representing uncertainty in model input parameters.

Parameters	**Default**	**Range [Min - Max]**	**Mean ± SD**	**Distribution type**	**References**
Mean daily air temperature, T_{mean} (°C)	variable	0-29.2	15.4 ± 5.1	Normal	(Government of Canada, 2018)
Mean daily dewpoint temperature, T_d (°C)	variable	-13.5-18.4	7.1 ± 4.9	Normal	(Government of Canada, 2018)
Minimum daily air temperature, T_{min} (°C)	variable	-6.4-20.5	8.2 ± 4.4	Normal	(Government of Canada, 2018)
Maximum daily air temperature, T_{max} (°C)	variable	0-41.3	22.7 ± 6.8	Normal	(Government of Canada, 2018)
Global solar radiation, R_s (Wh·m-2)	variable	1070-8735	5531 ± 1814	Normal	(Government of Canada, 2016)
Mean daily precipitation, P (mm)	variable	0-56.8	1.4 ± 4.4	Normal	(Government of Canada, 2018)
Mean daily relative humidity, RH (%)	variable	17.0-95.5	60.7 ± 14.8	Normal	(Government of Canada, 2018)
Mean daily wind speed at 2-m height, v (m·s-1)	variable	1.0-10.9	4.0 ± 1.5	Normal	(Government of Canada, 2018)
Growth length, GL (d)	variable	1-140		Uniform	(Government of Saskatchewan, 2018)
Ecosystem dependent empirical coefficient, D_r	0.75	0.6-0.9		Uniform	(Guenther et al., 1995)
Maximum light use efficiency, LUE_{max} (g C·MJ-1)	2.55	1.92-3.42		Uniform	(Gower et al., 1999; Sánchez et al., 2015)
Photosynthetic effective coefficient, η	0.5	0.47-0.53		Uniform	(Monteith, 1977)
PPFD/PAR conversion coefficient, u	4.61	4.4-4.8		Uniform	(Carruthers et al., 2001)
Canopy extinction coefficient, K	0.5	0.3- 0.7		Uniform	(Acevedo et al., 2006)
Optimal photosynthetic temperature, T_0 (°C)	22	18-27	27a	Triangular	(Xu et al., 2015b)
Minimum photosynthetic temperature, T_1 (°C)	5	5-14	14a	Triangular	(Xu et al., 2015b)

Maximum photosynthetic temperature, T_2 (°C)	35	27-35	33a	Triangular	(Xu et al., 2015b)
Sensitivity to water scarcity, K_y	variable	0-0.6	0.6a	Triangular	(Xu et al., 2015b)
Crop factor, K_c	variable	0.35-1.15	1.1a	Triangular	(Shi, 2019; Xu et al., 2015b)
Emission factor, ε (μg·g-1·h-1)	1		1.0 ± 0.1	Normal	(Gomez et al., 2019)
Production and loss factor, ρ	0.96	0.93-0.99		Uniform	(Guenther et al., 2006)
Leaf age factor, γ_A	variable	1.02-2.74	1.02a	Triangular	(Bachy et al., 2020)
Canopy environment factor, C_{ce}	variable	0.31-0.42	0.42a	Triangular	(Bachy et al., 2020)
Light-dependent fraction of the emissions, *LDF*	variable	0.8-0.93	0.93a	Triangular	(Bachy et al., 2020)
α-factor	0.0027		-6.05 ± 0.52b	Lognormal	(Zheng et al., 2010b)
β-factor	0.08		0.08 ± 0.017	Normal	(Zheng et al., 2010b)
Light empirical coefficient, C_p	1.066		1.06 ± 0.2	Normal	(Zheng et al., 2010b)
Activation energy, C_{T1} (kJ·mol-1)	60		4.53 ± 0.21b	Lognormal	(Zheng et al., 2010b)
Deactivation energy, C_{T2} (kJ·mol-1)	230		5.43 ± 0.09b	Lognormal	(Zheng et al., 2010b)
Maximum normalized emission capacity, E_{opt}	1.61	0.98-3.83		Uniform	(Zheng et al., 2010b)
The temperature when E_{opt}, T_{opt} (K)	313		312.83 ± 0.94	Normal	(Zheng et al., 2010b)

Notes: [a] mode value; [b] log value.

4.2.4. Quantifying the effect of climate change

Climate change has a great impact on the structure and function of ecosystems and its subsequent influences on vegetation composition will indirectly influence future BVOC emissions and composition, especially for the vegetation in cold zones (Peñuelas et al., 2013; Valolahti et al., 2015). Climate projections have been widely used for impact assessment and mitigation and adaptation measure design (Eyring et al., 2016). In our study, future temperature is obtained from the Coupled Model Intercomparison Project Phase 6 (CMIP6) which is an initiative of the World Climate Research Programme's Working Group of Coupled Modeling (data available at: https://esgf-node.llnl.gov/projects/esgf-llnl/). In CMIP6, a novel scenario matrix architecture combines the Representative Concentration Pathways (RCPs)—describing future GHGs and other radiative forcings—and the Shared Socioeconomic Pathways (SSPs)—modeling future socio-economic and technological development, i.e., population, economic growth, urbanization, and education. The impacts of a changing climate on MeOH emissions are assessed under two potential futures using the following SSP/RCP-based scenarios, SSP2-4.5 and SSP5-8.5. Specifically, SSP2-4.5 is a medium development (SSP2) achieving forcing levels of 4.5 $W \cdot m^{-2}$ while SSP5-8.5 means a high economic growth (SSP5) achieving forcing levels of 8.5 $W \cdot m^{-2}$. The simulations performed using CMIP6 meteorology spanning three periods—2020–2039, 2040–2069, and 2070–2099—are compared to the MeOH emissions for the year 2018 as follows:

$$RD = \frac{E_i - E_0}{E_0} \times 100 \tag{4.19}$$

where RD (%) is the relative difference in MeOH emissions between the projected periods (E_i, $\mu g \cdot m^{-2} \cdot h^{-1}$) and the control simulation in 2018 (E_0, $\mu g \cdot m^{-2} \cdot h^{-1}$) under two SSP scenarios.

Before inputting the projected temperatures into the updated emission model, a bias correction using the linear-scaling approach is conducted to correct the CMIP6 simulation temperatures as follows, as per Maraun (2016):

$$T_{f,corr}^{i,k} = T_{f,raw}^{i,k} + (\bar{T}_{obs}^{i,k} - \bar{T}_{contr}^{i,k}) \tag{4.20}$$

where T denotes daily air temperature (°C); the superscripts i and k represent the different crop districts and growing stages, respectively; and the subscripts *f*, *corr*, *raw*, *contr*, and *obs* represent the future values, corrected values, raw values, modeled values in the control case, and observed values in 2018, respectively.

4.3. Results

The MeOH emissions for spring wheat during different growing stages are estimated using the updated model for the year 2018 in Saskatchewan (Figure 4.3). Throughout the growing season, MeOH emissions are found to far exceed the canopy interception and loss, resulting in positive net emissions. This implies the presence of a MeOH source in the agriculture ecosystem. The average MeOH emission in 2018 for the various crop districts is found to be 37.94 ± 7.5 $\mu g \cdot m^{-2} \cdot h^{-1}$. Overall, MeOH emissions are found to increase moving from north to south, with the maximum emission level, in D3 (49.08 $\mu g \cdot m^{-2} \cdot h^{-1}$), being about double the minimum emission level, in D17 (25.39 $\mu g \cdot m^{-2}\, h^{-1}$). MeOH emissions exhibit phenological peak-to-valley characteristics, reaching maximum emissions (100.79 $\mu g \cdot m^{-2} \cdot h^{-1}$) in S6 (yield formation stage) and minimum emissions (≈ 0 $\mu g \cdot m^{-2} \cdot h^{-1}$) in S1 (germination stage).

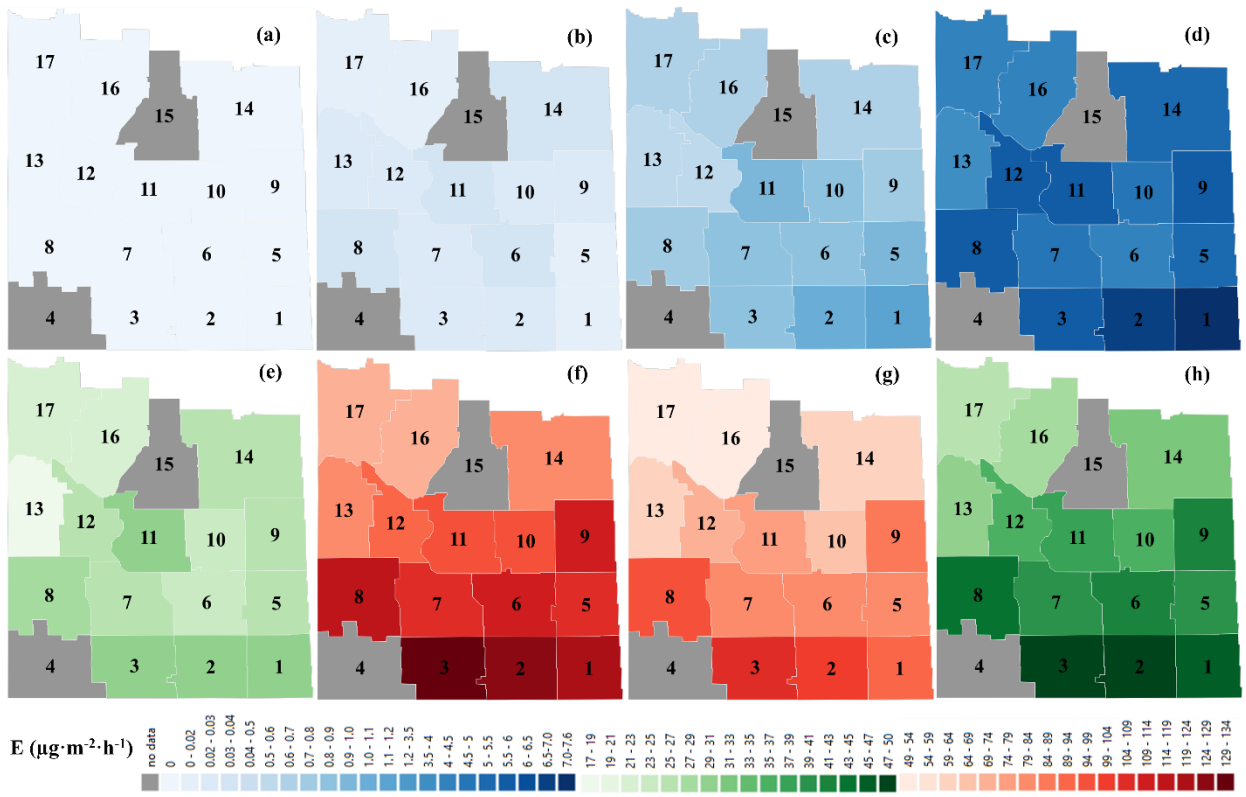

Figure 4.3. Spatial-temporal biogenic MeOH emissions (E, μg·m^{-2} ·h^{-1}) among different growing stages of spring wheat in 2018. (a) germination; (b) emergence; (c) tillering; (d) heading; (e) flowering; (f) yield formation; (g) ripening; (h) growing period.

Figure 4.4 shows the distribution and probability of forecast and fitted MeOH emissions in terms of daily increased biomass. The average forecast emission is averaged by 10,000 simulations from Monte Carlo sampling, with a mean value of 1.11 μg·m^{-2}·h^{-1}. Uncertainty in the MeOH estimation is found to be high, with a standard uncertainty of 2.07 μg·m^{-2}·h^{-1}. The MeOH emissions show a gamma probabilistic distribution, with a long tail in the high-value zone. The 95% confidence interval for the MeOH emissions can be evaluated as [0, 3.18]. There is a probability of nearly 84% in the range of MeOH emissions, [0, 2] μg·m^{-2}·h^{-1}, while a probability of approximately 30% in the range, [0, 0.05] μg·m^{-2}·h^{-1}.

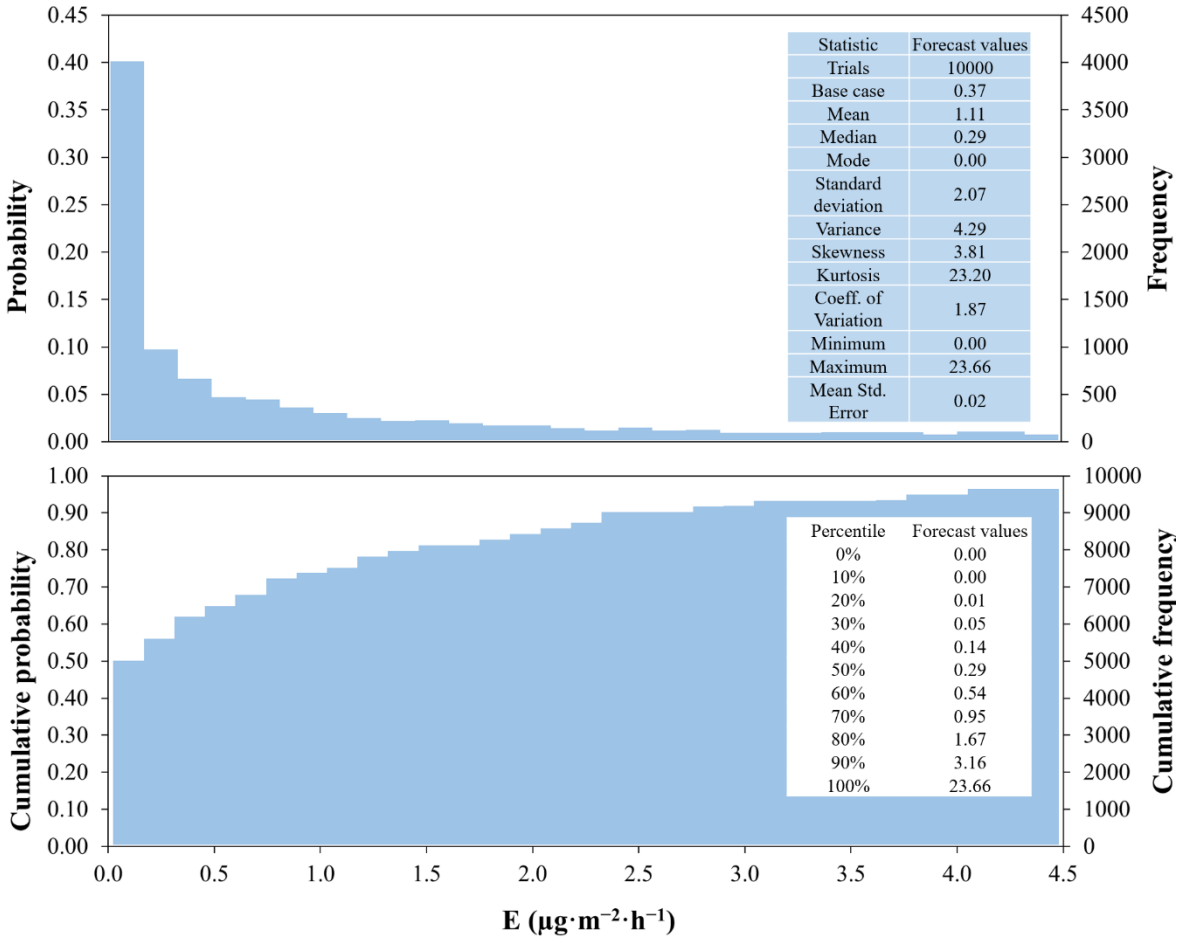

Figure 4.4. Uncertainty analysis of forecast MeOH emissions (E, $\mu g \cdot m^{-2} \cdot h^{-1}$) using Crystal Ball software.

The sensitivity results generated from the Crystal Ball software, as shown in Table 4.3, can preliminarily identify the key uncertainty sources in estimating MeOH emissions. Growth length (GL), mean daily temperature (T_{mean}), activation energy (C_{T1}), minimum photosynthetic temperature (T_1), global solar radiation (R_s), and maximum normalized emission capacity (E_{opt}) are found to be the top six sources of uncertainties in predicting MeOH emissions. To identify the primary and interactive effects of different variables on MeOH emissions, a 2-level fractional

factorial analysis of 15 factors—selected according to the contribution of these variables to variance and rank correlation as shown in Table 4.3—is performed using Minitab software.

Table 4.3. Sensitivity analysis of wheat biomass (B, g·m^{-2}) and MeOH emissions (E, μg·m^{-2}·h^{-1}) by Crystal Ball.

Sensitivity: B			**Sensitivity: E**		
Assumptions	Contribution to variance	Rank correlation	Assumptions	Contribution to variance	Rank correlation
GL	64%	0.690	GL	46.2%	0.601
T_{mean}	26%	0.439	T_{mean}	42.6%	0.577
T_1	3%	-0.160	CT_1	2.4%	-0.137
R_s	3%	0.159	T_1	2.0%	-0.125
T_0	1%	-0.088	R_s	1.7%	0.116
LUE_{max}	1%	0.086	E_{opt}	1.6%	0.110
K	1%	0.063	LUE_{max}	0.6%	0.066
P	0%	0.060	γ_A	0.5%	0.065
T_d	0%	0.035	C_p	0.5%	0.062
η	0%	0.029	K	0.4%	0.055
α	0%	0.019	T_0	0.3%	-0.049
K_y	0%	-0.016	RH	0.3%	-0.047
T_2	0%	0.014	T_{opt}	0.2%	-0.042
K_c	0%	-0.013	ε	0.2%	0.034
RH	0%	0.012	LDF	0.1%	-0.032
u	0%	-0.012	K_y	0.1%	-0.028
v	0%	-0.011	CT_2	0.1%	-0.023
CT_2	0%	0.010	C_{ce}	0.1%	0.023
β	0%	0.010	P	0.1%	0.021
C_{ce}	0%	0.009	β	0.0%	-0.020
LDF	0%	0.009	v	0.0%	-0.017
T_{max}	0%	-0.009	K_w	0.0%	-0.009
C_p	0%	0.009	α	0.0%	-0.008
CT_1	0%	-0.007	D_r	0.0%	0.006
ε	0%	-0.007	T_{max}	0.0%	-0.005
ρ	0%	-0.006	T_2	0.0%	0.005
T_{opt}	0%	-0.005	T_d	0.0%	0.005
E_{opt}	0%	0.004	η	0.0%	0.004
D_r	0%	-0.003	T_{min}	0.0%	0.002
T_{min}	0%	0.002	ρ	0.0%	0.002
γ_A	0%	-0.001	u	0.0%	0.000

Figure 4.5-4.6 show two scenarios of factorial analysis considering different uncertainty sources. When input data and model parameters are included in the analysis (Figure 4.5), in addition to the five most significant single factors ($SF_{p<0.05}$)—i.e., T_{mean}, GL, R_s, E_{opt}, and γ_A (leaf age factor), ten significant interactive factors ($IF_{p<0.05}$)— i.e., $T_{mean} \times GL$, $T_{mean} \times R_s$, $GL \times R_s$, $GL \times E_{opt}$, $T_{mean} \times E_{opt}$, $GL \times \gamma_A$, $T_{mean} \times \gamma_A$, T_0 (optimal photosynthetic temperature) × K (canopy extinction coefficient), C_{T2} (deactivation energy) × T_1, and $T_0 \times LUE_{max}$ (maximum light use efficiency)—are found to have significant positive effects on MeOH emissions. This means that several photosynthetic-related factors (i.e., T_0, T_1, K, C_{T2}, and LUE_{max}), although they do not have an obvious influence on the effect of $SF_{p<0.05}$ on MeOH emissions, can interact to double the effect of these insignificant-single-factors ($SF_{p>0.05}$). When only model parameters are included in the analysis, more factors, including seven $SF_{p<0.05}$ and nine $IF_{p<0.05}$, are found to affect MeOH emissions. Among them, K, γ_A, LUE_{max}, and E_{opt} are identified as positive $SF_{<0.05}$, while T_{opt} (temperature when E_{opt}), T_0, and T_1 are identified as negative $SF_{p<0.05}$, as shown in Figure 4.6. Notably, the double effect of negative $SF_{p<0.05}$, including $T_{opt} \times T_0$ and $T_{opt} \times T_1$, is positive, while $IF_{p<0.05}$, such as $T_{opt} \times \gamma_A$, $T_0 \times \gamma_A$, $T_{opt} \times LUE_{max}$, and $T_{opt} \times K$, are found to be negative.

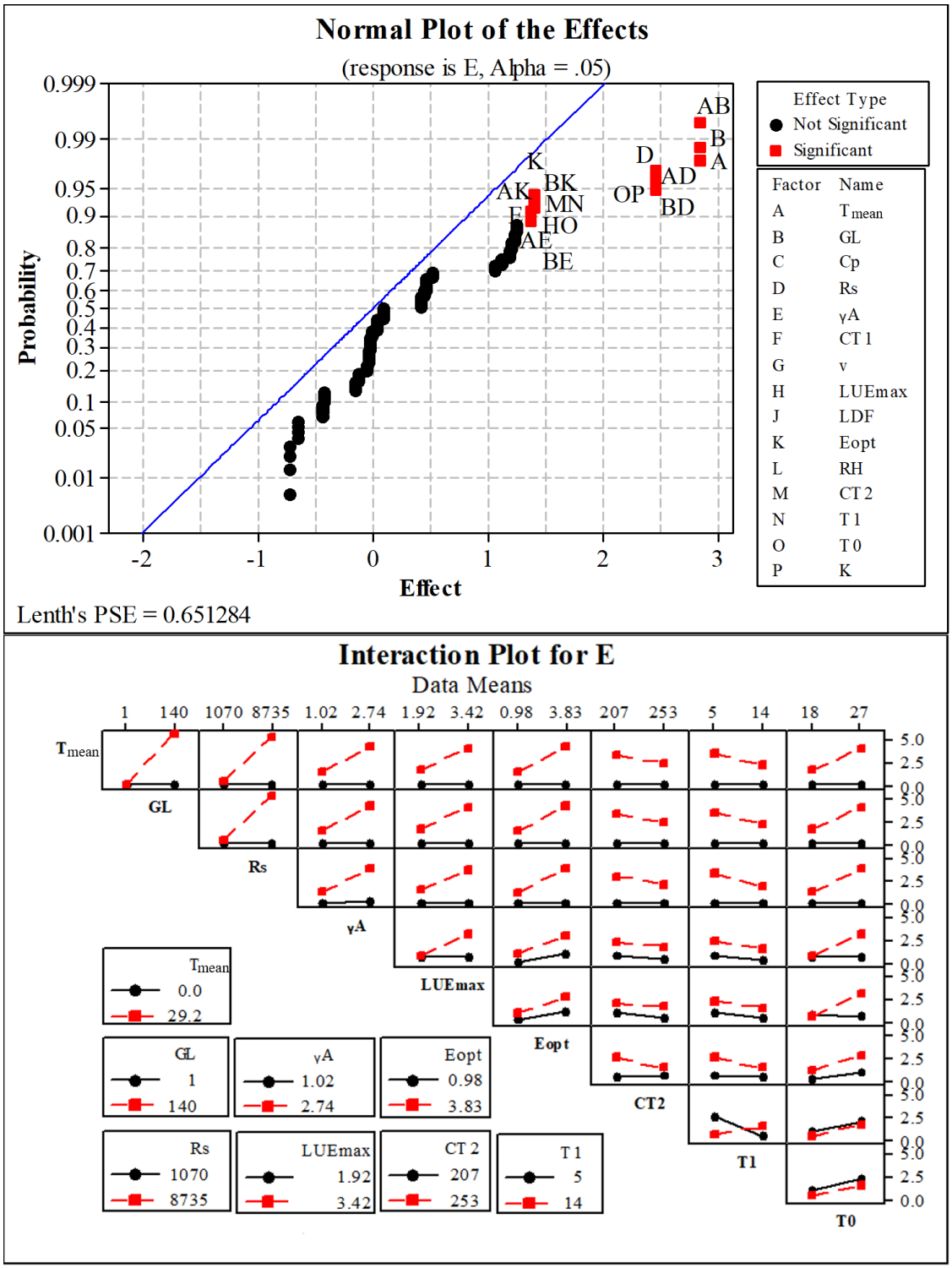

Figure 4.5. Normal and interaction plots of the effects for MeOH emissions considering input data and model parameters using Minitab 16.0.

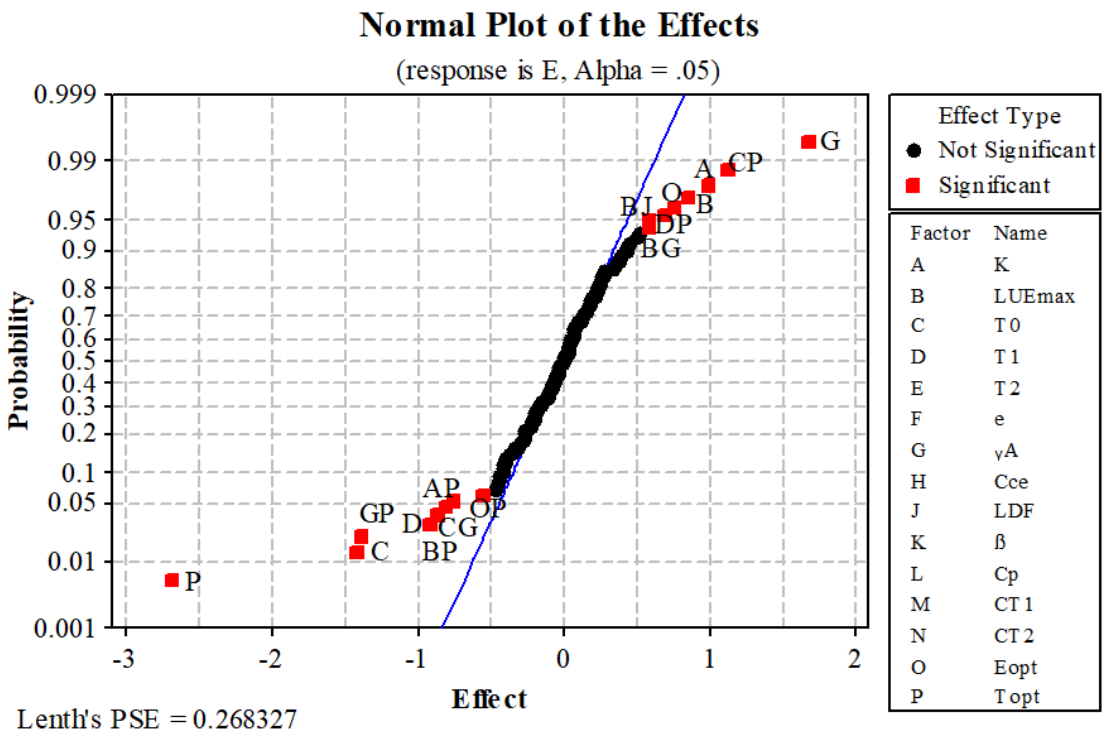

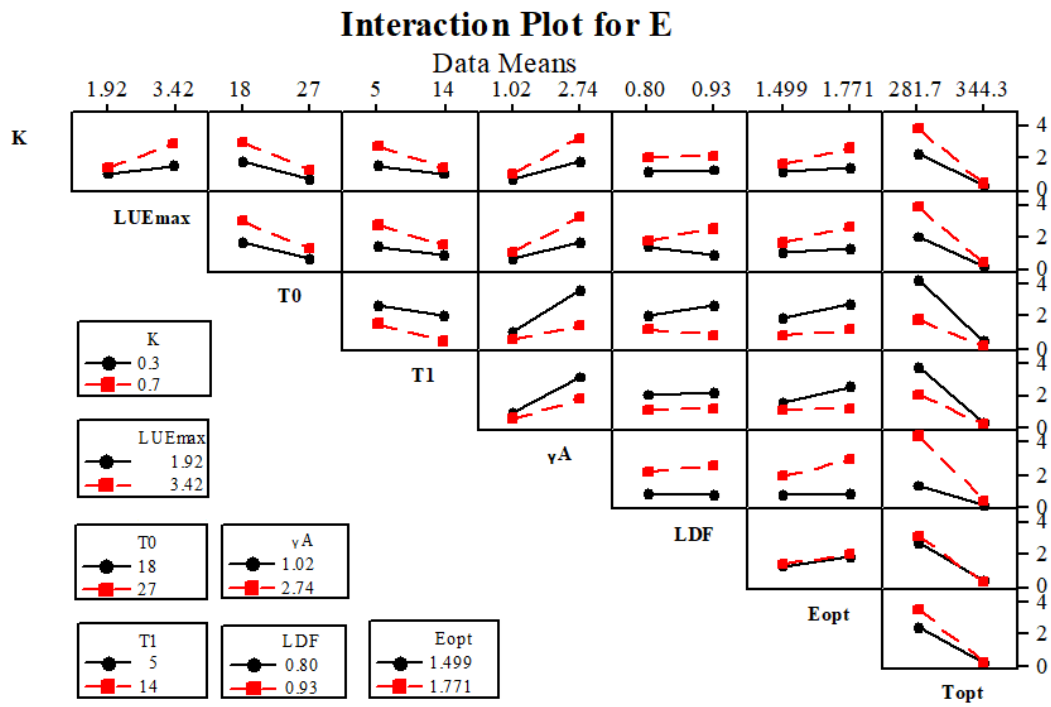

Figure 4.6. Normal and interaction plots of the effects for MeOH emissions only considering model parameters using Minitab 16.0.

The impact of temperature change on MeOH emissions according to the different SSP scenarios is shown in Figure 4.7. Generally, differences in MeOH emissions by -35 to +25% (2020–2039), -25 to +39% (2040–2069), and -19 to +60% (2070–2099) are observed under the SSP2-4.5 scenarios, and changes of -26 to +6% (2020–2039), -38 to +34% (2040–2069), and -24 to +82% (2070–2099) under the SSP5-8.5 scenarios, compared to the control observations (the year 2018) among crop districts. Moreover, the more pronounced increases are generally observed in northwestern Saskatchewan. This spatial distribution is opposite to the variations of biogenic MeOH emissions for the growing period in 2018 (Figure 4.3), but it is consistent with the changes in temperatures and wheat biomass in future scenarios (Figure 4.8-4.9).

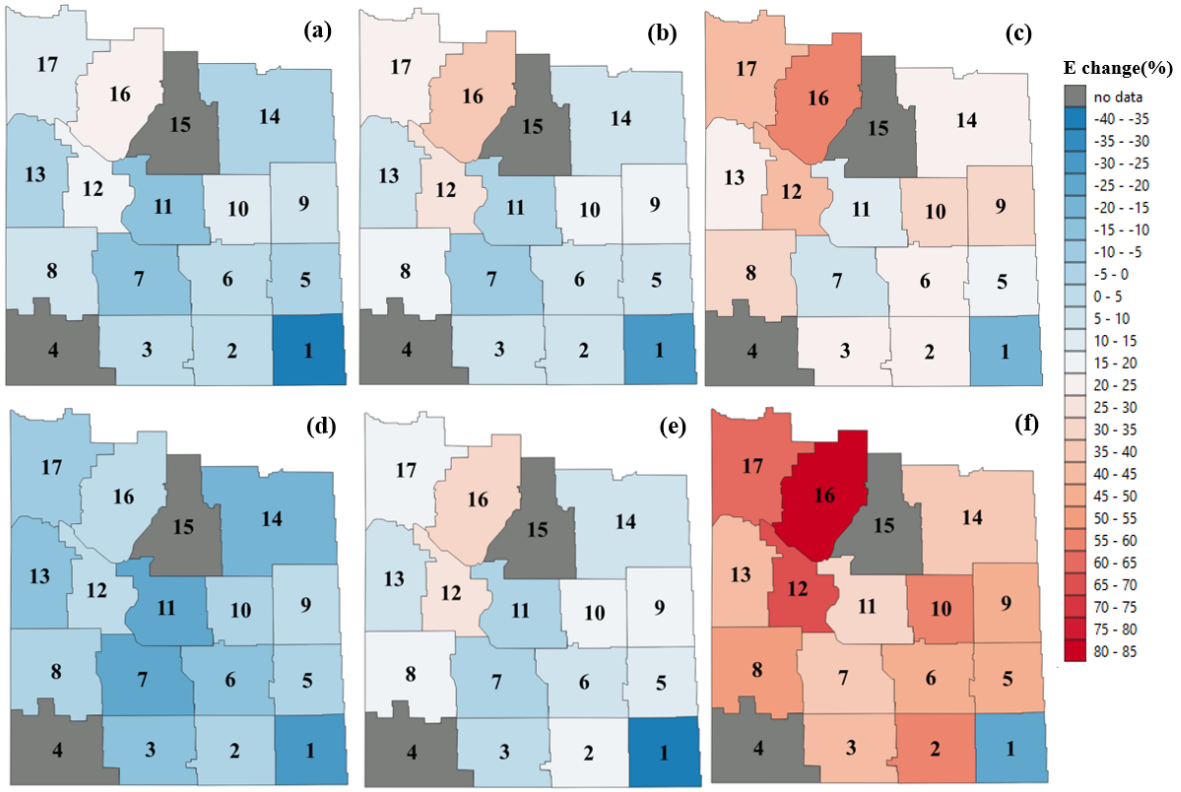

Figure 4.7. Relative differences in MeOH emissions (E, %) between the 2018 observation and three periods under two SSP scenarios. (a) SSP2-4.5 scenario during 2020-2039; (b) SSP2-4.5 scenario during 2040-2069; (c) SSP2-4.5 scenario during 2070-2099; (d) SSP5-8.5 scenario during 2020-2039; (e) SSP5-8.5 scenario during 2040-2069; (f) SSP5-8.5 scenario during 2070-2099.

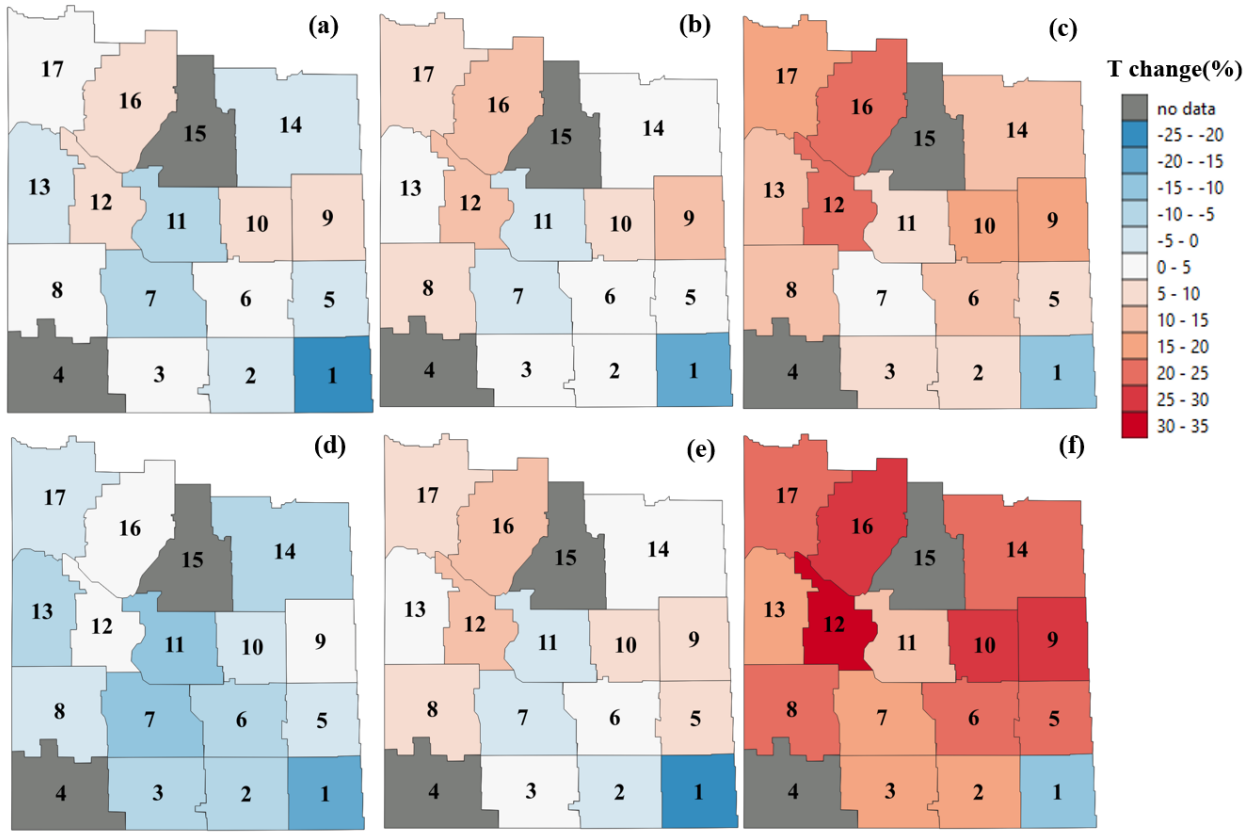

Figure 4.8. Relative temperature differences (T, %) between the 2018 observation and three periods under two SSP/RCP-based scenarios. (a) SSP2-4.5 scenario during 2020-2039; (b) SSP2-4.5 scenario during 2040-2069; (c) SSP2-4.5 scenario during 2070-2099; (d) SSP5-8.5 scenario during 2020-2039; (e) SSP5-8.5 scenario during 2040-2069; (f) SSP5-8.5 scenario during 2070-2099.

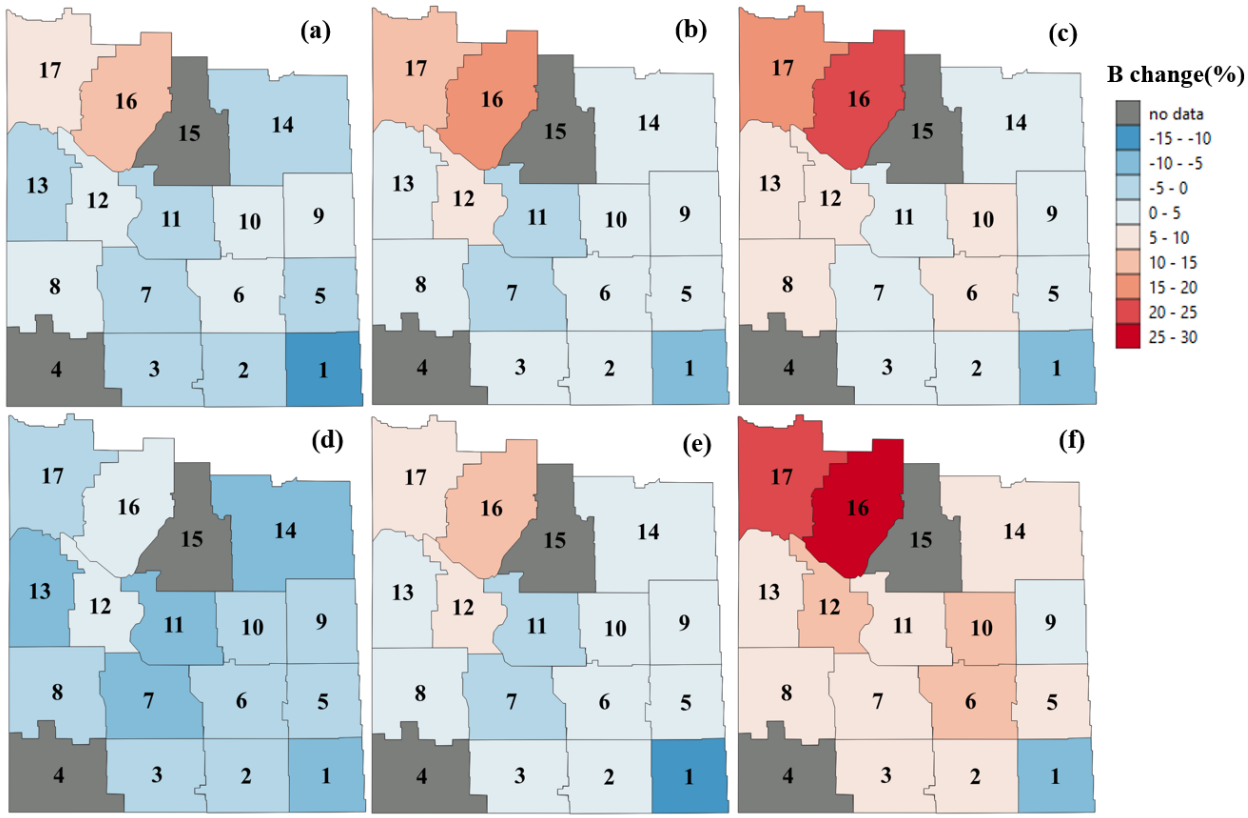

Figure 4.9. Relative differences in wheat biomass (B, %) between the 2018 observation and three periods under two SSP/RCP-based scenarios. (a) SSP2-4.5 scenario during 2020-2039; (b) SSP2-4.5 scenario during 2040-2069; (c) SSP2-4.5 scenario during 2070-2099; (d) SSP5-8.5 scenario during 2020-2039; (e) SSP5-8.5 scenario during 2040-2069; (f) SSP5-8.5 scenario during 2070-2099.

4.4. Discussion

4.4.1. Comparison with previous studies

MeOH emission of spring wheat in Saskatchewan in 2018 was found to be 37.94 ± 7.5 $\mu g \cdot m^{-2} \cdot h^{-1}$ (Figure 4.3), much lower than the findings reported by Gomez et al. (2019) and Bachy et al. (2020).

This variance may be the result of differences between stages, crop species, and measurement techniques (Table 4.4). For instance, chamber emissions are found to be more than fourfold higher than the EC measurements during the ripening stage (Gomez et al., 2019).

Table 4.4. Comparison of MeOH emissions from crop and grass species.

Species	Emission[s] ($\mu g \cdot m^{-2} \cdot h^{-1}$)	Biomass[a] ($g \cdot m^{-2}$)	Climate	Measuring techniques	Measuring period	Reference
Spring wheat	37.94 ± 7.5 or 0~131.03	611.2 ± 50.14 or 0~689	Dfb	Model	01/05~17/09/ 2018 (G~R)	(Cai et al., 2021b)
Winter wheat	62 ± 3.3 or -459~1128	0~2000	Cfb	Field /DEC-MS /PTR-MS	05/03~28/07/ 2013 (E~R)	(Bachy et al., 2020)
Winter wheat	900	1000	Cfb	Chamber /In situ cuvette /PTR-TOF-MS	12–9/06/2017 (R)	(Gomez et al., 2019)
Agricultural soil	0~200	N.A.	Cfb	Field /REA-EC /PTR-MS	Summer	(Schade and Custer, 2004)

Notes: [a] The annotation xx ± yy denotes the mean of emission or biomass ± its standard deviation, and the formalism xx ~ yy denotes the range of emission or biomass. [b] Dfb is a warm-summer humid continental climate and Cfb is a temperate oceanic climate according to the World Map of Köppen-Geiger climate classification (Kottek et al., 2006). [c] DEC-MS: disjunct eddy covariance by mass scanning technique; REA-EC: relaxed eddy accumulation - eddy covariance.

Furthermore, the predicted biomass range in the present study is found to fall within the observed biomass range of common classes of wheat in North America (*HI* = 0.33 to 0.61) but to be generally lower than the observed biomass of spring wheat in Canada in particular (*HI* = 0.4), shown in the Figure 4.10. Moreover, spring wheat normally has a shorter growing period and yields higher

biomass compared to winter wheat, and wheat biomass has a very strong relationship with MeOH emissions because the two are both predominantly influenced by similar factors such as *GL* and T_{mean} (Table 4.3). Therefore, the MeOH emissions from winter wheat measured by Gomez et al. (2019) are much higher than the results both of Bachy et al. (2020) and the present study. Notably, bi-directional exchanges of MeOH, including emission, uptake, and deposition, occur simultaneously on surfaces of the crop canopy and the soil, and this may lead to negative fluxes under dark, wet, and cold conditions or augmented emission from the soils under light, dry, and warm conditions (Bachy et al., 2020; Bachy et al., 2016; Mozaffar, 2017; Schade and Custer, 2004). Thus, Bachy et al. (2020) have identified negative fluxes corresponding to these conditions, while neither Gomez et al. (2019) nor the present study considers the MeOH sink phenomenon, and thus negative fluxes are not observed.

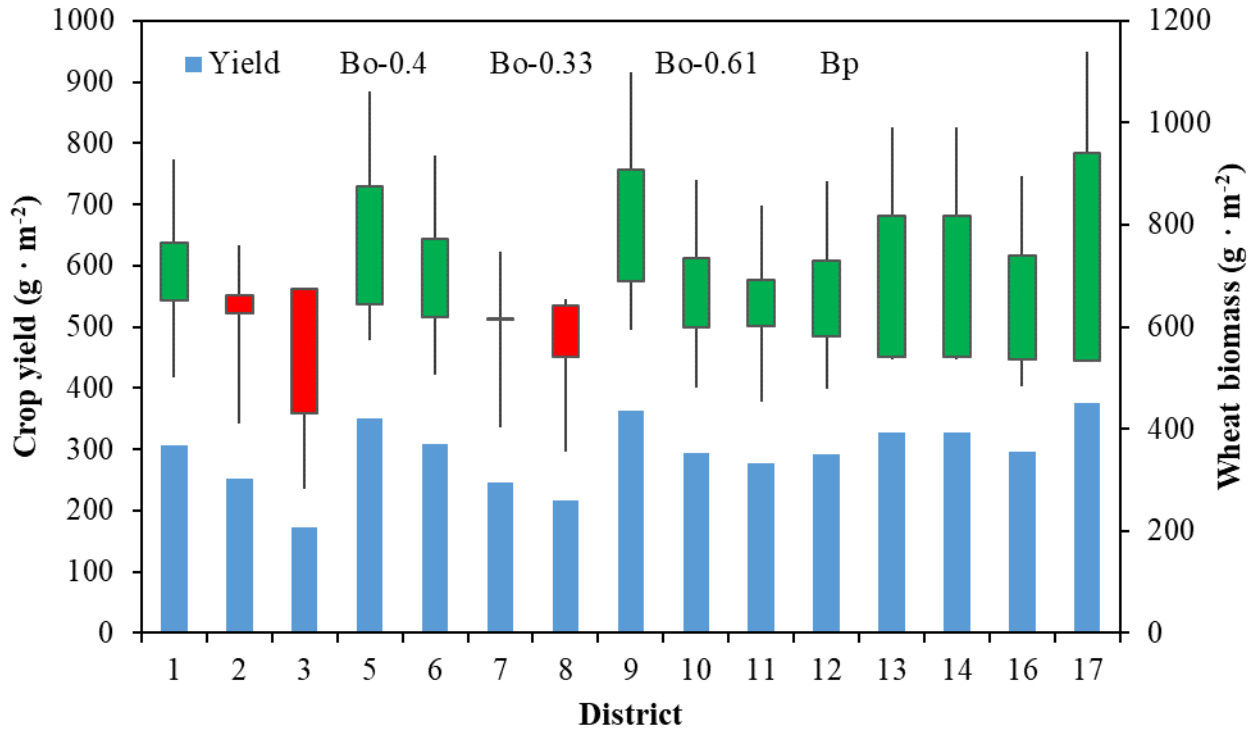

Figure 4.10. The stock chart for comparison of predicted biomass ($g \cdot m^{-2}$) of spring wheat from different studies. Yield (blue column) means the observed crop yield of spring wheat in 2018 (Government of Saskatchewan, 2018). $B_{o\text{-}0.4}$, $B_{o\text{-}0.33}$, and $B_{o\text{-}0.61}$ mean the calculated wheat biomass using Equation (3) when the harvest index is 0.4 for spring wheat in Canada (Bolinder et al., 2007b) and varies from 0.33 to 0.61 for five classes of wheat in North America (Dai et al., 2016b). B_p is the predicted wheat biomass in this study. The red column represents that B_p is more than $B_{o\text{-}0.4}$ while green is on the contrary.

The large uncertainty in MeOH emissions is observed in the present study, which is similar to that reported by Smiatek and Bogacki (2005) concerning the estimation of OVOC emissions from forests in Poland (they used a semi-empirical BVOC model). The sensitivity analysis suggests that MeOH emissions show a Gamma probabilistic distribution, and growth length, air temperature,

solar radiation and leafage are the most important influencing variables. However, Zheng et al. (2010a) found emission factor (ε), foliar density (D_m), and β-factor rather than temperature to be important sources of uncertainty in the estimation of OVOC emissions in the Pearl River Delta Metropolitan Region of China. Compared to the former two models, Zheng et al. (2010a) comparatively introduced fewer model input parameters and hourly observed meteorological data to estimate regional OVOC emissions. This demonstrates that meteorological data that is more precise than what is currently on hand, especially T_{mean} and R_s, may help reduce uncertainty in estimating dynamic MeOH emissions. Moreover, according to results shown in Table 4.3 and Figure 4.5-4.6, GL, T_1, T_0, and LUE_{max} are closely related to photosynthetic period and efficiency, which, in turn, affect leaf biomass directly and MeOH production indirectly, and γA, K, T_{opt}, and E_{opt} directly affect the production and emission of leaf MeOH. Thus, more robust biomass and emission parameters are required that consider specific wheat subspecies, climate zones, and wheat phenology.

4.4.2. MeOH emissions affected by climate change

The warming and drought brought by global climate change will alter MeOH emissions depending on the doses and timing of environmental factors (Penuelas and Staudt, 2010). Considering that P and RH have not been identified as significant influencing factors (Figure 4.5-4.6), only the effect of future climate change on MeOH emissions is discussed here. Temperature can strengthen the synthetase activity, lift the MeOH vapor pressure, reduce the diffusion resistance, and consequently increase MeOH emissions exponentially (Galbally and Kirstine, 2002). In most cases, MeOH emissions increase with temperature within a certain temperature range of 5–35 °C in the short- or medium-term, as per Figure 4.1-4.3 and Table 4.2. Harley et al. (2007) have reported that

each 10 °C increase in leaf temperature may cause MeOH emissions to increase by as much as 2.4 times. However, enzyme degradation and physiologic responses to heat stress will also influence the emission pattern, and in some cases increasing temperatures may, in fact, result in decreased or even inactivated enzyme activity (Feng et al., 2019). Stored volatiles, including MeOH, can be emitted when the cell walls of the storage pools become seriously damaged at temperatures >45 °C (Guidolotti et al., 2019). Accordingly, wounding induced by excessive temperatures may strongly increase instantaneous MeOH emissions.

In the long term, VOC emissions could increase with climate change due to its direct effect of warming and indirect effects on growing length, plant biomass, and vegetation composition (Lindwall et al., 2016). In the present study, there is no reduction of air temperature (Figure 4.8), wheat biomass (Figure 4.9), and MeOH emissions (Figure 4.7) in most crop districts in 2040–2069 and 2070–2099 compared to 2018. Compared to warmer southern regions in Saskatchewan, higher increases in both air temperature and wheat biomass are projected to occur in colder crop districts, e.g., D16 and D17, resulting in larger increases in emissions there. Previous studies have reported that projected climate change in 2040–2069 might cause higher grain yield, earlier seeding dates, and shorter maximum growing length (MGL) in Saskatchewan compared to the period of 1961–1990 (He et al., 2012). Crops in the southwest of Saskatchewan have earlier seeding dates and shorter MGL in most scenarios, but northeast districts have a higher potential of MGL reduction in 2041–2070 compared to the baseline period of 1971–2000 (Qian et al., 2016). Thus, the projected temperature change probably causes spatial-temporal differences in the MGL of spring wheat, consequently affecting long-term MeOH emissions.

Although few studies have focused on long-term MeOH emissions of spring wheat, studies about BVOC emissions including isoprene or monoterpene could provide relevant comparisons. Guenther et al. (1995) estimated that a rise of 2 °C increased global BVOC emissions by 25% and Feng et al. (2019) found that warming increased significantly the emission of isoprene (a 22% increase by +6.6 °C) and monoterpenes (a 39% increase by +1.7 °C). In general, cold zones are associated with a higher increase in air temperatures compared to the global average. For example, Subarctic and Arctic areas could have an increase in air temperatures at twice the global mean rate (Huang et al., 2015a). Thus, BVOC emissions in cold zones may increase more than the global mean level in response to climate warming. For example, a 1.9–2.5 °C rise in ambient temperature resulted in a doubling of emissions of MTs and SQTs from a wet subarctic tundra heath (Faubert et al., 2010). 2 °C warming caused 2-fold and 5-fold increases in emissions of MTs and SQTs, respectively, in northern Sweden (Valolahti et al., 2015). Notably, warming-caused increases in plant emissions cannot be fully attributed to leaf biomass because direct effects were more significant than indirect effects (Kramshøj et al., 2016; Rinnan et al., 2020). Previous studies have found that temperature—given its influence on vegetation coverage—is the primary driver of seasonal and inter-annual changes in BVOC emissions (Wang et al., 2016b). For example, BVOC emissions might adapt to 3-year warming and barely change in the next decade (Tang et al., 2018). Therefore, the higher increase of MeOH emissions in colder northwestern Saskatchewan is probably due to the larger temperature increases compared to that in the warmer southeastern region.

4.4.3. The effect of leaf development on MeOH emission

In addition to meteorological factors such as T_{mean} and R_s, γ_A is also an important factor influencing MeOH emissions, as per Figure 4.1, Figure 4.3, Figure 4.5, and Figure 4.6. In the present study, γ_A values of 1.02 and 2.74 are respectively assigned to stages G–F and stages YF–R in the updated model for spring wheat, as per Bachy et al. (2020). Accordingly, MeOH emissions are predicted to be highest in the Y stage and lowest in the G stage. The emission intensity and pattern of biogenic MeOH, it should be noted, depend on plant development. Leaf MeOH is typically produced through pectin biosynthesis during cell wall growth and expansion, leading to the highest biogenic MeOH emissions being observed in spring and early summer at both the individual and local scales (Fall and Benson, 1996; Galbally and Kirstine, 2002; Hu et al., 2011). It has also been reported that plant leaves during adulthood and the harvesting period emit MeOH at a rate several times higher than leaves during the growing period (Brunner et al., 2007; Huve et al., 2007). Notably, Mozaffar (2017) conducted a study in which strong emission peaks and guttation droplets were observed from young wheat plants following light/dark transitions, while no MeOH increases or guttation droplets were found in mature plants. Moreover, as demonstrated by Oikawa et al. (2011), PME activity is expected to decrease with leaf development, and the degree of methyl esterification is known to be lower in mature cell walls than in immature leaves; as such, mature leaves have a lower potential for MeOH production via the PME pathway compared to young leaves. Furthermore, a substantial proportion of MeOH production in deciduous trees with mature leaves is produced in pectin demethylation during root or stem growth and transported to stomata by the transpiration stream (Folkers et al., 2008). On the other hand, Oikawa et al. (2011) demonstrated in a similar study that root MeOH production is not the dominant contributor to daytime MeOH emissions from mature and immature leaves of tomato plants. Interestingly, MeOH

emissions may be affected by inducible factors such as mechanical wounding, herbivore attacks, fungal infection, and senescence (Harrison et al., 2013b). For instance, several recent studies have found that senescence-induced MeOH is emitted from herbaceous plants with yellow and dry leaves (Bachy et al., 2020; Bachy et al., 2018; Gomez et al., 2019; Mozaffar, 2017). These studies have observed strong increases in MeOH emissions from wheat leaves during ear formation, fruiting, and early senescence and from maize leaves with leaf chlorosis. These observations suggest that PME and guttation could be the major pathways of biogenic MeOH for immature leaves, while induced emission of MeOH produced and stored in roots and leaves may be the principal emission sources in mature spring wheat leaves.

4.4.4. The Fate of biogenic MeOH emissions over rural croplands

The MeOH produced by plants can have several fates. It can be stored in water and tissue within the plant, it can diffuse out through stomata to the atmosphere, or it can be oxidized to formaldehyde by the gas-phase reaction. BVOC–NO_x interaction generates highly chemically active species such as •OH and nitrate radical, which, in turn, are responsible for the formation of pollutants such as O_3 and peroxyacetyl nitrate (Margarita et al., 2013). Presumably, a portion of the MeOH within the leaf will be ultimately converted to CO_2 (Galbally and Kirstine, 2002).

In the present study, the seasonality of MeOH emissions is found to be positively correlated to concentrations of CO ($r = 0.176$, $p = 0.037$), FPM ($r = 0.205$, $p = 0.015$), and PM_{10} ($r = 0.345$, $p < 0.001$) but negatively related to NO_2 ($r = -0.204$, $p = 0.016$) and O_3 ($r = -0.506$, $p < 0.001$), as per Figure 4.11 and Table 4.5.

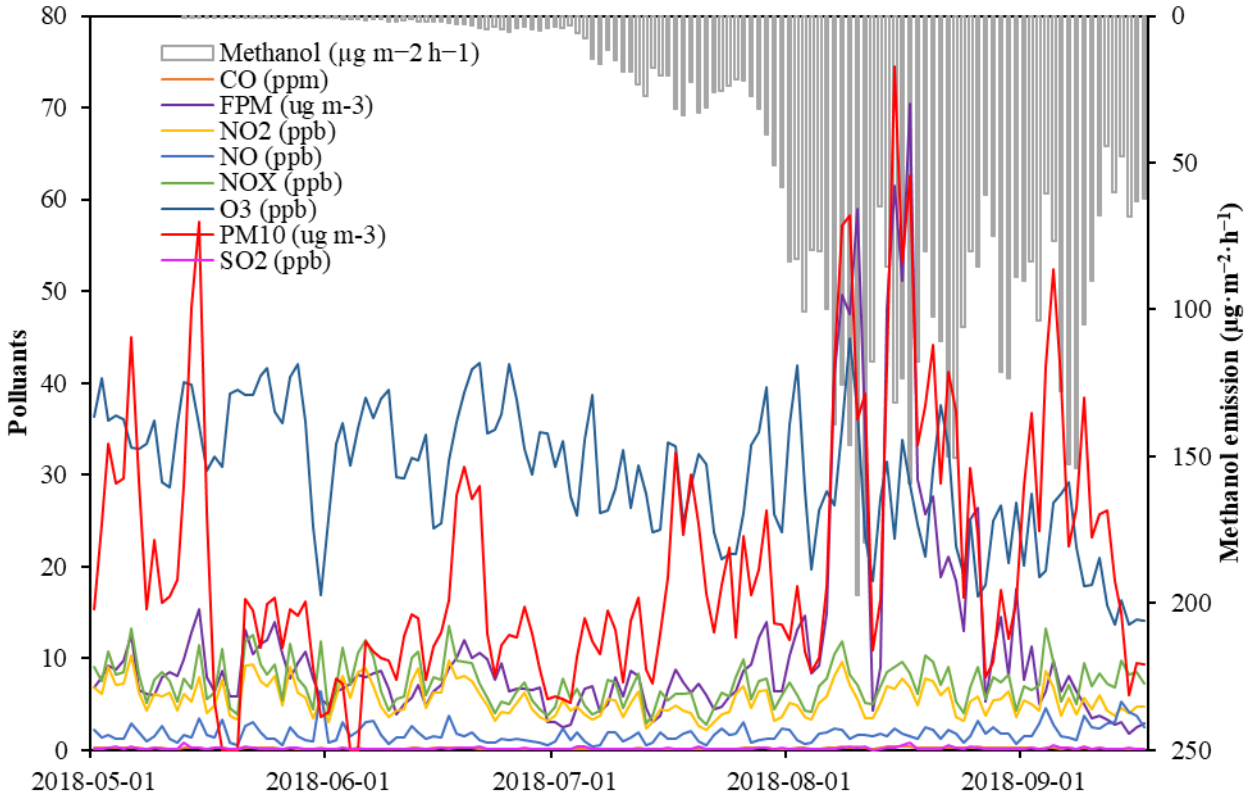

Figure 4.11. Temporal trend of the simulated MeOH fluxes (E, $\mu g \cdot m^{-2} \cdot h^{-1}$) and the observed concentrations of six common air pollutants among Districts 6, 8, and 11 in 2018.

However, it has been estimated that global MeOH emission could produce an increase of approximately 1–2% in O_3, a 1–3% decrease in •OH, a 3–5% increase in HO_2, and a 3–9% increase in HCHO (Tie et al., 2003). The differences in O_3 formation between the two studies may be related to the sensitivity of O_3 formation to NO_x and VOCs in environments with different concentrations of anthropogenic pollutants (Vermeuel et al., 2019). O_3 formation over highly polluted urban areas is strongly VOC-sensitive and progresses towards a more NO_x-sensitive regime when the plume transports to suburban and rural areas. Limited NO_x with long-distance transport from urban areas or released by local anthropogenic activities may result in a high relative ratio of rural biogenic

VOCs/NO_x, thereby maintaining •OH rather than contributing to chemical O_3 production (Jeon et al., 2014; MacKenzie et al., 2011). Moreover, the O_3 uptake by plants and soils in rural croplands and the destruction of the ozone by terpene emissions during nighttime might reduce O_3 concentrations (Im et al., 2011). Besides anthropogenic sources, VOC oxidation also contributes to CO in the atmosphere. When MeOH is oxidized by •OH, HCHO and CO are sequentially produced with essentially equal yields (Hu et al., 2011). Wells et al. (2014) found that MeOH explains more than 25% of the photochemical source of HCHO and CO in the north temperate zone in spring and accounts for 6% of global SOA annually. The positive relationship between MeOH emissions and CO concentration was also noted by Hu et al. (2011). For instance, when MeOH emissions are high in the early growing season, a large contribution to tropospheric CO and HCHO (~20%) has been observed because of a pronounced photochemical role in this period.

Our results have found that FPM and PM_{10} both exhibit significant positive relationships with CO, SO_2, NO_2, and NO_x concentrations. Previous studies have reported that BVOCs can produce SOA and PM via different formation pathways, e.g., gas-phase reactions and aqueous-phase oxidation. For instance, organosulfates can be produced by nitrates and organic peroxides via gas-phase partitioning into particle-phase (Pratt et al., 2013), and sulfates and organic aerosol are responsible for most of the change in $PM_{2.5}$ concentrations (Day and Pandis, 2015). However, although MeOH emissions may increase CO and PM concentrations, they have little impact on the concentrations of SO_2, NO, and NO_x ($|r| < 0.15$, $p > 0.05$). This means that MeOH might have another pathway to produce PM rather than gas-phase reactions with nitrates and sulfates. This assumption is supported by the findings of Hansel et al. (2015). The isoprenoid photochemical oxidation will enhance the formation of sulfate and SOA, and further promote the formation and growth of new

particles. However, biogenic MeOH is more likely to partition into aqueous phases—i.e., mist, fog, rain, and dew—and be oxidized by •OH. Besides, the addition reactions—e.g., dimerization, the addition reaction of hydroxyl functional groups and oxygen—will promote these aqueous-phase reactions to produce derivatives with lower vapor pressures, higher polarity, and larger molecular weights, and eventually form SOA after droplet evaporation.

Table 4.5. Spearman's correlation of the simulated MeOH fluxes and the observed concentrations of six common air pollutants among Districts 6, 8, and 11 in 2018.

Correlation	MeOH	CO	FPM	NO_2	NO	NO_x	O_3	PM_{10}	SO_2
MeOH	1.000	0.176*	0.205*	-0.204*	0.092	-0.116	-0.506**	0.345**	0.044
	—	(0.037)	(0.015)	(0.016)	(0.280)	(0.173)	(0.000)	(0.000)	(0.607)
CO	0.176*	1.000	0.749**	0.681**	0.336**	0.630**	0.118	0.574**	0.527**
	(0.037)	—	(0.000)	(0.000)	(0.000)	(0.000)	(0.164)	(0.000)	(0.000)
FPM	0.205*	0.749**	1.000	0.488**	0.000	0.332**	0.355**	0.557**	0.515**
	(0.015)	(0.000)	—	(0.000)	(0.995)	(0.000)	(0.000)	(0.000)	(0.000)
NO_2	-0.204*	0.681**	0.488**	1.000	0.532**	0.928**	0.338**	0.383**	0.479**
	(0.016)	(0.000)	(0.000)	—	(0.000)	(0.000)	(0.000)	(0.000)	(0.000)
NO	0.092	0.336**	0.000	0.532**	1.000	0.778**	-0.309**	0.223**	0.208*
	(0.280)	(0.000)	(0.995)	(0.000)	—	(0.000)	(0.000)	(0.008)	(0.014)
NO_x	-0.116	0.630**	0.332**	0.928**	0.778**	1.000	0.110	0.345**	0.421**
	(0.173)	(0.000)	(0.000)	(0.000)	(0.000)	—	(0.196)	(0.000)	(0.000)
O_3	-0.506**	0.118	0.355**	0.338**	-0.309**	0.110	1.000	0.026	0.323**
	(0.000)	(0.164)	(0.000)	(0.000)	(0.000)	(0.196)	—	(0.756)	(0.000)
PM_{10}	0.345**	0.574**	0.557**	0.383**	0.223**	0.345**	0.026	1.000	0.545**
	(0.000)	(0.000)	(0.000)	(0.000)	(0.008)	(0.000)	(0.756)	—	(0.000)
SO_2	0.044	0.527**	0.515**	0.479**	0.208*	0.421**	0.323**	0.545**	1.000
	(0.607)	(0.000)	(0.000)	(0.000)	(0.014)	(0.000)	(0.000)	(0.000)	—

Notes: * and ** mean that correlation is significant at the 0.05 and 0.01 level (2-tailed), respectively. NO: nitrogen monoxide; SO_2: sulfur dioxide.

4.4.5. Limitations and uncertainties

Besides the sources of uncertainty considered in the uncertainty and sensitivity analysis, there are still some other factors influencing MeOH modeling. Firstly, the seeding and harvesting periods vary slightly among different crop districts in the present study and thus the classification of growth length and growing stages may increase the uncertainty of spatial-temporal simulations. Secondly, the effects of CO_2 and inducible stress (wounding, etc.) on MeOH emissions are not incorporated in the present study, meaning that the long-term constitutive MeOH emissions due to the CO2 fertilization effect on wheat biomass as well as short-term induced-MeOH emissions may have been underestimated. Thirdly, it's important to note that our modeling process relies on certain assumptions. For example, in the Monte Carlo simulation, we assume that parameters are randomly distributed and independent. In reality, these relationships are more complex. Also, because of limited data, we use triangular distributions for random parameters, which are simpler to work with but can increase uncertainty in emission simulations. Finally, in the present study, the bias correction is calculated using daily observed and control run temperatures in 2018. Using long-term climate data to correct the bias of projected temperature might increase the accuracy of the bias-corrected temperature that is used to drive the MeOH emission model.

4.5. Summary

In this study, MeOH emissions from spring wheat during the growing period were estimated using a developed emission model. The temporal and spatial variations of MeOH emissions of spring wheat in a Canadian province were investigated. The averaged MeOH emission of spring wheat is found to be 37.94 ± 7.5 $\mu g \cdot m^{-2} \cdot h^{-1}$, increasing from north to south and exhibiting phenological peak-to-valley characteristics. Moreover, cold crop districts are projected to have higher increases

in air temperature and consequent MeOH emissions during 2020-2099. Furthermore, the seasonality of MeOH emissions is found to be positively correlated to concentrations of CO, FPM, and PM_{10} but negatively related to NO_2 and O_3. The uncertainty and sensitivity analysis results suggest that MeOH emissions show a Gamma probabilistic distribution, and growth length, air temperature, solar radiation and leafage are the most important influencing variables. In most cases, MeOH emissions increase with temperature in the range of 3-35 ℃ while the excessive temperature may result in decreased MeOH emissions because of inactivated enzyme activity or increased instant MeOH emissions due to heat injury. Notably, induced emission might be the major source of biogenic MeOH of mature leaves. The results of this study can be used to develop appropriate strategies for regional emission management of the cropping system.

CHAPTER 5. CHARACTERIZATION AND QUANTIFICATION OF THE BIODEGRADABLE MICROPLASTICS IN CROPPING SYSTEMS

5.1. Background

Plastic film mulching is widely used to enhance crop production. However, traditional non-biodegradable mulches may undergo fragmentation by mechanical abrasion, oxidation, photodegradation, and biodegradation, breaking into small segments, including MaPs (aerodynamic diameter $D_p > 5$ mm), MPs ($D_p < 5$ mm), and NPs ($D_p < 1$ μm) (Qin et al., 2021). Completely removing these small plastic residues from croplands is difficult, and they can accumulate in the soil for decades, even lasting up to 200–400 years (Jiang et al., 2017). These MPs and NPs may harm soil microorganisms, enter the surface water and groundwater, and transfer into the food chain (Hayes et al., 2017; Wang et al., 2022b). In agricultural soil environments, the physicochemical properties of plastic films, such as surface microstructure and chemistry, particle size, shape, and color, will change with the aging process and further pose negative effects on soil health, such as soil permeability, microbial activities, soil biota, and crop yield and quality (Wang et al., 2022a).

Over the past decades, BMs have been regarded as an alternative to mitigate the environmental and disposal problems caused by plastic residues (Miles et al., 2017). However, most commercially available BMs contain certain fossil fuel-based ingredients or additives, which limit their use in organic agriculture. Some BMs have no longer been regarded as an allowable input to certified

organic farming in Canada (CAN/CGSB-32.311, 2015). The environmental impacts of BMs have drawn increasing attention from researchers.

Current research has mainly focused on the effects of BMs on crop production and the degradation characteristics of BMs (Brodhagen et al., 2015; Tofanelli and Wortman, 2020). BMs are commonly tilled into the soil without removal, disposal, or recycling, and they are required to biodegrade 90% in two years (ASTM International, 2002). Theoretically, they are 100% degraded through natural microorganism mineralization and contemporaneously converted into CO_2, H_2O, and microbial biomass. Therefore, BMs may be more effective at reducing carbon footprint and negative impacts on soil health, as well as labor time and farm expenses, compared with PE mulches (Malinconico, 2017; Sintim, 2018; Waterer, 2010). However, it has been reported that BMs can hardly be 100% degraded in natural environments; they also generate biodegradable MaPs, MPs, and NPs (BMaPs, BMPs, and BNPs), which may persist in the soil for a few months or even several years (Flury et al., 2017; Shruti and Kutralam-Muniasamy, 2019; Sintim, 2018). BMs may produce more BMPs than non-degradable mulches during the same period because they are more vulnerable to biodegradation (Zhao et al., 2021). Several water incubation and leaching experiments have reported the released compounds, such as plastic additives and carbon black, from BMs (e.g., Mater-Bi®, BioFilm®A, Ecovio®, Bio-Flex®, PBAT, PLA, and PLA/PHA), which can cause negative effects to soils and/or crops (Balestri et al., 2019; Qin et al., 2021; Serrano-Ruíz et al., 2020; Sintim et al., 2020). Some in situ field experiments about diverse BMs, including PBAT,

PLA, PLA/PHA, Ecovio®, Mater-Bi®, BioAgri, Naturecycle, Organix, vegetable starch, and paper/WGP, have identified that different weathering conditions, such as photodegradation, hydrolytic, and oxidative reactions, caused increased surface wettability, decreased mechanical properties, and changed chemical bonding (e.g., increased hydrophilic end groups), thereby increasing BM biodegradation in soils (Hayes et al., 2017; La Mantia et al., 2020; Moreno et al., 2017; Sintim et al., 2020; Yang et al., 2020).

Notably, UV-induced abiotic oxidation can damage BMs and promote the subsequent abiotic (i.e., pyrolysis and hydrolysis) and biotic degradation in the soil (La Mantia et al., 2020; Qin et al., 2021; Wang et al., 2021c). However, these studies focused more on the changes in tensile strength and chemical bonding of BMs rather than the particle distribution of fragmented BMs. Only a few studies have reported the fragmentation and degradation of BMaPs into BMPs and BNPs in soils (Napper and Thompson, 2019; Weinstein et al., 2020). However, these studies observed the production of microplastic particles using visual inspection without quantitative analysis. Research regarding the weathering process of BMPs under abiotic conditions, especially UV irradiation, is scarce. More simulated research is needed to quantify the fragmentation process of BMPs into smaller particles, including BNPs. Therefore, this study aims to explore the effects of weathering on BMs under complex conditions. The physicochemical changes of weathered BMaPs and BMPs (including BioAgri and WGP), the particle distributions of micro- and nano-plastics, and the

chemical characteristics of BMP-derived DOM (DOM_{BMP}) released into the soil-water environment were studied.

5.2. Materials and Methods

5.2.1. Sample preparation

Two types of commercial BMs, namely, WGP (Sunshine Paper, Aurora, CO, USA) and BioAgri (BioBag Americas, Dunevin, FL, USA), were used in this study (Table 5.1). WGP is a brown paper mulch mainly composed of cellulose, while BioAgri is a black bioplastic mulch primarily consisting of PBAT and starch. Compared with WGP, BioAgri has significantly different physicochemical characteristics such as lower density, thickness, and peak load but higher elongation and carbon content. The soil used in the experiment was sampled from the 0–15 cm topsoil layer of the experimental field at the Emile A. Lods Agronomy Research Center (N 45°25′34″, W 73°55′40″), Macdonald Campus of McGill University, Sainte-Anne-de-Bellevue, Québec, Canada. The soil was characterized as Humic Gleysol, a well-drained sandy loam (62% sand, 32% silt, 6% clay) with a 1.28 g/cm^3 bulk density, 2.53 g/cm^3 particle density, pH 6.8, 52% water holding capacity, 48 g/kg organic-C content, and 2.5 g/kg total-N content. After sampling, the soil was air-dried in the fume hood for 48 h, ground, screened with a 2-mm sieve, and then stored in dry, dark, and sealed glass jars at room temperature.

Table 5.1. Basic information on the used BMs

Properties		WGP	BioAgri
Manufacturer		Sunshine Paper, Aurora, CO, USA	BioBag Americas, Dunevin, FL, USA
Color		Brown	Black
[a] Density, g/m^2		110.88 ± 0.533	22.81 ± 0.411
[a] Thickness (μm)		562 ± 13.0	29 ± 1.2
[a] Peak load (N)		88.22 ± 7.144	12.05 ± 0.586
[a] Elongation (%)		7.70 ± 0.300	295.00 ± 30.000
[b] Main polymer structure		Cellulosic paper: cellulose 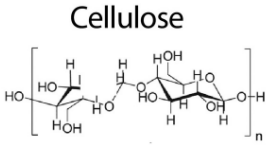	Mater-Bi® bioplastic: PBAT + starch 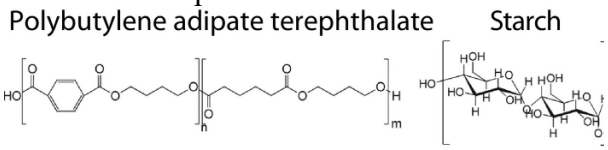
Element content (%)	C ± SD.	42.98 ± 0.016	59.70 ± 0.227
	N ± SD.	0.080 ± 0.005	0.051 ± 0.005
	H ± SD.	6.710 ± 0.006	6.748 ± 0.032
	S ± SD.	0.046 ± 0.0006 *	0.015 ± 0.003*

SD is standard deviation; * denotes sulfur via infrared detector (IR), and other via thermal conductivity detector (TCD); a (Hayes et al., 2017); b (Sintim et al., 2020).

5.2.2. Batch experimental design

The batch experimental design is shown in Figure 5.1. The BMs were stored in a dry and dark place at room temperature before batch experiments. They were cut into two sizes of debris: BMaPs (2–10 cm × 5 cm) and BMPs (2 mm × 6 mm). Pristine BM debris was placed in uncovered glass Petri dishes and weathered in a UV chamber (CX-2000 Crosslinker, Analytik Jena, USA) for different irradiation durations: 4K, 8K, 12K, 16K, 20K, 24K, 28K, and 32K (K=1,000) minutes. UV irradiation is generally less than 10% of the total solar irradiation (about 1367 W/m^2), so UV rays (254 nm, 20 mW/cm^2) were selected to simulate the accelerated weathering conditions.

Control samples (0K) were wrapped in aluminum foil and placed in the UV chamber under the same conditions as the weathered samples.

After UV irradiation, BMaPs were collected for the physiochemical characterization of the BM surface, whereas BMPs were used for particle analysis and DOM_{BMP} identification. To explore the process of BMPs releasing particles into the water environment, a dry weight of 0.3 g BMPs with various irradiation durations and 35 mL of deionized water were mixed in 50 mL centrifuge tubes. The tubes were shaken at 300 rpm and 25 °C for 15 h in an incubator shaker (New Brunswick Innova 42R, Eppendorf, USA). The mixture was separated into BMPs and leachates using a 0.5-mm sieve. The BMPs were air-dried in the fume hood for 48 h for the further physiochemical characterization of the BM surface as described in section 5.2.3. The leachate was collected for particle analysis as described in section 5.2.4. Then it was separated into the particulate organic matter (POM_{BMP}) and DOM_{BMP} through vacuum filtration with 0.45-μm membranes. Notably, DOM_{BMP} is considered a stable colloidal suspension of BNPs released from BMPs in this study (Docter et al., 2015). The particle morphology of POM_{BMP} remaining on the membranes was analyzed as described in section 5.2.3, whereas DOM_{BMP} was used for chemical identification and nanoparticle analysis as described in sections 5.2.4 and 5.2.5.

After entering the soil-water environment, the property of BMPs will be influenced by soil particles, such as due to mechanical abrasion. To explore the interactions between BMPs and soil

particles, a total dry weight of 0.3 g BMPs and soils in a 1:9 ratio was added into a 50 mL centrifuge tube. The BMPs were collected for analysis following the same procedures. Before air-drying, the BMPs were softly washed for 30 s using flowing deionized water to remove soil particles unstably adhering to the BMP surface.

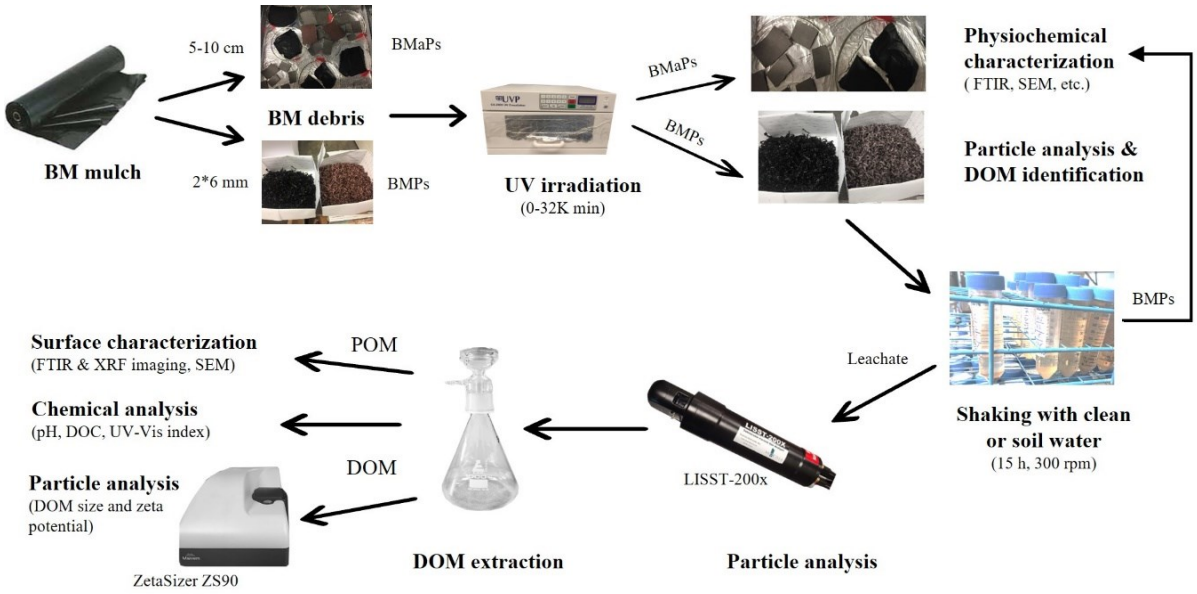

Figure 5.1. Batch experimental design.

5.2.3. Physiochemical characterization of BMaPs

The mechanical tensile strength (peak load) of the BMaPs (1 cm × 5 cm) was tested using the Model 42 Material Test System (MTS Criterion, USA). The changing rate of the peak load relative to the pristine BMaPs was adopted to characterize the effect of UV irradiation on the mechanical tensile strength of different BMaPs. The hydrophobicity of the BMaP surface was characterized by the water contact angle (CA_w) between the BMaP surface and the deionized water. A contact

angle goniometer (VCA Optima, AST Products, USA) recorded the changing of the 1.5 μL water droplet within 10 s after starting the recording at an ambient temperature of 20 °C and humidity of 45%. Microstructural changes on the BMaP surface were observed using an S-3400N scanning electron microscope (SEM, Hitachi, Japan) with a 5 kV electron accelerating voltage. Before observation, the BMaP were affixed to the sample holder using carbon tape, metalized with a 2-nm gold layer using JEOL device JFC 1100E ion sputter, and fine coated at 10 mA for 1 min.

The surface functional groups of the BMaPs were measured using attenuated total reflection−fourier transform infrared spectroscopy (ATR−FTIR, Optics Tensor 27, Bruker, USA). Six measurements were conducted for each sample on the surface. In each measurement, background spectrum and sample spectra were obtained in wavenumber ranges of 4000–400 cm^{-1} with 32 scans. The carbonyl index (CI) was applied to evaluate the changes in the carbonyl band (C=O) using the following equation (Almond et al., 2020):

$$Carbonyl\ index\ (CI) = \frac{Area\ under\ band 1850 - 1650 cm^{-1}}{Area\ under\ band\ 1500 - 1420 cm^{-1}} \quad (5.1)$$

To observe the functional group distribution of BMPs after soil-water washing, the FTIR images of the BMP surface were collected in reflectance mode, with a resolution of 4 cm^{-1} and the co-addition of 128 scans over the range of 4000−1000 cm^{-1}, at the Canadian Light Source (CLS) in Saskatoon, Canada. Bruker Vertex 70v coupled with a confocal microscope (Hyperion 3000) at

the Mid Infrared Spectromicroscopy (MID-IR) beamline was used to measure these samples. The whole set facility included a motored sample stage and a liquid nitrogen (LN)-cooled mercury cadmium telluride (MCT) detector (Bruker Optics, MA). The imaging data of the detected surface (64×64-pixel array) were acquired for each sample. FTIR mapping cannot detect much metal-O binding information below 1000 cm^{-1}, so synchrotron X-ray fluorescence (SR-XRF) spectra and mappings were further measured to identify the element distribution of trace metals on the BMP surface at the Very Sensitive Elemental and Structural Probe Employing Radiation From A Synchrotron (VESPERS) beamline (07B2–1). The SR-XRF maps of titanium (Ti), manganese (Mn), iron (Fe), cobalt (Co), Ni, Cu, zinc (Zn), and calcium (Ca) were scanned under an area of 200 μm × 200 μm with a step size of 5 μm.

5.2.4. Particle analysis of leachate from BMPs

The average and distribution of micro- and nano-particle sizes in the leachate from BMPs were measured using a laser in-situ scattering and transmissometer (LISST-200X, Sequoia Scientific, USA) and a Zetasizer analyzer (Nano ZS90, Malvern, UK). The detection range of the LISST-200X was 1–500 μm. The particle concentration (μL/L) was calculated by the equivalent volume of the irregular spheres. Samples of 20 mL were placed in the test chamber of LISST-200X and a total of 60 data points were collected for each minute in live data collecting mode. Deionized water as the control sample was used as the background for each measurement. After measurements, the samples were extracted from the test chamber of the LISST-200X and then filtrated through a 0.45-

μm membrane to separate the POM_{BMP} and DOM_{BMP}. The Nano ZS90 has been used to measure the average and distribution of nanoplastic size in the previous study (Murray and Örmeci, 2020). Its measurement range was 0.3 nm–10.0 μm. The size intensity and size distribution were measured by dynamic light scattering (DLS) and calculated using the Stokes-Einstein relationship. 1 mL DOM_{BMP} was added to the corresponding cells of the Nano ZS90 to measure its particle distribution and zeta potential (ZP). The POM_{BMP} remaining on the membranes was dried and its particle morphology was observed using SEM imaging following the procedures in section 5.2.3. The particle size distribution can be typically expressed by D10 (d10), D50 (d50), and D90 (d90). In this study, D and d represented the diameter of the microparticles (1-458.5 μm) and nanoparticles (0.3–5560 nm), respectively. D10 (d10), D50 (d50), and D90 (d90) mean that 10%, 50%, and 90% of the total particles were smaller than the corresponding size in the cumulative distribution function (CDF) of microparticles (or nanoparticles) measured by LISST-200X (or Nano ZS90), respectively. The particle size exceeding D10 (d10) and D90 (d90) can be ignored, and D50 (d50) is the median size of the particle distribution.

5.2.5. Identification and quantification of BMP-derived DOM

The pH of DOM_{BMP} was measured by a dual channel pH/Ion meter (Model AR25, Accumet Research, Fisher Scientific, Canada) calibrated with Fisher Scientific pH buffer standards at room temperature. DOC content was determined according to the high-temperature combustion method using a Shimadzu total organic carbon-VCSH analyzer (Kyoto, Japan). The Zeta potentials (ZPs)

of DOM_{BMP} were measured using the Nano ZS90 with a fixed scattering angle of 90° at 25 °C. Three replicates with over 20 runs per measurement were conducted for each sample. Deionized water as the control sample was used as the background for each DOC and ZP measurement. The organic carbon yield of BMPs (W_{SOC}, mg/g) was used to represent the organic carbon released from BMPs to water, which was obtained using the following equation:

$$W_{SOC} = C_{DOC} \times \frac{V_{solution}}{m_{BMPs}} \tag{5.2}$$

where $V_{solution}$ is the solution volume used for water extraction and m_{BMPs} (g) is the mass of BMPs used for water extraction.

Soil DOM parameters based on UV-vis spectroscopy have been widely used in recent years. Therefore, UV-vis spectra were obtained at wavelengths of 600–200 nm with 1 nm stepwise increments using a UV-vis spectrophotometer (UV-6700, Shimadzu, Japan). Blanks of deionized water were used as a reference. All DOM_{BMP} samples were returned to room temperature before measurements. The main UV-vis spectroscopy-based DOM parameters were calculated and described in Table 5.2.

Table 5.2. UV-Vis spectroscopy-based DOM parameters.

Index	Calculation	Characteristics	Relationships	Reference
$S_{275–295}$ (nm^{-1})	The slope of linear regression on the log-transformed spectra in the range of 275-295 nm	Molecular weight (MW)	Negative	(Zhang et al., 2021)

$A_{240\text{-}400}$ (m^{-2})	The integral of the area from 240-400 nm ($A_{240\text{-}400}$)	Electron transfer (ET)	Positive	(Chen et al., 2022)
$SUVA_{254}$ [L/(mg-C · m)]	The absorption coefficient at 254 nm divided by DOC concentration	Aromaticity	Positive	(Chen et al., 2022)
E_3/E_4	The ratio of absorbances at 300 and 400 nm, A_{300}/A_{400}	Humification	Negative	(Li and Hur, 2017)
A_{220}/A_{254}	The ratio of absorbances at 220 and 254 nm, A_{220}/A_{254}	Polarity	Negative	(Li and Hur, 2017)
A_{254}/A_{204}	The ratio of absorbances at 254 and 204 nm, A_{254}/A_{204}	Hydrophobicity	Positive	(Li and Hur, 2017)

5.2.6. Quality assurance/quality control (QA/QC) and statistical analysis

Batch experiments were conducted in triplicate and the average was used for further analysis. Blank control experiments with only deionized water were conducted for correction. All containers were cleaned using tap water with specific laboratory detergents in an ultrasonic cleaner (Model 97043-944, VWR International, USA) for 30 min, rinsed five times with deionized water, and dried at 50 °C in an oven (Blue M, USA) for 24 h. Most graphs were plotted using Origin 2021 (OriginLab Corporation, USA). Notably, the CI was calculated using mathematical area and integration methods. The typical indexes of particle size distribution, namely, D10 (d10), D50 (d50), and D90 (d90), were calculated using linear interpolation and intersection methods. Besides, the area and size of particles shown in SEM images were measured using ImageJ software (https://imagej.nih.gov/ij/index.html). FTIR spectra were corrected for the background signal attributable to the ATR crystal and manipulated for averaging smooth, baseline correction, and

vector normalization using the OPUS 7.2 software (Bruker Optics Inc., USA). FTIR images were processed by Cytospec 2.00.01 (Cytospec Inc., Boston, MA) and SR-XRF spectra and maps were plotted by SigmaPlot 14.0 (Systat Software Inc., USA).

5.3. Results and Discussion

5.3.1. Physicochemical changes of BMaPs during UV irradiation

The environmental processes can be affected by many factors (Babamiri et al., 2021; Yadav et al., 2022). The main spectral band assignments of BMaPs during UV irradiation are listed in Table 5.3. The spectra obtained for pristine WGP and BioAgri mostly matched the published spectra of respective polymer constituents (Hayes et al., 2017). Bands in the hydroxyl groups (O-H) stretching and bending regions (3600–3000 cm^{-1} and 1100–900 cm^{-1}, respectively) were partially attributable to polysaccharides because starch and cellulose are the main components of BioAgri and WGP, respectively. The peak within the 3000–2800 cm^{-1} spectral range was attributed to C-H stretching. The stretching of carbonyl groups (C=O bonds) led to the different peaks at 1710 and 1640 cm^{-1} for pristine BioAgri and WGP, probably attributed to the ester groups (-COO, peaking at 1710 cm^{-1}) of PBAT in BioAgri and conjugated C=O (peaking at 1640 cm^{-1}) of dye on WGP surface, respectively. The CI index of WGP increased linearly with UV irradiation, whereas BioAgri showed a reverse "U" relationship between them (Figure 5.2), possibly suggesting different dominant chemical photoreactions between two BaMPs during UV irradiation.

Table 5.3. Peak assignments for FTIR analysis of biodegradable mulches (Hayes et al., 2017).

Wavenumber (cm^{-1})	**Mulch**	**Bond assignments**
3000-3800	WGP, BioAgri	OH stretch
2924, 2852	BioAgri	C-H stretch
1710	BioAgri	C=O stretch
1646, 1700-1720	WGP	C=O stretch
1456	BioAgri (PBAT)	phenylene group
1409	BioAgri (PBAT)	$C\text{-}H_2$
1456, 1410, 1390	BioAgri	$\text{-}CH_2\text{-}$ bend
1428, 1368, 1336, 1316	WGP	C-H bend
1163	BioAgri (Starch)	CH_2OH
1118, 1081, 1270	BioAgri (Starch)	C-O
1018	PBAT	phenyl ring
1268, 1252, 1166, 1118, 1102, 1082	BioAgri	C-O stretch (polyester)
1100–900	WGP, BioAgri	O-H bend
874	BioAgri,	C-H stretch
726-728	BioAgri (PBAT)	$[\text{-}C\text{-}H_2\text{-}]n \geq 4$ bend

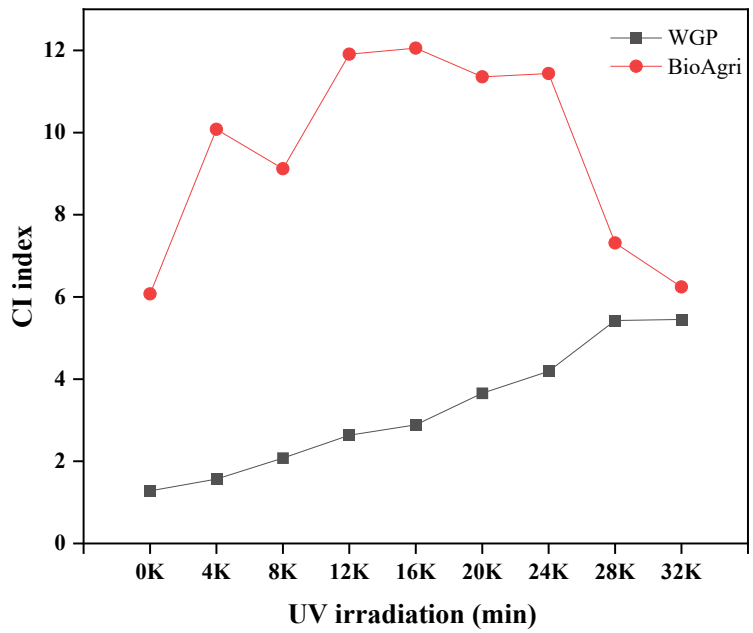

Figure 5.2. CI index of WGP and BioAgri with different UV irradiation durations (K: 1000 min).

The FTIR spectra of BMaPs during UV irradiation are shown in Figure 5.3. For the weathered WGP, a reduction of conjugated C=O and O-H groups (3600–3000 cm^{-1}) was observed after 4K min, whereby, its color changed from brown to grey. This result suggested that UV irradiation might promote the dye to produce VOCs emitted into the air (Cai et al., 2021a; Cai et al., 2021b). Since 8K min, a new peak at 1715 cm^{-1} assigned to C=O was detected, which was possibly due to the photooxidation of free radicals. Oxygenated functional groups (e.g., C=O) can be produced when UV radiation initiates the breaking of the C-H and O-O bonds and the generation of free radicals (e.g., hydroxyl, alkoxy, and peroxy radicals) in the oxygen environment (Feng et al., 2022a). The decrease of C-H bonds was also observed for BioAgri since 4K min, which may produce ester bonds (C=O). However, for the weathered BioAgri, the -COO and C-O (peaking at

1270 cm^{-1}) stretching bands decreased and became broad since 4K min, consistent with the Norrish I photodegradation reactions of PBAT and resulting in chemical cross-linking via the formation of free radicals on aromatic groups (Ar-) (Kijchavengkul et al., 2010). An increase of C=C (peaking at 1650 cm^{-1}), aromatic C=C (Ar C=C, 1580–1500 cm^{-1}), and free OH (3900–3600 cm^{-1}) was observed for BioAgri since 16K min, indicating the Norrish II photodegradation reaction of C=O bonds, which produced terminal carboxylic compounds (-COOH) and terminal double bond compounds ($CH=CH_2$) (Kijchavengkul et al., 2010). An increase of C=C, Ar C=C, and free OH bonds was also observed for WGP since 20K min, which may have resulted from the Norrish I and II chain scission of C=O and the formation of OH and C=C bonds (Hayes et al., 2017; Kijchavengkul et al., 2010; Kijchavengkul et al., 2008). Therefore, it can be inferred that there is a combination of the photooxidation-dominated production and photodegradation-dominated cleavage of ester bonds (C=O) during UV irradiation.

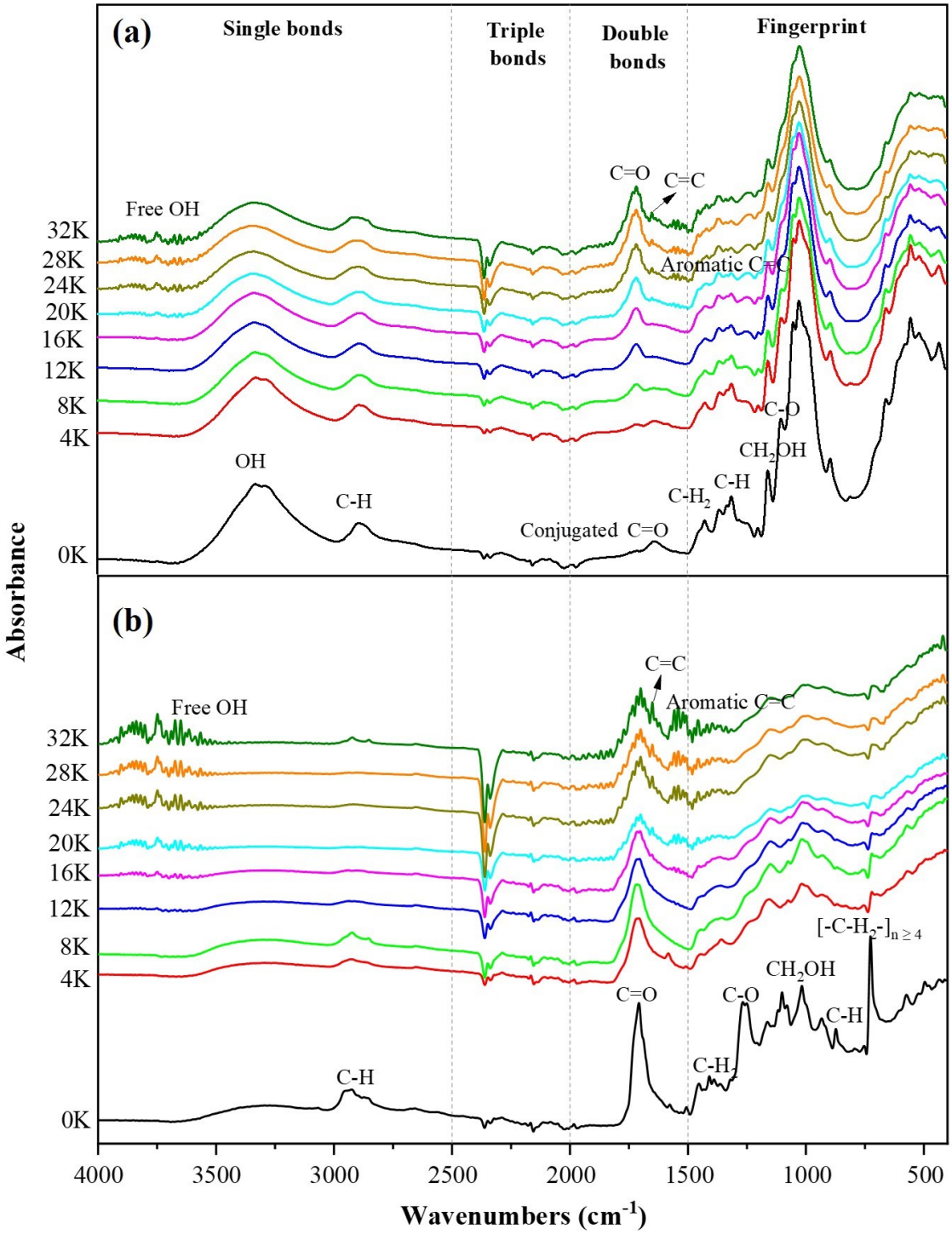

Figure 5.3. Surface chemical changes during UV irradiation. FTIR spectra for (a) WGP and (b) BioAgri with different UV irradiation durations (K: 1000).

Tensile tests, CA_w, SEM, and FTIR mapping were further used to observe the mechanical tensile strength of BaMPs as well as the microstructure changes and chemical distributions on the BaMP surface before and after UV irradiation (Figure 5.4-5.6). As shown in Figure 5.4 (a), with the UV irradiation duration, the peak load of WGP and BioAgri both showed a downtrend. Compared to the pristine BaMPs, their tensile strength decreased by 58.8% and 93.9% after 32K min UV irradiation, respectively. This result was consistent with previous studies that peak load decreased with the photo-oxidation time (Hayes et al., 2017; La Mantia et al., 2020), probably due to the damage to the BaMP surface caused by the photoreaction, such as Norrish I and II chain scission.

The hydrophilicity of the BaMP surface can also change during UV irradiation, which can be represented by droplet-mulch CA_w. As shown in Figure 5.4 (b), the mean CA_w of WGP and BioAgri both decreased with the UV irradiation duration. Compared to the pristine BaMPs, their mean CA_w decreased by 66.2% and 63.5% after 32K min UV irradiation, respectively (WGP: from 54.0 to 18.3 °; BioAgri: from 82.1 to 30.0 °). As shown in Figure 5.5, the water droplet can be absorbed by WGP and spread over the BioAgri surface; therefore, their CA_ws decreased quickly in the 10 s video recording. The changing rates of CA_ws for WGP and BioAgri in each dynamic observation both increased with UV irradiation duration and WGP had a higher changing rate than BioAgri (WGP: from -22 to -99 °/s; BioAgri: from -6 to -47 °/s). This meant that WGP had a lower mean CA_w and higher hydrophilicity than BioAgri before and after UV irradiation, respectively.

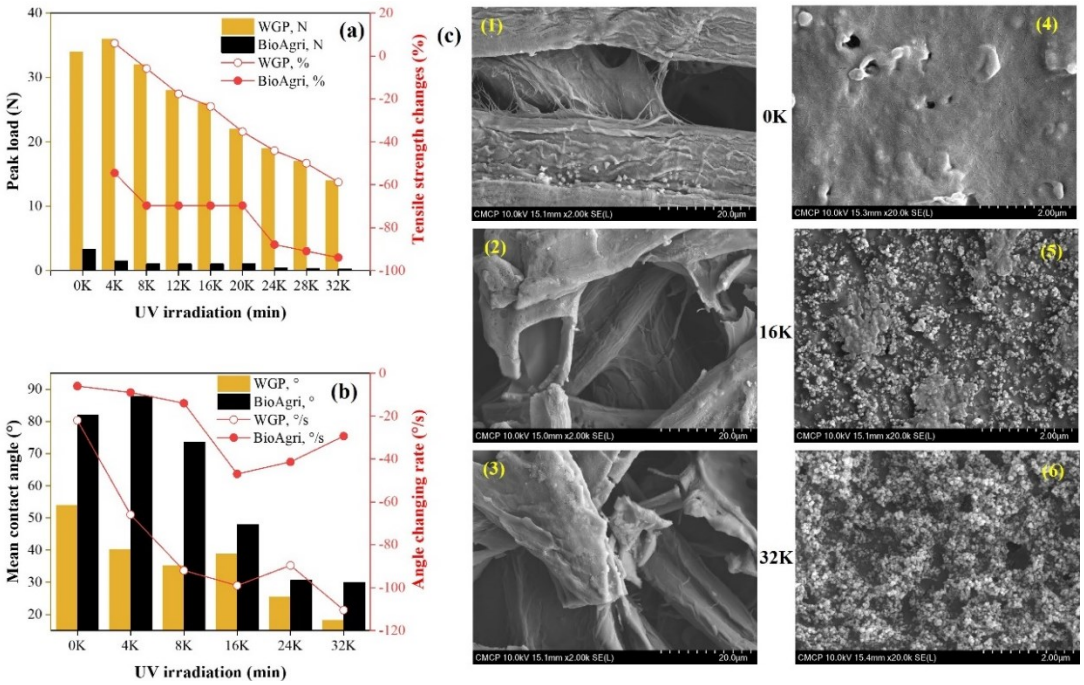

Figure 5.4. Surface physical changes during different UV irradiation durations (K: 1000). (a) mechanical tensile strength (peak load, N); (b) water contact angles (°); (c) SEM images for WGP (1-3) at 2K magnification and BioAgri (4-6) at 20K magnification.

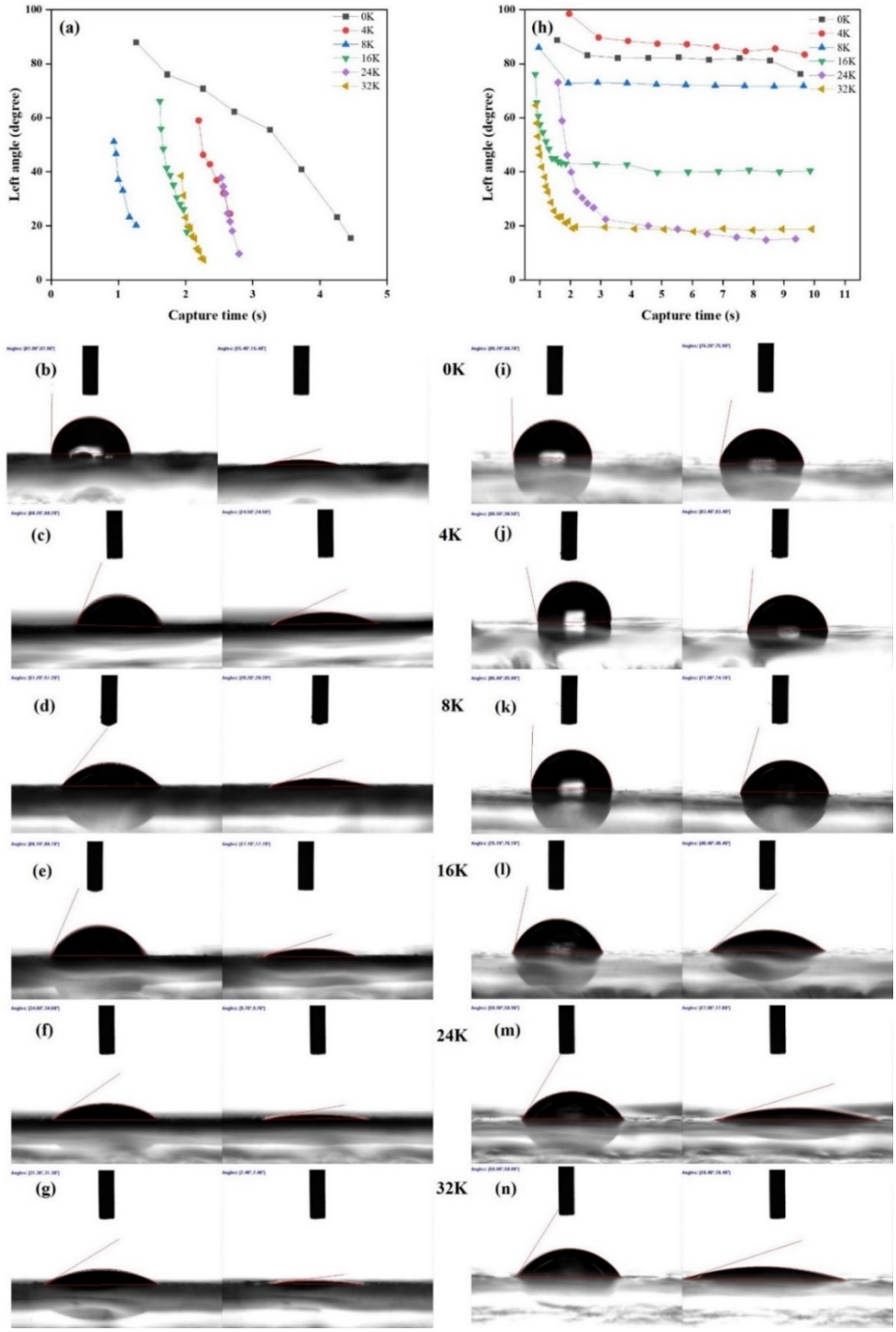

Figure 5.5. Dynamic water contact angles of WGP (a–g) and BioAgri (h-n) with different UV irradiation durations (K: 1000). The left and right of each image are the start and end of each video recording of dynamic water contact angles.

The variations of CA_w can be partially explained by the change in the contents of hydrophilic groups on the BaMP surface. The pristine WGP had a larger oxygen elemental content (50%) than pristine BioAgri (33%) (Table 5.1), which may cause a higher content of the hydrophilic group on their surface. As shown in Figure 5.6, compared to the pristine BioAgri, the weathered one had higher contents of functional groups. The increased surface hydrophilicity of BioAgri after UV irradiation can be partially attributed to the formation of hydrophilic groups, such as hydrophilic double-bond groups (C=O bonds) and oxygen-containing groups (O-H bonds). However, no significant changes in the contents of functional groups were observed on the pristine and weathered WGP surface. This meant the changes in hydrophilicity of the WGP surface were probably due to other surface factors, such as surface roughness (Wang et al., 2021d; Wang et al., 2022c).

The SEM images and FTIR maps of BaMPs showed that BioAgri had a smooth surface, with a heterogeneous microstructure where circular starch spots (C-H, C-O, and O-H bonds) were dispersed in a continuous three-dimension PBAT matrix (CO and C=O bonds) before weathering. With the increase in UV irradiation duration, BioAgri underwent significant changes in surface microstructure and chemical distributions. Specifically, the ratio of exposed starch to the total measured area increased from 6.6% (0K) to 41.9% (16K) and 70.1% (32K) as shown in Figure 5.4 (c4-c6) and Figure 5.7 (10-18), probably because of the photodegradation of the PBAT matrix. As shown in Figure 5.4 (c1-c3) and Figure 5.7 (1-9), the WGP surface was neatly lined with cellulosic

fibers. After 16K min UV irradiation, some fractures of fiber occurred on the WGP surface, causing small particles and fiber fragments. As the UV irradiation duration increased to 32K min, no significant increase in surface cracks and small particles was observed, showing the discontinuous linear distribution of functional groups. These results were consistent with previous studies that UV irradiation promoted the generation of cracks and particles on polymer surfaces, which increased surface roughness and hydrophilicity (Wang et al., 2021d; Wang et al., 2022c).

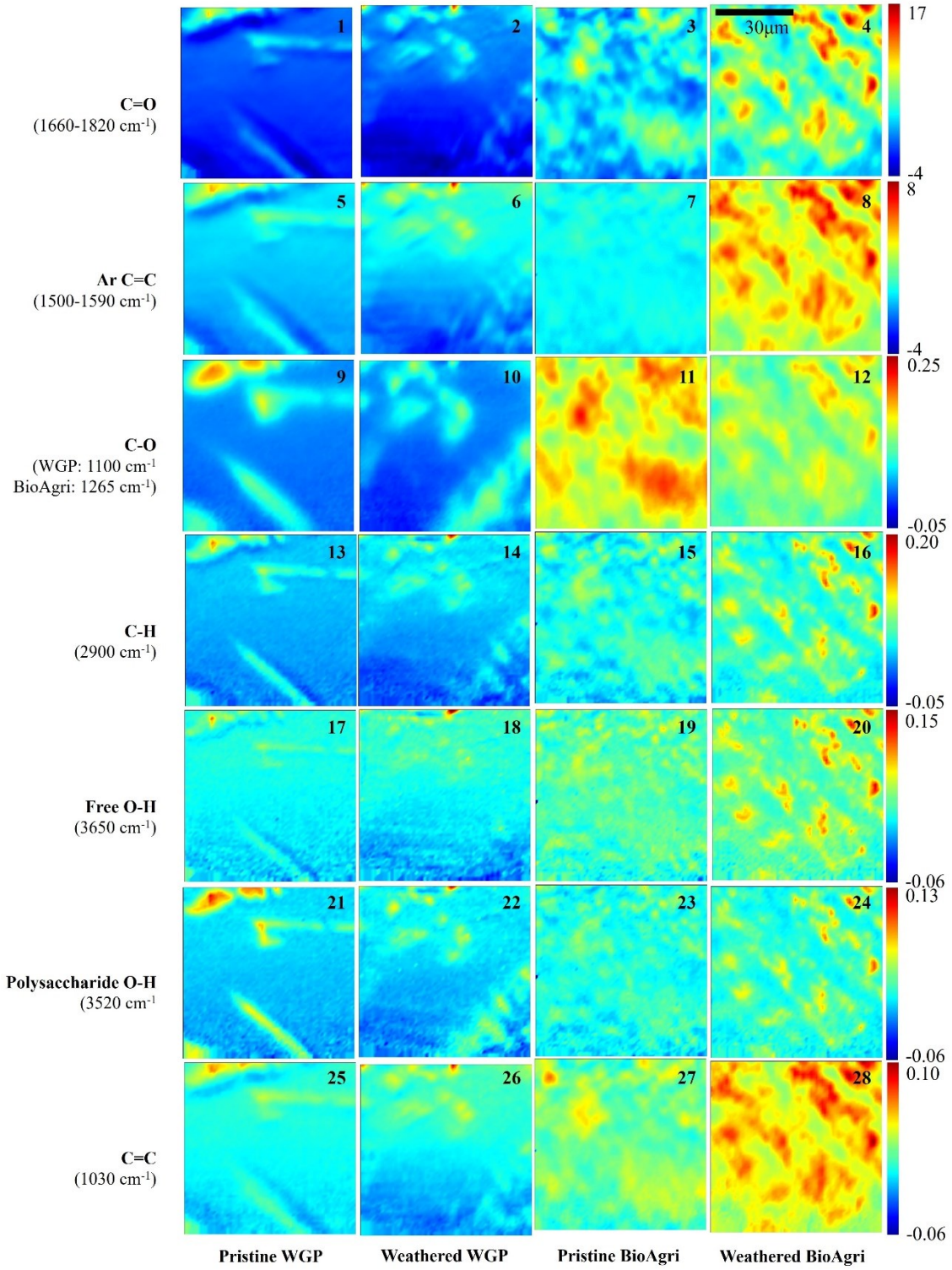

Figure 5.6. FTIR mapping of functional groups on pristine and weathered BMP surface.

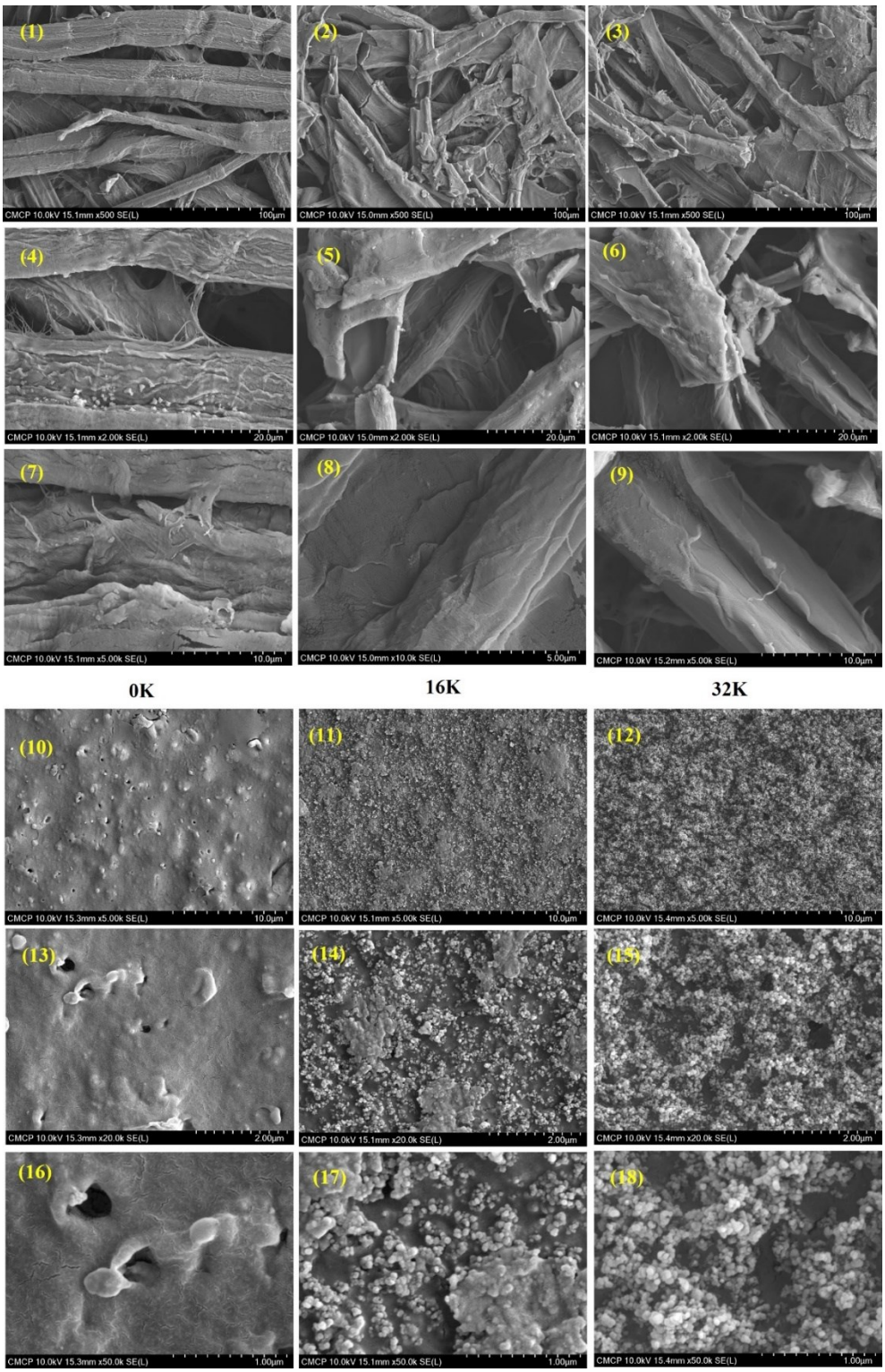

Figure 5.7. SEM images for WGP (1-9) and BioAgri (10-18) with different UV irradiation durations (K: 1000) at different magnifications.

5.3.2. Chemical analysis of BMP-derived DOM

The chemical analysis results of DOM_{BMP} derived from the pristine and weathered BMPs are shown in Figure 5.8. BioAgri released much more DOC (W_{DOC}, mg/g) than WGP before and after UV irradiation, while their W_{DOC} both increased from 0K to 32K min (WGP: from 1.19 ± 0.12 to 16.18 ± 0.41; BioAgri: from 12.52 ± 0.37 to 23.74 ± 2.19). The DOM_{BMP} caused significant chemical changes in the water. The pristine WGP and BioAgri both released basic DOM_{BMP}, with a pH greater than 6.5, which is consistent with the reported findings (Serrano-Ruíz et al., 2020). With increasing UV irradiation duration, the pH of weathered DOM_{BMP} significantly decreased. When the UV irradiation duration was extended to 32K min, the DOM_{BMP} derived from the weathered WGP and BioAgri showed strong acidity, with a pH of 4.5 and 3.7, respectively. This result may be attributed to the acid oxygen-containing groups, such as carboxyl groups (COO-bonds), released from the weathered BMPs after UV irradiation.

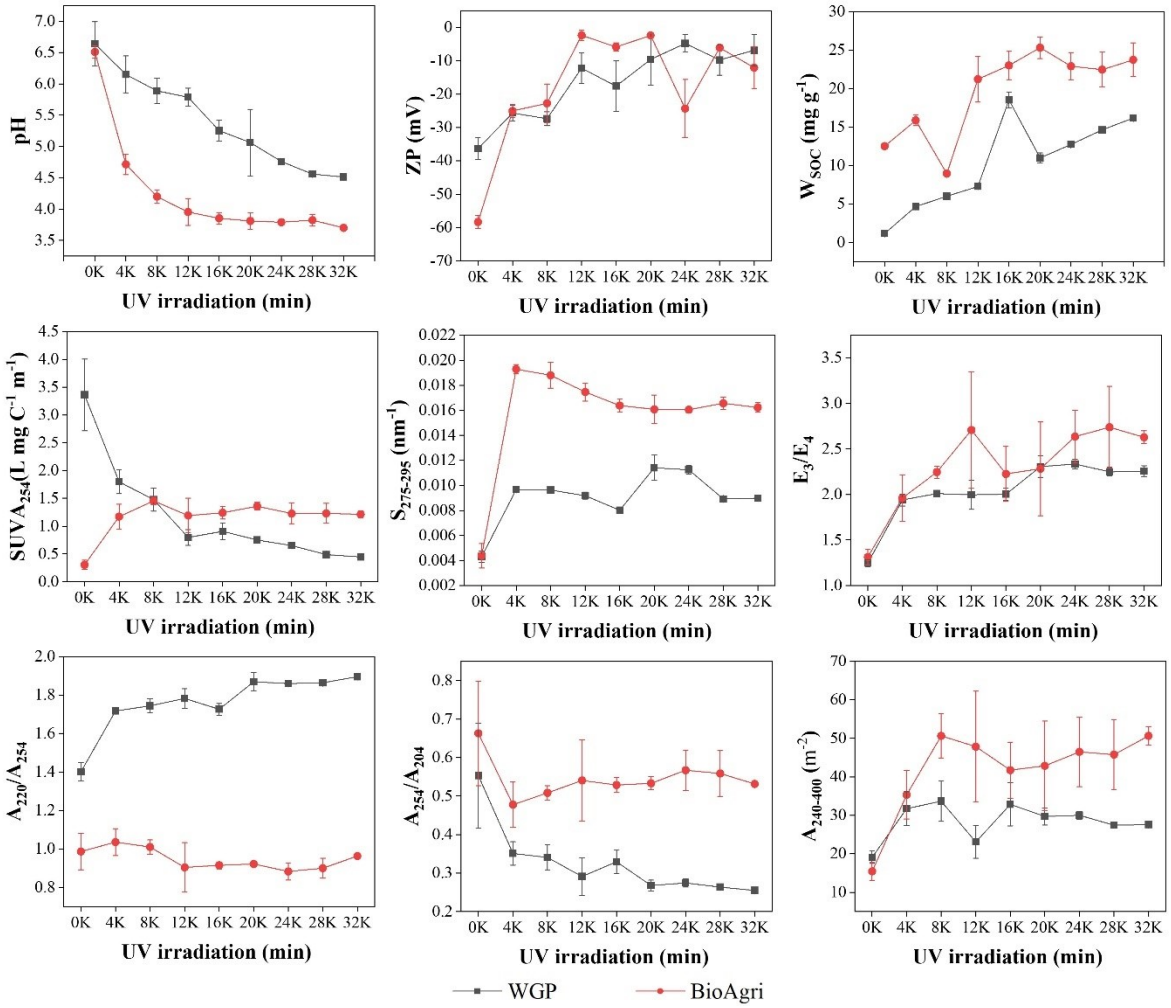

Figure 5.8. Chemical analysis of DOM_{BMP} released into the water environment.

According to the FTIR maps of the BMP surface before and after water washing (Figure 5.6 and Figure 5.9), the C=O bonds of the WGP surface significantly decreased after washing, which meant that acid carboxyl groups were released into water from the WGP. However, the C=O bonds on the BioAgri surface increased, whereas the C-H bonds decreased after washing, which indicated the hydrolysis of PBAT (Hayes et al., 2017; Sintim et al., 2020). This may cause more acid carboxyl groups to be released into the water and retained on the BMP surface compared with the

unwashed BioAgri. The carboxylic acid was negatively charged, so the DOM from the pristine and weathered BMPs had negative ZP values (-7–-58mV), which coincided with previous research (Fan et al., 2021; Feng et al., 2022b; Yang et al., 2022b). With the increase in UV irradiation duration, the ZP values of the DOM_{BMP} derived from WGP and BioAgri largely increased from -36 and -58 mV (0K min) to -7 and -12 mV (32K min), respectively. This was different from the findings of previous studies, wherein the weathered DOM_{BMP} became more negatively charged because of UV irradiation (Fan et al., 2021; Feng et al., 2022b), possibly due to proton neutralization at a low pH level (3.7–4.5). The ZP values of WGP and BioAgri both showed a significant negative relationship with pH under UV irradiation; with the decreased pH, BNPs became less ionized and negatively charged (Bi et al., 2022; Yin et al., 2021).

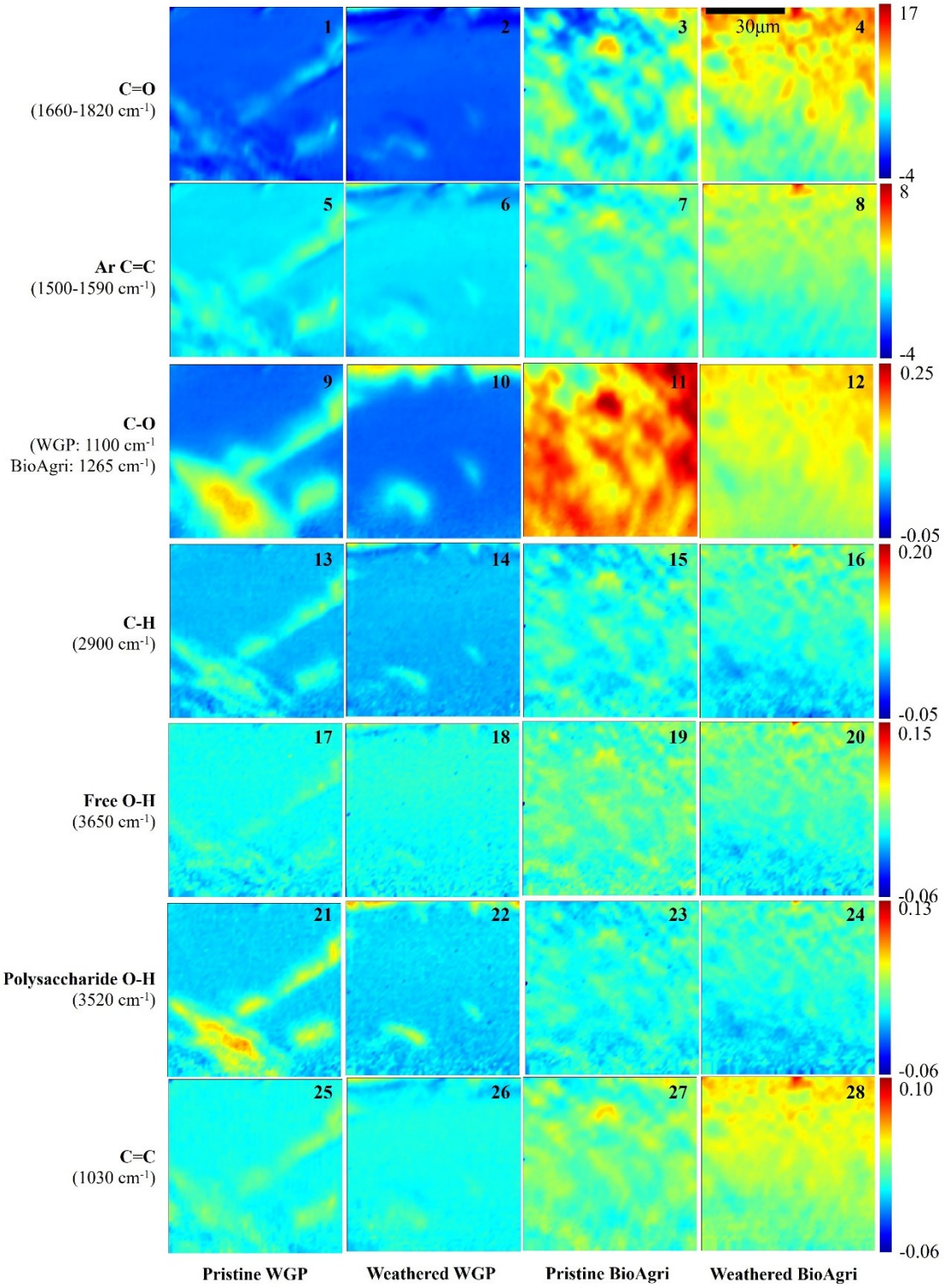

Figure 5.9. FTIR mapping of functional groups on BMP surface after water washing.

The UV-vis spectral signal peak at 300–250 nm is due to the aromatic structure-containing chemicals, including low-ring PAHs (2–4 rings) and their derivatives (Huang et al., 2020a; Zhang et al., 2021). Therefore, the $SUVA_{254}$ (L/(mg-C·m)) was used to evaluate the aromaticity of DOM_{BMP}. The UV-vis spectral index of $S_{275-295}$ is usually adopted to represent the molecular size of DOM_{BMP}, which is negatively related to molecular size. The E_3/E_4 ratio and A_{220}/A_{254} ratio are negatively related to humification and polarity, respectively. The A_{254}/A_{204} ratio and $A_{240–400}$ index are positively correlated with hydrophobicity and electron transfer (ET) capacity, respectively (Chen et al., 2022; Li and Hur, 2017). Generally, the pristine BioAgri had smaller $SUVA_{254}$ and A_{220}/A_{254} values, as well as larger $S_{275-295}$, E_3/E_4, A_{254}/A_{204}, and $A_{240–400}$ values than WGP, which suggested that BioAgri-DOM_{BMP} had higher aromaticity, polarity, hydrophobicity, and ET capacity, as well as smaller molecular size and humification, than WGP-DOM_{BMP}. With increasing UV irradiation duration, the $SUVA_{254}$ values of BioAgri-DOM_{BMP} significantly increased by about threefold that of the pristine one at 4K min (1.17 ± 0.21) and then maintained at a relatively high level (1.19–1.43), indicating that UV irradiation enhanced the aromaticity of DOM_{BMP}. However, compared with the pristine WGP-DOM_{BMP}, the $SUVA_{254}$ values of the weathered WGP-DOM_{BMP} sharply dropped by 46.5% at 4K min and 85.4% at 28K min, respectively. Meanwhile, UV irradiation significantly decreased the molecular size, humification, and hydrophobicity but increased ET capacity compared with the pristine BMPs. As mentioned in section 5.3.1, UV irradiation caused the Norrish I and II chain scission of C=O and the formation of OH and C=C bonds, which can transform a large molecule into a small one (Kijchavengkul et al., 2010;

Kijchavengkul et al., 2008), thereby decreasing the humification of DOM_{BMP}. According to the FTIR results shown in Figure 5.6 and Figure 5.8, polar functional groups such as hydroxyl, carbonyl, and carboxyl are produced in photoreaction, which enhances the hydrophobicity and ET capacity of the weathered DOM_{BMP}. The hydrolysis of PBAT may produce lactic acid, adipic acid, terephthalic acid, and 1,4-butanediol (Serrano-Ruíz et al., 2020), which also increases the contents of C=O bonds in BioAgri-DOM_{BMP}. The aromaticity of DOM_{BMP} derived from pristine WGP may be attributed to the release of brown dye into the water, while the production of Ar C=C bonds under UV irradiation contributed to the aromaticity of DOM_{BMP} derived from the weathered BioAgri.

5.3.3. Particles released from BMPs into the water environment

The particles released from BMPs into the water under different UV irradiation durations were investigated. The volume concentration and size distribution of the microparticles (1–458.5 μm) were measured by LISST-200X. The total concentration and mean size of the microparticles released from the pristine BMPs of WGP and BioAgri were 9.9 ± 0.7 and 7.5 ± 0.7 μL/L, and 34.9 ± 4.4 and 61.0 ± 21.2 μm, respectively, shown in Figure 5.10 and Figure 5.11. With increasing UV irradiation duration, the total volume concentration and mean diameter of the microparticles released from BMPs mostly increased, which was following the SEM images of POM_{BMP} (Figure 5.12). These trends were mostly in agreement with previous studies that UV irradiation increased the concentration of microparticles released from polymers (Wang et al., 2021d; Wang et al.,

2022c). Moreover, WGP released more microparticles than BioAgri in any UV irradiation duration. As the UV irradiation duration extended to 32K min, the total concentrations and mean size of the microparticles released from the weathered BMPs of WGP and BioAgri were 429.8 ± 83.2 and 66.6 ± 5.8 μL/L and 50.2 ± 2.3 and 56.1 ± 0.8 μm, respectively. Unlike BioAgri, WGP microparticles manifested a similar increasing trend among D10, D50, D90, and mean size with the increased UV irradiation duration. Meanwhile, their corresponding error bars became more significant, suggesting a more unstable particle size distribution (Figure 5.11). This is because WGP microparticles usually showed an unimodal pattern, whereas BioAgri microparticles mostly had a bimodal pattern in particle size distribution (Figure 5.10 (a, b, e, f)). For example, as the UV irradiation duration extended to 12K min, WGP microparticles mostly ranged between 19.2–61.2 μm, contributing 47.8% to the total concentration, respectively, whereas BioAgri microparticles were primarily distributed in two size ranges, namely, 13.79–51.86 μm and 195.02–385.55 μm, accounting for 43.6% and 23.8% of the total concentration, respectively.

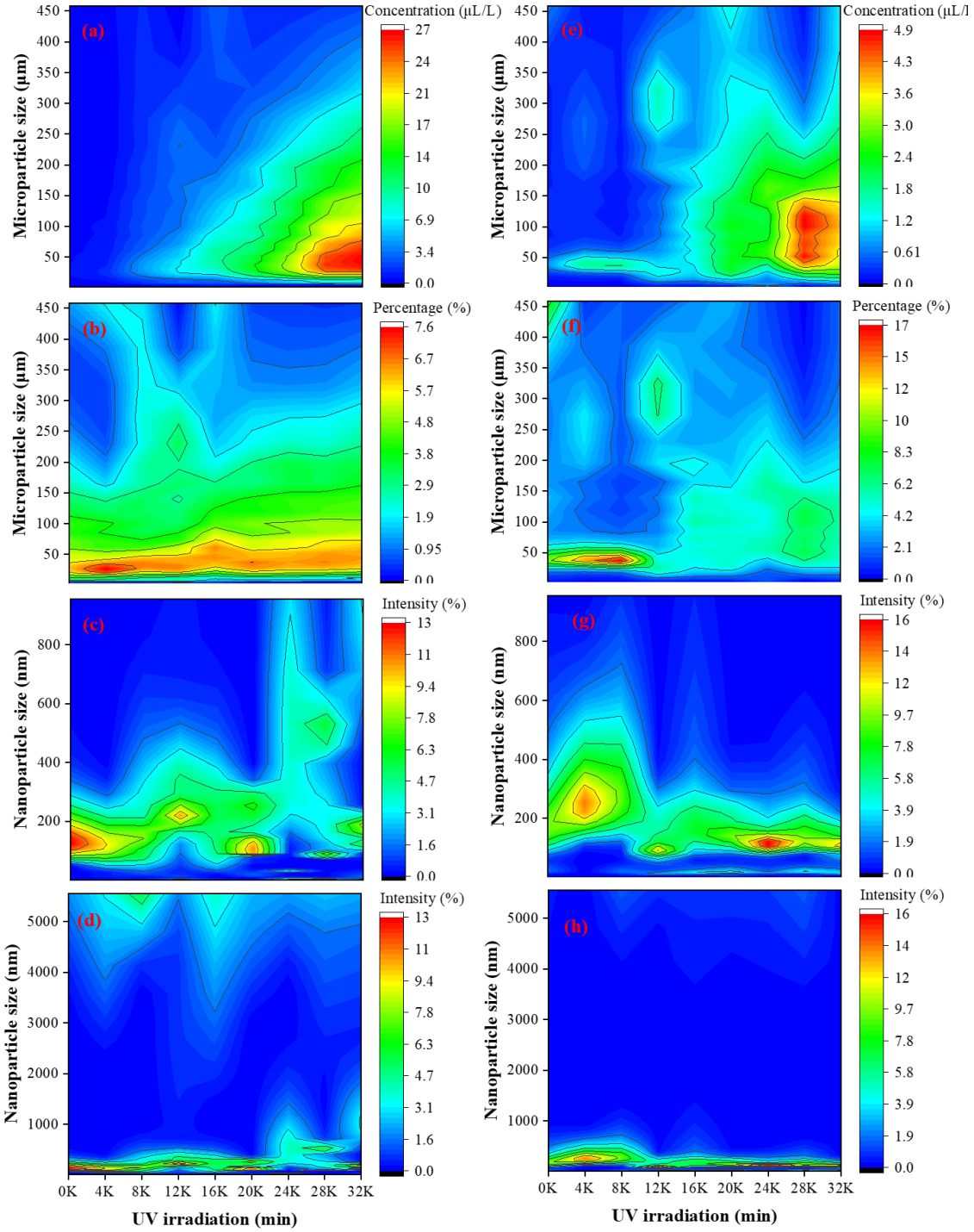

Figure 5.10. Size distributions of particles released from WGP (a-d) and BioAgri (e-h) with different UV irradiation durations (K: 1000).

Considering that most particles less than 1 μm can not be detected by the LISST-200X, the intensity and size distribution of the DOM_{BMP} under different UV irradiation durations were further investigated using the Nano ZS90. The size distribution of DOM_{BMP} in the range of 0.3–955.4 and 0.3–5560 nm was shown in Figure 5.10 (c, d, g, h), respectively. DOM_{BMP} generally showed an unimodal pattern in the size distribution of nanoparticles less than 1 μm. With the increase of UV irradiation duration, the median size (d50) of WGP-DOM_{BMP} increased from 129 ± 3 nm (0K) to 321 ± 53 nm (32K), whereas that of BioAgri-DOM_{BMP} decreased from 155 ± 72 nm (0K) to 88 ± 32 nm (32K). Previous studies have reported that with the decreasing pH, nanocellulose molecules will be less ionized, the surface negative charge will decrease, and ZP values will increase, causing an increase in the particle size of nanocellulose (Yang et al., 2022b; Yue et al., 2022). However, the decrease in DOM_{BMP} size of weathered BioAgri may be due to the decrease in pH caused by the increase in organic acids released from BMPs (Pace et al., 2012). These organic acids can promote the formation of energy-driven intra- and inter-molecular hydrogen bonds, altering the micelle-like aggregates stabilized mainly by the weaker hydrophobic association at neutral pH (Romera-Castillo et al., 2014). Notably, a proportion of particles released from the weathered BMPs of WGP (24K and 28K) and BioAgri (4K and 8K) had a particle size larger than 0.45 μm which is the pore size of the membrane used for filtration in this study. As shown in Figure 5.11 (d, f), WGP generally had much larger d90 values with corresponding error bars than BioAgri because microparticles (around 5 μm) were observed in the DOM_{BMP} derived from the pristine and weathered WGP, shown in Figure 5.10 (d, h). Previous studies have found that the increase in

nanoparticle size may be due to the nanoparticle aggregation in aquatic environments because of the flocculation effects driven by the particle surface charge and van der Waals force, as well as the particle collision enhanced by Brownian motion and differential settling (Fettweis and Lee, 2017; Wang et al., 2020c). In addition, WGP released a higher concentration of particles than BioAgri, which may increase the probability of particle agglomeration in water, leading to the generation of microparticles (around 5 μm) in the WGP-DOM_{BMP}. Owing to the sieving standard being 0.45 μm, the molecular weight distribution may be more accurate to represent the DOM_{BMP} fractions than the particle size. Therefore, the molecular weight distribution would be an optional measurement in our future research.

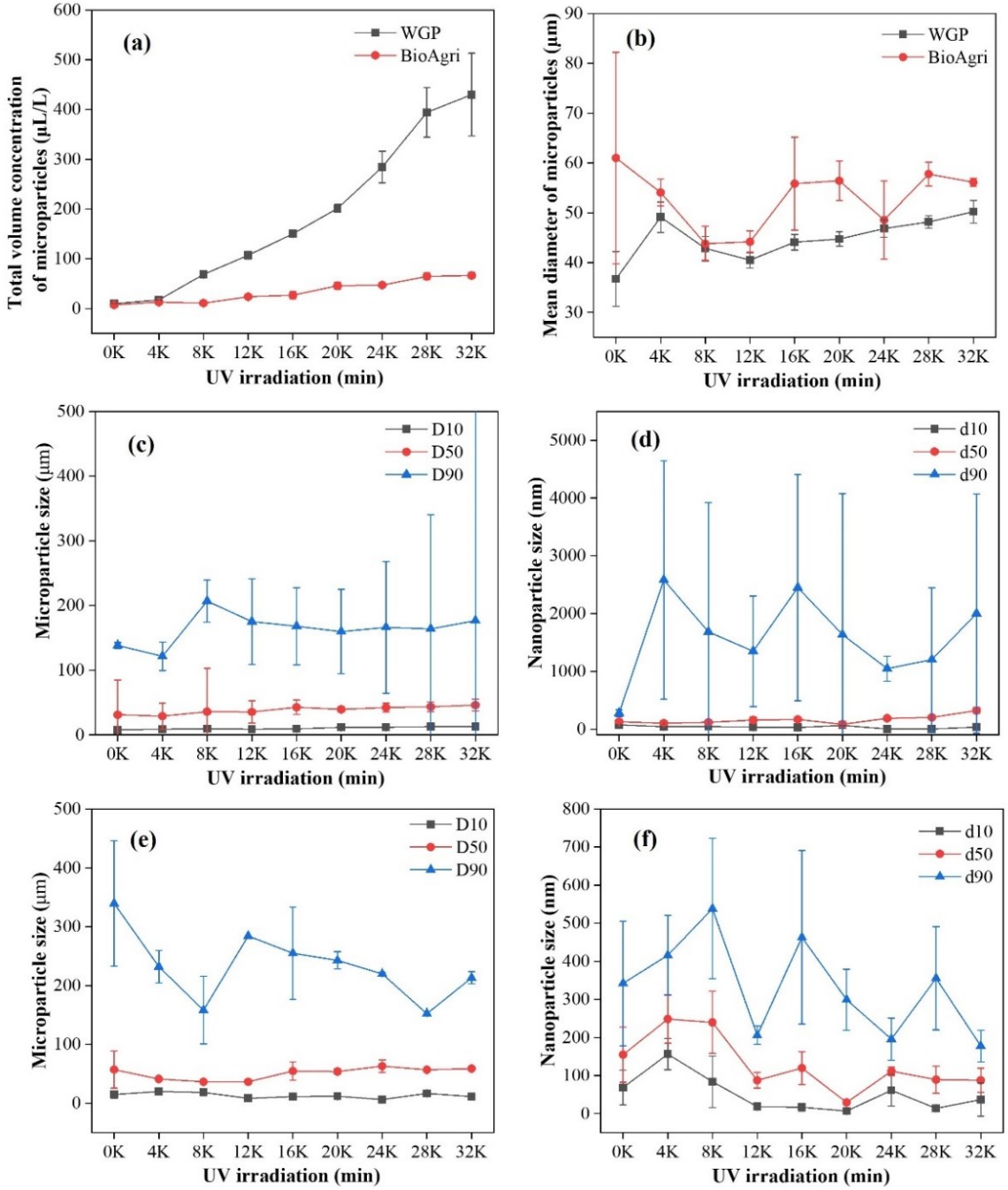

Figure 5.11. Particle concentration (a), mean diameter (b), and typical size indexes for WGP (c–d) and BioAgri (e–f) with different UV irradiation durations (K: 1000). A large error bar means a more unstable distribution of particle size.

The fragmentation of BMPs under UV weathering can be revealed via the number and morphology of POM_{BMP} particles released from WGP and BioAgri (Figure 5.12). The pristine BioAgri were smooth, intact, and thin films with pores, grooves, and attached particles on their surfaces. However, the WGP surface was neatly lined with long fibers with pits, threads, protrusions, and cracks (Figure 5.7). The pristine BioAgri released very few thin films, whereas the pristine WGP released more long fibers and downsized fragments. This suggests that the WGP was more easily damaged by water friction than the BioAgri. With the increase in UV irradiation duration, the weathered BMPs released more fragments and granules with abundant flakes and pores corresponding to a significant decrease in mechanical tensile strength. A proportion of weathered BMPs (32K) had a larger particle size than the pristine ones (0K), which was contrary to some previous results reporting that fibers and films had larger sizes than fragments and granules (Wang et al., 2021c). This may be attributed to the accumulation and aggregation of particles enhanced by the high concentration released from the weathered BM debris during water evaporation.

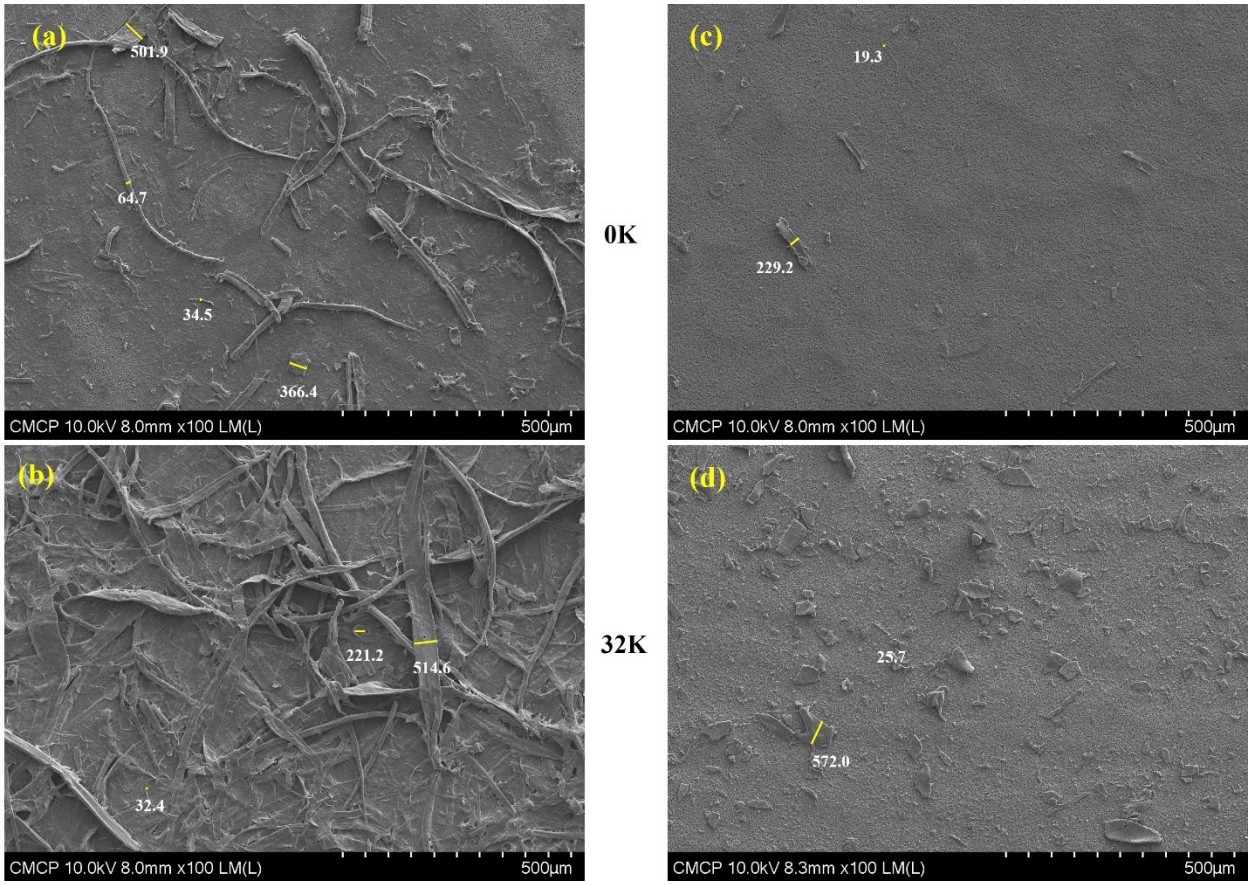

Figure 5.12. SEM images of POM_{BMP} released from WGP (a-b) and BioAgri (c-d) with different UV irradiation durations (K: 1000).

5.3.4. Spatial distributions of metal elements and functional groups on BMP surface

After entering the soil-water environment, the characteristics of BMPs will be influenced by soil particles. As a vector, BMPs can transport soil pollutants, such as heavy metals. To explore the transfer of trace metals between soils and BMPs, SR-XRF mapping was performed to study the spatial distributions of trace metals on the surfaces of the pristine and weathered BMPs after soil-water washing. As shown in Figure 5.13, the presence of Fe, Zn, and Mn on the BMP surface

proved the transport of heavy metals from soils to the BMP surface because organic matter (OM) had a high adsorption capacity for Fe-Mn concretions which were the predominant soil components (Gupta et al., 2021; Yin et al., 2021). The contents of trace metal elements (Fe and Zn) of the weathered BioAgri were higher compared with the pristine one (Figure 5.13 (a)). This was consistent with the previous study that the weathered PBAT absorbed more heavy metals because the increased roughness enlarged the specific surface area (Li et al., 2020b). Besides surface microstructure, oxygen-containing groups on the surface of MPs also significantly affected the adsorption of trace metals by MPs (Wang et al., 2022a). The adsorption of metals by MPs was primarily driven by physical sorption and electrostatic interaction (Zou et al., 2020). With the increasing UV irradiation durations, the CI index of BioAgri increased, which meant that the weathered BioAgri had higher contents of oxygen-containing groups on the surface, such as hydroxyl and carboxyl groups. It was reported that negatively charged ions (i.e., -COOH and -OH) in the weathered starches and cellulose surfaces had a strong coordination affinity with positively charged metallic cations (i.e., divalent Fe) due to the electrostatic attractions, thereby readily forming complexes (Gupta et al., 2021; Yin et al., 2021). However, the weathered WGP with a rougher surface showed lower contents of trace metal elements (i.e., Fe, Zn, and Mn) than the pristine one (Figure 5.13 (b)). This might be because the weathered WGP was more easily damaged by water and soil friction than the pristine one, releasing more fragments and granules and reducing specific surface area and negatively charged cellulosic fibers as shown in Figure 5.12.

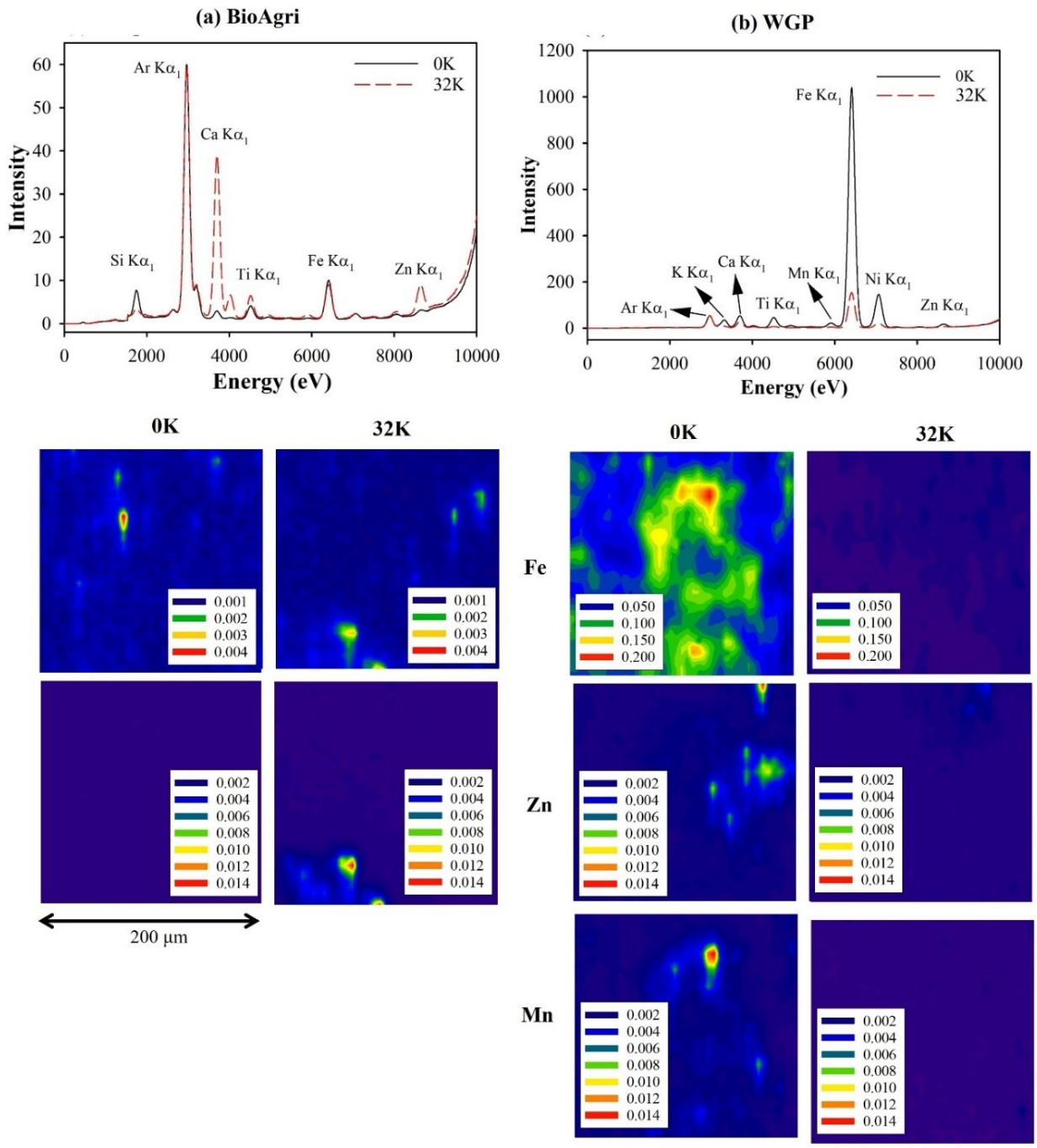

Figure 5.13. Synchrotron-XRF spectra and distributions of trace metals (Fe, Zn, and Mn) on pristine (0K) and weathered (32K) BioAgri (a) and WGP (b) after soil washing.

To observe the interactions between heavy metals and functional groups on the BMP surface, FTIR imaging was also performed after different washing conditions, including ultra-water washing (W, Figure 5.9) and soil-water washing (S+W, Figure 5.14) compared to the control without washing (C, Figure 5.6). As shown in Figure 5.14, multiple functional groups were respectively distributed on the edges of the fibers of WGP and circular spots of BioAgri in a consistent pattern. Overall, the pristine WGP had higher contents of functional groups compared to the weathered one, which was opposite to that of BioAgri. According to Figure 5.6 and Figure 5.9, water washing could reduce the contents of C=O, Ar C=C, C-H, O-H (free radical), and C=C bonds on the pristine and weathered WGP surfaces, whereas soil-water washing increased the amounts of these functional groups on the pristine WGP surface. However, the contents of the above functional groups on the surface of the pristine BioAgri did not change obviously after both water washing and soil-water washing, except for the increased contents of C=O, C-O, and Ar C=C bonds. For the weathered BioAgri, water washing also reduced the contents of Ar C=C, C-H, O-H (free radical), O-H (polysaccharide), and C=C bonds but increased the amounts of C=O and C-O bonds. Meanwhile, soil-water washing also increased the contents of these functional groups, except for the C=C bond.

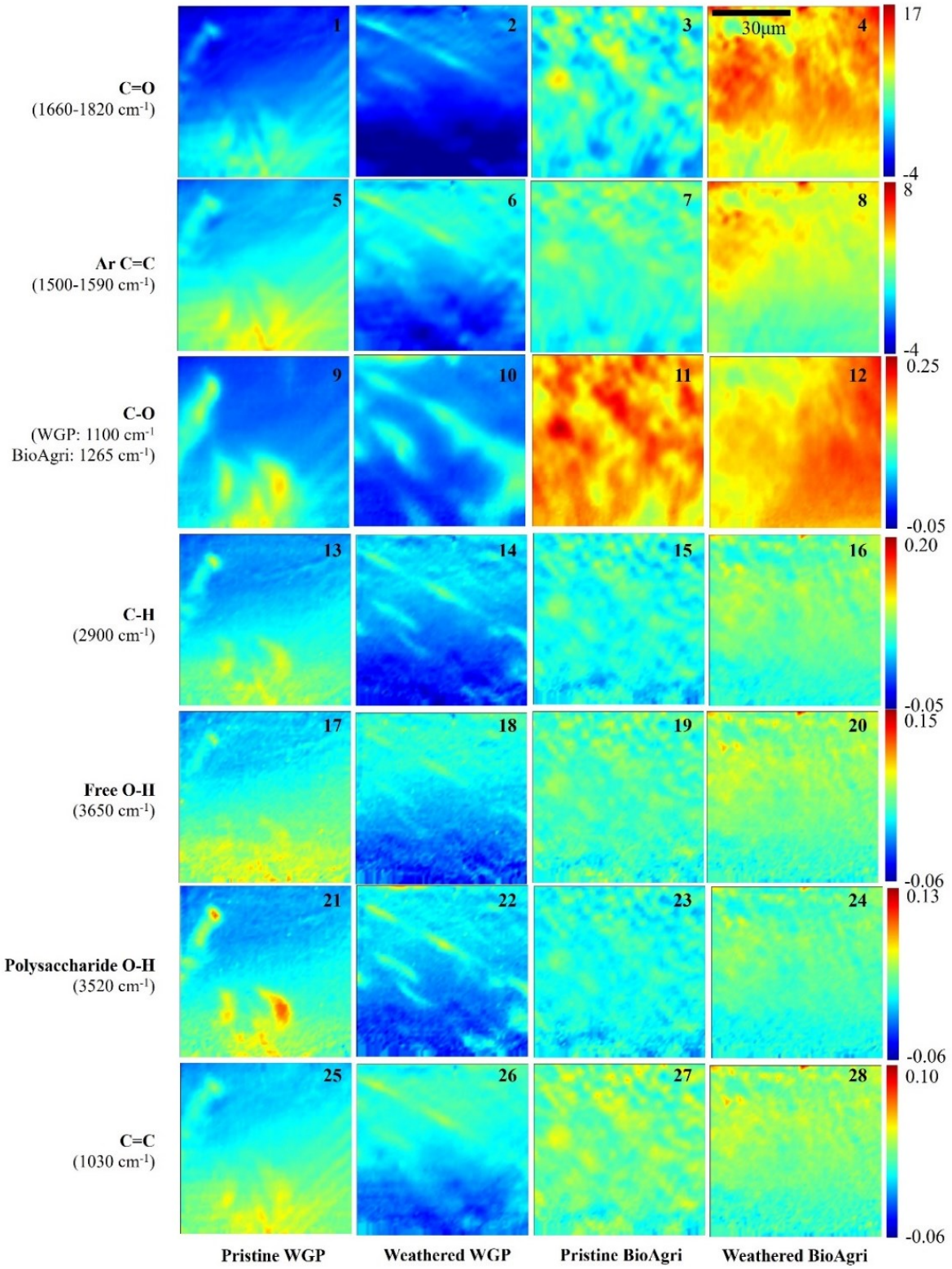

Figure 5.14. FTIR mapping of functional groups on BMP surface after soil water washing.

As mentioned in sections 5.3.1 and 5.3.2, functional groups, i.e., C=O and Ar C=C bonds, were probably from carboxylic acids (-COOH) and aromatic compounds (Ar C=C). As shown in Figure 5.15, compared to C washing, water washing reduced the content of Ar C=C bonds but increased the amount of C=O bonds on the weathered BioAgri. Meanwhile, the contents of the above functional groups on the pristine BioAgri increased, whereas their contents on the pristine and weathered WGP surfaces both decreased. This meant that carboxylic acids and aromatic compounds were released into the water from BMP surfaces, whereas the hydrolysis of PBAT in BioAgri produced the C=O bonds and retained them on its surface. Compared to C washing, soil-water washing increased the amounts of C=O and Ar C=C bonds on the BMP surface except for the weathered WGP surface. This might be because cellulosic fibers on the weathered WGP surface were largely washed by water and soil friction, causing a decrease in the specific surface area of binding sites for functional groups and heavy metals. This was consistent with previous studies that the adsorption capacity of MPs was largely affected by their weathering degree, particle size, porosity, and surface morphology (Feng et al., 2022a; Wang et al., 2022a). Compared to W washing, soil-water washing increased the amounts of C=O and Ar C=C bonds on the pristine WGP and weathered BioAgri, indicating BMPs probably adsorbed acids and aromatics from soils. This may be because the hydrophobic fraction of BMPs has an affinity to the aromatic structure of SOM because of hydrophobic partitioning (Yin et al., 2021). The increased acidic functional groups were stronger metal-binding and higher electronegative than SOM, which improved the adsorption capacity of BMPs to metals in soils. Therefore, the roughness of microstructures and the contents of oxygen-containing functional groups significantly affected the capacity of BMPs to adsorb aromatic compounds and heavy metals from soils.

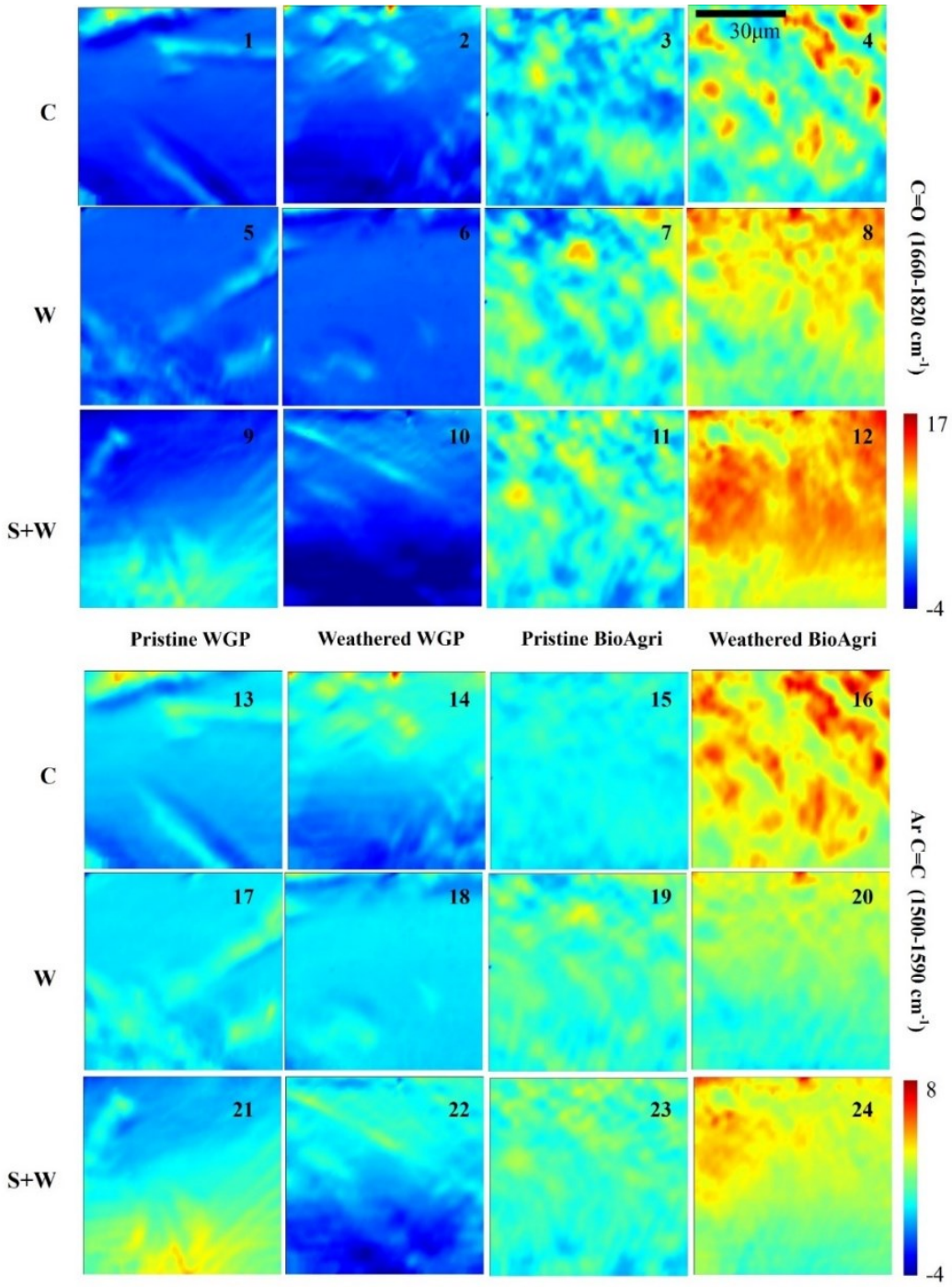

Figure 5.15. FTIR imaging of functional groups (C=O: 1660-1820 cm^{-1} and Ar C=C: 1500-1590 cm^{-1}) on BMP surface after different washing conditions (C: control without washing; W: water washing; S+W: soil-water washing).

5.3.5. Environmental implications

Agricultural health and safety are facing some new challenges (Eryiğit and Engel, 2022; Yang et al., 2022a). BMPs can influence soil microbiological and physicochemical properties and the effects are controlled by polymer type, size, dose, and shape (Wang et al., 2022a). BMPs can be the carbon addition to the agricultural soils, which will change soil DOM composition, such as aromatic functional groups (Feng et al., 2020). This may result in excessive carbon input into the soil and carbon emission into the air (Cai et al., 2021a; Cai et al., 2021b; Liu et al., 2022a). After exposure to the soil, the fragmentation from BMs to BMaPs then BMPs caused by abiotic and biotic processes will elevate the mobility of BMPs and BNPs in the soil, aquatic environment, and atmosphere (Cai et al., 2017; 2019b; Wang et al., 2021c). MPs and NPs may lead to various chemical and/or physical toxic effects on plants, such as mechanical blockage of pores in the seed capsule and a decrease in chlorophyll content (Wang et al., 2022a). Soil microorganisms, such as earthworms, snails, collembolan, springtails, and nematodes, may suffer tissue damage and inflammatory responses after ingesting MPs (Leonov and Tiunov, 2020). Several studies have documented that BMPs, such as Mater-Bi and starch-cellulose, pose fewer hazards to soil animals (e.g., woodlice, earthworms, and burrowing worms) than non-BMPs (Sforzini et al., 2016; Wood and Zimmer, 2014; Zhang et al., 2018). However, BMPs have a stronger affinity to soil pollutants, such as organic pollutants and heavy metals; thus, BMPs may have a greater negative impact than non-BMPs in certain conditions (Qin et al., 2021). For example, a study found that the number of MPs increased with the continuous addition of bio-debris. Moreover, BMPs account for the majority of the increment, reaching up to 35−73%. In light of the foregoing, it has been inferred that BMPs pose a greater negative effect on soil structure (Zhao et al., 2021). The degradation process of BMs and the ecotoxicity of the degradation products, especially BMPs and plastic

additives, have attracted the attention of researchers in the soil environment (Liu et al., 2022a). With the increasing UV irradiation durations, the weathered BMPs (i.e., BioAgri) had higher contents of negatively charged ions (i.e., -COOH and -OH) and a strong coordination affinity with positively charged metallic cations (i.e., divalent heavy metals). If the weathered BMPs were tilled into soils, they could transport more soil pollutants as a vector compared to the pristine BMPs. Although there are scarce studies on the ecotoxicity of BMPs on terrestrial organisms, we can speculate their hazards to crops, animals, and humans considering the transfer of BMPs via the terrestrial food web in the agroecosystem. Therefore, it is necessary to determine the environmental risk and disposal strategy after the use of mulching in future studies.

5.4. Summary

BMs are widely used in agroecosystems. They can be tilled into the soil as a source of carbon addition, which can help mitigate BM disposal and reduce environmental problems. However, the contents of MPs in the soil would increase with the addition of bio-debris. The combination of BMPs and soil pollutants may also harm soil health. This study investigated the characteristics of weathered BaMPs and the DOM_{BMP} released into soil-water environments. With the increase of UV irradiation time, the mechanical strength of BaMPs decreased and its chemical composition changed, thus introducing oxygenated functional groups on its surface. The photooxidation-dominated production and photodegradation-dominated cleavage of ester bonds on the BaMPs surface during UV irradiation were identified through FTIR analysis. After entering the water environment, the pH of the solution with DOM_{BMP} decreased, whereas the concentration of DOC increased. Polar functional groups, such as hydroxyl, carbonyl, and carboxyl, were produced in photoreaction processes, which enhanced the hydrophobicity and ET capacity of weathered

DOM_{BMP}. Compared with paper mulch (i.e., WGP), bioplastic mulch (i.e., BioAgri) contributed a larger amount of DOM_{BMP}, such as aromatic structure-containing chemicals and carboxylic acids, to the water environment but released fewer and smaller particles. After entering the soil-water environment, the analyses of FTIR and SR-XRF results revealed that the rough microstructure and oxygenated functional groups on the surfaces of BMPs, such as C-O and C=O bonds, played a crucial role in the adsorption of aromatic compounds and heavy metals from soils. The results obtained in this study can help manage environmental risks and determine disposal strategies after the use of mulching.

CHAPTER 6. CONCLUSIONS AND PERSPECTIVES

6.1. Overall conclusions

This dissertation assessed the emerging environmental concerns from bio-originated organic pollutants in cropping systems, including conducting the appropriate assessment of BVOC emissions and exploring the degradation and fragmentation of BMs. Generally, BVOC emissions are affected by temperature, drought, solar radiation, humidity, availability of nutrients, CO_2, O_3, etc. Growth length, air temperature, solar radiation and leafage were the most important variables influencing the temporal and spatial variations of MeOH emissions of spring wheat during the growing period in a Canadian province. Soils can act as both the sink and source of BVOCs through various soil processes that are affected by soil temperature, pH, SOM, and soil moisture. The seasonality of MeOH emissions was found to be positively correlated to concentrations of CO, FPM, and PM_{10} but negatively related to NO_2 and O_3. Anthropogenic activities can affect BVOC emissions and promote the formation of BVOC-derived pollutants (e.g., O_3, SOA, and PM).

Furthermore, the characterization and quantification of the BMPs in cropping systems were conducted to investigate the physicochemical changes of weathered BMPs, the particle distributions of micro- and nano-plastics, and the chemical characteristics of BMP leachate released into the soil-water environment. Compared with paper mulch, bioplastic mulch contributed a higher amount of aromatic structure-containing chemicals and carboxylic acids to the water environment but released fewer and smaller plastic particles. After entering the soil-water environment, the analyses of FTIR and SR-XRF results revealed that the rough microstructure and oxygenated functional groups on the surfaces of BMPs, such as C-O and C=O bonds, played a crucial role in the adsorption of aromatic compounds and heavy metals from soils.

6.2. Contribution and significance of thesis research

The main contribution of the research work presented in this dissertation is the assessment of emerging environmental concerns related to bio-originated organic pollutants in cropping systems. This includes conducting an appropriate assessment of BVOC emissions and exploring the degradation and fragmentation of BMs.

The scientometric analysis offers several advantages compared to critical reviews, as it helps minimize subjectivity and bias by providing a holistic and quantitative analysis of previous BVOC studies. It also plays a crucial role in identifying research gaps and future directions in this area. The findings obtained from scientometric analysis can provide researchers with a deeper understanding of BVOC emission mechanisms, while also offering decision-makers valuable insights for emission mitigation and environmental management.

A new BVOC assessment approach was developed to assess the biogenic MeOH emitted from crops during growing seasons. This approach enables the identification of relationships between MeOH emissions and major influencing factors. The results obtained from this assessment can be utilized to enhance the adaptation and mitigation strategies for agricultural systems. By understanding the factors influencing BVOC emissions, agricultural practices can be optimized to minimize their impact on the environment and promote sustainable farming. For example, using the ratio of BVOC emissions to biomass production or energy transformation can be a useful tool for cropping designers and decision-makers when weighing the trade-offs between the costs and benefits of ecosystem services.

The characterization and quantification of BMPs in cropping systems involved studying the fragmentation and degradation of BMPs under UV irradiation through visual inspection and quantitative analysis. The obtained results are valuable for managing environmental risks associated with BMPs and determining appropriate disposal strategies following their use in mulching. By understanding the behavior of BMPs under UV irradiation and their potential impact on the environment, effective measures can be implemented to mitigate any adverse effects and ensure sustainable agricultural practices. For instance, BM manufacturers are advised to explore protective coatings or treatments to mitigate UV-induced degradation and to select materials that combine UV stability with biodegradability. Crop farmers are recommended to choose mulch materials that have been tested for UV resistance while still ensuring their effectiveness. To facilitate this selection process, government regulators are suggested to collaborate with industry experts to establish standardized testing methods, develop a labeling system, and implement a rating system, which informs consumers about the expected lifespan and environmental benefits of different BM products.

Overall, the dissertation could help better understand the mechanisms of biogenic MeOH emission from crops or plants as well as the weathering, degradation, and fragmentation of BMs and their environmental behaviors and health risks, thus providing the theoretical basis for better handling these new environmental challenges for regulators and industries. The findings and sharing of the publications relevant to the thesis research listed in the Section Publications include peer-reviewed journal articles and conference publications, which provide scientific support for further research and development regarding the impact of BVOC emissions and BMP generation on environmental management.

6.3. Recommendations and perspectives

Based on the studies conducted in this dissertation, several recommendations are proposed for future research in this field:

- Further investigation of the specific mechanisms and factors influencing BVOC emissions is recommended to enhance our understanding of this field. Specifically, conducting more detailed studies on the effects of nutrient availability and CO_2/O_3 concentrations is crucial. It is important to note that the present study does not incorporate the effects of O_3. Previous studies have found that short-term exposure to O_3 rapidly reduced the SQTs (Li and Blande, 2015), the effect of O_3 on BVOC emissions varies over seasons (Yu and Blande, 2021), and the long-term exposure of O_3 to vegetation degraded yearly GPP (by about 22%) and LAI (by 15–20%) (Anav et al., 2011). Therefore, the effects of O_3 on MeOH emissions remain unclear and should be an important consideration in future studies. Addressing this knowledge gap will provide valuable insights into the complex interactions between BVOCs and the environment.
- Although the standard emission factor (ε) is not identified as a significant factor because of its smaller range compared to other factors, the use of a constant ε for common wheat (winter wheat) at the ripening stage to represent spring wheat throughout the whole growing period (which was done due to the lack of experimental data) may increase uncertainty concerning the base MeOH emissions calculated. To reduce this uncertainty and improve the accuracy of MeOH emission estimates, future research should focus on including missing environmental and physicochemical factors in the development of empirical algorithms. This can be achieved through conducting more extensive field and laboratory measurements of MeOH emissions,

specifically targeting different wheat subspecies, climate zones, and wheat phenologies. By incorporating these additional factors and data, more accurate and representative emission factors can be derived, leading to a better understanding of MeOH emissions from specific crops and growing conditions.

- RS data can provide valuable information such as cropland area, LAI, foliar densities, meteorological data, etc. Compared to ground station data, by incorporating these interpretative data from RS images, it becomes possible to estimate gridded MeOH emissions with a finer spatial-temporal resolution and quantify the impact of continuous changes in MeOH emissions on air pollution at the surface level. Future studies can explore integrating RS and GIS techniques to improve the estimation and monitoring of MeOH emissions, facilitate a better understanding of their distribution and potential impact on the environment, and contribute to more effective air pollution management strategies.
- In addition to leaf MeOH emissions, it is important to consider other significant contributors to MeOH emissions, namely soil and litter. Previous studies have shown that MeOH emissions from decomposing litterfalls can account for a substantial portion (28-99%) of total VOC emissions (Gray and Fierer, 2012). MeOH fluxes from bare and plowed soil can range from 0 to 200 $\mu g \cdot m^{-2} \cdot h^{-1}$ (Schade and Custer, 2004). The variability in MeOH emissions from these sources can be influenced by factors such as N additions, warming, wildfire, and drainage conditions in soils (Huang et al., 2020b; Kramshøj et al., 2019; Zhang-Turpeinen et al., 2020b). It is important to note that in the present study, only leaf MeOH emissions were calculated. Therefore, future research should consider several additional sources of MeOH emissions. These sources include above-ground fruits and flowers, shedding of leaves and stem on the surface, underground living roots, microbial decomposition of litter and SOM, dissolved

MeOH in soil water, and MeOH exchange in soil-plant-atmosphere ecosystems (Cai et al., 2020; Chen et al., 2020; Feng et al., 2020). By including these additional sources, a more comprehensive understanding of MeOH emissions and their environmental impact can be achieved.

- While the information obtained through FTIR mapping and UV-vis spectroscopy is valuable, combining these techniques with others such as chromatography or microscopy can provide complementary data and enhance the understanding of the samples. For example, chromatography can provide detailed information on the chemical components present, while microscopy can offer insights into the physical characteristics and morphology of the sample. By employing a multi-technique approach, a piece of more comprehensive information and a robust analysis of the chemical composition, structure, and properties of the samples can be achieved.
- The presence of SOM can have a significant impact on the functional groups present on the BMP surface. To gain a clearer understanding of surface interactions between soil particles and BMPs, it is important to examine the effect of residual SOM. Therefore, it is recommended to gather more detailed information about the soil particles, including the SOM content and composition. This additional information will provide insights into the influence of SOM on the surface properties of BMPs and help elucidate the nature of the interactions between soil particles and BMPs.
- Further research is recommended to investigate the fate and transport of BMPs in the environment and prioritize the assessment of ecological and health risks associated with BMPs. It is important to understand the degradation pathways of BMPs in different environments, such as soil, water, and air, and assess their potential ecological implications in BMPs on soil

and water quality, as well as their potential to accumulate in the food chain. By examining the fate and transport of BMPs, we can gain insights into their persistence, mobility, and potential hazards and adverse effects posed by BMPs to ecosystems and human health. This information will aid in developing appropriate risk assessment frameworks and effective mitigation strategies to minimize the environmental and health risks associated with BMPs in cropping systems.

Following these recommendations in future research can help us better understand BVOC emissions and BMPs in cropping systems. This will lead to more effective environmental management and sustainable agricultural practices.

PUBLICATIONS

Peer-Reviewed Journal Articles:

[1] **Cai, M**., Qi, Z., Guy, C., An, C., Chen, X., Wang, Z., Feng, Q. (2023). Insights into the abiotic fragmentation of biodegradable mulches under accelerated weathering conditions. *Journal of Hazardous Materials*. 454, 131477

[2] **Cai, M**., An, C., Guy, C. (2021). A scientometric analysis and review of biogenic volatile organic compound emissions: Research hotspots, new frontiers, and environmental implications. *Renewable and Sustainable Energy Reviews*, 149, 111317.

[3] **Cai, M**., An, C., Guy, C., Lu, C., Mafakheri, F. (2021). Assessing the regional biogenic methanol emission from spring wheat during the growing season: A Canadian case study. *Environmental Pollution*, 117602.

Conference Publications:

[1] **Cai, M**., An, C., Guy, C., Lu, C., Feng, Q. An emission model for regional biogenic oxygenated volatile organic compounds from crops. *In Proceedings of the Canadian Society of Civil Engineering Annual Conference 2021: CSCE21 Environmental Track* (pp. 323-327). Singapore: Springer Nature Singapore, September 2022.

[2] **Cai, M**., An, C. Effects of accelerated weathering on the abiotic fragmentation of biodegradable mulches. *Persistent, Emerging and Organic Pollution in the Environment 2023 (PEOPLE 2023)*. Montreal, Quebec, August 7-11, 2023.

[3] **Cai, M**., An, C. Release of microparticles into soil-water environments from weathered petroleum-derived polymers. *International Oil Spill Science Conference 2022 (IOSSC 2022)*. Halifax, Nova Scotia, Canada, October 4-7, 2022.

[4] **Cai, M**., An, C. Spectroscopic characterization of weathered biodegradable mulches and their dissolved organic matter released into soil-water environments. *Persistent, Emerging and Organic Pollution in the Environment 2022 (PEOPLE 2022)*. Online, August 23-26, 2022.

[5] **Cai, M**., An, C., Guy, C., Feng, Q. A bibliometric analysis of research trends of biogenic volatile organic compounds emitted from terrestrial ecosystems. *In American Geophysical Union (AGU) Fall Meeting Abstracts* (Vol. 2020, pp. A038-0003), December 2020.

[6] **Cai, M**., An, C. Emissions of biogenic volatile organic compounds in a regional cropping system. *Canadian Society of Civil Engineering (CSCE) Annual Conference*. Laval, Quebec, Canada, June 12-15, 2019.

[7] **Cai, M**., An, C. Emissions of biogenic volatile organic compounds in a regional cropping system. *Global Joint Seminar on Geo-Environmental Engineering*. Montreal, Quebec, Canada, May 30-31, 2019.

REFERENCES

Abis, L., Loubet, B., Ciuraru, R., Lafouge, F., Dequiedt, S., Houot, S., Maron, P. A. and Bourgeteau-Sadet, S. (2018) Profiles of volatile organic compound emissions from soils amended with organic waste products. Science of the Total Environment 636, 1333-1343.

Acevedo, E., Silva, P. and Silva, H. (2006) Growth and wheat physiology, development. Laboratory of Soil-Plant-Water Relations. Faculty of Agronomy and Forestry Sciences. University of Chile. Casilla 1004.

Al-Jaibachi, R., Cuthbert, R. N. and Callaghan, A. (2019) Examining effects of ontogenic microplastic transference on Culex mosquito mortality and adult weight. Science of the Total Environment 651, 871-876.

Albrizio, R. and Steduto, P. (2003) Photosynthesis, respiration and conservative carbon use efficiency of four field grown crops. Agricultural and Forest Meteorology 116(1-2), 19-36.

Almond, J., Sugumaar, P., Wenzel, M. N., Hill, G. and Wallis, C. (2020) Determination of the carbonyl index of polyethylene and polypropylene using specified area under band methodology with ATR-FTIR spectroscopy. e-Polymers 20(1), 369-381.

Amereh, F., Babaei, M., Eslami, A., Fazelipour, S. and Rafiee, M. (2020) The emerging risk of exposure to nano (micro) plastics on endocrine disturbance and reproductive toxicity: From a hypothetical scenario to a global public health challenge. Environmental Pollution 261, 114158.

Ameye, M., Allmann, S., Verwaeren, J., Smagghe, G., Haesaert, G., Schuurink, R. C. and Audenaert, K. (2018) Green leaf volatile production by plants: a meta-analysis. New Phytologist 220(3), 666-683.

Ameztoy, K., Baslam, M., Snchez-Lpez, A. M., Muoz, F. J., Bahaji, A., Magro, G. A., Garca-Gmez, P., Baroja-Fernndez, E., De Diego, N., Humplk, J. F., Ugena, L., Spchal, L., Dolezal, K., Kaneko, K., Mitsui, T., Cejudo, F. J. and Pozueta-Romero, J. (2019) Plant responses to fungal volatiles involve global posttranslational thiol redox proteome changes that affect photosynthesis. Plant Cell and Environment 42(9), 2627-2644.

Amin, H. S., Russo, R. S., Sive, B., Hoebeke, E. R., Dodson, C., McCubbin, I. B., Hallar, A. G. and Hartz, K. E. H. (2013) Monoterpene emissions from bark beetle infested *Engelmann spruce* trees. Atmospheric Environment 72, 130-133.

An, J. L., Zhu, B., Wang, H. L., Li, Y. Y., Lin, X. and Yang, H. (2014) Characteristics and source apportionment of VOCs measured in an industrial area of Nanjing, Yangtze River Delta, China. Atmospheric Environment 97, 206-214.

Anav, A., Menut, L., Khvorostyanov, D. and Viovy, N. (2011) Impact of tropospheric ozone on the Euro-Mediterranean vegetation. Global Change Biology 17(7), 2342-2359.

Antar, M., Lyu, D., Nazari, M., Shah, A., Zhou, X. and Smith, D. L. (2021) Biomass for a sustainable bioeconomy: An overview of world biomass production and utilization. Renewable and Sustainable Energy Reviews 139, 110691.

Arneth, A., Niinemets, U., Pressley, S., Back, J., Hari, P., Karl, T., Noe, S., Prentice, I. C., Serca, D., Hickler, T., Wolf, A. and Smith, B. (2007) Process-based estimates of terrestrial ecosystem isoprene emissions: incorporating the effects of a direct CO_2-isoprene interaction. Atmospheric Chemistry and Physics 7, 31-53.

Arneth, A., Schurgers, G., Lathiere, J., Duhl, T., Beerling, D., Hewitt, C., Martin, M. and Guenther, A. (2011) Global terrestrial isoprene emission models: sensitivity to variability in climate and vegetation. Atmospheric Chemistry and Physics 11(15), 8037-8052.

Arnts, R. R., Mowry, F. L. and Hampton, G. A. (2013) A high-frequency response relaxed eddy accumulation flux measurement system for sampling short-lived biogenic volatile organic compounds. Journal of Geophysical Research: Atmospheres 118(10), 4860-4873.

ASTM International (2002) Standard guide for determination of biobased content, resources consumption, and environmental profile of materials and products (withdrawn 2011), ASTM International, West Conshohocken, PA, United States.

Astner, A., Hayes, D., O'Neill, H., Evans, B., Pingali, S., Urban, V. and Young, T. (2019) Mechanical formation of micro-and nano-plastic materials for environmental studies in agricultural ecosystems. Science of the Total Environment 685, 1097-1106.

Babamiri, O., Vanaei, A., Guo, X., Wu, P., Richter, A. and Ng, K. (2021) Numerical simulation of water quality and self-purification in a mountainous river using QUAL2KW. Journal of Environmental Informatics 37(1), 26-35.

Bachy, A., Aubinet, M., Amelynck, C., Schoon, N., Bodson, B., Delaplace, P., De Ligne, A., Digrado, A., du Jardin, P. and Fauconnier, M.-L. (2020) Dynamics and mechanisms of volatile organic compound exchanges in a winter wheat field. Atmospheric Environment 221, 117105.

Bachy, A., Aubinet, M., Amelynck, C., Schoon, N., Bodson, B., Moureaux, C., Delaplace, P., De Ligne, A. and Heinesch, B. (2018) MeOH exchange dynamics between a temperate cropland soil and the atmosphere. Atmospheric Environment 176, 229-239.

Bachy, A., Aubinet, M., Schoon, N., Amelynck, C., Bodson, B., Moureaux, C. and Heinesch, B. (2016) Are BVOC exchanges in agricultural ecosystems overestimated? Insights from fluxes measured in a maize field over a whole growing season. Atmospheric Chemistry and Physics 16(8), 5343-5356.

Balestri, E., Menicagli, V., Ligorini, V., Fulignati, S., Galletti, A. M. R. and Lardicci, C. (2019) Phytotoxicity assessment of conventional and biodegradable plastic bags using seed germination test. Ecological indicators 102, 569-580.

Bandopadhyay, S., Martin-Closas, L., Pelacho, A. M. and DeBruyn, J. M. (2018) Biodegradable plastic mulch films: impacts on soil microbial communities and ecosystem functions. Frontiers in Microbiology 9, 819.

Baudic, A., Gros, V., Sauvage, S., Locoge, N., Sanchez, O., Sarda-Esteve, R., Kalogridis, C., Petit, J. E., Bonnaire, N., Baisnee, D., Favez, O., Albinet, A., Sciare, J. and Bonsang, B. (2016) Seasonal variability and source apportionment of volatile organic compounds (VOCs) in the Paris megacity (France). Atmospheric Chemistry and Physics 16(18), 11961-11989.

Bauwens, M., Stavrakou, T., Müller, J.-F., Van Schaeybroeck, B., De Cruz, L., De Troch, R., Giot, O., Hamdi, R., Termonia, P. and Laffineur, Q. (2018) Recent past (19792014) and future (20702099) isoprene fluxes over Europe simulated with the MEGANMOHYCAN model. Biogeosciences (15), 3673-3690.

Bergami, E., Rota, E., Caruso, T., Birarda, G., Vaccari, L. and Corsi, I. (2020) Plastics everywhere: first evidence of polystyrene fragments inside the common Antarctic collembolan *Cryptopygus antarcticus*. Biology letters 16(6), 20200093.

Bi, H., An, C., Mulligan, C. N., Zhang, K., Lee, K. and Yue, R. (2022) Treatment of oiled beach sand using a green and responsive washing fluid with nonionic surfactant-modified nanoclay. Journal of Cleaner Production 333, 130122.

Blanch, J. S., Penuelas, J. and Llusia, J. (2007) Sensitivity of terpene emissions to drought and fertilization in terpene-storing Pinus halepensis and non-storing *Quercus ilex*. Physiologia Plantarum 131(2), 211-225.

Bolinder, M., Janzen, H., Gregorich, E., Angers, D. and VandenBygaart, A. (2007a) An approach for estimating net primary productivity and annual carbon inputs to soil for common agricultural crops in Canada. Agriculture, Ecosystems & Environment 118(1-4), 29-42.

Bolinder, M. A., Janzen, H. H., Gregorich, E. G., Angers, D. A. and VandenBygaart, A. J. (2007b) An approach for estimating net primary productivity and annual carbon inputs to soil for common agricultural crops in Canada. Agriculture, Ecosystems & Environment 118(1-4), 29-42.

Brodhagen, M., Peyron, M., Miles, C. and Inglis, D. A. (2015) Biodegradable plastic agricultural mulches and key features of microbial degradation. Applied Microbiology and Biotechnology 99(3), 1039-1056.

Brown, S. G., Frankel, A. and Hafner, H. R. (2007) Source apportionment of VOCs in the Los Angeles area using positive matrix factorization. Atmospheric Environment 41(2), 227-237.

Brunner, A., Ammann, C., Neftel, A. and Spirig, C. (2007) MeOH exchange between grassland and the atmosphere. Biogeosciences 4(3), 395-410.

Bryant, J. P., Chapin III, F. S. and Klein, D. R. (1983) Carbon/nutrient balance of boreal plants in relation to vertebrate herbivory. Oikos, 357-368.

Cai, B., Mao, X., Wang, J. and Wang, M. (2019a) Fine resolution carbon dioxide emission gridded data and their application for China. Journal of Environmental Informatics 33(2), 82-95.

Cai, C., Geng, F., Tie, X., Yu, Q. and An, J. (2010) Characteristics and source apportionment of VOCs measured in Shanghai, China. Atmospheric Environment 44(38), 5005-5014.

Cai, M., An, C. and Guy, C. (2021a) A scientometric analysis and review of biogenic volatile organic compound emissions: Research hotspots, new frontiers, and environmental implications. Renewable and Sustainable Energy Reviews 149, 111317.

Cai, M., An, C., Guy, C. and Lu, C. (2020) Assessment of soil and water conservation practices in the loess hilly region using a coupled rainfall-runoff-erosion model. Sustainability 12(3), 934.

Cai, M., An, C., Guy, C., Lu, C. and Mafakheri, F. (2021b) Assessing the regional biogenic MeOH emission from spring wheat during the growing season: A Canadian case study. Environmental Pollution 287, 117602.

Cai, M., Qi, Z., Guy, C., An, C., Chen, X., Wang, Z. and Feng, Q. (2023) Insights into the abiotic fragmentation of biodegradable mulches under accelerated weathering conditions. Journal of Hazardous materials 454, 131477.

Cai, M., Xin, Z. and Yu, X. (2017) Spatio-temporal variations in PM leaf deposition: A meta-analysis. Environmental Pollution 231, 207-218.

Cai, M., Xin, Z. and Yu, X. (2019b) Particulate matter transported from urban greening plants during precipitation events in Beijing, China. Environmental Pollution 252, 1648-1658.

Calfapietra, C., Fares, S., Manes, F., Morani, A., Sgrigna, G. and Loreto, F. (2013) Role of biogenic volatile organic compounds (BVOC) emitted by urban trees on ozone concentration in cities: A review. Environmental Pollution 183, 71-80.

CAN/CGSB-32.311 (2015) Organic production systems : permitted substances lists, Canadian General Standards Board, Gatineau, Canada.

CAN/CGSB-32.311 (2020) Organic production systems-permitted substances lists, Canadian General Standards Board, Gatineau, Canada.

Caravan, R. L., Khan, M. A. H., Zádor, J., Sheps, L., Antonov, I. O., Rotavera, B., Ramasesha, K., Au, K., Chen, M.-W. and Rösch, D. (2018) The reaction of hydroxyl and methylperoxy radicals is not a major source of atmospheric MeOH. Nature Communications 9(1), 1-9.

Carruthers, T. J., Longstaff, B. J., Dennison, W. C., Abal, E. G. and Aioi, K. (2001) Measurement of light penetration in relation to seagrass. Global seagrass research methods. Elsevier, Amsterdam, 369-392.

Caser, M., D'Angiolillo, F., Chitarra, W., Lovisolo, C., Ruffoni, B., Pistelli, L., Pistelli, L. and Scariot, V. (2018) Ecophysiological and phytochemical responses of Salvia sinaloensis Fern. to drought stress. Plant Growth Regulation 84(2), 383-394.

Chae, Y. and An, Y.-J. (2020) Nanoplastic ingestion induces behavioral disorders in terrestrial snails: trophic transfer effects via vascular plants. Environmental Science: Nano 7(3), 975-983.

Chen, C. (2006) CiteSpace II: Detecting and visualizing emerging trends and transient patterns in scientific literature. Journal of the American Society for Information Science and Technology 57(3), 359-377.

Chen, C. (2014) The citespace manual. College of Computing and Informatics, Drexel University, Philadelphia, PA, USA (1), 1-84.

Chen, J., Yue, W. and Yang, T. (2011) A study on the relationship between leaf temperature of rice and meteorological factors. Chin. Agric. Sci. Bull 27, 19-23.

Chen, M., Liu, S., Bi, M., Yang, X., Deng, R. and Chen, Y. (2022) Aging behavior of microplastics affected DOM in riparian sediments: From the characteristics to bioavailability. Journal of Hazardous materials 431, 128522.

Chen, Z., An, C., Fang, H., Zhang, Y., Zhou, Z., Zhou, Y. and Zhao, S. (2020) Assessment of regional greenhouse gas emission from beef cattle production: A case study of Saskatchewan in Canada. Journal of environmental management 264, 110443.

Cheng, S., Zhang, J., Wang, Y., Zhang, D., Teng, G., Chang-Chien, G., Huang, Q., Zhang, Y. and Yan, P. (2019) Global research trends in health effects of volatile organic compounds during the last 16 Years: A bibliometric analysis. Aerosol and Air Quality Research 19(8), 1834-1843.

Choi, W., Hong, H., Lee, Y., Ryu, J., Park, J. and Lee, H. (2019) First-time estimation of HCHO column over Asia using multiple regression with OMI and MODIS data. Journal of Environmental Informatics 34(2), 88-98.

Choi, Y., Kim, G., Park, S., Kim, E. and Kim, S. (2021) Prediction of natural volatile organic compounds emitted by Bamboo Groves in urban forests. Forests 12(5), 543.

Chuang, K.-Y., Huang, Y.-L. and Ho, Y.-S. (2007) A bibliometric and citation analysis of stroke-related research in Taiwan. Scientometrics 72(2), 201-212.

Ciccioli, P., Centritto, M. and Loreto, F. (2014) Biogenic volatile organic compound emissions from vegetation fires. Plant Cell and Environment 37(8), 1810-1825.

Collalti, A., Tjoelker, M. G., Hoch, G., Mäkelä, A., Guidolotti, G., Heskel, M., Petit, G., Ryan, M. G., Battipaglia, G. and Matteucci, G. (2020) Plant respiration: controlled by photosynthesis or biomass? Global Change Biology 26(3), 1739-1753.

Collet, S., Kidokoro, T., Karamchandani, P., Jung, J. and Shah, T. (2018) Future year ozone source attribution modeling study using CMAQ-ISAM. Journal of the Air & Waste Management Association 68(11), 1239-1247.

Conti, G. O., Ferrante, M., Banni, M., Favara, C., Nicolosi, I., Cristaldi, A., Fiore, M. and Zuccarello, P. (2020) Micro-and nano-plastics in edible fruit and vegetables. The first diet risks assessment for the general population. Environmental Research 187, 109677.

Cortés, C., Domenech, J., Salazar, M., Pastor, S., Marcos, R. and Hernández, A. (2020) Nanoplastics as a potential environmental health factor: effects of polystyrene nanoparticles on human intestinal epithelial Caco-2 cells. Environmental Science: Nano 7(1), 272-285.

Courty, L., Chetehouna, K., Lemee, L., Fernandez-Pello, C. and Garo, J. P. (2014) Biogenic volatile organic compounds emissions at high temperatures of common plants from Mediterranean regions affected by forest fires. Journal of Fire Sciences 32(5), 459-479.

Covey, K., Soper, F., Pangala, S., Bernardino, A., Pagliaro, Z., Basso, L., Cassol, H., Fearnside, P., Navarrete, D., Novoa, S., Sawakuchi, H., Lovejoy, T., Marengo, J., Peres, C. A., Baillie, J., Bernasconi, P., Camargo, J., Freitas, C., Hoffman, B., Nardoto, G. B., Nobre, I., Mayorga, J., Mesquita, R., Pavan, S., Pinto, F., Rocha, F., Mello, R. D., Thuault, A., Bahl, A. A. and Elmore, A. (2021) Carbon and beyond: The biogeochemistry of climate in a rapidly changing Amazon. Frontiers in Forests and Global Change 4, 20.

Custer, T. and Schade, G. (2007) MeOH and acetaldehyde fluxes over ryegrass. Tellus Series B-Chemical and Physical Meteorology 59(4), 673-684.

Dai, J., Bean, B., Brown, B., Bruening, W., Edwards, J., Flowers, M., Karow, R., Lee, C., Morgan, G. and Ottman, M. (2016a) Harvest index and straw yield of five classes of wheat. Biomass and Bioenergy 85, 223-227.

Dai, J., Bean, B., Brown, B., Bruening, W., Edwards, J., Flowers, M., Karow, R., Lee, C., Morgan, G., Ottman, M., Ransom, J. and Wiersma, J. (2016b) Harvest index and straw yield of five classes of wheat. Biomass and Bioenergy 85, 223-227.

Day, M. C. and Pandis, S. N. (2015) Effects of a changing climate on summertime fine particulate matter levels in the eastern US. Journal of Geophysical Research-Atmospheres 120(11), 5706-5720.

de Castilhos Ghisi, N., Zuanazzi, N. R., Fabrin, T. M. C. and de Oliveira, E. C. (2020) Glyphosate and its toxicology: A scientometric review. Science of the Total Environment 733, 139359.

de Gouw, J. and Warneke, C. (2007) Measurements of volatile organic compounds in the earth's atmosphere using proton-transfer-reaction mass spectrometry. Mass Spectrometry Reviews 26(2), 223-257.

de Souza Machado, A. A., Lau, C. W., Kloas, W., Bergmann, J., Bachelier, J. B., Faltin, E., Becker, R., Görlich, A. S. and Rillig, M. C. (2019) Microplastics can change soil properties and affect plant performance. Environmental Science & Technology 53(10), 6044-6052.

Detournay, A., Sauvage, S., Riffault, V., Wroblewski, A. and Locoge, N. (2013) Source and behavior of isoprenoid compounds at a southern France remote site. Atmospheric Environment 77, 272-282.

Docter, D., Westmeier, D., Markiewicz, M., Stolte, S., Knauer, S. and Stauber, R. (2015) The nanoparticle biomolecule corona: lessons learned–challenge accepted? Chemical Society Reviews 44(17), 6094-6121.

Dolar, A., Selonen, S., van Gestel, C. A., Perc, V., Drobne, D. and Kokalj, A. J. (2021) Microplastics, chlorpyrifos and their mixtures modulate immune processes in the terrestrial crustacean Porcellio scaber. Science of the Total Environment 772, 144900.

Domenech, J., Hernández, A., Rubio, L., Marcos, R. and Cortés, C. (2020) Interactions of polystyrene nanoplastics with in vitro models of the human intestinal barrier. Archives of Toxicology 94, 2997-3012.

Dong, C., Chen, C., Chen, Y., Chen, H., Lee, J. and Lin, C. (2020a) Polystyrene microplastic particles: In vitro pulmonary toxicity assessment. Journal of Hazardous materials 385, 121575.

Dong, Y., Gao, M., Qiu, W. and Song, Z. (2021) Uptake of microplastics by carrots in presence of As (III): Combined toxic effects. Journal of Hazardous materials 411, 125055.

Dong, Y., Gao, M., Song, Z. and Qiu, W. (2020b) Microplastic particles increase arsenic toxicity to rice seedlings. Environmental Pollution 259, 113892.

Dorokhov, Y. L., Sheshukova, E. V. and Komarova, T. V. (2018) MeOH in plant life. Frontiers in plant science 9, 1623.
Du, F., Cai, H., Zhang, Q., Chen, Q. and Shi, H. (2020) Microplastics in take-out food containers. Journal of Hazardous materials 399, 122969.
Dunker, A. M., Koo, B. and Yarwood, G. (2019) Source apportionment of organic aerosol and ozone and the effects of emission reductions. Atmospheric Environment 198, 89-101.
Effmert, U., Kalderas, J., Warnke, R. and Piechulla, B. (2012) Volatile mediated interactions between bacteria and fungi in the soil. Journal of Chemical Ecology 38(6), 665-703.
Ehrlich, J. and Cahill, T. M. (2018) Identification of broadleaf and coniferous trees as a primary source of acrolein. Atmospheric Environment 191, 414-419.
El Haddad, I., Marchand, N., Wortham, H., Piot, C., Besombes, J. L., Cozic, J., Chauvel, C., Armengaud, A., Robin, D. and Jaffrezo, J. L. (2011) Primary sources of PM2.5 organic aerosol in an industrial Mediterranean city, Marseille. Atmospheric Chemistry and Physics 11(5), 2039-2058.
Eller, A. S. D., Sekimoto, K., Gilman, J. B., Kuster, W. C., de Gouw, J. A., Monson, R. K., Graus, M., Crespo, E., Warneke, C. and Fall, R. (2011) Volatile organic compound emissions from switchgrass cultivars used as biofuel crops. Atmospheric Environment 45(19), 3333-3337.
EN-17033 (2018) Plastics-biodegradable mulch films for use in agriculture and horticulture-requirements and test methods, European Committee for Standardization, Brussels, Belgium
Eryiğit, M. and Engel, B. (2022) Spatiotemporal modelling of groundwater flow and nitrate contamination in an agriculture-dominated watershed. Journal of Environmental Informatics 39(2), 125-135.
Escudero, M., Viana, M., Querol, X., Alastuey, A., Diez Hernandez, P., Dos Santos, S. and Anzano, J. (2015) Industrial sources of primary and secondary organic aerosols in two urban environments in Spain. Environmental Science and Pollution Research 22(14), 10413-10424.
Eyring, V., Bony, S., Meehl, G. A., Senior, C. A., Stevens, B., Stouffer, R. J. and Taylor, K. E. (2016) Overview of the Coupled Model Intercomparison Project Phase 6 (CMIP6) experimental design and organization. Geoscientific Model Development 9(5), 1937-1958.
Faiola, C. L., VanderSchelden, G. S., Wen, M., Elloy, F. C., Cobos, D. R., Watts, R. J., Jobson, B. T. and VanReken, T. M. (2014) SOA formation potential of emissions from soil and leaf litter. Environmental Science & Technology 48(2), 938-946.
Fall, R. (2003) Abundant oxygenates in the atmosphere: a biochemical perspective. Chemical Reviews 103(12), 4941-4952.
Fall, R. and Benson, A. A. (1996) Leaf MeOH—the simplest natural product from plants. Trends in Plant Science 1(9), 296-301.
Fan, X., Zou, Y., Geng, N., Liu, J., Hou, J., Li, D., Yang, C. and Li, Y. (2021) Investigation on the adsorption and desorption behaviors of antibiotics by degradable MPs with or without UV ageing process. Journal of Hazardous materials 401, 123363.
Fang, J., Pan, L., Gu, Q., Juengpanich, S., Zheng, J., Tong, C., Wang, Z., Nan, J. and Wang, Y. (2020) Scientometric analysis of mTOR signaling pathway in liver disease. Annals of Translational Medicine 8(4).
Fang, Y., Yin, J. and Wu, B. (2017) Climate change and tourism: a scientometric analysis using CiteSpace. Journal of Sustainable Tourism 26(1), 108-126.
FAO (2018) Crops data from Food and Agriculture Organization of the United Nations (FAO). http://www.fao.org/faostat/en/?#data/QC.

FAOSTAT (2020) Land use in agriculture by the numbers. https://www.fao.org/sustainability/news/detail/en/c/1274219/.
Fares, S., Weber, R., Park, J. H., Gentner, D., Karlik, J. and Goldstein, A. H. (2012) Ozone deposition to an orange orchard: Partitioning between stomatal and non-stomatal sinks. Environmental Pollution 169, 258-266.
Farooqui, Z. M., John, K., Biswas, J. and Sule, N. (2013) Modeling analysis of the impact of anthropogenic emission sources on ozone concentration over selected urban areas in Texas. Atmospheric Pollution Research 4(1), 33-42.
Faubert, P., Tiiva, P., Rinnan, A., Michelsen, A., Holopainen, J. K. and Rinnan, R. (2010) Doubled volatile organic compound emissions from subarctic tundra under simulated climate warming. New Phytologist 187(1), 199-208.
Favero, A., Daigneault, A. and Sohngen, B. (2020) Forests: Carbon sequestration, biomass energy, or both? Science advances 6(13), eaay6792.
Feng, Q., An, C., Chen, Z. and Wang, Z. (2020) Can deep tillage enhance carbon sequestration in soils? A meta-analysis towards GHG mitigation and sustainable agricultural management. Renewable and Sustainable Energy Reviews 133, 110293.
Feng, Q., An, C., Chen, Z., Yin, J., Zhang, B., Lee, K. and Wang, Z. (2022a) Investigation into the impact of aged microplastics on oil behavior in shoreline environments. Journal of Hazardous materials 421, 126711.
Feng, Q., Chen, Z., Greer, C. W., An, C. and Wang, Z. (2022b) Transport of microplastics in shore substrates over tidal cycles: roles of polymer characteristics and environmental factors. Environmental Science & Technology.
Feng, Z. Z., Yuan, X. Y., Fares, S., Loreto, F., Li, P., Hoshika, Y. and Paoletti, E. (2019) Isoprene is more affected by climate drivers than monoterpenes: A meta-analytic review on plant isoprenoid emissions. Plant Cell and Environment 42(6), 1939-1949.
Fettweis, M. and Lee, B. J. (2017) Spatial and seasonal variation of biomineral suspended particulate matter properties in high-turbid nearshore and low-turbid offshore zones. Water 9(9), 694.
Flury, M., Sintim, H., Bary, A., English, M. and Schaefer, S. (2017) Nanoparticles from degradation of biodegradable plastic mulch, p. 4138.
Folkers, A., Hüve, K., Ammann, C., Dindorf, T., Kesselmeier, J., Kleist, E., Kuhn, U., Uerlings, R. and Wildt, J. (2008) MeOH emissions from deciduous tree species: dependence on temperature and light intensity. Plant Biology 10(1), 65-75.
Galbally, I. E. and Kirstine, W. (2002) The production of MeOH by flowering plants and the global cycle of MeOH. Journal of Atmospheric Chemistry 43(3), 195-229.
Gao, C., Xiu, A. J., Zhang, X. L., Chen, W. W., Liu, Y., Zhao, H. M. and Zhang, S. C. (2020) Spatiotemporal characteristics of ozone pollution and policy implications in Northeast China. Atmospheric Pollution Research 11(2), 357-369.
Gao, M., Liu, Y., Dong, Y. and Song, Z. (2021) Effect of polyethylene particles on dibutyl phthalate toxicity in lettuce (Lactuca sativa L.). Journal of Hazardous materials 401, 123422.
Gaurav, N., Sivasankari, S., Kiran, G., Ninawe, A. and Selvin, J. (2017) Utilization of bioresources for sustainable biofuels: a review. Renewable and Sustainable Energy Reviews 73, 205-214.
Giorgetti, L., Spanò, C., Muccifora, S., Bottega, S., Barbieri, F., Bellani, L. and Castiglione, M. R. (2020) Exploring the interaction between polystyrene nanoplastics and Allium cepa during germination: Internalization in root cells, induction of toxicity and oxidative stress. Plant Physiology and Biochemistry 149, 170-177.

Giuntoli, J., Searle, S., Jonsson, R., Agostini, A., Robert, N., Amaducci, S., Marelli, L. and Camia, A. (2020) Carbon accounting of bioenergy and forest management nexus. A reality-check of modeling assumptions and expectations. Renewable and Sustainable Energy Reviews 134, 110368.

Gomez, L. G., Loubet, B., Lafouge, F., Ciuraru, R., Buysse, P., Durand, B., Gueudet, J. C., Fanucci, O., Fortineau, A., Zurfluh, O., Decuq, C., Kammer, J., Duprix, P., Bsaibes, S., Truong, F., Gros, V. and Boissard, C. (2019) Comparative study of biogenic volatile organic compounds fluxes by wheat, maize and rapeseed with dynamic chambers over a short period in northern France. Atmospheric Environment 214, 16.

Government of Canada (2016) Canadian Weather Energy and Engineering Datasets (CWEEDS2016). https://climate.weather.gc.ca/prods_servs/engineering_e.html.

Government of Canada (2018) 2018 Crop reports. https://publications.saskatchewan.ca/#/categories/2629.

Government of Saskatchewan (2018) Historical data. https://climate.weather.gc.ca/historical_data/search_historic_data_e.html.

Gower, S. T., Kucharik, C. J. and Norman, J. M. (1999) Direct and indirect estimation of leaf area index, fAPAR, and net primary production of terrestrial ecosystems. Remote Sensing of Environment 70(1), 29-51.

Graus, M., Eller, A. S., Fall, R., Yuan, B., Qian, Y., Westra, P., de Gouw, J. and Warneke, C. (2013) Biosphere-atmosphere exchange of volatile organic compounds over C4 biofuel crops. Atmospheric Environment 66, 161-168.

Gray, C. M. and Fierer, N. (2012) Impacts of nitrogen fertilization on volatile organic compound emissions from decomposing plant litter. Global Change Biology 18(2), 739-748.

Greenberg, J., Asensio, D., Turnipseed, A., Guenther, A., Karl, T. and Gochis, D. (2012) Contribution of leaf and needle litter to whole ecosystem BVOC fluxes. Atmospheric Environment 59, 302-311.

Grote, R. (2007) Sensitivity of volatile monoterpene emission to changes in canopy structure: a model-based exercise with a process-based emission model. New Phytologist 173(3), 550-561.

Grote, R., Monson, R. K. and Niinemets, Ü. (2013) Biology, controls and models of tree volatile organic compound emissions, pp. 315-355, Springer, Dordrecht, Netherlands.

Grote, R., Morfopoulos, C., Niinemets, Ü., Sun, Z., Keenan, T. F., Pacifico, F. and Butler, T. (2014) A fully integrated isoprenoid emissions model coupling emissions to photosynthetic characteristics. Plant, Cell and Environment 37(8), 1965-1980.

Grote, R. and Niinemets, U. (2008) Modeling volatile isoprenoid emissions - a story with split ends. Plant Biology 10(1), 8-28.

Guenther, A., Archer, S., Greenberg, J., Harley, P., Helmig, D., Klinger, L., Vierling, L., Wildermuth, M., Zimmerman, P. and Zitzer, S. (1999) Biogenic hydrocarbon emissions and landcover/climate change in a subtropical savanna. Physics and Chemistry of the Earth Part B-Hydrology Oceans and Atmosphere 24(6), 659-667.

Guenther, A., Baugh, W., Davis, K., Hampton, G., Harley, P., Klinger, L., Vierling, L., Zimmerman, P., Allwine, E., Dilts, S., Lamb, B., Westberg, H., Baldocchi, D., Geron, C. and Pierce, T. (1996) Isoprene fluxes measured by enclosure, relaxed eddy accumulation, surface layer gradient, mixed layer gradient, and mixed layer mass balance techniques. Journal of Geophysical Research-Atmospheres 101(D13), 18555-18567.

Guenther, A., Hewitt, C. N., Erickson, D., Fall, R., Geron, C., Graedel, T., Harley, P., Klinger, L., Lerdau, M. and McKay, W. (1995) A global model of natural volatile organic compound emissions. Journal of Geophysical Research: Atmospheres 100(D5), 8873-8892.

Guenther, A., Karl, T., Harley, P., Wiedinmyer, C., Palmer, P. I. and Geron, C. (2006) Estimates of global terrestrial isoprene emissions using MEGAN (Model of Emissions of Gases and Aerosols from Nature). Atmospheric Chemistry and Physics 6, 3181-3210.

Guenther, A. B., Jiang, X., Heald, C. L., Sakulyanontvittaya, T., Duhl, T., Emmons, L. K. and Wang, X. (2012) The Model of Emissions of Gases and Aerosols from Nature version 2.1 (MEGAN2.1): an extended and updated framework for modeling biogenic emissions. Geoscientific Model Development 5(6), 1471-1492.

Guidolotti, G., Pallozzi, E., Gavrichkova, O., Scartazza, A., Mattioni, M., Loreto, F. and Calfapietra, C. (2019) Emission of constitutive isoprene, induced monoterpenes, and other volatiles under high temperatures in Eucalyptus camaldulensis: A C-13 labelling study. Plant Cell and Environment 42(6), 1929-1938.

Guo, H., So, K. L., Simpson, I. J., Barletta, B., Meinardi, S. and Blake, D. R. (2007) C-1-C-8 volatile organic compounds in the atmosphere of Hong Kong: Overview of atmospheric processing and source apportionment. Atmospheric Environment 41(7), 1456-1472.

Guo, P., Guo, K., Ren, Y., Shi, Y., Chang, J., Tani, A. and Ge, Y. (2013) Biogenic volatile organic compound emissions in relation to plant carbon fixation in a subtropical urban–rural complex. Landscape and Urban Planning 119, 74-84.

Gupta, A. D., Rawat, K., Bhadauria, V. and Singh, H. (2021) Recent trends in the application of modified starch in the adsorption of heavy metals from water: a review. Carbohydrate Polymers 269, 117763.

Gustavsson, L., Nguyen, T., Sathre, R. and Tettey, U. Y. A. (2021) Climate effects of forestry and substitution of concrete buildings and fossil energy. Renewable and Sustainable Energy Reviews 136, 110435.

Haberstroh, S., Kreuzwieser, J., Boeddeker, H., Eiblmeier, M., Gutte, H., Lobo-do-Vale, R., Caldeira, M. C. and Werner, C. (2019) Natural carbon isotope composition distinguishes compound groups of biogenic volatile organic compounds (BVOC) in two Mediterranean woody species. Frontiers in Forests and Global Change 2, 55.

Haberstroh, S., Kreuzwieser, J., Lobo-do-Vale, R., Caldeira, M. C., Dubbert, M. and Werner, C. (2018) Terpenoid emissions of two Mediterranean woody species in response to drought stress. Frontiers in plant science 9, 1071.

Hansel, A. K., Ehrenhauser, F. S., Richards-Henderson, N. K., Anastasio, C. and Valsaraj, K. T. (2015) Aqueous-phase oxidation of green leaf volatiles by hydroxyl radical as a source of SOA: Product identification from methyl jasmonate and methyl salicylate oxidation. Atmospheric Environment 102, 43-51.

Hantson, S., Knorr, W., Schurgers, G., Pugh, T. A. M. and Arneth, A. (2017) Global isoprene and monoterpene emissions under changing climate, vegetation, CO2 and land use. Atmospheric Environment 155, 35-45.

Harley, P., Greenberg, J., Niinemets, Ü. and Guenther, A. (2007) Environmental controls over MeOH emission from leaves.

Harrison, S. P., Morfopoulos, C., Dani, K. G. S., Prentice, I. C., Arneth, A., Atwell, B. J., Barkley, M. P., Leishman, M. R., Loreto, F., Medlyn, B. E., Niinemets, U., Possell, M., Penuelas, J. and Wright, I. J. (2013a) Volatile isoprenoid emissions from plastid to planet. New Phytologist 197(1), 49-57.

Harrison, S. P., Morfopoulos, C., Dani, K. S., Prentice, I. C., Arneth, A., Atwell, B. J., Barkley, M. P., Leishman, M. R., Loreto, F. and Medlyn, B. E. (2013b) Volatile isoprenoid emissions from plastid to planet. New Phytologist 197(1), 49-57.

Hassanzadeh, E., Elshorbagy, A., Wheater, H. and Gober, P. (2014) Managing water in complex systems: An integrated water resources model for Saskatchewan, Canada. Environmental Modelling & Software 58, 12-26.

Hayes, D. G., Wadsworth, L. C., Sintim, H. Y., Flury, M., English, M., Schaeffer, S. and Saxton, A. M. (2017) Effect of diverse weathering conditions on the physicochemical properties of biodegradable plastic mulches. Polymer Testing 62, 454-467.

He, M., Kimball, J. S., Maneta, M. P., Maxwell, B. D., Moreno, A., Beguería, S. and Wu, X. (2018) Regional crop gross primary productivity and yield estimation using fused landsat-MODIS data. Remote Sensing 10(3), 372.

He, Y., Li, J., Chen, J., Miao, X., Li, G., He, Q., Xu, H., Li, H. and Wei, Y. (2020) Cytotoxic effects of polystyrene nanoplastics with different surface functionalization on human HepG2 cells. Science of the Total Environment 723, 138180.

He, Y., Wang, H., Qian, B., McConkey, B. and DePauw, R. (2012) How early can the seeding dates of spring wheat be under current and future climate in Saskatchewan, Canada? PLoS ONE 7(10), e45153.

Heal, M. R., Naysmith, P., Cook, G. T., Xu, S., Duran, T. R. and Harrison, R. M. (2011) Application of C-14 analyses to source apportionment of carbonaceous PM2.5 in the UK. Atmospheric Environment 45(14), 2341-2348.

Heikes, B. G., Chang, W. N., Pilson, M. E. Q., Swift, E., Singh, H. B., Guenther, A., Jacob, D. J., Field, B. D., Fall, R., Riemer, D. and Brand, L. (2002) Atmospheric MeOH budget and ocean implication. Global Biogeochemical Cycles 16(4), 13.

Holopainen, J. K. and Gershenzon, J. (2010) Multiple stress factors and the emission of plant VOCs. Trends in plant science 15(3), 176-184.

Hu, J., Ma, Y., Zhang, L., Gan, F. and Ho, Y. (2010) A historical review and bibliometric analysis of research on lead in drinking water field from 1991 to 2007. Science of the Total Environment 408(7), 1738-1744.

Hu, L., Millet, D. B., Mohr, M. J., Wells, K. C., Griffis, T. J. and Helmig, D. (2011) Sources and seasonality of atmospheric MeOH based on tall tower measurements in the US Upper Midwest. Atmospheric Chemistry and Physics 11(21), 11145-11156.

Huang, L., McDonald-Buller, E., McGaughey, G., Kimura, Y. and Allen, D. T. (2015a) Comparison of regional and global land cover products and the implications for biogenic emission modeling. Journal of the Air & Waste Management Association 65(10), 1194-1205.

Huang, L., McGaughey, G., McDonald-Buller, E., Kimura, Y. and Allen, D. T. (2015b) Quantifying regional, seasonal and interannual contributions of environmental factors on isoprene and monoterpene emissions estimates over eastern Texas. Atmospheric Environment 106, 120-128.

Huang, R., Yang, L., Shen, J., Yuan, W., Gong, Y., Guo, J., Cao, W., Duan, J., Ni, H. and Zhu, C. (2020a) Water-insoluble organics dominate brown carbon in wintertime urban aerosol of China: chemical characteristics and optical properties. Environmental Science & Technology 54(13), 7836-7847.

Huang, W., Yin, H., Yang, Y., Jin, L., Lu, G. and Dang, Z. (2021) Influence of the co-exposure of microplastics and tetrabromobisphenol A on human gut: Simulation in vitro with human cell Caco-2 and gut microbiota. Science of the Total Environment 778, 146264.

Huang, X., Lai, J., Liu, Y., Zheng, L., Fang, X., Song, W. and Yi, Z. (2020b) Biogenic volatile organic compound emissions from Pinus massoniana and Schima superba seedlings: Their responses to foliar and soil application of nitrogen. Science of the Total Environment 705, 135761.

Huerta Lwanga, E., Gertsen, H., Gooren, H., Peters, P., Salánki, T., Van Der Ploeg, M., Besseling, E., Koelmans, A. A. and Geissen, V. (2016) Microplastics in the terrestrial ecosystem: implications for Lumbricus terrestris (Oligochaeta, Lumbricidae). Environmental Science & Technology 50(5), 2685-2691.

Huerta Lwanga, E., Mendoza Vega, J., Ku Quej, V., Chi, J. d. l. A., Sanchez del Cid, L., Chi, C., Escalona Segura, G., Gertsen, H., Salánki, T. and van der Ploeg, M. (2017) Field evidence for transfer of plastic debris along a terrestrial food chain. Scientific Reports 7(1), 14071.

Huve, K., Christ, M. M., Kleist, E., Uerlings, R., Niinemets, U., Walter, A. and Wildt, J. (2007) Simultaneous growth and emission measurements demonstrate an interactive control of MeOH release by leaf expansion and stomata. Journal of Experimental Botany 58(7), 1783-1793.

Hwang, J., Choi, D., Han, S., Choi, J. and Hong, J. (2019) An assessment of the toxicity of polypropylene microplastics in human derived cells. Science of the Total Environment 684, 657-669.

Im, U., Poupkou, A., Incecik, S., Markakis, K., Kindap, T., Unal, A., Melas, D., Yenigun, O., Topcu, S., Odman, M. T., Tayanc, M. and Guler, M. (2011) The impact of anthropogenic and biogenic emissions on surface ozone concentrations in Istanbul. Science of the Total Environment 409(7), 1255-1265.

Jeon, W. B., Lee, S. H., Lee, H., Park, C., Kim, D. H. and Park, S. Y. (2014) A study on high ozone formation mechanism associated with change of NOx/VOCs ratio at a rural area in the Korean Peninsula. Atmospheric Environment 89, 10-21.

Jiang, J. H., Aksoyoglu, S., El-Haddad, I., Ciarelli, G., van der Gon, H., Canonaco, F., Gilardoni, S., Paglione, M., Minguillon, M. C., Favez, O., Zhang, Y. J., Marchand, N., Hao, L. Q., Virtanen, A., Florou, K., O'Dowd, C., Ovadnevaite, J., Baltensperger, U. and Prevot, A. S. H. (2019a) Sources of organic aerosols in Europe: a modeling study using CAMx with modified volatility basis set scheme. Atmospheric Chemistry and Physics 19(24), 15247-15270.

Jiang, X., Chen, H., Liao, Y., Ye, Z., Li, M. and Klobučar, G. (2019b) Ecotoxicity and genotoxicity of polystyrene microplastics on higher plant Vicia faba. Environmental Pollution 250, 831-838.

Jiang, X. J., Liu, W., Wang, E., Zhou, T. and Xin, P. (2017) Residual plastic mulch fragments effects on soil physical properties and water flow behavior in the Minqin Oasis, northwestern China. Soil and Tillage Research 166, 100-107.

Jiang, X. Y., Guenther, A., Potosnak, M., Geron, C., Seco, R., Karl, T., Kim, S., Gu, L. H. and Pallardy, S. (2018) Isoprene emission response to drought and the impact on global atmospheric chemistry. Atmospheric Environment 183, 69-83.

Jorquera, H. and Rappengluck, B. (2004) Receptor modeling of ambient VOC at Santiago, Chile. Atmospheric Environment 38(25), 4243-4263.

Ju, H., Zhu, D. and Qiao, M. (2019) Effects of polyethylene microplastics on the gut microbial community, reproduction and avoidance behaviors of the soil springtail, Folsomia candida. Environmental Pollution 247, 890-897.

Kader, M., Senge, M., Mojid, M. and Ito, K. (2017) Recent advances in mulching materials and methods for modifying soil environment. Soil and Tillage Research 168, 155-166.

Karamchandani, P., Long, Y., Pirovano, G., Balzarini, A. and Yarwood, G. (2017) Source-sector contributions to European ozone and fine PM in 2010 using AQMEII modeling data. Atmospheric Chemistry and Physics 17(9), 5643-5664.

Karami, A., Golieskardi, A., Choo, C. K., Larat, V., Karbalaei, S. and Salamatinia, B. (2018) Microplastic and mesoplastic contamination in canned sardines and sprats. Science of the Total Environment 612, 1380-1386.

Karlsson, T., Rinnan, R. and Holst, T. (2020) Variability of BVOC emissions from commercially used willow (*Salix spp.*) varieties. Atmosphere 11(4), 356.

Kashyap, P., Kumar, A., Kumar, R. P. and Kumar, K. (2019) Biogenic and anthropogenic isoprene emissions in the subtropical urban atmosphere of Delhi. Atmospheric Pollution Research 10(5), 1691-1698.

Kellomaki, S., Rouvinen, I., Peltola, H., Strandman, H. and Steinbrecher, R. (2001) Impact of global warming on the tree species composition of boreal forests in Finland and effects on emissions of isoprenoids. Global Change Biology 7(5), 531-544.

Kijchavengkul, T., Auras, R., Rubino, M., Alvarado, E., Montero, J. R. C. and Rosales, J. M. (2010) Atmospheric and soil degradation of aliphatic–aromatic polyester films. Polymer Degradation and Stability 95(2), 99-107.

Kijchavengkul, T., Auras, R., Rubino, M., Ngouajio, M. and Fernandez, R. T. (2008) Assessment of aliphatic–aromatic copolyester biodegradable mulch films. Part I: Field study. Chemosphere 71(5), 942-953.

Kim, J., Lee, H., Kim, S. and Kim, H. (2018) Global pattern of microplastics (MPs) in commercial food-grade salts: sea salt as an indicator of seawater MP pollution. Environmental Science & Technology 52(21), 12819-12828.

Kim, L., Galbally, I. E., Porter, N., Weeks, I. A. and Lawson, S. J. (2011) BVOC emissions from mechanical wounding of leaves and branches of Eucalyptus sideroxylon (red ironbark). Journal of Atmospheric Chemistry 68(3), 265-279.

Kim, S., Lee, M., Kim, S., Choi, S., Seok, S. and Kim, S. (2013) Photochemical characteristics of high and low ozone episodes observed in the Taehwa Forest observatory (TFO) in June 2011 near Seoul South Korea. Asia-Pacific Journal of Atmospheric Sciences 49(3), 325-331.

Kosuth, M., Mason, S. A. and Wattenberg, E. V. (2018) Anthropogenic contamination of tap water, beer, and sea salt. PloS one 13(4), e0194970.

Kottek, M., Grieser, J., Beck, C., Rudolf, B. and Rubel, F. (2006) World map of the Köppen-Geiger climate classification updated.

Kramer, R. and Abraham, W. R. (2012) Volatile sesquiterpenes from fungi: what are they good for? Phytochemistry Reviews 11(1), 15-37.

Kramshøj, M., Albers, C. N., Svendsen, S. H., Björkman, M. P., Lindwall, F., Björk, R. G. and Rinnan, R. (2019) Volatile emissions from thawing permafrost soils are influenced by meltwater drainage conditions. Global Change Biology 25(5), 1704-1716.

Kramshøj, M., Vedel-Petersen, I., Schollert, M., Rinnan, Å., Nymand, J., Ro-Poulsen, H. and Rinnan, R. (2016) Large increases in Arctic biogenic volatile emissions are a direct effect of warming. Nature Geoscience 9(5), 349-352.

Kumar, A., Bali, K., Singh, S., Naja, M. and Mishra, A. K. (2019) Estimates of reactive trace gases (NMVOCs, CO and NOx) and their ozone forming potentials during forest fire over Southern Himalayan region. Atmospheric Research 227, 41-51.

Kutralam-Muniasamy, G., Pérez-Guevara, F., Elizalde-Martínez, I. and Shruti, V. (2020) Branded milks–Are they immune from microplastics contamination? Science of the Total Environment 714, 136823.

La Mantia, F. P., Ascione, L., Mistretta, M. C., Rapisarda, M. and Rizzarelli, P. (2020) Comparative investigation on the soil burial degradation behaviour of polymer films for agriculture before and after photo-oxidation. Polymers 12(4), 753.

Lahive, E., Walton, A., Horton, A. A., Spurgeon, D. J. and Svendsen, C. (2019) Microplastic particles reduce reproduction in the terrestrial worm *Enchytraeus crypticus* in a soil exposure. Environmental Pollution 255, 113174.

Lathiere, J., Hauglustaine, D. A., Friend, A. D., De Noblet-Ducoudre, N., Viovy, N. and Folberth, G. A. (2006) Impact of climate variability and land use changes on global biogenic volatile organic compound emissions. Atmospheric Chemistry and Physics 6, 2129-2146.

Lavoir, A. V., Staudt, M., Schnitzler, J. P., Landais, D., Massol, F., Rocheteau, A., Rodriguez, R., Zimmer, I. and Rambal, S. (2009) Drought reduced monoterpene emissions from the evergreen Mediterranean oak *Quercus ilex*: results from a throughfall displacement experiment. Biogeosciences 6(7), 1167-1180.

Leonov, V. and Tiunov, A. (2020) Interaction of invertebrates and synthetic polymers in soil: a review. Russian Journal of Ecology 51, 503-517.

Li, B., Lan, Z., Wang, L., Sun, H., Yao, Y., Zhang, K. and Zhu, L. (2019) The release and earthworm bioaccumulation of endogenous hexabromocyclododecanes (HBCDDs) from expanded polystyrene foam microparticles. Environmental Pollution 255, 113163.

Li, J., Yang, D., Li, L., Jabeen, K. and Shi, H. (2015a) Microplastics in commercial bivalves from China. Environmental Pollution 207, 190-195.

Li, L., An, J. Y., Shi, Y. Y., Zhou, M., Yan, R. S., Huang, C., Wang, H. L., Lou, S. R., Wang, Q., Lu, Q. and Wu, J. (2016) Source apportionment of surface ozone in the Yangtze River Delta, China in the summer of 2013. Atmospheric Environment 144, 194-207.

Li, L., An, J. Y., Zhou, M., Yan, R. S., Huang, C., Lu, Q., Lin, L., Wang, Y. J., Tao, S. K., Qiao, L. P., Zhu, S. H. and Chen, C. H. (2015b) Source apportionment of fine particles and its chemical components over the Yangtze River Delta, China during a heavy haze pollution episode. Atmospheric Environment 123, 415-429.

Li, L., Luo, Y., Li, R., Zhou, Q., Peijnenburg, W. J., Yin, N., Yang, J., Tu, C. and Zhang, Y. (2020a) Effective uptake of submicrometre plastics by crop plants via a crack-entry mode. Nature sustainability 3(11), 929-937.

Li, M., Liu, Y., Xu, G., Wang, Y. and Yu, Y. (2021) Impacts of polyethylene microplastics on bioavailability and toxicity of metals in soil. Science of the Total Environment 760, 144037.

Li, P. and Hur, J. (2017) Utilization of UV-Vis spectroscopy and related data analyses for dissolved organic matter (DOM) studies: a review. Critical Reviews in Environmental Science and Technology 47(3), 131-154.

Li, R., Liu, Y., Sheng, Y., Xiang, Q., Zhou, Y. and Cizdziel, J. V. (2020b) Effect of prothioconazole on the degradation of microplastics derived from mulching plastic film: Apparent change and interaction with heavy metals in soil. Environmental Pollution 260, 113988.

Li, T. and Blande, J. D. (2015) Associational susceptibility in broccoli: mediated by plant volatiles, impeded by ozone. Global Change Biology 21(5), 1993-2004.

Li, Y. Q., Li, J. and Xie, S. D. (2017) Bibliometric analysis: global research trends in biogenic volatile organic compounds during 1991-2014. Environmental Earth Sciences 76(1), 13.

Lian, J., Liu, W., Meng, L., Wu, J., Chao, L., Zeb, A. and Sun, Y. (2021) Foliar-applied polystyrene nanoplastics (PSNPs) reduce the growth and nutritional quality of lettuce (*Lactuca sativa L.*). Environmental Pollution 280, 116978.

Liebezeit, G. and Liebezeit, E. (2015) Origin of synthetic particles in honeys. Polish Journal of Food and Nutrition Sciences 65(2).

Lindwall, F., Schollert, M., Michelsen, A., Blok, D. and Rinnan, R. (2016) Fourfold higher tundra volatile emissions due to arctic summer warming. Journal of Geophysical Research-Biogeosciences 121(3), 895-902.

Ling, Z. H., He, Z. R., Wang, Z., Shao, M. and Wang, X. M. (2019) Sources of methacrolein and methyl vinyl ketone and their contributions to methylglyoxal and formaldehyde at a receptor site in Pearl River Delta. Journal of Environmental Sciences 79, 1-10.

Liu, L., Zou, G., Zuo, Q., Li, S., Bao, Z., Jin, T., Liu, D. and Du, L. (2022a) It is still too early to promote biodegradable mulch film on a large scale: a bibliometric analysis. Environmental Technology & Innovation, 102487.

Liu, P., Qian, L., Wang, H., Zhan, X., Lu, K., Gu, C. and Gao, S. (2019) New insights into the aging behavior of microplastics accelerated by advanced oxidation processes. Environmental Science & Technology 53(7), 3579-3588.

Liu, S., Wang, J., Zhu, J., Wang, J., Wang, H. and Zhan, X. (2021) The joint toxicity of polyethylene microplastic and phenanthrene to wheat seedlings. Chemosphere 282, 130967.

Liu, Y., Guo, R., Zhang, S., Sun, Y. and Wang, F. (2022b) Uptake and translocation of nano/microplastics by rice seedlings: Evidence from a hydroponic experiment. Journal of Hazardous materials 421, 126700.

Loreto, F. and Schnitzler, J.-P. (2010) Abiotic stresses and induced BVOCs. Trends in Plant Science 15(3), 154-166.

Loreto, F. and Sharkey, T. (1993) Isoprene emission by plants is affected by transmissible wound signals. Plant, Cell & Environment 16(5), 563-570.

Lozano, Y. M. and Rillig, M. C. (2020) Effects of microplastic fibers and drought on plant communities. Environmental Science & Technology 54(10), 6166-6173.

Lu, S., Qiu, R., Hu, J., Li, X., Chen, Y., Zhang, X., Cao, C., Shi, H., Xie, B. and Wu, W.M. (2020) Prevalence of microplastics in animal-based traditional medicinal materials: Widespread pollution in terrestrial environments. Science of the Total Environment 709, 136214.

Lun, X. X., Lin, Y., Chai, F. H., Fan, C., Li, H. and Liu, J. F. (2020) Reviews of emission of biogenic volatile organic compounds (BVOCs) in Asia. Journal of Environmental Sciences 95, 266-277.

Ma, J., Sheng, G. D., Chen, Q.-L. and O'Connor, P. (2020) Do combined nanoscale polystyrene and tetracycline impact on the incidence of resistance genes and microbial community disturbance in Enchytraeus crypticus? Journal of Hazardous materials 387, 122012.

MacKenzie, A. R., Langford, B., Pugh, T. A. M., Robinson, N., Misztal, P. K., Heard, D. E., Lee, J. D., Lewis, A. C., Jones, C. E., Hopkins, J. R., Phillips, G., Monks, P. S., Karunaharan, A., Hornsby, K. E., Nicolas-Perea, V., Coe, H., Gabey, A. M., Gallagher, M. W., Whalley, L. K., Edwards, P. M., Evans, M. J., Stone, D., Ingham, T., Commane, R., Furneaux, K. L., McQuaid, J. B., Nemitz, E., Seng, Y. K., Fowler, D., Pyle, J. A. and Hewitt, C. N. (2011) The atmospheric chemistry of trace gases and particulate matter emitted by different land uses in Borneo. Philosophical Transactions of the Royal Society B-Biological Sciences 366(1582), 3177-3195.

Maki, M., Krasnov, D., Hellen, H., Noe, S. M. and Back, J. (2019) Stand type affects fluxes of volatile organic compounds from the forest floor in hemiboreal and boreal climates. Plant and Soil 441(1-2), 363-381.

Malinconico, M. (2017) Soil degradable bioplastics for a sustainable modern agriculture, Springer.

Maraun, D. (2016) Bias correcting climate change simulations-a critical review. Current Climate Change Reports 2(4), 211-220.

Margarita, P., Karina, C. and Johanna, M. (2013) Emission factors of biogenic volatile organic compounds in various stages of growth present in the urban forest of the Metropolitan Region, Chile. Research Journal of Chemistry and Environment 17(11), 1-9.

Martre, P. and Dambreville, A. (2018) A model of leaf coordination to scale-up leaf expansion from the organ to the canopy. Plant Physiology 176(1), 704-716.

Maulé, C., Helgason, W., McGinn, S. and Cutforth, H. (2006) Estimation of standardized reference evapotranspiration on the Canadian Prairies using simple models with limited weather data. Canadian Biosystems Engineering 48, 1.

Miles, C., DeVetter, L., Ghimire, S. and Hayes, D. G. (2017) Suitability of biodegradable plastic mulches for organic and sustainable agricultural production systems. HortScience 52(1), 10-15.

Mochizuki, T., Miyazaki, Y., Ono, K., Wada, R., Takahashi, Y., Saigusa, N., Kawamura, K. and Tani, A. (2015) Emissions of biogenic volatile organic compounds and subsequent formation of secondary organic aerosols in a Larix kaempferi forest. Atmospheric Chemistry and Physics 15(20), 12029-12041.

Monforti, F., Lugato, E., Motola, V., Bodis, K., Scarlat, N. and Dallemand, J.-F. (2015) Optimal energy use of agricultural crop residues preserving soil organic carbon stocks in Europe. Renewable and Sustainable Energy Reviews 44, 519-529.

Monson, R., Harley, P., Litvak, M., Wildermuth, M., Guenther, A., Zimmerman, P. and Fall, R. (1994) Environmental and developmental controls over the seasonal pattern of isoprene emission from aspen leaves. Oecologia 99, 260-270.

Monteith, J. L. (1977) Climate and the efficiency of crop production in Britain. Philosophical Transactions of the Royal Society of London. B, Biological Sciences 281(980), 277-294.

Moreno, M. M., González-Mora, S., Villena, J., Campos, J. A. and Moreno, C. (2017) Deterioration pattern of six biodegradable, potentially low-environmental impact mulches in field conditions. Journal of environmental management 200, 490-501.

Mozaffar, A. (2017) Exchanges of biogenic volatile organic compounds between the atmosphere and agricultural plants/ecosystems in controlled and field conditions, Université de Liège, Liège, Belgique.

Muhammad, A., Zhou, X., He, J., Zhang, N., Shen, X., Sun, C., Yan, B. and Shao, Y. (2021) Toxic effects of acute exposure to polystyrene microplastics and nanoplastics on the model insect, silkworm Bombyx mori. Environmental Pollution 285, 117255.

Müller, J., Stavrakou, T., Wallens, S., De Smedt, I., Van Roozendael, M., Potosnak, M., Rinne, J., Munger, B., Goldstein, A. and Guenther, A. (2007) Global isoprene emissions estimated using MEGAN, ECMWF analyses and a detailed canopy environment model. Atmos. Chem. Phys. Discuss. EGU 7(6), 15373-15407.

Murray, A. and Örmeci, B. (2020) Removal effectiveness of nanoplastics (< 400 nm) with separation processes used for water and wastewater treatment. Water 12(3), 635.

Muzika, R., Pregitzer, K. and Hanover, J. (1989) Changes in terpene production following nitrogen fertilization of grand fir (*Abies grandis (Dougl.) Lindl.*) seedlings. Oecologia 80(4), 485-489.

Napper, I. E. and Thompson, R. C. (2019) Environmental deterioration of biodegradable, oxo-biodegradable, compostable, and conventional plastic carrier bags in the sea, soil, and open-air over a 3-year period. Environmental Science & Technology 53(9), 4775-4783.

Niinemets, Ü. (2010) Mild versus severe stress and BVOCs: thresholds, priming and consequences. Trends in plant science 15(3), 145-153.

Niinemets, Ü., Monson, R., Arneth, A., Ciccioli, P., Kesselmeier, J., Kuhn, U., Noe, S., Peñuelas, J. and Staudt, M. (2010) The emission factor of volatile isoprenoids: caveats, model algorithms, response shapes and scaling.

Oikawa, P. Y., Giebel, B. M., Sternberg, L., Li, L., Timko, M. P., Swart, P. K., Riemer, D. D., Mak, J. E. and Lerdau, M. T. (2011) Leaf and root pectin methylesterase activity and C-13/C-12 stable isotopic ratio measurements of MeOH emissions give insight into MeOH production in *Lycopersicon esculentum*. New Phytologist 191(4), 1031-1040.

OMRI (2015) Report on biodegradable biobased mulch films. https://www.ams.usda.gov/sites/default/files/media/Biobased%20mulches%20report.pdf.

Ormeno, E., Fernandez, C., Bousquet-Melou, A., Greff, S., Morin, E., Robles, C., Vila, B. and Bonin, G. (2007) Monoterpene and sesquiterpene emissions of three Mediterranean species through calcareous and siliceous soils in natural conditions. Atmospheric Environment 41(3), 629-639.

Ormeno, E., Olivier, R., Mevy, J. P., Baldy, V. and Fernandez, C. (2009) Compost may affect volatile and semi-volatile plant emissions through nitrogen supply and chlorophyll fluorescence. Chemosphere 77(1), 94-104.

Ouyang, C., Liao, W., Wang, P., Fan, G., Hsiao, C., Chuang, M., Chang, C., Lin, N. and Wang, J. (2016) Construction of a cryogen-free thermal desorption gas chromatographic system with off-the-shelf components for monitoring ambient volatile organic compounds. Journal of Separation Science 39(8), 1489-1499.

Ouyang, W., Wang, Y., Lin, C., He, M., Hao, F., Liu, H. and Zhu, W. (2018) Heavy metal loss from agricultural watershed to aquatic system: A scientometrics review. Science of the Total Environment 637, 208-220.

Pace, M. L., Reche, I., Cole, J. J., Fernández-Barbero, A., Mazuecos, I. P. and Prairie, Y. T. (2012) pH change induces shifts in the size and light absorption of dissolved organic matter. Biogeochemistry 108(1), 109-118.

Pacifico, F., Harrison, S. P., Jones, C. D. and Sitch, S. (2009) Isoprene emissions and climate. Atmospheric Environment 43(39), 6121-6135.

Pakkattil, A., Muhsin, M. and Varma, M. R. (2021) COVID-19 lockdown: Effects on selected volatile organic compound (VOC) emissions over the major Indian metro cities. Urban Climate, 100838.

Pallozzi, E., Guidolotti, G., Ciccioli, P., Brilli, F., Feil, S. and Calfapietra, C. (2016) Does the novel fast-GC coupled with PTR-TOF-MS allow a significant advancement in detecting VOC emissions from plants? Agricultural and Forest Meteorology 216, 232-240.

Palmer, P. I., Barkley, M. P., Kurosu, T. P., Lewis, A. C., Saxton, J. E., Chance, K. and Gatti, L. V. (2007) Interpreting satellite column observations of formaldehyde over tropical South America. Philosophical Transactions of the Royal Society a-Mathematical Physical and Engineering Sciences 365(1856), 1741-1751.

Patel, N., Dadhwal, V., Saha, S., Garg, A. and Sharma, N. (2010) Evaluation of MODIS data potential to infer water stress for wheat NPP estimation. Tropical Ecology 51(1), 93.

Peñuelas, J., Asensio, D., Tholl, D., Wenke, K., Rosenkranz, M., Piechulla, B. and Schnitzler, J.-P. (2014) Biogenic volatile emissions from the soil. Plant Cell and Environment 37(8), 1866-1891.

Penuelas, J., Filella, I., Stefanescu, C. and Llusia, J. (2005) Caterpillars of *Euphydryas aurinia* (*Lepidoptera : Nymphalidae*) feeding on Succisa pratensis leaves induce large foliar emissions of MeOH. New Phytologist 167(3), 851-857.

Peñuelas, J., Sardans, J., Estiarte, M., Ogaya, R., Carnicer, J., Coll, M., Barbeta, A., Rivas-Ubach, A., Llusià, J. and Garbulsky, M. (2013) Evidence of current impact of climate change on life: a walk from genes to the biosphere. Global Change Biology 19(8), 2303-2338.

Penuelas, J. and Staudt, M. (2010) BVOCs and global change. Trends in Plant Science 15(3), 133-144.

Pierce, T. E. and Waldruff, P. S. (1991) PC-BEIS - A personal computer version of the biogenic emissions inventory system. Journal of the Air & Waste Management Association 41(7), 937-941.

Pignattelli, S., Broccoli, A. and Renzi, M. (2020) Physiological responses of garden cress (*L. sativum*) to different types of microplastics. Science of the Total Environment 727, 138609.

Pratt, K. A., Fiddler, M. N., Shepson, P. B., Carlton, A. G. and Surratt, J. D. (2013) Organosulfates in cloud water above the Ozarks' isoprene source region. Atmospheric Environment 77, 231-238.

Prendez, M., Carvajal, V., Corada, K., Morales, J., Alarcon, F. and Peralta, H. (2013) Biogenic volatile organic compounds from the urban forest of the Metropolitan Region, Chile. Environmental Pollution 183, 143-150.

Qi, Y., Yang, X., Pelaez, A. M., Lwanga, E. H., Beriot, N., Gertsen, H., Garbeva, P. and Geissen, V. (2018) Macro-and micro-plastics in soil-plant system: effects of plastic mulch film residues on wheat (*Triticum aestivum*) growth. Science of the Total Environment 645, 1048-1056.

Qian, B., De Jong, R., Huffman, T., Wang, H. and Yang, J. (2016) Projecting yield changes of spring wheat under future climate scenarios on the Canadian Prairies. Theoretical and Applied Climatology 123(3-4), 651-669.

Qin, M., Chen, C., Song, B., Shen, M., Cao, W., Yang, H., Zeng, G. and Gong, J. (2021) A review of biodegradable plastics to biodegradable microplastics: another ecological threat to soil environments? Journal of Cleaner Production 312, 127816.

Ren, Y., Ge, Y., Ma, D. P., Song, X. L., Shi, Y., Pan, K. X., Qu, Z. L., Guo, P. P., Han, W. J. and Chang, J. (2017) Enhancing plant diversity and mitigating BVOC emissions of urban green spaces through the introduction of ornamental tree species. Urban Forestry & Urban Greening 27, 305-313.

Rinnan, R., Gierth, D., Bilde, M., Rosenorn, T. and Michelsen, A. (2013) Off-season biogenic volatile organic compound emissions from heath mesocosms: responses to vegetation cutting. Frontiers in Microbiology 4, 10.

Rinnan, R., Iversen, L. L., Tang, J., Vedel-Petersen, I., Schollert, M. and Schurgers, G. (2020) Separating direct and indirect effects of rising temperatures on biogenic volatile emissions in the Arctic. Proceedings of the National Academy of Sciences 117(51), 32476-32483.

Rohr, A. C. (2013) The health significance of gas- and particle-phase terpene oxidation products: A review. Environment International 60, 145-162.

Romera-Castillo, C., Chen, M., Yamashita, Y. and Jaffé, R. (2014) Fluorescence characteristics of size-fractionated dissolved organic matter: implications for a molecular assembly based structure? Water Research 55, 40-51.

Rosenkranz, M., Pugh, T. A. M., Schnitzler, J. P. and Arneth, A. (2015) Effect of land-use change and management on biogenic volatile organic compound emissions - selecting climate-smart cultivars. Plant Cell and Environment 38(9), 1896-1912.

Roviello, V. and Roviello, G. N. (2021) Lower COVID-19 mortality in Italian forested areas suggests immunoprotection by Mediterranean plants. Environmental chemistry letters 19(1), 699-710.

Sakulyanontvittaya, T., Duhl, T., Wiedinmyer, C., Helmig, D., Matsunaga, S., Potosnak, M., Milford, J. and Guenther, A. (2008) Monoterpene and sesquiterpene emission estimates for the United States. Environmental Science & Technology 42(5), 1623-1629.

Sánchez, M., Pardo, N., Pérez, I. and García, M. (2015) GPP and maximum light use efficiency estimates using different approaches over a rotating biodiesel crop. Agricultural and Forest Meteorology 214, 444-455.

Sarkar, C., Sinha, V., Sinha, B., Panday, A. K., Rupakheti, M. and Lawrence, M. G. (2017) Source apportionment of NMVOCs in the Kathmandu Valley during the SusKat-ABC international field campaign using positive matrix factorization. Atmospheric Chemistry and Physics 17(13), 8129-8156.

Sbai, S. E., Mejjad, N., Norelyaqine, A. and Bentayeb, F. (2021) Air quality change during the COVID-19 pandemic lockdown over the Auvergne-Rhône-Alpes region, France. Air Quality, Atmosphere & Health, 1-12.

Schade, G. W. and Custer, T. G. (2004) OVOC emissions from agricultural soil in northern Germany during the 2003 European heat wave. Atmospheric Environment 38(36), 6105-6114.

Schade, G. W., Solomon, S. J., Dellwik, E., Pilegaard, K. and Ladstatter-Weissenmayer, A. (2011) MeOH and other VOC fluxes from a Danish beech forest during late springtime. Biogeochemistry 106(3), 337-355.

Schirinzi, G. F., Pérez-Pomeda, I., Sanchís, J., Rossini, C., Farré, M. and Barceló, D. (2017) Cytotoxic effects of commonly used nanomaterials and microplastics on cerebral and epithelial human cells. Environmental Research 159, 579-587.

Schollert, M., Kivimaenpaa, M., Valolahti, H. M. and Rinnan, R. (2015) Climate change alters leaf anatomy, but has no effects on volatile emissions from arctic plants. Plant Cell and Environment 38(10), 2048-2060.

Schwabl, P., Köppel, S., Königshofer, P., Bucsics, T., Trauner, M., Reiberger, T. and Liebmann, B. (2019) Detection of various microplastics in human stool: a prospective case series. Annals of internal medicine 171(7), 453-457.

Seewald, M., Bonfanti, M., Singer, W., Knapp, B., Hansel, A., Franke-Whittle, I. and Insam, H. (2010) Substrate induced VOC emissions from compost amended soils under aerobic and anaerobic incubation. Biol Fertil Soils 46, 371-382.

Selonen, S., Dolar, A., Kokalj, A. J., Skalar, T., Dolcet, L. P., Hurley, R. and van Gestel, C. A. (2020) Exploring the impacts of plastics in soil–The effects of polyester textile fibers on soil invertebrates. Science of the Total Environment 700, 134451.

Serrano-Ruíz, H., Eras, J., Martín-Closas, L. and Pelacho, A. (2020) Compounds released from unused biodegradable mulch materials after contact with water. Polymer Degradation and Stability 178, 109202.

Sforzini, S., Oliveri, L., Chinaglia, S. and Viarengo, A. (2016) Application of biotests for the determination of soil ecotoxicity after exposure to biodegradable plastics. Frontiers in Environmental Science 4, 68.

Shi, Q., Tang, J., Wang, L., Liu, R. and Giesy, J. P. (2021a) Combined cytotoxicity of polystyrene nanoplastics and phthalate esters on human lung epithelial A549 cells and its mechanism. Ecotoxicology and environmental safety 213, 112041.

Shi, Y., Huang, G., An, C., Zhou, Y. and Yin, J. (2021b) Assessment of regional greenhouse gas emissions from spring wheat cropping system: A case study of Saskatchewan in Canada. Journal of Cleaner Production 301, 126917.

Shrivastava, M., Cappa, C. D., Fan, J., Goldstein, A. H., Guenther, A. B., Jimenez, J. L., Kuang, C., Laskin, A., Martin, S. T. and Ng, N. L. (2017) Recent advances in understanding secondary organic aerosol: Implications for global climate forcing. Reviews of Geophysics 55(2), 509-559.

Shruti, V. and Kutralam-Muniasamy, G. (2019) Bioplastics: missing link in the era of microplastics. Science of the Total Environment 697, 134139.

Simon, H., Fallmann, J., Kropp, T., Tost, H. and Bruse, M. (2019) Urban trees and their impact on local ozone concentration-A microclimate modeling study. Atmosphere 10(3), 24.

Simpraga, M., Verbeeck, H., Bloemen, J., Vanhaecke, L., Demarcke, M., Joo, E., Pokorska, O., Amelynck, C., Schoon, N., Dewulf, J., Van Langenhove, H., Heinesch, B., Aubinet, M. and Steppe, K. (2013) Vertical canopy gradient in photosynthesis and monoterpenoid emissions: An insight into the chemistry and physiology behind. Atmospheric Environment 80, 85-95.

Simpraga, M., Verbeeck, H., Demarcke, M., Joo, E., Pokorska, O., Amelynck, C., Schoon, N., Dewulf, J., Van Langenhove, H., Heinesch, B., Aubinet, M., Laffineur, Q., Muller, J. F. and Steppe, K. (2011) Clear link between drought stress, photosynthesis and biogenic volatile organic compounds in Fagus sylvatica L. Atmospheric Environment 45(30), 5254-5259.

Sindelarova, K., Granier, C., Bouarar, I., Guenther, A., Tilmes, S., Stavrakou, T., Muller, J. F., Kuhn, U., Stefani, P. and Knorr, W. (2014) Global data set of biogenic VOC emissions calculated by the MEGAN model over the last 30 years. Atmospheric Chemistry and Physics 14(17), 9317-9341.

Singh, J., Singh, P., Vaishnav, A., Ray, S., Rajput, R. S., Singh, S. M. and Singh, H. B. (2021) Belowground fungal volatiles perception in okra (*Abelmoschus esculentus*) facilitates plant growth under biotic stress. Microbiological Research 246, 14.

Sintim, H. Y. (2018) Biodegradable plastic mulch: degradation and impacts on soil health, Washington State University.

Sintim, H. Y., Bary, A. I., Hayes, D. G., Wadsworth, L. C., Anunciado, M. B., English, M. E., Bandopadhyay, S., Schaeffer, S. M., DeBruyn, J. M. and Miles, C. A. (2020) In situ degradation of biodegradable plastic mulch films in compost and agricultural soils. Science of the Total Environment 727, 138668.

Smiatek, G. and Bogacki, M. (2005) Uncertainty assessment of potential biogenic volatile organic compound emissions from forests with the Monte Carlo method: Case study for an episode from 1 to 10 July 2000 in Poland. Journal of Geophysical Research: Atmospheres 110(D23).

Song, C. B., Liu, B. S., Dai, Q. L., Li, H. R. and Mao, H. J. (2019a) Temperature dependence and source apportionment of volatile organic compounds (VOCs) at an urban site on the north China plain. Atmospheric Environment 207, 167-181.

Song, S. K., Shon, Z. H., Kang, Y. H., Kim, K. H., Han, S. B., Kang, M., Bang, J. H. and Oh, I. (2019b) Source apportionment of VOCs and their impact on air quality and health in the megacity of Seoul. Environmental Pollution 247, 763-774.

Song, Y., Cao, C., Qiu, R., Hu, J., Liu, M., Lu, S., Shi, H., Raley-Susman, K. M. and He, D. (2019c) Uptake and adverse effects of polyethylene terephthalate microplastics fibers on terrestrial snails (*Achatina fulica*) after soil exposure. Environmental Pollution 250, 447-455.

Spielmann, F., Langebner, S., Ghirardo, A., Hansel, A., Schnitzler, J. P. and Wohlfahrt, G. (2017) Isoprene and alpha-pinene deposition to grassland mesocosms. Plant and Soil 410(1-2), 313-322.

Sporre, M. K., Blichner, S. M., Karset, I. H. H., Makkonen, R. and Berntsen, T. K. (2019) BVOC-aerosol-climate feedbacks investigated using NorESM. Atmospheric Chemistry and Physics 19(7), 4763-4782.

Squire, O. J., Archibald, A. T., Abraham, N. L., Beerling, D. J., Hewitt, C. N., Lathiere, J., Pike, R. C., Telford, P. J. and Pyle, J. A. (2014) Influence of future climate and cropland expansion on isoprene emissions and tropospheric ozone. Atmospheric Chemistry and Physics 14(2), 1011-1024.

Staudt, M. and Bertin, N. (1998) Light and temperature dependence of the emission of cyclic and acyclic monoterpenes from holm oak (*Quercus ilex L.*) leaves. Plant Cell and Environment 21(4), 385-395.

Staudt, M. and Lhoutellier, L. (2007) Volatile organic compound emission from holm oak infested by gypsy moth larvae: evidence for distinct responses in damaged and undamaged leaves. Tree Physiology 27(10), 1433-1440.

Stavrakou, T., Guenther, A., Razavi, A., Clarisse, L., Clerbaux, C., Coheur, P. F., Hurtmans, D., Karagulian, F., De Maziere, M., Vigouroux, C., Amelynck, C., Schoon, N., Laffineur, Q., Heinesch, B., Aubinet, M., Rinsland, C. and Muller, J. F. (2011) First space-based derivation of the global atmospheric MeOH emission fluxes. Atmospheric Chemistry and Physics 11(10), 4873-4898.

Su, X., Li, X. and Kang, Y. (2019) A bibliometric analysis of research on intangible cultural heritage using CiteSpace. SAGE Open 9(2), 2158244019840119.

Sun, H., Lei, C., Xu, J. and Li, R. (2021) Foliar uptake and leaf-to-root translocation of nanoplastics with different coating charge in maize plants. Journal of Hazardous materials 416, 125854.

Sun, X., Yuan, X., Jia, Y., Feng, L., Zhu, F., Dong, S., Liu, J., Kong, X., Tian, H. and Duan, J. (2020) Differentially charged nanoplastics demonstrate distinct accumulation in Arabidopsis thaliana. Nature nanotechnology 15(9), 755-760.

Svendsen, S. H., Lindwall, F., Michelsen, A. and Rinnan, R. (2016) Biogenic volatile organic compound emissions along a high arctic soil moisture gradient. Science of the Total Environment 573, 131-138.

Sytar, O., Brestic, M., Hajihashemi, S., Skalicky, M., Kubeš, J., Lamilla-Tamayo, L., Ibrahimova, U., Ibadullayeva, S. and Landi, M. (2021) COVID-19 prophylaxis efforts based on natural antiviral plant extracts and their compounds. Molecules 26(3), 727.

Tai, A. P. K., Mickley, L. J., Heald, C. L. and Wu, S. L. (2013) Effect of CO2 inhibition on biogenic isoprene emission: Implications for air quality under 2000 to 2050 changes in climate, vegetation, and land use. Geophysical Research Letters 40(13), 3479-3483.

Tang, J., Schurgers, G. and Rinnan, R. (2019a) Process understanding of soil BVOC fluxes in natural ecosystems: a review. Reviews of Geophysics.

Tang, J., Schurgers, G. and Rinnan, R. (2019b) Process understanding of soil BVOC fluxes in natural ecosystems: a review. Reviews of Geophysics 57(3), 966-986.

Tang, J., Valolahti, H., Kivimaenpaa, M., Michelsen, A. and Rinnan, R. (2018) Acclimation of biogenic volatile organic compound emission from subarctic heath under long-term moderate warming. Journal of Geophysical Research-Biogeosciences 123(1), 95-105.

Tani, A. and Mochizuk, T. (2021) Review: Exchanges of volatile organic compounds between terrestrial ecosystems and the atmosphere. Journal of Agricultural Meteorology 77(1), 66-80.

Tie, X., Guenther, A. and Holland, E. (2003) Biogenic MeOH and its impacts on tropospheric oxidants. Geophysical Research Letters 30(17).

Tiwary, A. and Kumar, P. (2014) Impact evaluation of green-grey infrastructure interaction on built-space integrity: An emerging perspective to urban ecosystem service. Science of the Total Environment 487, 350-360.

Tofanelli, M. B. and Wortman, S. E. (2020) Benchmarking the agronomic performance of biodegradable mulches against polyethylene mulch film: a meta-analysis. Agronomy 10(10), 1618.

Uchimiya, M., Chang, S. and Klasson, K. T. (2011) Screening biochars for heavy metal retention in soil: role of oxygen functional groups. Journal of Hazardous materials 190(1-3), 432-441.

Urbina, M. A., Correa, F., Aburto, F. and Ferrio, J. P. (2020) Adsorption of polyethylene microbeads and physiological effects on hydroponic maize. Science of the Total Environment 741, 140216.

Valentini, R., Greco, S., Seufert, G., Bertin, N., Ciccioli, P., Cecinato, A., Brancaleoni, E. and Frattoni, M. (1997) Fluxes of biogenic VOC from Mediterranean vegetation by trap enrichment relaxed eddy accumulation. Atmospheric Environment 31, 229-238.

Valolahti, H., Kivimäenpää, M., Faubert, P., Michelsen, A. and Rinnan, R. (2015) Climate change-induced vegetation change as a driver of increased subarctic biogenic volatile organic compound emissions. Global Change Biology 21(9), 3478-3488.

Vedel-Petersen, I., Schollert, M., Nymand, J. and Rinnan, R. (2015) Volatile organic compound emission profiles of four common arctic plants. Atmospheric Environment 120, 117-126.

Vermeuel, M. P., Novak, G. A., Alwe, H. D., Hughes, D. D., Kaleel, R., Dickens, A. F., Kenski, D., Czarnetzki, A. C., Stone, E. A. and Stanier, C. O. (2019) Sensitivity of ozone production to NOx and VOC along the lake Michigan coastline. Journal of Geophysical Research: Atmospheres 124(20), 10989-11006.

von Schneidemesser, E., Bonn, B., Butler, T. M., Ehlers, C., Gerwig, H., Hakola, H., Hellen, H., Kerschbaumer, A., Klemp, D., Kofahl, C., Kura, J., Ludecke, A., Nothard, R., Pietsch, A., Quedenau, J., Schafer, K., Schauer, J. J., Singh, A., Villalobos, A. M., Wiegner, M. and Lawrence, M. G. (2018) BAERLIN2014-stationary measurements and source apportionment at an urban background station in Berlin, Germany. Atmospheric Chemistry and Physics 18(12), 8621-8645.

Waked, A., Favez, O., Alleman, L. Y., Piot, C., Petit, J. E., Delaunay, T., Verlinden, E., Golly, B., Besombes, J. L., Jaffrezo, J. L. and Leoz-Garziandia, E. (2014) Source apportionment of PM10 in a north-western Europe regional urban background site (Lens, France) using positive matrix factorization and including primary biogenic emissions. Atmospheric Chemistry and Physics 14(7), 3325-3346.

Wang, D. F., Zhou, B., Fu, Q. Y., Zhao, Q. B., Zhang, Q., Chen, J. M., Yang, X., Duan, Y. S. and Li, J. (2016a) Intense secondary aerosol formation due to strong atmospheric photochemical reactions in summer: observations at a rural site in eastern Yangtze River Delta of China. Science of the Total Environment 571, 1454-1466.

Wang, F., Wang, Q., Adams, C. A., Sun, Y. and Zhang, S. (2022a) Effects of microplastics on soil properties: current knowledge and future perspectives. Journal of Hazardous materials 424, 127531.

Wang, F., Wang, X. and Song, N. (2021a) Polyethylene microplastics increase cadmium uptake in lettuce (Lactuca sativa L.) by altering the soil microenvironment. Science of the Total Environment 784, 147133.

Wang, H., Ding, J., Xiong, C., Zhu, D., Li, G., Jia, X., Zhu, Y. and Xue, X. (2019a) Exposure to microplastics lowers arsenic accumulation and alters gut bacterial communities of earthworm Metaphire californica. Environmental Pollution 251, 110-116.

Wang, H., Wang, X., Zhang, Y., Mu, Y. and Han, X. (2016b) Evident elevation of atmospheric monoterpenes due to degradation-induced species changes in a semi-arid grassland. Science of the Total Environment 541, 1499-1503.

Wang, H. L., Chen, C. H., Wang, Q., Huang, C., Su, L. Y., Huang, H. Y., Lou, S. R., Zhou, M., Li, L., Qiao, L. P. and Wang, Y. H. (2013) Chemical loss of volatile organic compounds and its impact on the source analysis through a two-year continuous measurement. Atmospheric Environment 80, 488-498.

Wang, J., Coffin, S., Sun, C., Schlenk, D. and Gan, J. (2019b) Negligible effects of microplastics on animal fitness and HOC bioaccumulation in earthworm Eisenia fetida in soil. Environmental Pollution 249, 776-784.

Wang, K., Li, J., Zhao, L., Mu, X., Wang, C., Wang, M., Xue, X., Qi, S. and Wu, L. (2021b) Gut microbiota protects honey bees (Apis mellifera L.) against polystyrene microplastics exposure risks. Journal of Hazardous materials 402, 123828.

Wang, L., Li, P., Zhang, Q., Wu, W., Luo, J. and Hou, D. (2021c) Modeling the conditional fragmentation-induced microplastic distribution. Environmental Science & Technology 55(9), 6012-6021.

Wang, M., Qin, W., Chen, W. T., Zhang, L., Zhang, Y., Zhang, X. Z. and Xie, X. (2020a) Seasonal variability of VOCs in Nanjing, Yangtze River delta: Implications for emission sources and photochemistry. Atmospheric Environment 223, 11.

Wang, P., Chen, Y., Hu, J. L., Zhang, H. L. and Ying, Q. (2019c) Source apportionment of summertime ozone in China using a source-oriented chemical transport model. Atmospheric Environment 211, 79-90.

Wang, Q., Bai, J., Ning, B., Fan, L., Sun, T., Fang, Y., Wu, J., Li, S., Duan, C. and Zhang, Y. (2020b) Effects of bisphenol A and nanoscale and microscale polystyrene plastic exposure on particle uptake and toxicity in human Caco-2 cells. Chemosphere 254, 126788.

Wang, W., Do, A. T. N. and Kwon, J. (2022b) Ecotoxicological effects of micro-and nanoplastics on terrestrial food web from plants to human beings. Science of the Total Environment, 155333.

Wang, Z., An, C., Chen, X., Lee, K., Zhang, B. and Feng, Q. (2021d) Disposable masks release microplastics to the aqueous environment with exacerbation by natural weathering. Journal of Hazardous materials 417, 126036.

Wang, Z., An, C., Lee, K., Chen, X., Zhang, B., Yin, J. and Feng, Q. (2022c) Physicochemical change and microparticle release from disposable gloves in the aqueous environment impacted by accelerated weathering. Science of the Total Environment 832, 154986.

Wang, Z., Li, W., Zhang, K., Agrawal, Y. and Huang, H. (2020c) Observations of the distribution and flocculation of suspended particulate matter in the North Yellow Sea cold water mass. Continental Shelf Research 204, 104187.

Waterer, D. (2010) Evaluation of biodegradable mulches for production of warm-season vegetable crops. Canadian Journal of Plant Science 90(5), 737-743.

Way, D. A., Ghirardo, A., Kanawati, B., Esperschutz, J., Monson, R. K., Jackson, R. B., Schmitt-Kopplin, P. and Schnitzler, J. P. (2013) Increasing atmospheric CO_2 reduces metabolic and physiological differences between isoprene- and non-isoprene-emitting poplars. New Phytologist 200(2), 534-546.

Weinstein, J. E., Dekle, J. L., Leads, R. R. and Hunter, R. A. (2020) Degradation of bio-based and biodegradable plastics in a salt marsh habitat: another potential source of microplastics in coastal waters. Marine pollution bulletin 160, 111518.

Wells, K. C., Millet, D. B., Cady-Pereira, K. E., Shephard, M. W., Henze, D. K., Bousserez, N., Apel, E. C., de Gouw, J., Warneke, C. and Singh, H. B. (2014) Quantifying global terrestrial MeOH emissions using observations from the TES satellite sensor. Atmospheric Chemistry and Physics 14(5), 2555-2570.

Wiedinmyer, C., Tie, X. X., Guenther, A., Neilson, R. and Granier, C. (2006) Future changes in biogenic isoprene emissions: How might they affect regional and global atmospheric chemistry? Earth Interactions 10, 19.

Wood, C. T. and Zimmer, M. (2014) Can terrestrial isopods (Isopoda: Oniscidea) make use of biodegradable plastics? Applied Soil Ecology 77, 72-79.

Wu, K., Yang, X. Y., Chen, D., Gu, S., Lu, Y. Q., Jiang, Q., Wang, K., Ou, Y. H., Qian, Y., Shao, P. and Lu, S. H. (2020) Estimation of biogenic VOC emissions and their corresponding impact on ozone and secondary organic aerosol formation in China. Atmospheric Research 231, 11.

Xiao, F., Li, C., Sun, J. and Zhang, L. (2017) Knowledge domain and emerging trends in organic photovoltaic technology: a scientometric review based on CiteSpace analysis. Frontiers in chemistry 5, 67.

Xie, S., Zhang, J. and Ho, Y.-S. (2008) Assessment of world aerosol research trends by bibliometric analysis. Scientometrics 77(1), 113-130.

Xing, C. Z., Liu, C., Hu, Q. H., Fu, Q. Y., Lin, H., Wang, S. T., Su, W. J., Wang, W. W., Javed, Z. and Liu, J. G. (2020) Identifying the wintertime sources of volatile organic compounds (VOCs) from MAX-DOAS measured formaldehyde and glyoxal in Chongqing, southwest China. Science of the Total Environment 715, 12.

Xu, G., Liu, Y. and Yu, Y. (2021) Effects of polystyrene microplastics on uptake and toxicity of phenanthrene in soybean. Science of the Total Environment 783, 147016.

Xu, L., Guo, H. Y., Boyd, C. M., Klein, M., Bougiatioti, A., Cerully, K. M., Hite, J. R., Isaacman-VanWertz, G., Kreisberg, N. M., Knote, C., Olson, K., Koss, A., Goldstein, A. H., Hering, S. V., de Gouw, J., Baumann, K., Lee, S. H., Nenes, A., Weber, R. J. and Ng, N. L. (2015a) Effects of anthropogenic emissions on aerosol formation from isoprene and monoterpenes in the southeastern United States. Proceedings of the National Academy of Sciences of the United States of America 112(1), 37-42.

Xu, M., Halimu, G., Zhang, Q., Song, Y., Fu, X., Li, Y., Li, Y. and Zhang, H. (2019) Internalization and toxicity: A preliminary study of effects of nanoplastic particles on human lung epithelial cell. Science of the Total Environment 694, 133794.

Xu, Y., Pu, L. and Zhu, M. (2015b) Calculation of climate potential productivity at coastal zone of Jiangsu province based on crop growing period. Scientia Geographica Sinica 35(5), 658-664.

Yadav, D., Singh, R., Kumar, A. and Sarkar, B. (2022) Reduction of pollution through sustainable and flexible production by controlling by-products. Journal of Environmental Informatics 40(2), 106-124.

Yadav, R., Sahu, L. K., Tripathi, N., Pal, D., Beig, G. and Jaaffrey, S. N. A. (2019) Investigation of emission characteristics of NMVOCs over urban site of western India. Environmental Pollution 252, 245-255.

Yang, C., Gao, X., Huang, Y. and Xie, D. (2020) An alternative to polyethylene film mulch: field evaluation of biodegradable film mulch on winter potato in the south of China. Agronomy Journal 112(6), 4752-4764.

Yang, G., Li, M. and Guo, P. (2022a) Monte Carlo-based agricultural water management under uncertainty: a case study of Shijin irrigation district, China. Journal of Environmental Informatics 39(2), 152-164.

Yang, W. Y., Chen, H. S., Wang, W. D., Wu, J. B., Li, J., Wang, Z. F., Zheng, J. Y. and Chen, D. H. (2019) Modeling study of ozone source apportionment over the Pearl River Delta in 2015. Environmental Pollution 253, 393-402.

Yang, X., An, C., Feng, Q., Boufadel, M. and Ji, W. (2022b) Aggregation of microplastics and clay particles in the nearshore environment: characteristics, influencing factors, and implications. Water Research, 119077.

Yao, Y., Huang, G., An, C., Chen, X., Zhang, P., Xin, X., Shen, J. and Agnew, J. (2020) Anaerobic digestion of livestock manure in cold regions: Technological advancements and global impacts. Renewable and Sustainable Energy Reviews 119, 109494.

Yin, J., Huang, G., An, C., Zhang, P., Xin, X. and Feng, R. (2021) Exploration of nanocellulose washing agent for the green remediation of phenanthrene-contaminated soil. Journal of Hazardous materials 403, 123861.

Yu, H. and Blande, J. D. (2021) Diurnal variation in BVOC emission and CO_2 gas exchange from above-and belowground parts of two coniferous species and their responses to elevated O_3. Environmental Pollution, 116830.

Yu, Y., Chen, H., Hua, X., Dang, Y., Han, Y., Yu, Z., Chen, X., Ding, P. and Li, H. (2020) Polystyrene microplastics (PS-MPs) toxicity induced oxidative stress and intestinal injury in nematode Caenorhabditis elegans. Science of the Total Environment 726, 138679.

Yuan, Z. B., Lau, A. K. H., Shao, M., Louie, P. K. K., Liu, S. C. and Zhu, T. (2009) Source analysis of volatile organic compounds by positive matrix factorization in urban and rural environments in Beijing. Journal of Geophysical Research-Atmospheres 114, 14.

Yue, R., An, C., Ye, Z., Chen, X., Lee, K., Zhang, K., Wan, S. and Qu, Z. (2022) Exploring the characteristics, performance, and mechanisms of a magnetic-mediated washing fluid for the cleanup of oiled beach sand. Journal of Hazardous materials 438, 129447.

Zabini, F., Albanese, L., Becheri, F. R., Gavazzi, G., Giganti, F., Giovanelli, F., Gronchi, G., Guazzini, A., Laurino, M., Li, Q., Marzi, T., Mastorci, F., Meneguzzo, F., Righi, S. and Viggiano, M. P. (2020) Comparative study of the restorative effects of forest and urban videos during COVID-19 lockdown: Intrinsic and benchmark values. International Journal of Environmental Research and Public Health 17(21), 13.

Zhang-Turpeinen, H., Kivimaenpaa, M., Aaltonen, H., Berninger, F., Koster, E., Koster, K., Menyailo, O., Prokushkin, A. and Pumpanen, J. (2020a) Wildfire effects on BVOC emissions from boreal forest floor on permafrost soil in Siberia. Science of the Total Environment 711, 12.

Zhang-Turpeinen, H., Kivimäenpää, M., Aaltonen, H., Berninger, F., Köster, E., Köster, K., Menyailo, O., Prokushkin, A. and Pumpanen, J. (2020b) Wildfire effects on BVOC emissions from boreal forest floor on permafrost soil in Siberia. Science of the Total Environment 711, 134851.

Zhang, H., Wu, L., Qian, W., Ni, J., Wei, R., Qi, Z. and Chen, W. (2021) Spectral characteristics of dissolved organic carbon derived from biomass-pyrogenic smoke (SDOC) in the aqueous environment and its solubilization effect on hydrophobic organic pollutants. Water Research 203, 117515.

Zhang, L., Sintim, H. Y., Bary, A. I., Hayes, D. G., Wadsworth, L. C., Anunciado, M. B. and Flury, M. (2018) Interaction of Lumbricus terrestris with macroscopic polyethylene and biodegradable plastic mulch. Science of the Total Environment 635, 1600-1608.

Zhang, R., Cohan, A., Biazar, A. P. and Cohan, D. S. (2017) Source apportionment of biogenic contributions to ozone formation over the United States. Atmospheric Environment 164, 8-19.

Zhang, X. F., Yin, Y. Y., Wen, J. H., Huang, S. L., Han, D. M., Chen, X. J. and Cheng, J. P. (2019) Characteristics, reactivity and source apportionment of ambient volatile organic compounds (VOCs) in a typical tourist city. Atmospheric Environment 215, 13.

Zhao, S., Zhu, L. and Li, D. (2016) Microscopic anthropogenic litter in terrestrial birds from Shanghai, China: Not only plastics but also natural fibers. Science of the Total Environment 550, 1110-1115.

Zhao, Y., Mao, P., Zhou, Y. D., Yang, Y., Zhang, J., Wang, S. K., Dong, Y. P., Xie, F. J., Yu, Y. Y. and Li, W. Q. (2017) Improved provincial emission inventory and speciation profiles of anthropogenic

non-methane volatile organic compounds: a case study for Jiangsu, China. Atmospheric Chemistry and Physics 17(12), 7733-7756.

Zhao, Z., Wang, P., Wang, Y., Zhou, R., Koskei, K., Munyasya, A. N., Liu, S., Wang, W., Su, Y. and Xiong, Y. (2021) Fate of plastic film residues in agro-ecosystem and its effects on aggregate-associated soil carbon and nitrogen stocks. Journal of Hazardous materials 416, 125954.

Zheng, J., Zheng, Z., Yu, Y. and Zhong, L. (2010a) Temporal, spatial characteristics and uncertainty of biogenic VOC emissions in the Pearl River Delta region, China. Atmospheric Environment 44(16), 1960-1969.

Zheng, J. Y., Zheng, Z. Y., Yu, Y. F. and Zhong, L. J. (2010b) Temporal, spatial characteristics and uncertainty of biogenic VOC emissions in the Pearl River Delta region, China. Atmospheric Environment 44(16), 1960-1969.

Zheng, Y. and Qiu, F. (2020) Bioenergy in the Canadian Prairies: Assessment of accessible biomass from agricultural crop residues and identification of potential biorefinery sites. Biomass and Bioenergy 140, 105669.

Zhou, C., Lu, C., Mai, L., Bao, L., Liu, L. and Zeng, E. Y. (2021) Response of rice (*Oryza sativa L.*) roots to nanoplastic treatment at seedling stage. Journal of Hazardous materials 401, 123412.

Zhou, L., Wang, T., Qu, G., Jia, H. and Zhu, L. (2020) Probing the aging processes and mechanisms of microplastic under simulated multiple actions generated by discharge plasma. Journal of Hazardous materials 398, 122956.

Zhu, J., Wang, S. S., Wang, H. L., Jing, S. G., Lou, S. R., Saiz-Lopez, A. and Zhou, B. (2020a) Observationally constrained modeling of atmospheric oxidation capacity and photochemical reactivity in Shanghai, China. Atmospheric Chemistry and Physics 20(3), 1217-1232.

Zhu, K., Jia, H., Sun, Y., Dai, Y., Zhang, C., Guo, X., Wang, T. and Zhu, L. (2020b) Long-term phototransformation of microplastics under simulated sunlight irradiation in aquatic environments: roles of reactive oxygen species. Water Research 173, 115564.

Zhu, Y. H., Huang, L., Li, J. Y., Ying, Q., Zhang, H. L., Liu, X. G., Liao, H., Li, N., Liu, Z. X., Mao, Y. H., Fang, H. and Hu, J. L. (2018) Sources of particulate matter in China: Insights from source apportionment studies published in 1987-2017. Environment International 115, 343-357.

Zou, J., Liu, X., Zhang, D. and Yuan, X. (2020) Adsorption of three bivalent metals by four chemical distinct microplastics. Chemosphere 248, 126064.